The Effect of Particles on the Phase Separation of Waxy Corn Starch plus Galactomannan gums

Nataricha Phisarnchananan

Submitted in accordance with the requirements for degree of Doctor of Philosophy

The University of Leeds

School of Food Science and Nutrition

October, 2015

The candidate confirms that the work submitted is her own, except where work which has formed part of jointly-authored publications has been included. The contribution of the candidate and the other authors to this work has been explicitly indicated below. The candidate confirms that appropriate credit has been given within the thesis where reference has been made to the work of others. Details of the jointly-authored publications are outlined on the next page.

Further details of the work from jointly-authored publications and the contributions of the candidate and the other authors to the work are included below:

This thesis has contributed to the following publication based on chapter 3, 4 and 6:

- Murray, B.S. and Phisarnchananan, N. 2014. The effect of nanoparticles on the phase separation of waxy corn starch + locust bean gum or guar gum. *Food Hydrocolloids*. 42, pp.92-99.
- Murray, B.S. and Phisarnchananan, N. 2016. Whey protein microgel particles as stabilizers of waxy corn starch + locust bean gum water-in-water emulsions. *Food Hydrocolloids*. 56, pp.161-169.

Details of authorship contributions:

Phisarnchananan: conducted the experimental design, data analysis, data interpretation, laboratory work and wrote a draft publication.

Murray: guidance, supervision, contributed to answer the reviewer's comments and manuscript editor

Acknowledgements

This report would never been completed without the support and guidance from many people who pleasantly involved themselves in helping me undertake this thesis. First of all I would like to express my gratitude to my supervisor, Professor. Brent S Murray for his support, advice, guidance and help with the research materials from the beginning to the end of the project and particularly for submitting publications to referred journals. I am deeply grateful to him for the long discussions that helped me explore the technical details of my work. I wish to acknowledge the help provided by Professor Bernard Binks and his students from University of Hull with regards to interfacial tension measurements and providing model silica particles.

I would also like to extend thanks to all lecturers, staff and my friends in School of Food Science and Nutrition, particularly in the food colloid group for supporting me in any respect and making my life in the laboratory enjoyable. A special thanks goes to Miles Ratcliffe who lent a hand when needed in the laboratory during my PhD.

I owe my deepest gratitude to my parents and my family for supporting and encouraging me to get through problems during research. I am also thankful to Samwise Wilson, who provided countless corrections and helped me whilst being patient. Lastly, thanks to Samwise's family for their care and cheering me up during tough times. This thesis is dedicated to all of you.

Abstract

This thesis was initiated with the aim of studying the effect of small particles on phase separation of polysaccharide mixtures with the expectation of stabilising the mixture for a longer period of time, completely inhibiting phase separation, or changing the phase-separated microstructure. The phase separation of a model system consisting 2 wt.% waxy corn starch + 0.25 wt.% guar gum or 0.3 wt.% locust bean gum was studied at 25 °C at pH 7. Phase separated networks occurred within 30 minutes after preparation where the upper phase was enriched with galactomannan gum whereas the lower phase contained starch. Macroscopic phase separation of mixed polysaccharides was studied at vary concentrations, i.e., 0.5 – 4 wt.% and 0.05 – 0.6 wt.% galactomannan gums. The phase diagram illustrating the binodal lines almost coincided with the axes representing the polysaccharide concentrations. Microscopic results showed that the morphology of both mixtures exhibited thermodynamic incompatibility via spinodal decomposition structure.

The model systems were also studied in the presence of different kinds of particles. There are three main types of particles that were selected in this thesis; silica nanoparticles (at different hydrophobicities), oil-in-water stable microdroplets and whey protein microgel particles with an initial particle size of 20 nm, 280 nm and 149 nm, respectively. The key parameters investigated were particle concentration, size and effect of pH.

This particle-stablised model W/W emulsion was shown to induce long-term stability. With silica particles, the results showed that the rate of phase separation was inversely proportional to particle concentration. The observation also showed that the phase separation of polysaccharide mixtures was significantly slowed down in the presence of 0.5 wt.% of the 80-SiOH and 65-SiOH particles and fully inhibited at 1 wt.% particle concentration. The microdroplets appeared to slow down the rate of phase separation but within one month of storage all mixtures showed the sign of phase separation. The phase separation of a model system, starch + locust bean gum, was significantly inhibited in the presence of 1 vol.% whey protein microgel particles at pH 4, whilst the microgel particles were not as effective in starch + guar gum systems.

Acknowledgements…… iv

Abstract…….. v

Contents……. vi

Figures…… xii

Table…… xix

Contents

Chapter 1. General Introduction……... 1

1.1 Aim of the research…… 2

1.1.1 Plan of thesis……..… 3

1.2 Food emulsions……..…… 4

1.3 Challenges raised by mixing biopolymers……. 5

1.4 Early sight of phase separation in polysaccharide mixtures…….. 8

1.5 Theory of emulsion stability…….. 8

1.5.1 Thermodynamics of stability……. 9

1.5.2 Gravitational separation……. 10

1.6 Phase diagram……..... 11

1.7 Rheology…….... 13

1.7.1 Flow models……..…. 15

1.7.2 Viscoelastic behaviour via frequency sweep tests……..… 17

1.7.3 Effect of concentration on zero-shear viscosity……..… 19

1.8 Microstructure of emulsions……..… 20

1.9 Particle-stabilised emulsions……. 21

1.9.1 Pickering emulsion……...……. 23

1.9.2 Bijels…… 25

1.9.3 Particle detachment energy, $\Delta \boldsymbol{E}$…… 26

1.10 Polysaccharides…… 28

1.10.1 Types of polysaccharide structure…… 29

1.10.2 Starch…… 30

1.10.3 Galactomannans…… 31

1.10.4 Binary polysaccharide gels…… 35

1.11 Fumed silica particles…… 36

1.12 Milk proteins…… 37

1.12.1 Sodium Caseinate…… 37

1.12.2 Whey protein isolates (WPI) …… 37

Chapter 2. General materials and methodology…… 39

2.1 General Materials…… 40

2.1.1 Phosphate buffer pH 7…… 40

2.1.2 Starch…… 40

2.1.3 Gum…… 40

2.1.4 Model fumed silica particles…… 40

2.1.5 Fluorescence labels…… 41

2.2 Preparation of solutions…… 41

2.2.1 Preparation of starch solution…… 41

2.2.2 Preparation of galactomannan gum solution…… 42

2.2.3 Preparation of the final solution…… 42

2.3 Particle size distribution and ζ-potential measurement…… 43

2.4 Phase diagrams……...…… 47

2.4.1 Mixture of polysaccharides…… 47

2.4.2 Determination of phase volumes……...…… 47

2.5 Rheological measurement……..…… 47

2.5.1 Cone (upper geometry) and Plate (lower geometry) with plate cartridge……..…… 49

2.5.2 Bob (upper geometry) and double gap cup (lower geometry) with cylinder cartridge…… 50

2.6 Confocal laser scanning microscopy (CLSM) …….. 50

2.6.1 Sample holder (slide) for CLSM observations…….. 53

2.6.2 Image analysis…… 53

Chapter 3. Phase diagrams, phase separation and rheology of waxy corn starch + locust bean gum or guar gum…….. 56

3.1 Introduction…… 57

3.2 Materials and methods……... 59

3.2.1 Materials…… 59

3.2.2 Methods……. 59

3.3 Results and discussion……... 63

3.3.1 Bulk rheology of different solutions……..… 63

3.3.2 Determination of phase separation and phase diagram……. 68

3.3.3 Measured viscosity of each layer in the mixtures……. 75

3.3.4 Interfacial tension measurement…… 76

3.3.5 Effect of changing pH…… 78

3.3.6 Microscopic observations on phase separation…….. 81

3.4 Conclusions…….. 83

Chapter 4. Effect of silica nanoparticles on phase separation of waxy corn starch + locust bean gum or guar gum…….… 85

4.1 Introduction…….. 86

4.2 Materials and methods…….… 88

4.2.1 Materials……..…… 88

4.2.2 Methods…… 88

4.3 Results and discussion……..…… 89

4.3.1 Determination of phase separation…… 89

4.3.2 Microscopic observations of phase separation….……..… 93

4.3.3 Image analysis…… 103

4.3.4 Estimated minimum domain size that could be covered by the given silica particles……..…… 105

4.3.5 Bulk rheology of different phases…… 107

4.4 Conclusion…….…….. 110

Chapter 5. Effect of bromohexadecane microemulsion droplets on phase separation of waxy corn starch + locust bean gum or guar gum……..…….. 111

5.1 Introduction…… 112

5.2 Materials and methods…….…….. 114

5.2.1 Materials……. 114

5.2.2 Methods……..…… 114

5.3 Results and discussion…… 116

5.3.1 BMDs characterisation……... 116

5.3.2 Bulk rheology of BMDs……..…….. 118

5.3.3 Determination of phase separation…...…….. 121

5.3.4 Microscopic observations on phase separation…….. 126

5.3.5 Image analysis……..…….. 130

5.3.6 Bulk rheology of different phases…….. 132

5.4 Conclusion……...…….. 134

Chapter 6. Effect of whey protein isolate microgel particles on phase separation of waxy corn starch + locust bean gum or guar gum…….…….. 136

6.1 Introduction…….…….. 137

6.2 Materials and methods…….. 139

6.2.1 Materials……..…….. 139

6.2.2 Methods……. 139

6.3 Results and discussion…..…….…… 141

6.3.1 WPI microgel particle characterisation……..…… 141

6.3.2 Bulk rheology of WPI microgel particles…….……..… 143

6.3.3 Macroscopic observations of the effect of particles on W/W emulsions…….... 146

6.3.4 Microscopic observations on phase separation…… 149

6.3.5 Estimate particle detachment energy……... 153

6.3.6 Image Analysis of phase separating microdomains…..…….... 153

6.3.7 Bulk rheology of different phases……..…..…… 155

6.4 Conclusions……..… 157

Chapter 7. Overall summaries and conclusions…… 158

7.1 Phase behaviour of starch + galactomannan…… 159

7.2 Rheology of each phase…… 160

7.3 Particle size distribution and rheology of particle dispersion…… 160

7.4 Effect of particle on phase separation…… 160

7.4.1 Detachment energy, ΔE…… 162

7.5 Future work …… 163

References…… 165

Publications and presentations…… 191

Nomenclature…… 193

Annotations…… 193

Greek letters…… 194

Abbreviations and subscripts…… 195

Figures

Figure 1-1 Schematic of segregative interaction……...…… 6

Figure 1-2 Schematics of 2 types of phase diagram; (*a*) typical phase diagram for polymer blend; (*b*) rectangular coordination phase diagram. ♦ critical point; (—) binodal line; (....) tie line……. 12

Figure 1-3 The diagram shows the relationship between shear stress and shear rate……..…… 14

Figure 1-4 Viscosity approximation with the (---) Power law and the (—) Cross model……..…… 17

Figure 1-5 Amplitude sweep……..…… 18

Figure 1-6 Typical frequencies response of (—) G' and (---) G" from frequency sweep (ω) test: (*a*) viscoelastic solid material; (*b*) gel-like material; (*c*) viscoelastic liquid material.……...…….. 19

Figure 1-7 Graph shows the double log graph of Zero-shear viscosity (η_0) against (bio)polymer concentration [C_b] ……..…….. 19

Figure 1-8 The model morphology of binary mixtures; (*a*) spinodal decomposition, (*b*) nucleation and growth. These images were reported by Garcia-Ojalvo *et al.* (1998) …….. 20

Figure 1-9 Schematic representation of Pickering stabilisation of O-W emulsion by spherical particles (*a*) single amphiphilic particle at the interface; (*b*) single hydrophobic particle at the interface (W/O); (*c*) single hydrophilic particle at the interface; (O/W) (*d*) close-packed monolayer particle at surface of dispersed oil droplet……. 24

Figure 1-10 Schematic representation bicontinuous morphology of mixed (bio)polymers that stabilised by particle and form a system called bijel. Black regions: aqueous$_1$; white regions: aqueous$_2$; grey regions: particles. …...… 26

Figure 1-11 The principle structure of guar gum. This diagram based on work reported by Wang and Somasundaran (2007) …….…..…. 33

Figure 1-12 The principle structure of locust bean gum. This diagram based on work reported by Wang and Somasundaran (2007) ……..…… 34

Figure 1-13 The model represent the possible gel structure that form in a binary mixture (*a*) phase separated networks; (*b*) swollen networks; (*c*) interpenetrating networks; (*d*) coupled networks. This diagram redrawn from work reported by Morris (1998) ……. 35

Figure 2-1 Flowchart of sample preparation…… 43

Figure 2-2 Schematic representation of negative charged particle…… 44

Figure 2-3 Schematic illustrating Hückel and Smoluchowski's approximations used for the conversion of electrophoretic mobility into zeta potential…….. 46

Figure 2-4 Image representation of Kinexus rheometer with cone and plate geometries. The images were obtained from Chemeurope.com (2012) …..... 48

Figure 2-5 Schematic representation of (*a*) cone and plate cartridge geometry; (*b*) Double gap and bob with cylinder cartridge geometry……..….. 49

Figure 2-6 Dimension of focal plane in CLSM as x-y-z plane……..… 50

Figure 2-7 The confocal principle in laser scanning microscope. This schematic based on book that wrote by Murphy, 2001, p.210……...…… 51

Figure 2-8 (*a*) a typical micrograph of spinodal decomposition in sample containing 2 wt% starch + 0.3 wt% locust bean gum. (*b*) the 2D FFT of (*a*) …… 53

Figure 2-9 Command menus in Image J software to obtain FFT and Radial profile..…...…….. 54

Figure 3-1 Flow chart of preparation method of the mixtures used in chapter 3…...…… …...…… ……..……. 61

Figure 3-2 Schematic of the spinning drop method…….…… 62

Figure 3-3 Viscosity (η) versus shear rate ($\dot{\gamma}$) for [S] = 4 wt.% (●); [S] = 1 wt.% (○); [GG] = 0.6 wt.% (■); [GG] = 0.2 wt.% (□); [LBG] = 0.6 wt.% (▲); [LBG] = 0.2 wt.% (△) ……. 63

Figure 3-4 Viscosity (η) at γ = 0.1 s^{-1} versus wt.% concentration (C_b) of different biopolymers: [S] (○); [LBG] (△); [GG] (□); (—) trend line……..…… 65

Figure 3-5 Frequency versus storage modulus (open symbol) and loss modulus (filled symbol) for (a) [S] = 4 wt.% (○,●); (b) [GG] = 0.5 wt.% (□,■); (c) [LBG] = 0.6 wt.% (△,▲).…… 67

Figure 3-6 Visual observation of 2 wt.% S + different wt.% LBG concentration after centrifugation. Arrow indicates boundary between the two-phases. ……..... 68

Figure 3-7 Phase diagram showing the estimated binodal (—) between single-phase (○) and biphasic (●) mixtures of (*a*) S + GG; (*b*) S + LBG, as determined by the centrifugation procedure described in the text.……..… 70

Figure 3-8 Volume of upper (*a*) GG phase and (*b*) LBG phase as a % of the overall volume (%vol gum) versus wt.% of galactomannan in the mixtures at different [S]: 0.15 (□); 0.25 (△); 0.5 (○); 1 (■); 1.5 (▲); 2 (●). The dashed line at 50% indicates initial %volume of gum solution (since equal volumes of solutions were mixed) ……...……..…….. 72

Figure 3-9 Hypothetical maximum concentration (*a*) [GG']; (*b*) [LBG'] of gum in the gum phase separated regions, calculated (see text) on the basis of Figure 3-8, versus initial wt.% of gum in the mixtures at different [S]: 0.15 (□); 0.25 (△); 0.5 (○); 1 (■); 1.5 (▲); 2 (●). Dashed line indicate the volume were [GG'] = [GG_0] or [LBG'] = [LBG_0] ……..……..... 73

Figure 3-10 Hypothetical maximum viscosity (η') at $\gamma = 0.1s^{-1}$ of the (*a*) GG; (*b*) LBG phase separated regions, calculated (see text) on the basis of Figure 3-4 and 3-9, versus viscosity (η) of the original gum phase after mixing with different [S]: 0.15 (□); 0.25 (△); 0.5 (○); 1 (■); 1.5 (▲); 2 (●). The dashed diagonal line indicates the case where η' = η.……. 74

Figure 3-11 Representative confocal micrographs of mixture of 2 wt.% S + 0.3 wt.% LBG. The system was observed at 24 h. Dark regions are gum-rich phase and brighter regions are starch-rich phase……..…… 77

Figure 3-12 Viscosity at $\dot{\gamma}$ = 0.1 s^{-1} versus wt.% concentration [C_b] of different biopolymers: (*a*) waxy corn starch; (*b*) GG; (*c*) LBG at different pH; pH7 (○); pH8 (△); pH5.4 (□). "I" indicates standard error bar……. 78

Figure 3-13 Visual observation of 2 wt.% S + 0.25 wt.% GG after strorage at room temperature under normal gravity for 3 days. From left to right: pH 5.4, pH 7 pH 8. Arrow indicates boundary between two-phase……..…….... 80

Figure 3-14 Visual observation of 2 wt.% S + 0.3 wt.% LBG after strorage at room temperature under normal gravity for 3 days. From left to right: pH 5.4, pH 7 pH 8. Arrow indicates boundary between two-phase……..…….. 80

Figure 3-15 CLSM images of (*a*) upper LBG-rich phase; (*b*) lower starch-rich phase in transmission mode……..…… 81

Figure 3-16 Representative confocal micrographs of mixture of 2 wt.% S + 0.25 wt.% GG. The system was observed at different times (*a*) 5min; (*b*) 10 min; (*c*) 20 min; (*d*) 24 h…….. 82

Figure 3-17 Representative confocal micrographs of mixture of 2 wt.% S + 0.3 wt.% LBG. The system was observed at different times (*a*) 5min; (*b*) 10 min; (*c*) 20 min; (*d*) 24 h……..…… 82

Figure 4-1 Visual observation of centrifuged samples of 2 wt.% S + 0.3 wt.% LBG with the presence of silica particles of varying surface hydrophobicities. From left to right: no particles; 100-SiOH; 80-SiOH; 70-SiOH; 65-SiOH; food-grade silica particles. Left column = 0.5 wt.%; right column = 1 wt.%. Total volume = 15 ml……..……. 90

Figure 4-2 Evolution of W/W emulsions formed by S + LBG with the presence of silica particles of varying surface hydrophobicities after leaving under gravity for 45 days. From left to right: no particle; 100-SiOH; 80-SiOH; 70-SiOH; 65-SiOH; food-grade silica particles. Left column = 0.5 wt.%; right column = 1 wt.%. Total volume = 15 ml.……...……..…… … 90

Figure 4-3 Representative confocal micrographs of each layer of centrifuged mixtures of 2 wt.% starch + 0.3 wt.% LBG + 0.5 wt.% 100-SiOH; (*a*) top layer; (*b*) middle layer; (*c*) bottom layer…… 91

Figure 4-4 Representative confocal micrographs of 2 wt.% S + 0.3 wt.% LBG + 0.5 wt.% 100-SiOH; particles added into the starch phase first, (*a*) age 5 min; (*b*) age 30 min; particles added into the gum phase first, (*c*) age 5 min; (*d*) age 30 min. Dark regions are gum-rich, brighter regions are starch-rich and/or particle-rich, very bright regions are clusters of particles……..…… 93

Figure 4-5 Representative confocal micrographs of mixtures of 2 wt.% S + 0.3 wt.% LBG containing 0.5 wt.% 100-SiOH (i.e., unmodified) particles. Observed at (*a*) 5 min; (*b*) 10 min; (*c*) 30 min; (*d*) 3 h; (*e*) 6 h; (*f*) 24 h…….. 95

Figure 4-6 Representative confocal micrographs of mixtures of 2 wt.% starch + 0.3 wt.% LBG in the absence and presence of 0.5 wt.% silica particles of varying surface hydrophobicities: (*a*) no particles, age 5 min; (*b*) no particles, age 30 min; (*c*) 100-SiOH (i.e., unmodified) particles; (*d*) 80-SiOH particles; (*e*) 70-SiOH particles; (*f*) 65-SiOH particles; (*g*) Food-grade silica particles. Image *c-g* show micrographs at age 24 h…….……. 97

Figure 4-7 Representative confocal micrographs of mixtures of 2 wt.% S + 0.3 wt.% LBG age 24 h in the presence of various surface characteristics silica particle at [C_p] = 0.7 wt.% (left) 1 wt.% (right); (*a,b*) 100-SiOH, (*c,d*) 80-SiOH, (*e,f*) 70-SiOH, (*g,h*) 65-SiOH..……..…… 102

Figure 4-8 Representative confocal micrographs of mixtures of 2 wt.% S + 0.3 wt.% LBG age 24 h in the presence of food-grade silica particles at concentration of (*a*) 0.5 wt.%; (*b*) 1 wt.% …….…… 103

Figure 4-9 Characteristic length scale, *L*, versus time since mixing for mixtures of 2 wt.% starch + 0.3 wt.% LBG plus different [C_p]: (*a*) 0.5 wt.% (*b*) 0.7 wt.%; (*c*) 1 wt.%. Data and representative confocal micrographs are shown for systems with silica particles of different surface characteristics: (◊) 100-SiOH (i.e., unmodified); (□) (80-SiOH); (Δ) 70-SiOH; (X) 65-SiOH…….…….. 104

Figure 4-10 (*a*) Viscosity (η) at $\dot{\gamma}$ = 0.1 s^{-1}; (*b*) loss modulus (G") measured at 0.1 Hz; (*c*) storage modulus (G') at 0.01 Hz for varying concentration of the 100-SiOH particles (C_p) added to individual solutions of 4 wt.% starch (o); 0.6 wt.% LBG (Δ); 0.5 wt.% GG (□) …… 108

Figure 5-1 Distribution of BMDs dispersion (—) unheated age 1 day; (•••••) heated age 1 day; (- - -) unheated age 3 week…….…….. 116

Figure 5-2 CLSM of 1 vol.% of BMDs in phosphate buffer: (*a*) pH7; (*b*) pH4. Bright regions are BMDs, dark regions are phosphate buffer……..…….. 117

Figure 5-3 Viscosity (η) versus shear rate (γ) for BMDs; at pH 7 (open symbols) and pH 4 (filled symbols): 1 vol.% (○,●); 5 vol.% (△,▲); 10 vol.% (□,■); 15 vol.% (♢,♦)……..…….. 119

Figure 5-4 Viscosity (η) at $\dot{\gamma}$ = 0.1 s^{-1} of BMDs; at pH 7 (open symbols) and pH 4 (filled symbols) …….……. 120

Figure 5-5 W/W emulsions formed by 2 wt.% S + (*a*) 0.3 wt.% LBG; (*b*) 0.25 wt.% GG containing 0 to 15 vol.% BMDs at pH 7. Observed at 1, 3, 7 and 30 days. From left to right: no particle; 1 vol.%; 5 vol.%; 10 vol.%; 15 vol.% BMDs…..… 122

Figure 5-6 Representative confocal micrographs of each layer of 2 wt.% starch + 0.3 wt.% LBG or 0.25 wt.% GG with the presence of 5 vol.% BMDs. (a) S + LBG, bottom layer; (b) S +GG, bottom layer; (c) S+ LBG top layer; (d) S+GG top layer. Left stained with Nile Red; right stained with Rhodamine B…… 124

Figure 5-7 W/W emulsions formed by 2 wt.% S + (*a*) 0.3 wt.% LBG; (*b*) 0.25 wt.% GG containing 0 to 15 vol.% BMDs at pH 4. Observed at 1, 3, 7 and 30 days. From left to right: no particle; 1 vol.%; 5 vol.%; 10 vol.%; 15 vol.% BMDs.…… 125

Figure 5-8 Representative confocal micrographs of mixture containing 2wt.% S + 0.3 wt.% LBG in the absence and presence of BMDs captured at 5 ± 2 minute after mixing: (*a*) no particles at pH7, age 5 minute; (*b*) 1 vol.% at pH 7, age 5 minute; (*c*) 1 vol.% at pH 4, age 5 minute…… 127

Figure 5-9 Representative confocal micrographs of mixture of 2 wt.% S + 0.3 wt.% LBG in the absence and presence of BMDs captured after 24 h storage: (*a*) 1 vol.%,

pH 7; (*b*) 5 vol.%, pH 7; (*c*) 10 vol.%, pH 7; (*d*) 10 vol.%, pH 7; (e) 1 vol.%, pH 4; (*f*) 5 vol.%, pH4; (*g*) 10 vol.%, pH4; (*h*) 15 vol.%, pH4…… ….. 128

Figure 5-10 Characteristic length scale, *L*, versus time since mixing for mixtures of (*a*) S + LBG; (*b*) S + GG ; at pH 7 (filled symbols) and pH 4 (open symbols) :1 vol.% (●,○); 5 vol.% (▲,△); 10 vol.% (■,□) ……..…….... 130

Figure 5-11 At pH 4 (*a*) Viscosity (η) at $\gamma = 0.1\ s^{-1}$; (*b*) storage modulus (G') measure at 0.01 Hz; (*c*) loss modulus (G") at 0.1 Hz and 0.01 strain versus vol.% (f) of BMDs added to individual solutions of 4 wt.% starch (○); 0.6 wt.% LBG (△); 0.5 wt.% GG (□) ……..…… 133

Figure 6-1 Distribution of WPI nanogel before (- - -) sonication and (—) after sonication…….…….. 140

Figure 6-2 CLSM of 5 vol.% of WPI microgels in phosphate buffer: (*a*) pH7; (*b*) pH4. Bright regions are WPI microgel particles, dark regions are phosphate buffer…….. 141

Figure 6-3 Viscosity (η) versus shear rate (γ) for WPI microgel suspensions; (*a*) at pH 7 (open symbols); (*b*) at pH 4 (filled symbols): 1 vol.% (○,●); 5 vol.% (△,▲); 10 vol.% (□,■); 15 vol.% (♢,♦)……. 143

Figure 6-4 Viscosity (η) at $\dot{\gamma} = 0.1\ s^{-1}$ of WPI microgel particles; at pH 7 (open symbols) and pH 4 (filled symbols).……..…… 143

Figure 6-5 W/W emulsions formed by 2 wt.% S + (*a*) 0.3 wt.% LBG; (*b*) 0.25 wt.% GG containing 0 to 15 vol.% WPI microgel particles at pH 7. Observed at 1, 3, 7 and 30 days. From left to right: no particle; 1 vol.% WPI; 5 vol.% WPI; 7.5 vol.% WPI; 10 vol.% WPI; 15 vol.% microgels……..…….. 145

Figure 6-6 W/W emulsions formed by 2 wt.% S + (*a*) 0.3 wt.% LBG; (*b*) 0.25 wt.% GG containing 0 to 15 vol.% WPI microgel particles at pH 4. Observed at 1, 3, 7 and 30 days. From left to right: no particle; 1 vol.% WPI; 5 vol.% WPI; 7.5 vol.% WPI; 10 vol.% WPI; 15 vol.% microgels……..…….. 147

Figure 6-7 Representative confocal micrographs of mixture containing 2wt.% S + 0.3 wt.% LBG in the absence of WPI microgel particles: (*a*) age 5 min; (*b*) age 24 hour…… 148

Figure 6-8 Representative confocal micrographs of mixture of 2 wt.% S + 0.3 wt.% LBG in the presence WPI microgel particles, age 24 hour: (*a*) 1 vol.% particles, pH7; (*b*) 5 vol.% particles, pH7 h; (*c*) 10 vol.% particles, pH7; (*d*) 1 vol.% particles, pH4; (*e*) 5 vol.% particles, pH4; (*f*) 10 vol.% particles, pH4……..…… 151

Figure 6-9 Characteristic length scale, *L*, versus time since mixing for mixtures of 2 wt.% S + 0.3 wt.% LBG at (*a*) pH7 (open symbols); (*b*) pH4 (filled symbols). Data and representative micrographs are shown for system with different concentrations of added WPI microgel particles: 1 vol.% (○,●); 5 vol.% (△,▲); 10 vol.% (□,■)...……...…… 153

Figure 6-10 At pH 4 (*a*) Viscosity (η) at $\dot{\gamma}$ = 0.1 s^{-1}; (*b*) storage modulus (G') measured at 0.1 Hz; (*c*) loss modulus (G") at 0.1 Hz and 0.01 strain versus vol.% (ϕ) of WPI microgel particles added to individual solutions of 4 wt.% starch (○); 0.6 wt.% LBG (△); 0.5 wt.% GG (□).……...…… 155

Figure 7-1 Graph shows prediction of particle detachment enery at various particle sizes…… 161

Figure 7-2 Illustration of particles at the interface and the energy required to remove particles…….…… 162

Tables

Table 1-1 Properites of polysaccharides and their origins. ♦ very often used in the food industry; O often used in the food industry; [1)] does not form gel as a single ingredient but does when combined with another substance. This table is based on work reported by Funami (2009) ……...…… 28

Table 3-1 Measured viscosity η of starch + galactomannan mixtures…….. 75

Table 3-2 Measured density of starch, GG and LBG at 20 °C and 60 °C.… 77

Table 5-1 Fitting parameters of power law model (Equation 1-7) to viscosity of WPI microgel suspensions of different [C_p] as shown in Figure 5-3. *K* is the flow consistency index, *n* is flow behaviour index and R^2 is goodness-of-fit..…. 120

Table 6-1 Fitting parameters of power law model (Equation 6-1) to viscosity of WPI microgel suspensions of different concentrations (vol.%), as shown in Figure 6-3. *K* is the flow consistency index, *n* is flow behaviour index and R^2 is goodness-of-fit…… 144

Chapter 1

1 Chapter 1. General Introduction

1.1 Aim of the research

This research is inspired by the idea of using solid particles to stabilise incompatible polysaccharide-polysaccharide mixtures. In the food industry, there is little information about controlling the phase separation of this water-in-water emulsion for purposeful gain. The aims of this thesis are;

- To study the phase behaviour of mixed polysaccharides and understand the thermodynamics of the phase separation.
- To investigate the relationship between microstructure observed and the rheological properties of waxy corn starch + galactomannan mixtures.
- Experiment using three different types of particles to try to stabilise model polysaccharide systems.
- To observe the effect of adding particles to a phase separating polysaccharide mixture, to see if this can influence the rate of formation and/or morphology of the phase-separating structures.
- Extend the duration of the apparent mono-phase or inhibit phase separation by using small particles that interact with the interface between the two phases.
- Create food grade particles that have an ability to stabilise model polysaccharide systems.

1.1.1 Plan of thesis

This thesis is composed of the following chapters:

- Chapter one: general introduction.
- Chapter two: general materials and methodology.
- Chapter three: phase diagrams, phase separation and rheology of waxy corn starch + locust bean gum or guar gum.
- Chapter four: effect of silica nanoparticles on phase separation of waxy corn starch + locust bean gum or guar gum.
- Chapter five: effect of bromohexadecane microemulsion droplets on phase separation of waxy corn starch + locust bean gum or guar gum
- Chapter six: effect of whey protein isolate microgel particles on phase separation of waxy corn starch + locust bean gum or guar gum.
- Chapter seven: general conclusions.

1.2 Food emulsions

A colloidal solution is a system in which one substance is dispersed in another, such as solid-liquid dispersions, liquid-liquid dispersions and liquid-gas dispersions; called suspension, emulsion and foam, respectively. Therefore, emulsion science is an active subsection of colloid science. Colloidal particles, droplets or bubbles typically have a diameter between one nanometre to a few micrometres (McClements, 1999; Schramm, 2005). In the food industry, emulsion science has also incorporated other disciplines such as physiology and sensory science in an attempt to correlate emulsion function with the taste, odour, mouth-feel and appearance of food product.

The idea is to mix different ingredients in order to obtain food products with specific characteristics. The general characteristics of food emulsions can be described as mixtures of two or more immiscible liquids where one of the liquids is dispersed as small droplets (dispersed phase) in the other (continuous phase). The droplets usually range between 0.1 and 100 μm (Dickinson, 1992; McClements, 1999; 2005), which may exceed the usual size limit for colloidal particles (Schramm, 2005), and exhibit Brownian motion; random movement driven by thermal energy in the liquid. The study of emulsions is of great interest in terms of food function as they could provide encapsulation of specific ingredients offering increased product bioavailability and the possibility of controlled delivery (McClements, 2012; Berton-Carabin and Schroën, 2015).

A system containing oil and water, where oil is a dispersed phase, is called an oil-in-water or O/W emulsion. A system consisting of a water dispersed phase and an oil continuous phase is called a water-in-oil or W/O emulsion. The concentration of dispersed phase is usually described as disperse phase volume fraction which is equal to the volume of dispersed phase divided by the total volume of the emulsion. This volume fraction is one of the factors that is used in determining the cost, appearance, texture, flavour and stability of a particular food product. Typically, the type of emulsion formed depends upon volume fraction of dispersed phase. For example, at high volume of oil, a W/O emulsion tends to be formed and at low volume of oil an O/W emulsion tends to be formed (McClements, 2005). Apart from typical O/W, W/O and air-in-water (A/W) system, i.e. foams, there is also another

type of emulsion that is far less studied. These are water-in-water (W/W) emulsions where the incompatibility can be between different proteins, different polysaccharides or between protein and polysaccharide. An interface is a boundary area between two phases. It should be noted that the expression 'interfacial tension' is used when both phases are liquid whilst 'surface tension' is commonly used when one of the phases is gas. The interfacial tension was reported to be significantly low for W/W emulsions (10^{-4} – 10^{-6} N m^{-1}) (Shum *et al.,* 2012; Hanazawa and Murray, 2013) which is much lower than that of oil – water or air - water interface (10 mN m^{-1}: Sagis and Scholten, 2014).

Most food emulsions are made with raw materials that are not normally found together in nature except in some dairy products that have a naturally occurring emulsion; e.g. milk, (Dickinson and Stainsby, 1982). Food is a complex colloid system where a large number of food products consist of partly or wholely emulsions. They serve to impart mouth-feel characteristics and also play a key role in the formation of certain structures such as whipped cream, ice cream, mayonnaise etc. However, instability in some food is visually unattractive, undesirable to the consumer and adversely affects the taste and texture of food. Therefore, it is important to study the structure and properties of emulsions in order to understand the behaviour of processed foods and be able to control and stabilise the mixture under environmental conditions (e.g. transport, storage and usage). In addition, the arrangement of the molecules within the emulsion also depends upon the surrounding environment, which includes; the temperature, pressure, gravity and applied substance during its lifetime. Importantly, processors also require knowledge of food regulations because the use of certain ingredients may be restricted in some regions or countries.

1.3 Challenges raised by mixing biopolymers

Over the last two decades mixtures of aqueous biopolymers have been widely studied due to their important role in applications such as food, pharmaceuticals, nutraceuticals, etc. Biopolymers are macromolecules formed by living organisms, including proteins, nucleic acids and polysaccharides. The functional properties of

biopolymers are limited by their molecular characteristics, which are dependent on number and sequence of the monomers in the polymer chain. There has been increased scientific emphasis placed on exploring the mechanisms of aqueous biopolymer formation. Professor Beijerinck first discovered the incompatibility of biopolymer mixtures in 1896 (Tolstoguzov, 2006). His work shows that the mixture of starch + gelatin leads to a phase separated structure, so-called water-in-water emulsion (W/W). Dobry and Boyer-Kawenoki (1947) then reported that the incompatibility of macromolecules is commonly due to their nature.

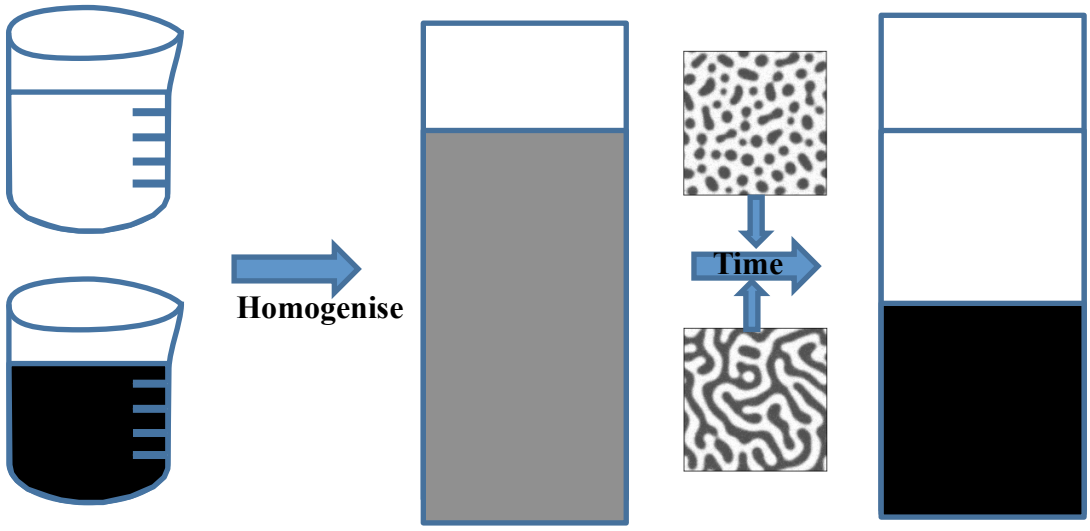

Figure 1-1 Schematic of segregative interaction.

The process of dispersing two immiscible liquids into an emulsion is called homogenisation or emulsification. When two solutions of macromolecules are mixed together, there are three types of structure that can be seen in the systems; interpenetration, couple formation and phase-separated networks. Nevertheless, incompatibility between different polymers in mixtures is a well-known phenomenon, referred to as *thermodynamic incompatibility*, where the mixture forms two distinctive layers with a denser one at the bottom and a lighter one is forming on top. Factors that influence the thermodynamic driving force for phase separation are the pH, chemical structure, ionic strength, concentration of solution, the presence of the other low-molecular weight solutes (sugars for example), conformation and flexibility of the biopolymer species present. For example; when the mixture contains charged molecules that can be influenced by the addition of salt or by

changing the pH. Moreover, in most systems studied, it has been shown that only small differences in the structure of molecules of the polysaccharides can lead to incompatibility (Garnier *et al.*, 1995).

Dickinson and Lorient (1995) and Tolstoguzov (2006) stated that there are two basic types of phase separation caused by thermodynamic incompatibility: associative and segregative phase separation. Associative interaction is the separation that one phase is rich in both biopolymers (normally the bottom phase), where interbiopolymers form a complex and the other phase contains mainly solvent. In this case, the complex formation is normally due to electrostatic attraction (Harrington *et al.*, 2009). On the other hand, segregative interaction shows two layers of different polymers in each phase. Figure 1-1 shows a basic formation of segregative interaction when mixing two immiscible solutions together. The separation appears in both micro- and macrostructure matrixes. After homogenisation, the mixed biopolymers usually show a microscopic phase separation network whereby the microdomains of one liquid form within the other liquid and these microdomains collide and coalesce with time to minimise the total energy within the system. This kind of incompatibility results from the fact that macromolecules tend to prefer to be surrounded by like molecules (Tolstoguzov, 2006). Moreover, this phenomenon is likely to occur in the mixtures with two similarly charged polyelectrolytes, two non-ionic polymers or polyelectrolyte plus a non-ionic polymer (Michon *et al.*, 1995).

The phase behaviour of mixed biopolymers is important in the food industry. Over the last three decades, there have been many case studies about immiscible biopolymer mixtures under various conditions in an attempt to create new components that improve stability, texture and appearance of products. The immiscibility mixture of two different polysaccharides have also become an area of interest (Morris, 1998).

1.4 Early sight of phase separation in polysaccharide mixtures

The mixture of two neutral or two charged polysaccharides commonly leads to phase separation. Funami (2009) also stated that the addition of food polysaccharides, i.e. galactomannan, to starch solution results in thermodynamic incompatibility. Albertsson (1962) first investigated incompatibility in polysaccharide-polysaccharide emulsions. Later on, the first phase diagrams for polysaccharide mixtures, amylose and amylopectin, were constructed by Kalichevsky and Ring (1987). Since then there were numerous works on the thermodynamic incompatibility of starch and hydrocolloid mixtures (Tolstoguzov, 1986a; Alloncle and Doublier, 1991; Kulicke, 1996; Conder-petit *et al.*, 1997; Closs *et al.* 1999; Tolstoguzov, 2006; Chaisawang and Suphantharika, 2006; Frith, 2010) since such mixtures form the basis of the texture in numerous food products. In the food industry, sensory properties and appearance are one of the most important factors that have been of concern since most of starch + non-starch hydrocolloid blends often lead to a W/W emulsion. It is important to understand its mechanism in order to control this phenomenon.

In addition, W/W emulsions tend to have significantly low interfacial tension compared with O/W and W/O emulsions. Once starch is mixed with a non-starch hydrocolloid, the droplets of starch or non-starch phase will eventually coalesce to decrease the amount of energy in the system. The reason polysaccharide mixtures show phase separation may be due their tendency to self-association and the differences in chemical structure (Tolstoguzov, 2006). At equilibrium, two distinctive layers can be seen, however, this macroscopic phase separation can be arrested by using surfactants, particles or by gelation of one of the components, which will be explained in detail in section 1.9.

1.5 Theory of emulsion stability

Emulsion stability refers to the ability to remain unchanged in its properties and appearance over a period of time. There are two types of instability (1) chemical instability (2) physical instability. Coalescence, creaming, flocculation are examples

of physical instability (Dickinson and Stainsby, 1982; Dickinson, 1992) whereas oxidation and hydrolysis are typical examples for chemical instability. In real food emulsions, it is indeed difficult to predict the stability of an emulsion due to the complex structure of food. Subsequently, combination of theoretical prediction and experimental measurements are often combined together in order to understand the influence of different ingredients and the change in stability.

1.5.1 Thermodynamics of stability

Before going into detail, it is important to distinguish the difference between thermodynamic and kinetic stability. The use of basic thermodynamics of polymer solutions addresses the incompatibility of mixed polymer solutions whereas kinetics refers to the rate at which the properties of an emulsion change with time. Within a system at constant pressure, thermodynamic incompatibility is demonstrated by comparing the Gibbs free energy of a system before and after emulsification, given by:

$$\Delta G_{mix} = \Delta H_{mix} - T\Delta S_{mix} \qquad \text{Equation 1-1}$$

where ΔH_{mix} is the difference in enthalpy, T is the absolute temperature and ΔS_{mix} is the difference in entropy. Enthalpy expresses the interchangeability of the different form of heat content of a system which relates to a particular chemical process. As a result of mixing the heat can be absorbed ($\Delta H_{mix} > 0$) or released ($\Delta H_{mix} < 0$). On the other hand, entropy is a measure of molecular disorder within a macroscopic system. According to the thermodynamics of mixing liquids, phase separation of mixed (bio)polymers takes place when ΔG_{mix} is *positive* whereas in homogeneous mixture, ΔG_{mix} is *negative* (Tolstoguzov, 2007). If $\Delta G_{mix} = 0$, it means the components are partly miscible. Stable mixtures can be achieved when specific interactions between molecules occur. The attractive forces between different molecules must be equal to or larger than interaction between the same molecules. However, in most cases, the interaction between pairs of the same monomer is usually stronger than pairs of different monomers which means that the enthalpy of the mixture is above zero. In other words, different molecule structures are incompatible when there is no specific attraction between them (Tolstoguzov, 1986a, b). Furthermore, the entropy of mixed (bio)polymers is commonly lower than that of low molecular weight or smaller molecules, hence the ΔS_{mix} is not sufficient to over come ΔH_{mix} value. Moreover,

Flory (1953) theorised that in mixed polymer solutions the entropy is significantly low so the dominant energy at equilibrium is from ΔH_{mix}.

1.5.2 Gravitational separation

The dispersed phase in an emulsion normally has a different density to that of the continuous phase.

Stokes' law

Stokes' law describes the influence of gravitational separation in the simple case of an isolated spherical droplet (dispersed phase) moving through a surrounding fluid. According to a gravitational force, if the dispersed phase has lower density than the continuous phase, they tend to form the upper phase. This is known as creaming. On the other hand, if the dispersed phase has higher density than the continuous phase, they tend to form the lower phase. This is known as sedimentation (McClements, 2005). The creaming or sedimentation of an isolated spherical droplet (dispersed phase) in an emulsion is thus described by:

$$V_s = \frac{g(\Delta\rho)d^2}{18\eta_c} \qquad \text{Equation 1-2}$$

Where V_s is the velocity of spherical droplet (m s^{-1}), g is gravitational acceleration = 9.8 m s^{-2}, $\Delta\rho$ is the density difference between dispersed phase and the continuous phase, d is the droplet diameter and η_c is the viscosity of the continuous phase. V_s determines whether the droplet moves upward (+) or downward (-). Equation 1-2 reveals that there are many ways to slow down the rate of creaming or sedimentation, such as increase continuous phase viscosity, reduce the droplet size or minimise the density difference between two phases.

1.6 Phase diagram

Phase separation of biopolymer mixtures can be described via phase diagrams. Phase diagrams depict the equilibrium phase behaviour of the mixed biopolymer systems. They graphically illustrate the boundary conditions for phase separation and the partitioning of the components between the phases and the effects of different variables (temperature, pH, ionic strength etc.). Phase separation can be identified by several techniques, e.g. light microscopy, centrifugation, turbidimetry and viscosimetry (Tolstoguzov, 1986b).

Figure 1-2*a* illustrates the typical behaviour of mixed solutions of two (bio)polymers. The graph shows the binodal line, which indicates the boundary between a homogeneous phase and two-phase mixtures. If the composition of the mixture lies between binodal (solid line) and spinodal (dotted line), then the mixture shows phase separation via nucleation and growth. Practically, phase separation via nucleation and growth occurs rarely, because the binodal and spinodal lines lie very close to each other on phase diagram, as illustrated. At the composition where the mixture lies outside the binodal line, the mixture is homogeneous. A critical point is the point where the binodal line and the spinodal line contact each other. At this point, the system changes from one-phase to biphasic-phase system without passing through a nucleation and growth region. On the Figure1-2*a*, it is also indicated that this mixture separates into two phases upon cooling.

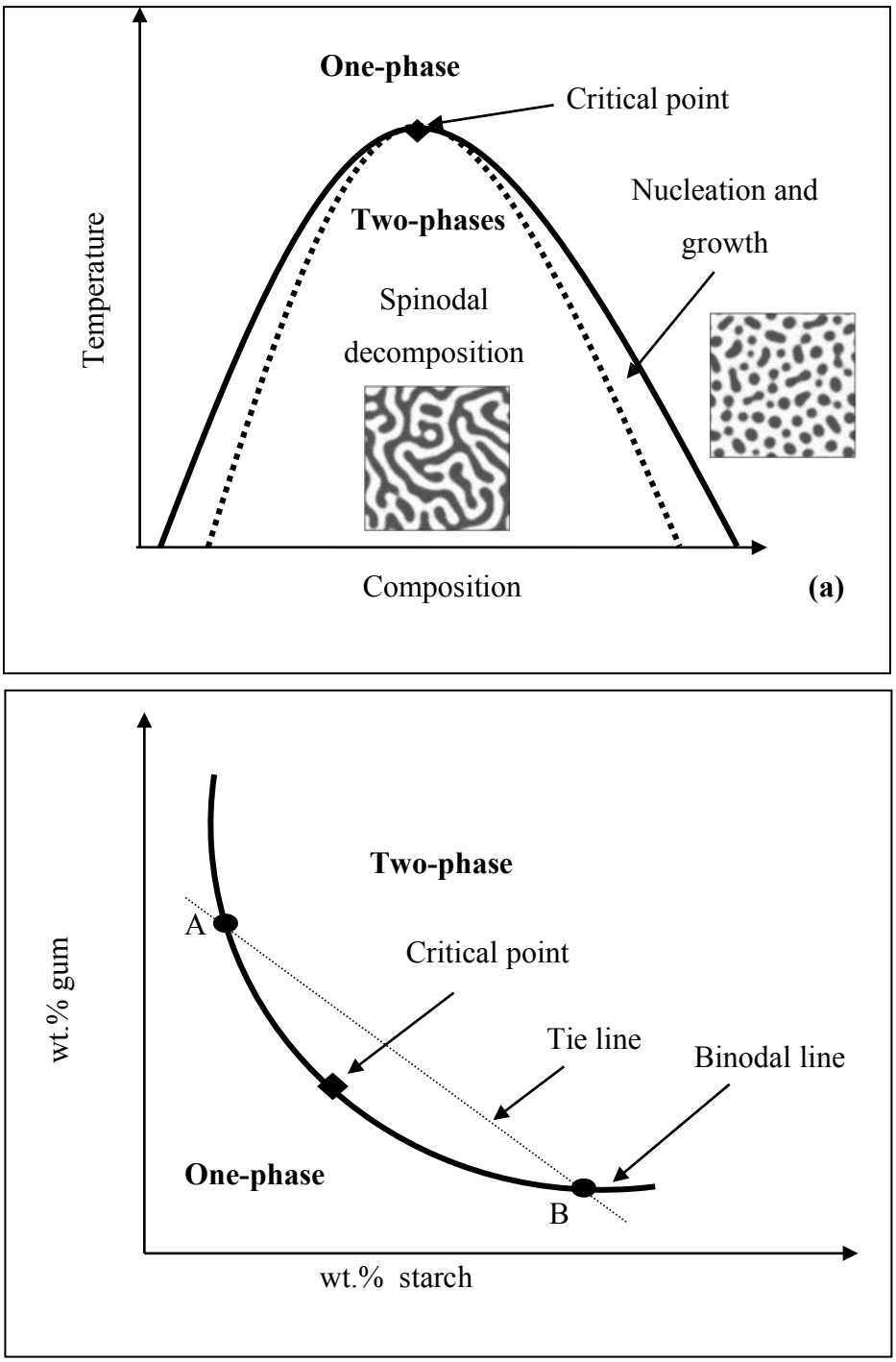

Figure 1-2 Schematics of 2 types of phase diagram; (*a*) typical phase diagram for polymer blend; (*b*) rectangular coordination phase diagram. ♦ critical point; (—) binodal line; (....) tie line

An alternative representation of the phase diagram is called the rectangular coordinate phase diagram – see Figure 1-2*b*. This phase diagram illustrates the composition of each polymer component in terms of the weight percentage. The binodal line separates the single-phase region and two-phase region. The area above binodal line corresponds to the two-phase region, while the area lying under the binodal line shows the single-phase region. The connecting line between points, for example A and B, is called the tie line. It is a line that connects pairs of equilibrium phases. For instance, any mixture with an overall composition along a tie line gives the same starch and gum compositions where phase A is rich in gum and phase B is rich in starch, but the volume ratio of the co-existing phases A and B are changed. The critical point represents the minimum concentration of polysaccharides required for phase separation to occur. A rectangular coordinate phase diagram is an example of a phase diagram for a ternary system (solvent, $solute_1$, $solute_2$) which shows thermodynamic incompatibility.

1.7 Rheology

The origin of the word "rheology" is from Greek roots; rheo meaning 'to flow' and 'logos' meaning science. It is a study of flow and deformation of fluid and semi-solids under specific conditions. The study of rheology in food is essential in understanding the properties of the product. The behaviour of fluid or semi-solid food is important in the quality control of food processing in order to control the sensory properties that are presented to consumers. Basically, material properties change due to the influence of forces that have been applied on the structure (Malkin and Isayev, 2006).

Food can be classified in different ways such as solid, homogeneous liquid, gel, suspension and emulsion. The main factors that affect food rheological properties are component structure (dissolved polymers or suspended solids), structure of food (homogeneous or heterogeneous), processing and storage conditions. An understanding of the rheology of mixed solutions may allow the control of food sensory properties by adjusting interactions in a desirable way (Semenova *et al.*, 2010).

A (bio)polymer solution normally has a wide range of rheological properties. Its rheology can be classified as Newtonian or non-Newtonian. Newtonian fluids are named after Isaac Newton (Rao, 1999) as he first postulated the relation between shear rate and shear stress for such fluids. For a Newtonian fluid, its viscosity does not depend upon the shear rate, whereas for a non-Newtonian fluid the change of shear rate affects its viscosity. Typical Newtonian fluids are commonly those containing low molecular weight molecules e.g. water, sugars, milk and most fizzy drinks etc. Most fluid foods that contain high molecular weight molecules and/or suspension of solids in liquid often show non-Newtonian behaviour.

In terms of fluid flow, there are two different kinds of behaviour: (1) shear-thinning (pseudoplastic) behaviour, where the curve of the viscosity-shear rate plot is concave downward, due to the breakdown of structural unit during shear and (2) shear-thickening behaviour, where the curve of the viscosity-shear rate plot is concave upward due to an increase of structural unit during shear. Shear-thinning flow is a common behaviour exhibited in food solution whereas shear-thickening is not commonly found in food, except in highly concentrated swollen starch granule solutions.

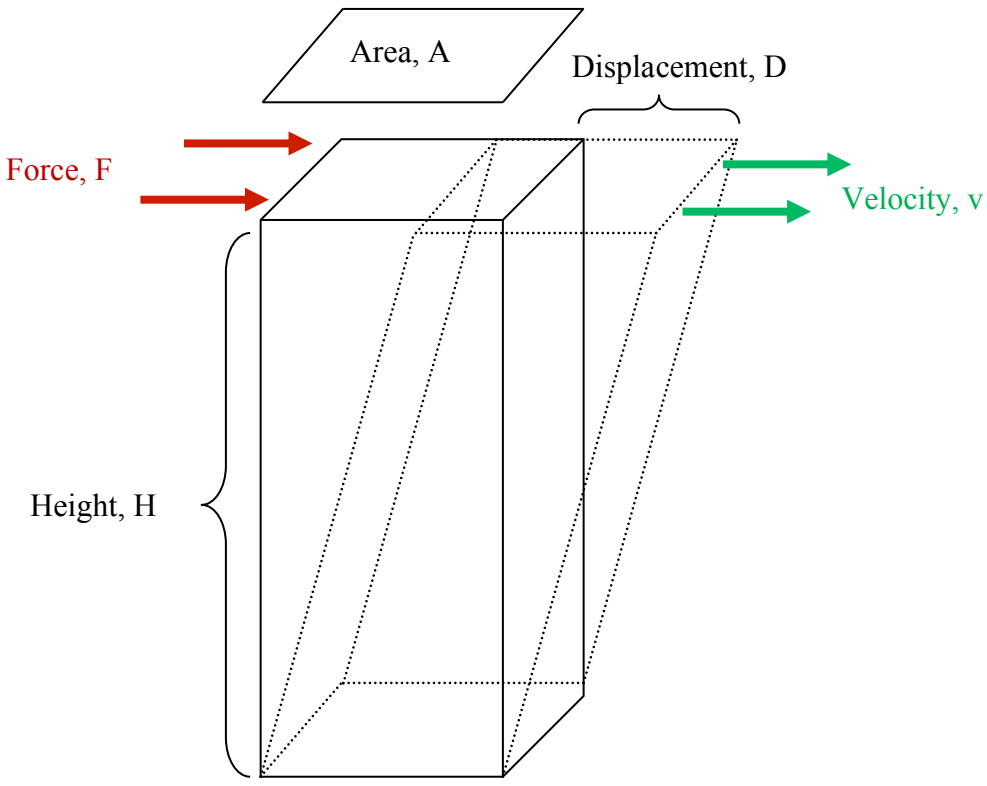

Figure 1-3 The diagram shows the relationship between shear stress and shear rate.

Figure 1-3 illustrates the relationship between each rheology parameter. Shear stress, denoted by the symbol σ, is the force per unit area (Equation 1-3), Shear rate, denoted by $\dot{\gamma}$, is the effect of applied stress, resulting in a change in velocity (Equation 1-4), where velocity is displacement of area divided by time (Equation 1-5).

$$\sigma = F/A \quad \text{Equation 1-3}$$

$$\dot{\gamma} = v/H \quad \text{Equation 1-4}$$

$$v = D/t \quad \text{Equation 1-5}$$

1.7.1 Flow models

A flow model is a mathematical equation that helps describe rheological data concisely. Sometimes more than one equation is needed. Rheological models can be categorised into three groups: (1) empirical, such as Power law, used to describe the experimental data (2) theoretical, which determines the fundamental concepts and helps in understanding the role of structure and (3) structural, such as Cross model, occasionally is used together with experimental data to help characterise the rheological behaviour of the samples (Rao, 2013).

Newtonian model

Viscosity (η) is the tendency to resist flow of a fluid, which means the higher the viscosity the better the resistance (McClements, 2005). Regarding Newton's law, the proportion of shear stress to shear rate is known as viscosity of ideal liquid (Equation 1-6). The mathematical model for this type of fluid flow behaviours can be written as:

$$\eta = \frac{\sigma}{\dot{\gamma}} \quad \text{Equation 1-6}$$

Power law

The Power law (or Ostwald) model describes the data of shear-thinning and shear-thickening fluids:

Shear-thinning $\eta = K\dot{\gamma}^{n-1}\ (n < 1)$ Equation 1-7

Shear-thickening $\eta = K\dot{\gamma}^{n-1}\ (n > 1)$ Equation 1-8

Where K is the flow consistency index (unit: Pa s^n), n is flow behaviour index. This mathematical equation is used to describe the behaviour of a non-Newtonian fluid. For example, if n is less than one, it predicts that the fluid exhibits shear-thinning behaviour. In the case of n equal to one, the shear stress is directly proportional to the shear rate, i.e. Newtonian. In non-Newtonian liquids, the viscosity depends upon the shear rate applied (shear-rate dependent) and/or the time (time-dependent). The parameters K and n are obtained from a plot of log η versus log $\dot{\gamma}$. On this plot the slope appears as a straight line with slope n-1. Parameters K and n normally correlate with polymer concentration, for example when concentration increases n decreases and K increases. One disadvantage of this model is that it does not indicate very well the viscosities at low and high shear rates.

In general, many emulsions have viscosities that depend on both shear rate and time duration that the emulsion is sheared (Dickinson, 1992). As the shear rate is increased, the viscosity may either increase or decrease. The viscosity at a selected shear rate is referred to as the apparent viscosity. It is important when analysing the rheology of products to mimic the flow rates that occur during manufacture.

Cross model

This model has been used to define shear-thinning flow behaviour of polymer solutions.

$$\eta = \eta_\infty + \frac{\eta_0 - \eta_\infty}{1 + C\dot{\gamma}^m} \qquad \text{Equation 1-9}$$

$$C = \frac{\eta_0}{\sigma^*} \qquad \text{Equation 1-10}$$

Where C is Cross constant, m is dimensionless exponents, σ^* is critical shear stress at the transition from the upper plateau value, η_∞ and η_0 are the limiting values of the viscosity at high and 'zero' shear rate, respectively. For small values of η_∞ ($\eta_0 \gg \eta_\infty$), m tends to be a value of 1-n, where n is the power law flow index (Launay *et al.*, 1986). In addition, the difference between a Power law and the Cross model is the Cross model fits the data at low shear rate whereas the Power law does not, see Figure 1-4. The dashed line shows the data fit Power law model.

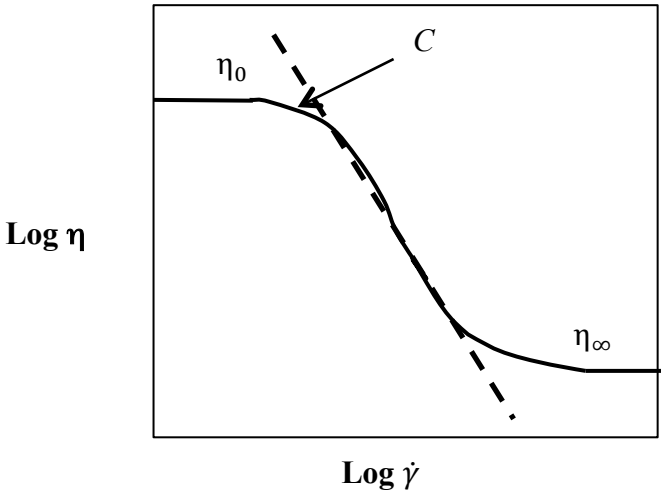

Figure 1-4 Viscosity approximation with the (---) Power law and the (—) Cross model.

1.7.2 Viscoelastic behaviour via frequency sweep tests

The principle of this measurement is to exert a sinusoidal shear deformation or strain in the sample at an angular frequency (ω) and determine the response. During the test the sample stores and loses its energy, described via the storage moduli (elastic component or G') and loss moduli (viscous component or G") (Rao, 2007). It is a measurement of *viscoelastic* behaviour of materials. Some materials may exhibit both viscous and elastic characteristics when undergoing deformation; Viscoelastic materials have an ability to return to their original shape when the forces are removed and resist motion when the forces are applied. Maxwell fluid is the simplest example of a viscoelastic material. However, the induced response must not overstrain the sample otherwise the elastic structure will be irreversibly destroyed. Furthermore, if the forces are applied for a long time the viscous element will also not return to its original shape.

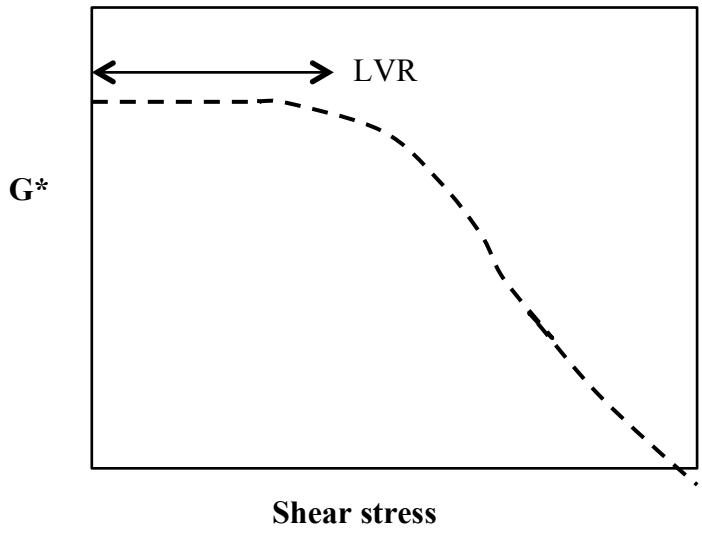

Figure 1-5 Amplitude sweep.

The linear viscoelastic region (LVR) must be defined before further oscillation analysis and all measurements should preferably be performed within LVR range because beyond this region, the sample can be deformed permanently. Within the LVR region the G' and G" are independent of strain. LVR is usually determined by amplitude sweep over a stress or strain range; an example result can be seen in Figure 1-5. It shows that when the applied stress is too high the sample starts to breakdown, which leads to decrease in complex modulus (G*).

The frequency sweep analysis can be used once the LVR is determined. This analysis involves oscillating the sample over a range of frequencies at constant strain. It shows how frequency affects the viscous and elastic behaviour of material. There are three typical frequency responses as shown in Figure 1-6. In LVR range the relationship between G*, G' and G" are defined:

$$G^* = G' + iG'' \qquad \text{Equation 1-11}$$

Figure 1-6 represents three typical types of deformation of materials under frequency sweep measurement. Figure 1-6*a* shows the typical response for a solid material where G' > G" with G' almost independent of frequency and G" increases with the increase in frequency. Figure 1-6*b* shows some frequency independence and G' is dominant over the entire frequency range, which is common behaviour for strong gels. Figure 1-6*c* shows the typical response for a dilute polymer solution

where G" > G' with G' ∝ ω^2 and G" ∝ ω at low frequencies. At higher frequencies there will be a cross over between G' and G".

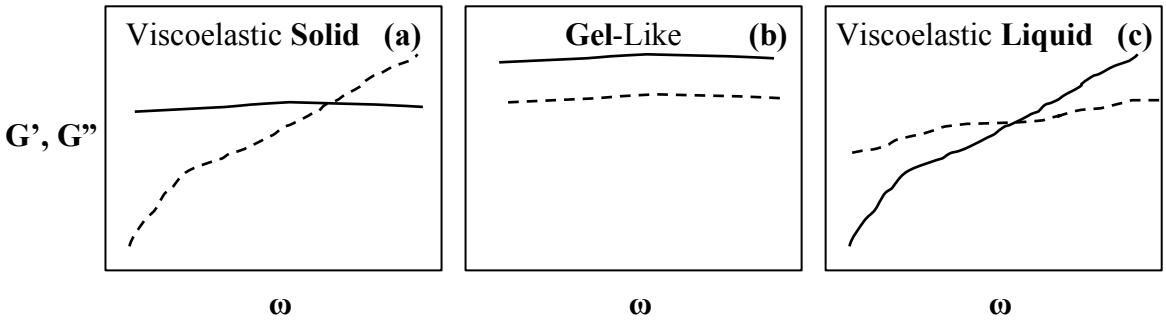

Figure 1-6 Typical frequencies response of (—) G' and (---) G" from frequency sweep (ω) test: (*a*) viscoelastic solid material; (*b*) gel-like material; (*c*) viscoelastic liquid material.

1.7.3 Effect of concentration on zero-shear viscosity

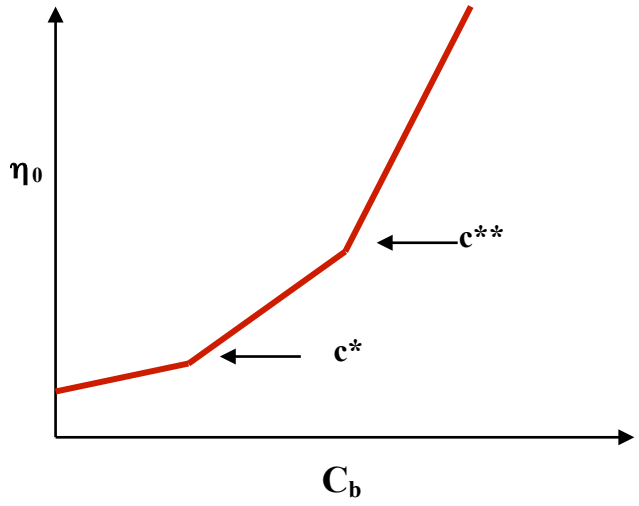

Figure 1-7 Graph shows the double log graph of Zero-shear viscosity (η_0) against (bio)polymer concentration [C_b].

Figure 1-7 shows the viscosity at $\dot{\gamma} = 0$ (η_0) of a typical polymer solution as a function of (bio)polymer concentration [C_b]. Polymer solutions are classified into three regions: dilute, semidilute and concentrated. At low concentration (c < c*), the polymer chains are rarely in contact with each other, hence there are no entanglements of the individual molecules. It appears that in the dilute regime

solutions conventionally exhibit Newtonian behaviour at concentrations below a critical point (Chaplin, 2012). This condition persists until the concentration increase up to the critical overlap concentration (c*). This is a transition where the fluid changes from dilute to semi-dilute or concentrated solution (c = c*) (Wang *et al.*, 2001), which is an overlap threshold, leading to rapid increase in viscosity. The individual molecules begin to interpenetrate or overlap. Above the critical concentration (c > c*) value, there is a progressive interpenetration of the coils and the polymer molecules become entangled. This region is said to be the semidilute regime. At certain concentrations where c > c**, the polymer solution becomes a hyperentangled network close to a polymer melt.

1.8 Microstructure of emulsions

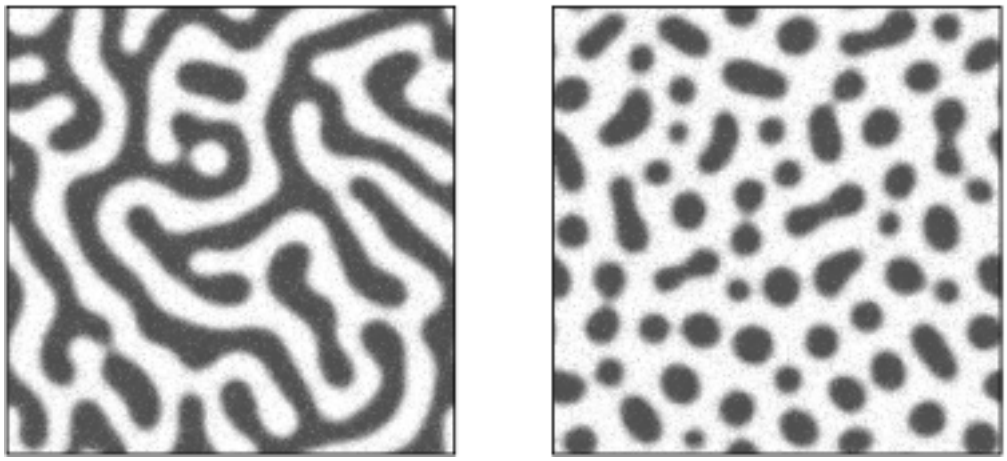

(a) **(b)**

Figure 1-8 The model morphology of binary mixtures; (*a*) spinodal decomposition, (*b*) nucleation and growth. These images were reported by Garcia-Ojalvo *et al.* (1998).

There are two levels of focus when studying a colloid system: (1) macroscopic which is explained in section 1.3 and (2) microscopic. To produce high-quality emulsion-based food products, an understanding of emulsion microstructure is required. However, under normal observation, human eyes cannot resolve an object that is smaller than 100 μm, hence microscopic techniques must be introduced. There are various microscopes, and each can be used to examine a different type and level of structure. Nevertheless, in order to observe really small objects, microscopes must

have suitable resolution, magnification and contrast options. Resolution is the ability to distinguish between two objects that are close together. Contrast is the ability to adjust specific regions/areas onto images in order to be differentiated from its background.

Using a microscope is vital in determining the interaction between two polymers. Figure 1-8 shows model micrographs of immiscible mixtures under a microscope. After leaving the immiscible mixture under normal gravity conditions the microstructure may appear as nucleation and growth separation (Figure 1-8*b*) which results in formation of small globular regions which grow over time. However, this stage of phase separation may not be seen as it can rapidly change to the spinodal decomposition stage (Figure 1-8*a*). The morphology of spinodal decomposition appears as interconnected and bicontinuous domains, meaning only changes in the scale factor occur but the overall morphology remains the same. Nevertheless, Loren and Hermansson (2003) also stated that, in some cases, the growth of mixed biopolymer structures may occur via either spinodal decomposition or nucleation and growth. In other words, the spinodal decomposition structure can occur spontaneously whilst the emulsion is demixing or it is a result of diffusional clustering from nucleation and growth.

1.9 Particle-stabilised emulsions

When two immiscible liquids are mixed together, they may form a biphasic solution and produce a bicontinuous network or a liquid$_1$-in-liquid$_2$ emulsion where the droplet of either liquid will form and eventually coalesce to decrease the amount of energy in the system. Even though emulsions are thermodynamically unstable some can remain kinetically stable. McClements (2005), for example, describes how these phenomena can be kinetically stabilised by addition of emulsifiers e.g. small surfactants, surface-active polymers (i.e., protein) or particles. Adding these substances into the system decreases the interfacial tension and creates a steric barrier between drop interfaces (Destribats *et al.*, 2014b). It is important that kinetic trapping of microstructures of mixed biopolymer should be achieved in some way (Dickinson Vliet, 2003). Emulsification may involve numerous steps or only a single step depending upon the nature of (bio)polymers. The interface is a narrow

region that separates two fluids of different kinds of molecules. To achieve a long-term stable emulsion, accumulation of stabiliser at the interface is required to create an energy barrier towards coalescence. A stabiliser is a substance that can be used to enhance the stability of an emulsion, classified as either an emulsifier or texture modifier (Dickinson, 1992; Krog and Sparso, 2004; McClements, 2005). Emulsifiers are a surface-active substance that can adsorb at the interface of dispersed droplets and prevent the droplets from coalescencing and/or aggregating. On the other hand, texture modifiers are substances that enhance emulsion stability by retarding the movement of droplets. Thickening agents, for example, increase the viscosity of one of the two phases and slow down the coalescence rate of the dispersed phase (Berton-Carabin and Schroën, 2015).

One of the most important aspects in formulating an emulsion product is to select the appropriate stabiliser. In the early years of food emulsion studies, small-molecule surfactants were necessary to control the kinetics of destabilisation of emulsion. However, in the past decades, particles have attracted scientific attention owing to their unique properties, which differ from those of surfactants. Solid particles require a strong trap at the interface to obtain a stable emulsion. A challenging concern is to be able to produce particles that are both effective at stabilising the emulsion and also acceptable for use in food industry (Morris, 2011). Although there is a large amount of research of particle-stabilised emulsions, there only a few examples that are applicable for use in real food (Berton-Carabin and Schroën, 2015). This is because most chemicals that are used to modify the surface of particles are not permitted or approved as safe in foods. However, the idea of using solid particles is gaining interest in food research (Dickinson 2012; Pawlik and Norton, 2014). Recent works on food-grade particles for emulsion stabilisation have proposed chitin nanocrystals (Tzoumaki *et al.*, 2011), cellulose microparticles (Wege *et al.*, 2008), soy protein particles (Liu and Tang, 2013), modified starch particles (Timgren *et al.*, 2011; Murray, 2011; Yusoff and Murray, 2011; Rayner *et al.*, 2012; Tan *et al.*, 2014), flavonoid particles (Luo *et al.*, 2011), solid lipid particles (Gupta and Rousseau, 2012; Hanazawa and Murray, 2013, 2014) and protein microgels/particles (de Folter *et al.*, 2012, Destribats *et al.*, 2014). The use of particles in emulsions can be from micro- to nanosize, especially nanoparticles that have large surface area to volume ratio. There are numerous advantages of using

particles instead of surfactants. Sometimes surfactant-stabilised emulsions appear to have adverse effects (Li and Ngai, 2013), i.e. irritancy, cytotoxicity, haemolytic behaviour etc., hence being a surfactant-free emulsion prevents these effects. The coating of particles at the interface can be used as a barrier to diffusion of drug/flavour molecules. Other properties of particle-stabilised emulsions include texture modification and quality enhancers. Ideally, these stabilisers should rapidly adsorb to the interface of dispersed phase during homogenisation.

1.9.1 Pickering emulsion

More than a century ago, Ramsden first reported the adsorption of solid particles at air-liquid interface. This kind of stabilisation was later known as a Pickering emulsion after S.U. Pickering (1907) published his paper on O/W emulsion stabilised by solid particles. In Ramsden's paper (Ramsden, 1903), proteins (i.e. albumin) were used as solid particles. In fact, these particles are not real solids and could be considered as soft-solids (Chevalier and Bolzinger, 2013).

Pickering emulsions were largely ignored after their discovery in 1903. However, in the past decades (since 2003) there has been renewed interest in this type of stabilisation, particularly using the increasingly novel and wide ranging types of small particles that are now available. Pickering stabilisation retains the basic properties of surfactant-stabilised emulsions (Chevalier and Bolzinger, 2013). It is a stabilisation of emulsion using micro- and nanoparticles that strongly adsorb at the interface between two phases, whereby solid particles protect droplets of dispersed phase from coalescing. Particles are required to be partially wetted by both liquids in order to adsorb at an interface (Finkle *et al.*, 1923). Ideally, Pickering stabilisation requires complete coverage of closely packed particles around dispersed droplets to ensure the highest capacity in stabilising the emulsion. The inhibition of a phase separating network also depends upon the density of packing of the particles at the interface. Pickering stabilisation is known to give long-term stability. In most systems studied, the particles commonly used as model particles are latex, silica and clay particles (Li and Ngai, 2013). Silica particles are the most popular due to the ease of surface modification to alter their hydrophobicity.

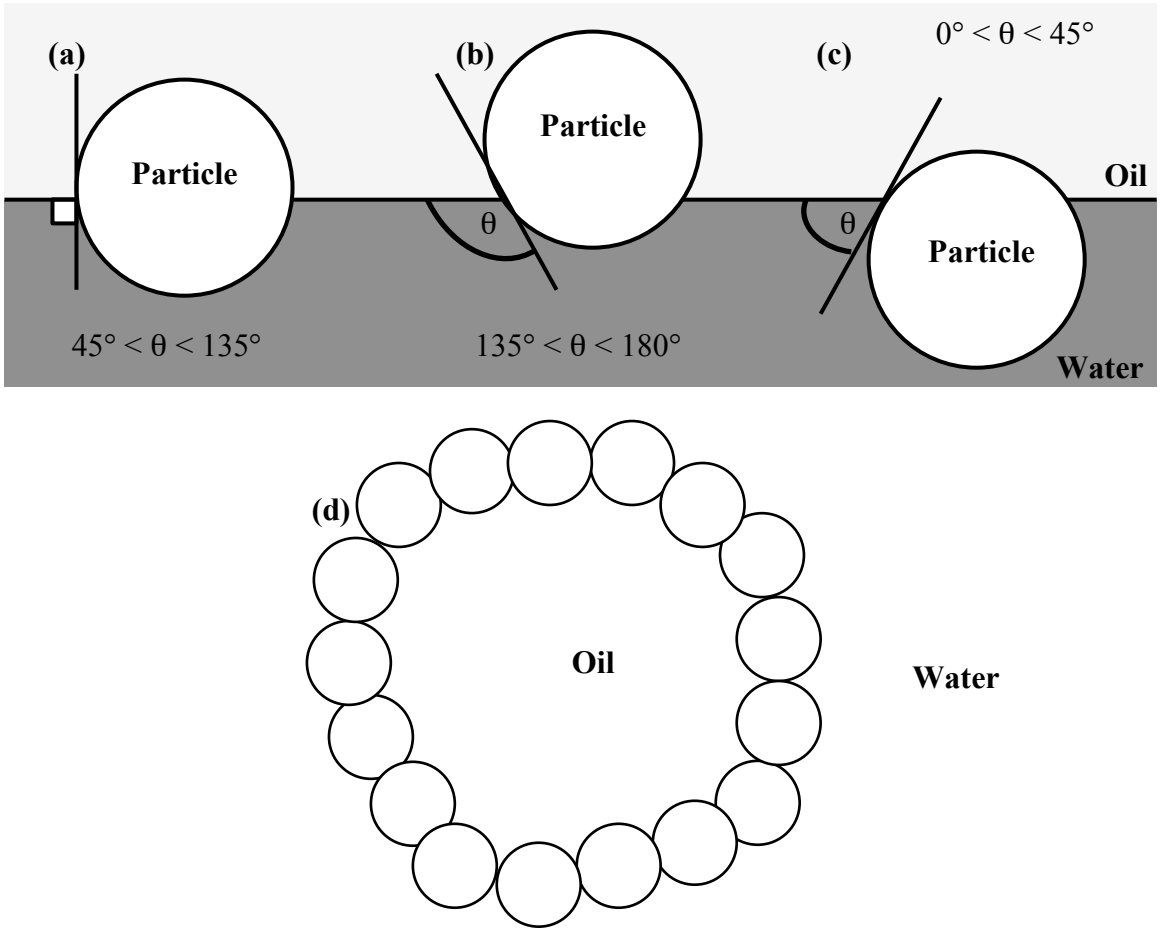

Figure 1-9 Schematic representation of Pickering stabilisation of O-W emulsion by spherical particles (*a*) single amphiphilic particle at the interface; (*b*) single hydrophobic particle at the interface (W/O); (*c*) single hydrophilic particle at the interface; (O/W) (*d*) close-packed monolayer particle at surface of dispersed oil droplet.

Solid particles in both nano- and micro- scales are widely used as stabilisers in emulsions, especially water-oil systems (Dickinson, 2011). The particles provide a physical barrier against droplet coalescence. Such structures can also be used to encapsulate some materials, such as proteins, pharmaceuticals, flavours etc., in order to control and deliver small molecules.

Key factors that control the stability of particle-stabilised emulsions are the contact angle, concentration, size and location of particles. The position of a particle can be quantified by the contact angle (θ) that depends upon how particles are wetted by the dispersed and continuous phase. The type of emulsion (e.g. oil-in-water or water-in-oil) can be predicted on a basic of particle wettability and contact angle.

Figure 1-9*a*, *b* and *c* show different locations of individual particles at the O-W interface. The location of particles at the interface depends upon the properties of the particle (i.e. amphiphilic, hydrophobic or hydrophilic). There are three surface tensions that occur in the system and are denoted by Young's equation (Young, 1855) ($\theta_o = \pi - \theta_w$):

$$\gamma_{ow} \cos\theta_o = \gamma_{op} - \gamma_{wp} \qquad \text{Equation 1-12}$$

where θ_o is the contact angle in oil, θ_w is contact angle in water, γ_{ow}, γ_{op}, γ_{wp} are the surface tension of the oil-water, oil-particle and water-particle, respectively. At $\theta \approx 90°$ (Figure 1-9*a*) the particle is wetted equally by both liquids, which is considered to be an inversion point (Aveyard *et al.* 2003). For $135° < \theta < 180°$ (Figure 1-9*b*), the particle is preferentially wetted by oil. This situation favours the stabilisation of water droplets in oil. Whereas for $0° < \theta < 45°$ the particle is wetted by the water (Figure 1-9*c*) and it is the stabilisation of oil droplets in water that is preferred (Figure 1-9*d*). However, pure hydrophobic or hydrophilic particles are more likely to stay in their preference phase. Another important factor is particle concentration. In a well-stabilised emulsion system, a sufficiently high particle concentration is required in order to obtain good coverage of dispersed droplets.

1.9.2 Bijels

Conventional Pickering emulsions normally occur in droplet form; this contrasts with a different stabilisation mechanism that was found recently. This new class of material has been defined when neutrally wetting particles adsorb at the interface and lock in or 'gel' the system through arrested spinodal decomposition; forming a so-called 'bijel'. Bijels were first proposed in 2005 by Stratford and his colleagues via lattice-Bolzmann computer simulations. Since then bijels have been extensively studied by the Edinburgh group (Herzing *et al*., 2007; 2008; Cates and Clegg, 2008). Witt *et al*. (2013) stated that the particles should be near-neutrally wetted to ensure irreversible adsorption at the interface. This occurrence leads to jamming the system in bicontinuous structure with the rigid particle monolayer at the interface - see Figure 1-10 (Cates and Clegg, 2008). In this case both liquids in the mixture are no longer distinguished as dispersed and continuous phases. The first bijel systems that were tested in the laboratory were silica particle-stabilised 2,6-

lutidine + water mixtures (Cates and Clegg, 2008). The interface then gained mechanical strength due to particle jamming. Later on in 2013, Witt *et al*. discovered a new class of bijel called bridged bijel. This system contains fluorescent silica particles where off-neutral wetting leads to partial affinity for one liquid phase. The result is a combination of interfacial jamming and bridging of dispersed droplets throughout the fluid domain. The appearance of bridged bijel was the outcome of addition of silica particles in binary mixtures, which arrested both spinodal decomposition and the nucleation and growth mechanism. The main factors effecting formation of bijels are therefore the same principles governing Pickering stabilisation.

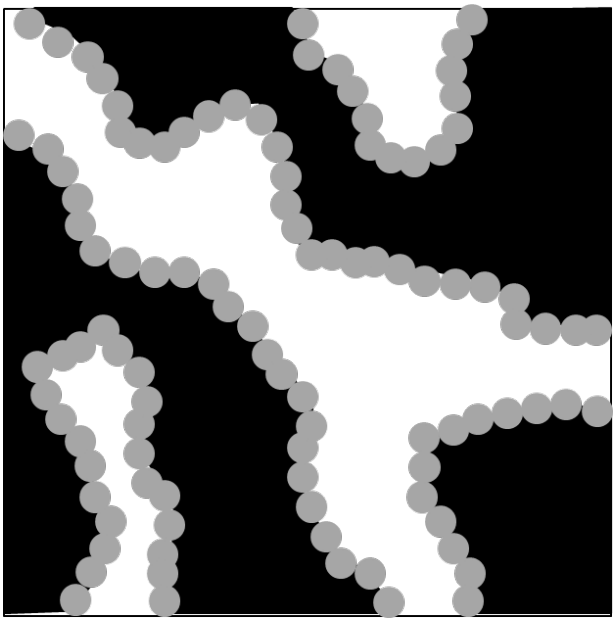

Figure 1-10 Schematic representation of bicontinuous morphology in mixed (bio)polymers stabilised by particles to form a system called a bijel. Black regions: aqueous$_1$; white regions: aqueous$_2$; grey regions: particles.

1.9.3 Particle detachment energy, ΔE

The energy barrier of detachment of particles is one of the factors that has been considered in term of producing an efficient stabiliser. In the case of small particles, e.g., less than a few microns in diameter, neglecting the effect of gravity, the energy barrier can be estimated using Equation 1-13 (Destribats *et al.*, 2014b). This equation was first quantified by Levine *et al.* (1989) using a particle-stabilised

water-oil emulsion as a model. The detachment energy must always be larger than the thermal energy (4.11 x 10^{-21} J = 1 k_BT at 25°*C*). Dickinson (2012b) stated that the detachment energy of particles at an interface leads to it being irreversibly absorbed if $\Delta E \gg 10\, k_BT$. Theoretically, a strong particle detachment energy will result in great steric barrier to coalescence, because more free energy is needed in order to disrupt the particle and allow coalescence (Levine *et al.*, 1989a). The energy barrier (ΔE) to particle desorption from the interface depends on three phase contact angle θ, the particles radius *r* (assumed spherical) and the liquid-liquid interfacial tension γ (Aveyard *et al.,* 2003; Chevalier and Bolzinger 2013; Murray and Phisarnchananan, 2014):

$$\Delta E = \pi r^2 \gamma_{ow} (1 - cos\theta_{ow})^2 \qquad \text{Equation 1-13}$$

In W/W emulsions the interfacial tension can be extremely low (γ = 10^{-4} – 10^{-6} N m^{-1}: Shum *et al.,* 2012; Hanazawa and Murray, 2013) which is expected to make ΔE significantly small. However, the detachment energy can be non-negligible if the particles are large enough. For example, if $\gamma = 10^{-6}\ N\ m^{-1}$, r = 300 nm and θ_w = *90*° the predicted desorption energy is 17 k_BT per particle, where k_B is Boltzmann's constant (1.38 x 10^{-23} m^2 kg s^{-2} K^{-1}) and T is the absolute temperature (300K). Thus, the particle will still be weakly adsorbed at the interface.

As can be seen in Equation 1-13, particle contact angle is important in calculating the detachment energy. Particles are irreversibly adsorbed when a particle is attached to the interface with θ_{ow} not too close to 0° or 180° (Levine *et al.,* 1989). The adsorption is strongest when θ_{ow} = 90° (Chevalier and Bolzinger, 2013). This has been agreed in numerous works (Dickinson, 2011; Destribats *et al.*, 2014b). In other words, particles that can only wetted by one of the phases do not act as emulsifiers. Apart from contact angle, another factor controlling the steric barrier energy is particle size (i.e $\Delta E \propto r^2$). However, the particles size should be smaller than the droplets of dispersed phase (Binks and Lumsdon, 2001; Dickinson, 2012b).

1.10 Polysaccharides

Table 1-1 Properites of polysaccharides and their origins. ♦ very often used in the food industry; O often used in the food industry; [1)] does not form gel as a single ingredient but does when combined with another substance. This table is based on work reported by Funami (2009).

Origin	Polysaccharide	Functions							
		Gelling	Thickening	Dispersing	Emulsifying	Binding	Water Holding	Foaming	Film forming
Plant Seeds	**Guar gum**		♦	O			♦	O	
	Locust bean gum	O[1)]	♦	♦		O	♦	O	
Plant Tubers	**Starch**	♦	♦			♦	♦		
Plant Fruits	Pectin	♦		♦					
Plant Tree Exudates	Gum Arabic				♦	♦		O	♦
Plant Pulps	Cellulose		O	♦	♦				
Seaweeds	Carrageenan	♦	O	♦	O	♦	O		O
	Alginate	♦	O	O	O		O		O
Microorganism	Xanthan gum	O[1)]	♦	♦	♦	O	O		

Polysaccharides are carbohydrates and attract a high interest due to their properties as food stock, health and dietary supplements. They are also a renewable resource material (Walther, 1998; Izydorczyk, 2005). Commercial polysaccharides are commonly available in powder form. The size of the particles varies with its origin and preparation method. Most polysaccharides are recognised as safe for

human consumption. The most common polysaccharides are glycogen (found in animal cells), chitin (found in the exoskeleton of arthropods and cell walls of fungi), starch and cellulose (found in plant cells).

Polysaccharides are biopolymers composed of simple sugar monomers (glycosides) that are linked together via glycosidic bonds. Polysaccharides can be either homopolymers or heteropolymers. Amylose and amylopectin are examples of homopolymers whilst guar gum and locust bean gum are examples of heteropolymers. In food products they are often used as thickening or gelling agents. Moreover, most gelling polysaccharides are heteropolymers (Morris, 2007). They are rich in hydroxyl groups so they are good in forming hydrogen bonds to one or more water molecules, this property gives them hydrophilic properties (Whistler and BeMiller, 1997). However, polysaccharides exhibit a wide range of solubility where some are highly soluble in water whereas others have lower solubility which take a long time to dissolve but can enhance the solubility when dispersed at high temperature (Wang and Cui, 2005). Solubility depends upon molecular structure and charge (Izydorczyk, 2005). The polymers can be neutral (e.g. amylose, amylopectin, cellulose etc.) or polyelectrolytes (e.g. xanthan, gellan, alginate etc.). Normally, charged polysaccharides are more soluble than the neutral ones (Wang and Cui, 2005). Polysaccharides are mainly found in plants, fungi and bacteria. A number of useful polysaccharides and their origin are listed in Table 1-1.

1.10.1 Types of polysaccharide structure

The functional properties of polysaccharides are n aturally controlled by their structure. Hence, the study of polysaccharide structure is of great importance since individual structures are also dependent upon the source of the biopolymers. The degree of structural heterogeneity of a polysaccharide depends upon its origin, extraction, purification and fractionation processes. There are two main types of polysaccharide structure (Semenova *et al.*, 2010) described as follows.

Linear polysaccharides

This type of structure is ostensibly a straight chain molecule formed from a single sugar. Linear polysaccharides are usually insoluble in water due to strong interchain attractions except under certain conditions; e.g., increasing temperature (Dumitriu, 2002). Locust bean and guar gum are considered to be examples of

substituted linear polysaccharides. They normally give high viscosity; as the molecules come into contact with each other more easily at much lower dilutions than highly branched molecules of the same overall molecular weight (Whistler and BeMiller, 1997).

Branched polysaccharides

Branched polysaccharides primary features are that they may contain a single branch or numerous branches. Complex structure formations can evolve where side chains may form on side chains to a give branch-on-branch structure. This kind of structure tends to have less interchain attraction, resulting in high solubility (Wang and Cui, 2005). In addition, they tend to give a higher stability and a less viscous solutions than linear polysaccharides of equal molecular mass (Glicksman,1982; Dumitriu, 2002).

1.10.2 Starch

Starch is the energy storage material that can be extracted and purified from seeds and tubers. It is the main storage carbohydrate in plant organs. It is one of the most important occurring natural biopolymer. Starch is also one of the most important and abundant human food sources due to its multifunctional properties as a thickener, gelling agent, stabiliser and fat substitute in processed food products as well as being a main ingredient in staple foods (Funami, 2009). Starch exists in the form of granules. Native starch granules are insoluble in cold water but normally become more soluble at higher temperature. The size of starch granules ranges from 1 to 100 μm depending upon the plant species (Eliasson and Gudmundsson, 2006).

The rheology of starch depends strongly on volume fraction and state of the granules in the dispersion. During heating starch dispersions at appropriate concentrations, its viscosity is changed due to the formation of gel and the swelling at the starch granules (gelatinisation). Some authors state that amylose is related to short-term development of gel structure, whereas amylopectin was the main factor in long-term development (Nagano *et al.*, 2008). Starch is comprised of glucose polymers, which consists of two different polysaccharides; amylopectin and amylose. Both components are homopolysaccharides. In starch granules, amylose and amylopectin are arranged into complex structures that consist of crystalline and amorphous regions. In most common starches, the percentages of amylose and

amylopectin are 20-30% and 70-80% respectively. However, waxy corn starch contains exclusively almost a hundred per cent of amylopectin. This type of starch tends to breakdown in highly acidic conditions, high shear or on prolonged heating (Achayuthakan and Suphantharika, 2008). In amylomaize, there is up to 60% of amylose in the granules.

Amylose

Amylose is a linear molecule of (1→4) – linked –D-α- glucopyranosyl units with a few branches. Typically, it has molecular weights ranging from 30 - 3200 kDa (Knill and Kennedy, 2005) with radius of gyration around 7-22 nm (Chaplin, 2015). In aqueous solution, amylose aligns in parallel, thus permitting molecular reassociation and hydrogen bonding between hydroxyl groups results in forming a network of junction zones and leads to strong gel formation.

Amylopectin

Amylopectin has a high degree of structural organisation. The degree of branching and length of chain varies within each sample and also its origin. It is a highly branched polymer of glucose, which is composed of (1→4) – linked –D –α-glucopyranosyl units that join together by (1→6) -α- glycosidic linkages. On average, it has one branch point every 20 to 25 residues and contains several hundreds of thousands of glucose units (Morris, 2007). Its molecular weight ranges from 10,000 to 1,000,000 kDa (Liu, 2005) with radius of gyration around 21-75 nm (Chaplin, 2015). Amylopectin has the ability to be solubilised in water and does not tend to gel strongly in aqueous solutions.

1.10.3 Galactomannans

Galactomannans consists of mannan backbone with short galactose side chains. One of the differences between each galactomannan is the degree of galactose substitution. Hence, the differences in the ratio of side chains strongly influence the functional properties of galactomannans. This type of polysaccharide is usually used to increase the viscosity of food products. These ‘gums’ are primarily non-ionic polymers, hence their rheological properties are not strongly affected by pH or ionic strength. However, the galactose side chains are easily hydrolysed by

acid which causes them to rapidly lose their viscosity at low pH. However, gums that are richer in galactose side chains are more likely to have higher acid stability (Chudzikowski, 1971). Galactomannan gums disperse in water to give a high viscosity to thickening or weakly gelling the system. They are commonly used at concentration of 0.25 – 0.50 wt.% in food products (Whistler and BeMiller, 1997). They are extensively used as thickening agents in food products such as sauces, dressings, desserts *etc*. due their low cost and wide range of functional properties (Bourbon *et al.*, 2010). Galactomannans are found around cell walls in numerous plant seeds. They are insoluble in many organic solvents such as hydrocarbon, alcohol, ester, oil etc., hence the important solvent for these gums is water (Chudzikowski, 1971) and their richness in hydroxyl groups gives them an ability to bind large quantities of water. Due to the fact that mannan backbone is relatively hydrophobic (Grenha and Dionísio, 2012), the larger the number of galactose side chains the more soluble it is in water (Tombs and Harding, 1998). To make a homogeneous gum dispersion, the gum must be added to solvent under controlled conditions (Whistler and BeMiller, 1997). Galactomannans, such as guar gum and locust bean gum, contain a wide range of molecular structures. Bourbon *et al.* (2010) reported that galactomannan viscosity depends mainly on molecular weight whilst their synergistic interactions depend on galatose side chains and molecular structure (Schorsch *et al.*, 1997). The molecules in solution can adopt any configuration compatible with its mannan backbone, exhibiting random coil-like behaviour mostly in solvent (Morris, 1998). When each polymer chain of galactomannan comes into contact with another they form an intermolecular attraction and this leads to a high viscosity solution.

In this experiment, two different galactomannans were used; guar gum (GG) and locust bean gum (LBG). Both gums are non-ionic molecules that are non-toxic and biodegrade and show high viscosity at low concentration, usually well below 1 wt.% (Glicksman,1982). The properties and rheology of each gum is different, hence they can be chosen for specific food formulations. For example, GG shows good stability to freeze-thaw hence it is commonly used as a stabiliser in ice cream products. The basic structure of GG and LBG are shown in Figure 1-11 and 1-12, respectively.

Guar gum

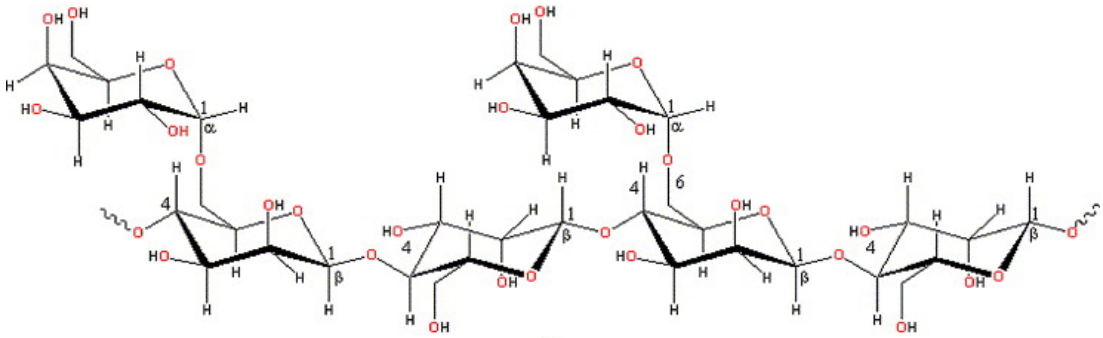

Figure 1-11 The principle structure of guar gum. This diagram is based on work reported by Wang and Somasundaran (2007)

Guar gum (GG) (also known as guaran) is a galactomannan extracted from Cyamopsis tetragonoloba seeds (an annual leguminous plant). Its seeds consist of 15% husk, 45% embryo and 40% endosperm. GG is obtained from milled endosperms. It is mainly composed of a linear chain of β- (1→4) linked mannose with α- (1→6) linked galactose residues as side chains. The mannose: galactose ratio is 2:1 (38-40% galactose side chain). GG has molecular weight around 250-5000 kDa depending on the source and the method used to extract it (Dea and Morrison, 1975). The radius of gyration of GG is between 55-169 nm (Picout *et al*., 2001). The main property of GG is that it is soluble in both hot and cold water but insoluble in organic solvents. Ptaszek *et al*. (2009) stated that some caking (a formation of gum particles which have adhered onto one another causing lumps) might occur due to fast water absorption. It gives a high viscosity at low concentration due to the strong hydrogen bonding properties. Its viscosity can be influenced by temperature, rate of agitation and the particle size of the guar gum powder. When the temperature is increased, the viscosity will decrease and vice versa. It is stable in the pH range 4 to 10.5 (Kawamura, 2008). In addition, commercial guar gum often contains impurities and insoluble matter such as protein from the germ, ash, phosphorus and husk residues. Thus, total GG can sometimes be only around 66% of the total powder (Panda, 2004).

Locust bean gum

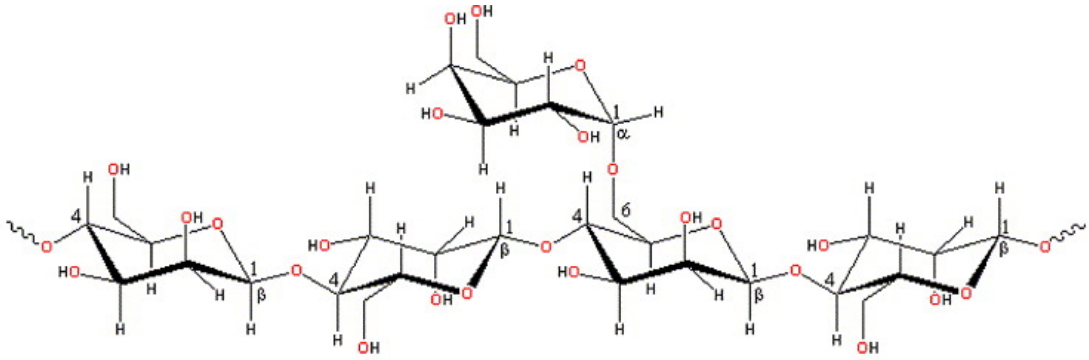

Figure 1-12 The principle structure of locust bean gum. This diagram is based on work reported by Wang and Somasundaran (2007).

Locust bean gum (LBG) or carob gum (from Ceratonia siliqua) mainly consists of a linear chain of β- (1→4) linked mannose with α-(1→6) linked galactose residues as side chains. The mannose: galactose ratio is 4:1 (22% galactose sidechain). Moreover, the molecular weight of LBG is about 50 - 1000 kDa (Dakia *et al.*, 2008; Grenha and Dionísio, 2012) with radius of gyration between 64-127 nm (Picout *et al*., 2002). The seed consists of 30-35% husk, 25-30% embryo and 34-45% endosperm. LBG is obtained from milled endosperms. It has lower solubility than GG because it has fewer branch points and normally gives lower viscosity. LBG is only partially soluble in cold water, hence it is important to solubilise it in hot water (typically it needs temperatures above 85 ^{o}C for 10 minutes). LBG has attracted scientific interest especially in the biopharmaceutical field in the past few years due to its defined drug delivery properties (Grenha and Dionísio, 2012).

Only a few gums can form a firm, rigid structure that is resistant to flow under pressure (i.e. a gel). LBG itself creates no gel, but it can yield gelling system when mixed with other polysaccharides upon aging (Garnier *et al.*, 1995; Goff *et al.*, 1999). In addition, it also yields an irreversible gel in freezing due to self-association of smooth regions along the backbone. Regarding the purity of commercial LBG, the percentage of galactomannan in the powder is often around 70% - 80% (Panda, 2004; Grenha and Dionísio, 2012). For food industrial uses, LBG has been used as a stabiliser in ice-cream, cheese spread and other dairy product due to its excellent water binding properties. The range of LBG content in food product can be from 0.05 – 0.6 wt.% (Tombs and Harding, 1998). LBG is widely used in textile,

pharmaceutical, biomedical and cosmetic industries as well as in food (Batal *et al.*, 2012).

1.10.4 Binary polysaccharide gels

Sometimes mixtures of polysaccharides form gels and these can ideally be categorised into 4 types: phase separated networks, swollen networks, interpenetrating networks and coupled networks. The gelation properties of a binary mixture offer an effective means to increase system stability. The type of gel formed depends upon the nature of components, the rate of phase separation and mechanism of gelation (Dumitriu *et al.*, 1996).

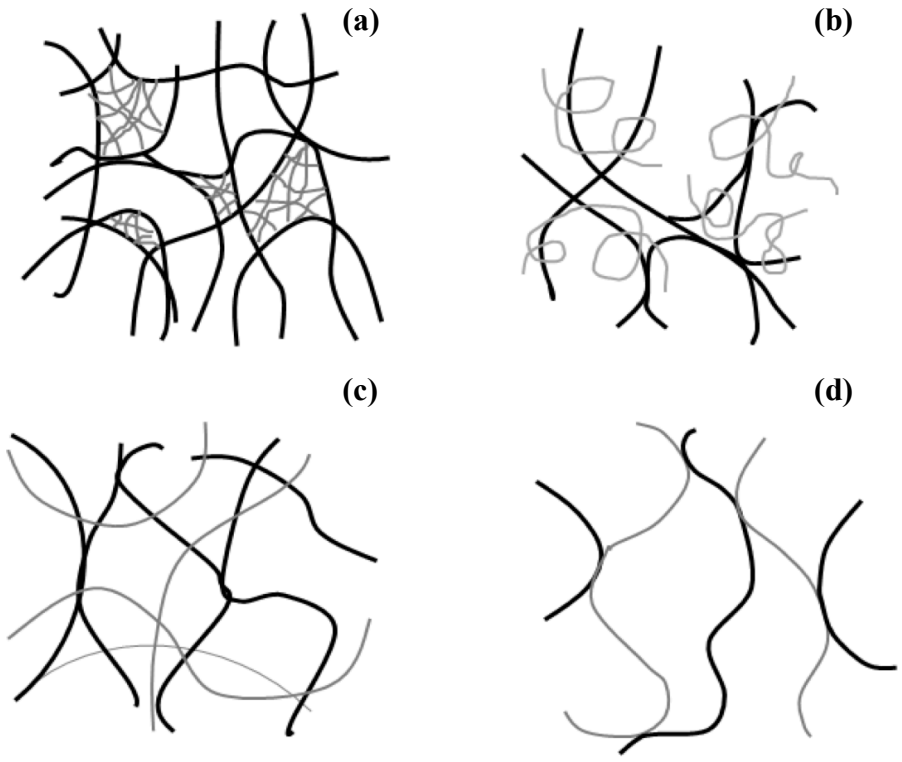

Figure 1-13 The model represent the possible gel structure that form in a binary mixture (*a*) phase separated networks; (*b*) swollen networks; (*c*) interpenetrating networks; (*d*) coupled networks. This diagram redrawn from work reported by Morris (1998).

Phase separated networks (Figure 1-13a)

The incompatible polysaccharides that mixed together form 3-dimensional (3D) phase separated gel structure when some degree of demixing occurs prior to

gelation in either one of the phases or both gels. It results in a non-equilibrium structure that is arrested and the polysaccharide(s) form a composite or filled gel.

Swollen networks (Figure 1-13b)

This type of structure forms when one of the components is induced to gel and the other component resides within and swell the gelled network. This type of network is likely to occur when the rate of gelation is higher than the rate of demixing of polysaccharides.

Interpenetrating networks (Figure 1-13c)

These types of networks form when both polysaccharide chains associate independently in the sample and interpenetrating through each other.

Coupled networks (Figure 1-13d)

These types of gel structure occur when both polysaccharides bind together through the formation of new heterotypic junction zones

1.11 Fumed silica particles

Silica particles are one of solid particles that are widely used for the stabilisation of emulsions. Fumed silica particles (pyrogenic silica) are extremely small particles ranging from 5-50 nm diameter they therefore have a high specific surface area. As it is a small particle it can easily become air-borne. The particles can be produced by burning silicontetrachloride in a flame. The molecular weight is 60.08 g/mol. It finds a wide variety of applications in industry such as in antiperspirants, coatings, thickeners, laminates etc. The major chemical companies that sell this type of particle are Cabot Corporation, Wacker Chemie and Dow Corning. Fumed silica particles are naturally hydrophilic, but they can be chemically modified to obtain different hydrophobicities using dichlorodimethylsilane or hexamethyldisilazane.

1.12 Milk proteins

Proteins consist of amino acids that are linked via peptide bonds. Amino acids are zwitterionic compounds which means the molecules can carry both negative and positive charges. Proteins are surface-active molecules that are widely used as stabilisers of emulsions or present naturally as the emulsifier (Hoffmann and Reger, 2014). Aggregation or gelation of protein can be induced by heating or changing pH. The most commonly used dairy proteins are casein and β-lactoglobulin (Dickinson, 1994; 1998; 2001).

1.12.1 Sodium Caseinate

Casein is a main protein component derived from bovine milk by acid or enzyme precipitation (McClements, 2005). Casein consists of α_1, α_2, β, κ caseins. Sodium caseinate is a sodium hydroxide solubilised precipitate of acid casein. It is a large complex molecule, 10 to 300 nm in diameter (Dickinson, 2006). It is widely use as emulsifying agent in many dairy products. Sodium caseinate is manufactured by removing calcium phosphate from casein via acidification to pH 4.6, precipitation and neutralisation with alkaline solution to pH 6.7 then pasteurising and spray drying (Dickinson, 2010a; Hanazawa and Murray, 2014) in order to increase its water solubility. It has a relatively high amount of negative charge, dependent on pH and ionic strength. It also can be made to aggregate (Hanazawa and Murray, 2014) to form viscous solutions or gel in various ways, for example, addition of ethanol, addition of salt or pH adjustment to the isoelectric point (McClements, 2005).

1.12.2 Whey protein isolates (WPI)

WPI is a mixture of globular proteins, mainly composed of β-lactoglobulin (60% in bovine whey) and α-lactalbumin (20% in bovine whey). β-lactoglobulin has molar mass of 18.2 kg mol^{-1} and contains two disulfide bridges and one free thiol whilst α-lactalbumin has molar mass of 14.2 kg mol^{-1} and contains four disulfide bridges (Nicolai *et al.*, 2011). WPI is well known for its excellent emulsifying, gelling and binding properties (Chun *et al.*, 2014). Generally, when a solution of the whey protein is heated above 70°C, the unfolding/expansion of protein molecules results in the molecules rearranging to form a three dimensional network via forming

intermolecular bonds. The interactions can be either covalent or non-covalent bonds. This heat-set gelling is irreversible.

Chapter 2

2 Chapter 2. General materials and methodology

This chapter provides detailed information about the materials and the methods used in this thesis.

2.1 General Materials

2.1.1 Phosphate buffer pH 7

A pH 7 phosphate buffer consisting of 0.05 mol dm^{-3} KH_2PO_4 + Na_2HPO_4 + 0.05 mol dm^{-3} NaCl. Additionally 0.02 wt.% sodium azide was added as a bactericide. The pH was adjusted by adding either 1M NaOH or 1M HCl. A Jenway 3310 pH meter (Jenway, Essex UK) was used to measure the pH of buffer.

2.1.2 Starch

Starch from corn (unmodified waxy corn starch) product code S-9679 was purchased from Sigma-Aldrich (Dorset UK).

2.1.3 Gum

In the experiment, two galactomannans were used; guar gum (product number. G-4129) and locust bean gum from Ceretonia siliqua seeds (product number. G-0753). They were supplied by Sigma-Aldrich.

2.1.4 Model fumed silica particles

The fumed silica particles with different hydrophobicity, characterised as having 100- (most hydrophilic), 80-, 70- and 65-SiOH (most hydrophobic) of the natural surface density of silica SiOH group remaining after treatment with dimethyldichloromethane (dimethylsilane) were a gift from Professor Binks, University of Hull, previously obtained from Wacker-Chemie GmbH (Munich, Germany). The nominal particle size was 20 nm with a specific surface area of 200 m^2 g^{-1} (Binks *et al.*, 2005).

2.1.5 Fluorescence labels

All dyes were stored in a dark place.

0.5 wt. % Rhodamine B (RB): ($C_{28}H_{31}ClN_2O_3$)

Product number R-6626 was obtained from Sigma-Aldrich (Sigma-Aldrich Company Ltd., Dorset, UK). It has an absorption maximum around 554 nm and emission maximum of 579 nm (Kristoffersen *et al.,* 2014). The powder was dissolved with Millipore water (Millipore, Bedford, UK), with a resistivity not less than 18.2 MΩ cm. This dye was used to stain starch.

0.5 wt.% Acridine Orange hemi (zinc chloride) salt (AO): ($C_{17}H_{20}ClN_3 \bullet HCl \bullet ½ ZnCl_2$)

Product number 158550 was obtained from Sigma-Aldrich. It has an absorption maximum around 431 - 490 nm and emission maximum of 510 - 520 nm (Heller, 1994; Greb, 2012). The powder was dissolved with Millipore water (Millipore, Bedford, UK), with a resistivity not less than 18.2 MΩ cm. The dye was used to stain silica particles and whey protein isolate microgel particles.

0.02 wt.% Nile Red: ($C_{20}H_{18}N_2O_2$)

Product number N3013 was purchased from Sigma-Aldrich. It excites at 514 - 546 nm and emits at 633 nm (Greenspan and Fowler, 1985; Girija and Stephen, 2003). The powder was dissolved with ethyl alcohol. The dye was used to stain stable oil microdroplets.

2.2 Preparation of solutions

Preparation of starch + galactomannan ± solid particles consisted of separate consecutive steps.

2.2.1 Preparation of starch solution

Stock solutions of starch (7 wt.%) were prepared by dispersing the starch powder in phosphate buffer pH 7 and leaving for 5 minutes, followed by heating in a Julabo F25 refrigerated and heating circulator (Julabo, Allentown USA) at 90 °C for 15 minutes

with constant manual stirring. The stock solutions were diluted with buffer to the required concentrations.

2.2.2 Preparation of galactomannan gum solution

If the gum powder hydrates too quickly it will produce a gelatinous coating on its surface and a dry interior which results in slowing the rate of water diffusion (Whistler and BeMiller, 1997). To prevent this problem, stock solutions of gums were prepared by slowly dispersing an appropriate amount of LBG or GG (1 – 2 wt.%) in the stirred buffer under the same conditions as for the starch. The gum solution was then left to cool and centrifuged at 11000 rpm and 25 °C for 1 hour in a high speed Beckman Coulter (Avanti J-301) centrifuge to remove insoluble materials. This centrifugation technique was also used in many galactomannan studies (Sittikijyothin *et al.,* 2005; Simonet *et al*., 2000; Bourbon *et al.*, 2010). After the insoluble particles had been removed the sample was put in an oven at 105 °C for 4 hours or until it is completely dry. The percentage of the removal and final concentration of gum were then calculated (because the concentration will change after removing insoluble materials). This contributed 20 ± 2 wt.% of the original powders. Panda (2004) has reported that commercial LBG and GG may contain up to 27% and 34% impurities respectively. However the variation depends upon its original source. Stock solutions were stored at room temperature before use. To make the stock solution reproducible, gum solutions were diluted with the buffer to the required concentration based on soluble part remaining.

2.2.3 Preparation of the final solution

To prepare polysaccharide mixtures, both stock solutions were heated separately at 90 °C for 5 minutes before blending together. Emulsions were composed of identical volumes of S and LBG or GG phase (50/50 vol%). Solutions were mixed immediately after removal from the oil bath by an Ultra Turrax T25 homogeniser (IKA-Werke GmbH &Co., Staufen Germany) at 24000 rpm for 1 minute and the temperature of the samples was 70 ± 5°C after mixing. Where appropriate particles were added to either gum or starch phase and mixed with Ultra Turrax before adding the other solution and blended with Ultra Turrax again - see Figure 2-1. Trials showed that the order of mixing did not significantly influence the structure of emulsion. In order to reduce the pH to pH 4, 0.25M HCl was added to the mixed solution during homogenising by Ultra Turrax.

For samples intended for confocal microscopy, Rhodamine B (RB), Acridine orange (AO) and/or Nile red (NR) were added during blending.

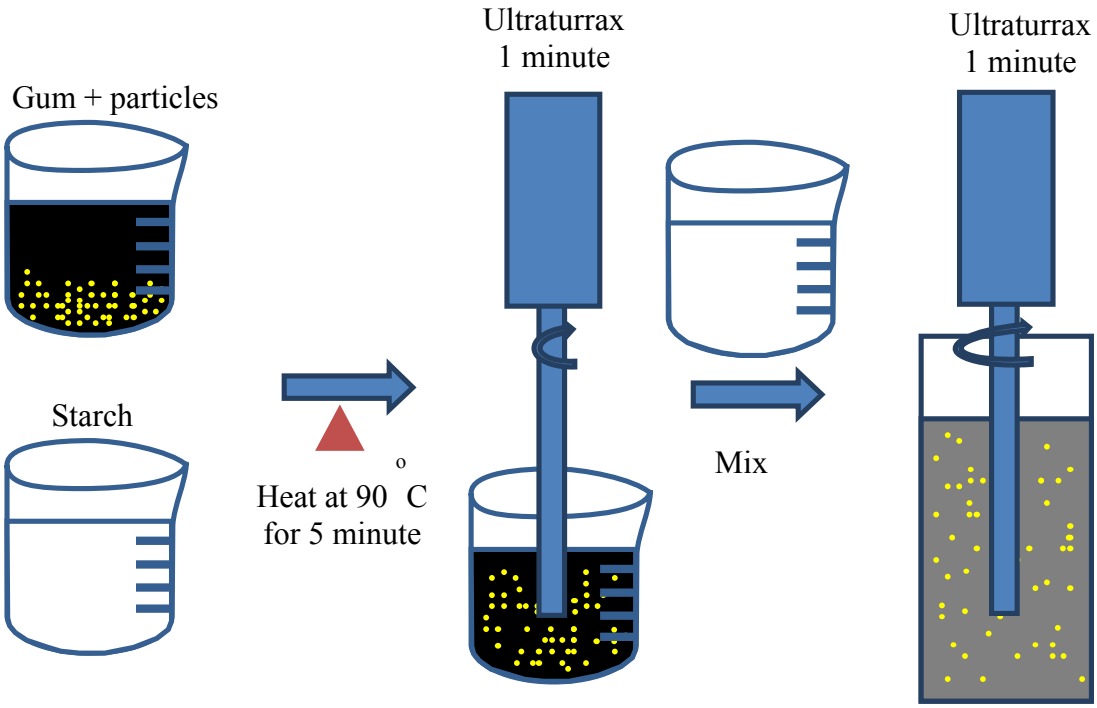

Figure 2-1 Flowchart of sample preparation

2.3 Particle size distribution and ζ-potential measurement

The size distribution of particles and their ζ-potential were determined by dynamic light scattering (DLS), also known as quasi-elastic light scattering (QELS). DLS is a well-established technique to measure particle size distribution, commonly in a sub-micron region. The Brownian motion of the particles causes an incident laser beam to be scattered at different intensities. This method works without knowledge of the concentration of particle dispersion (Nobbmann *et al.,* 2007). The particle hydrodynamic diameter is calculated using the Stokes – Einstein equation:

$$d = \frac{k_B T}{6\pi\eta D} \qquad \text{Equation 2-1}$$

Where d is particle hydrodynamic diameter, k_B is Boltzmann's constant, T is absolute temperature, D is translational diffusion coefficient, η is viscosity of the solvent (Pa s). An overall average particle diameter often called the z-average or

cumulants mean is calculated from the fitted particle size distribution (Malvern, Instruments Ltd., 2005).

The tests were run using a Zetasizer Nano-ZS (Malvern instruments, Worcestershire UK). The samples were diluted with phosphate buffer before being placed in a disposable PMMA standard disposal cuvette. The light is detected at an angle of 173° and a temperature of 25 °C. The particle sizes were then measured, typically requiring measurement duration of 150 seconds. Between each measurement the cuvettes had to be cleaned with Milli-Q water and phosphate buffer. The mean particle size was reported as the z-average which was calculated by the autocorrelation function from Zetasizer software.

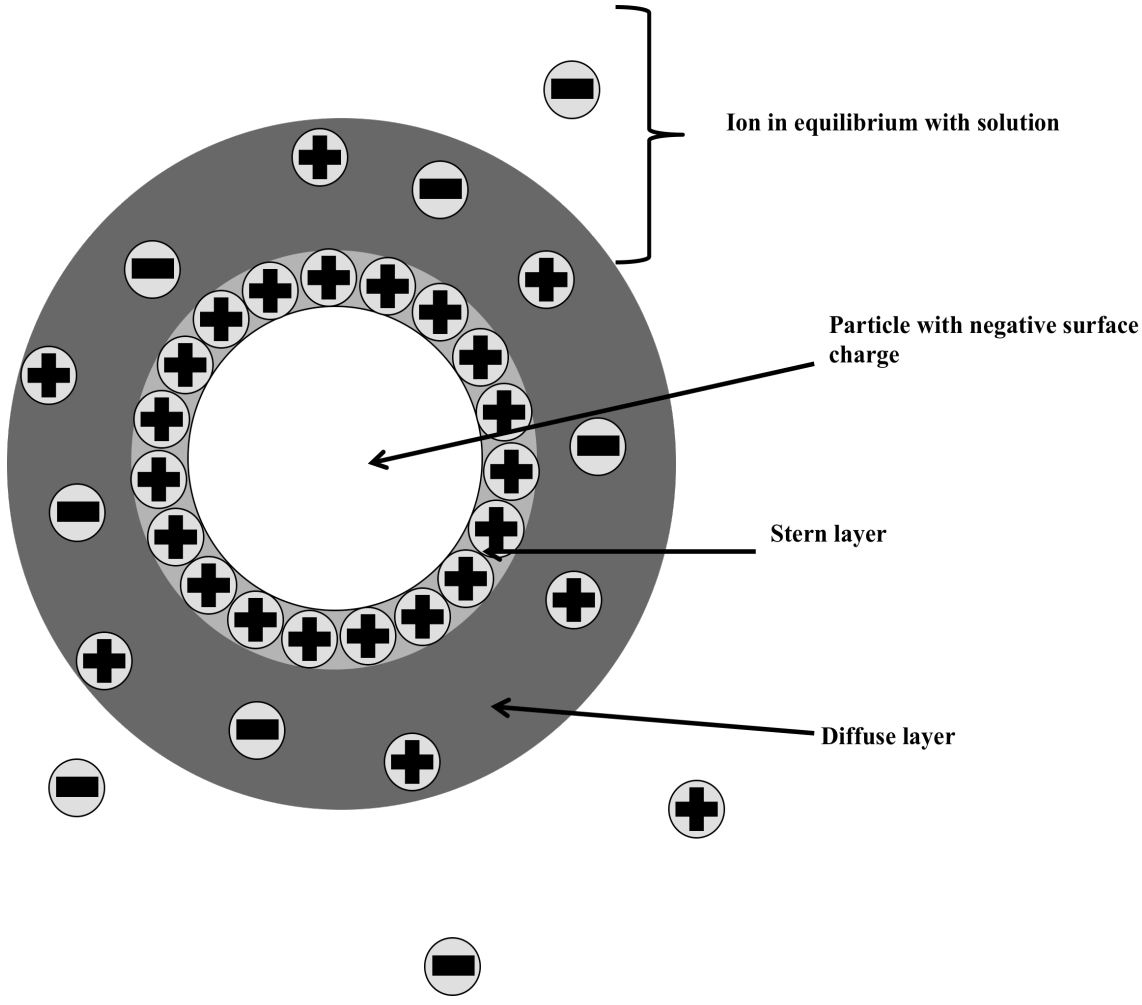

Figure 2-2 Schematic representation of negative charged particle.

Before explaining about the zeta potential it is worth mentioning about the double layer model of charged particles. This model explains how electrical repulsive forces occur. Figure 2-2 shows a diagram of a single negative particle to which positive ions (counter-ions) in solution are attracted which cause some of the counter ions to form a "Stern layer". In a "diffuse layer", additional counter ions are still attracted by the particle and also repelled by the Stern layer. Hence, counter ions are highly concentrated around particle surface and gradually decrease with distance. In contrast, additional negative ions (co-ions) have a low concentration near the particle surface and gradually increase with distance away from the surface until equilibrium between diffusion and repulsion is reached. The Stern layer and diffuse layer are usually known as the "double layer". The boundary between a layer of immobile liquid and associated ions is referred to as the slip plane. It is somewhere between where the Stern layer ends and diffuse layer ends. The electrostatic potential at the slip plane is know as zeta potential (ζ-potential).

The zeta potential gives some indication of the likely stability of the colloidal sample. For example, if the particles have a large negative or positive ζ-potential, they will repel each other significantly if the ionic strength is not too high. Particle charge can be controlled by the change in pH or ionic strength in solution. When an electric field (normally between 50-150 Volts) is applied to the particle dispersion (Schmitt *et al.,* 2014), the particles then move with a velocity related to their ζ-potential. The velocity of a particle relative to the field strength is referred to electrophoretic mobility, which can be calculated by following equation (Schmitt *et al.*, 2014):

$$V = U\,(\omega)\,E \qquad \text{Equation 2-2}$$

where V is the particle velocity (m s^{-1}), U is electrophoretic mobility, ω is frequency (s^{-1}) and E is electrical field.

Zeta potential is related to the electrophoretic mobility by the Henry's equation:

$$U = \frac{2\zeta\varepsilon\, f(\kappa a)}{3\eta} \qquad \text{Equation 2-3}$$

Where ε is dielectric constant and f(κa) is Henry's function. The units of κ are reciprocal length and k^{-1} is thickness of the double layer and "a" is the particle radius, thus κa is the ratio of particle radius to the thicken of the double layer.

The Smoluchowski is widely used in calculating ζ-potential however this equation is only valid for a sufficiently thin double layer, i.e., smaller than the mean particle radius. In the case of a thick double layer, Hückel approximation is used instead. For particles in polar media the maximum value of f(κa) is 1.5 and this is referred to as the Smoluchowski approximation. On the other hand, for particles in low or non-polar media the minimum value of f(κa) is 1 and this is referred to as the Hückel approximation (Malvern Instruments Ltd., 2005), see Figure 2-3.

In the ζ-potential measurements, samples were injected in a DTS1070 disposable capillary cell and were then measured via Zetasizer Nano-ZS.

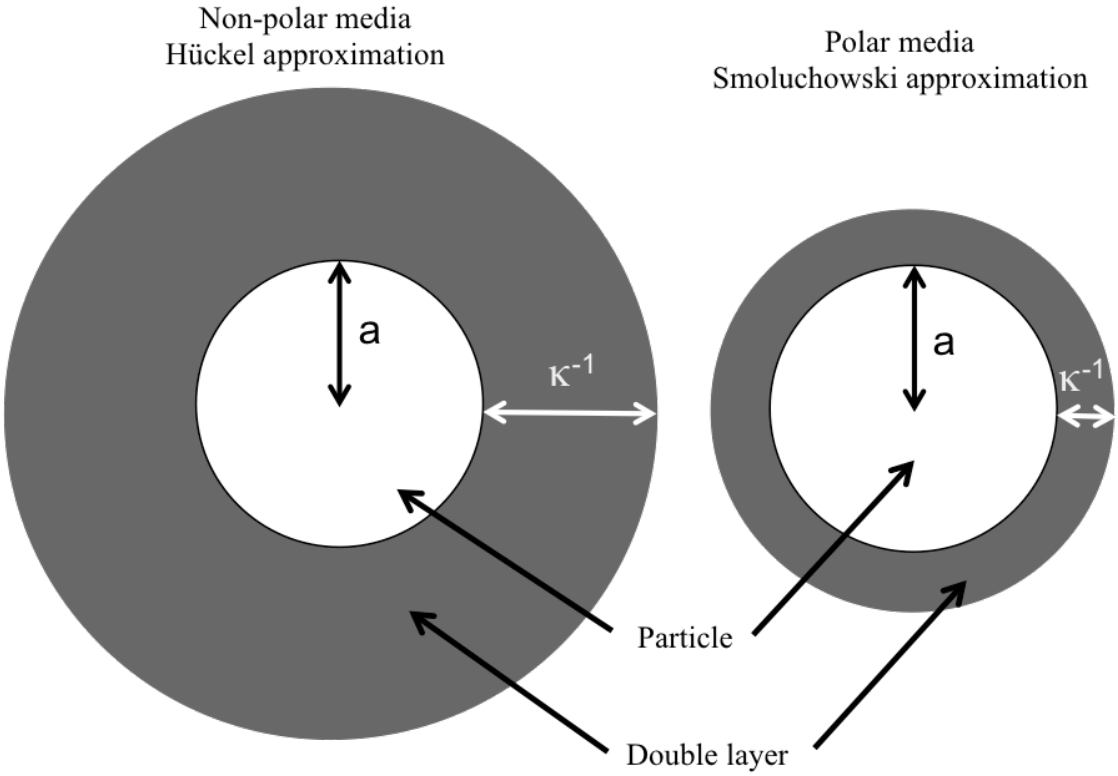

Figure 2-3 Schematic illustrating Hückel and Smoluchowski's approximations used for the conversion of electrophoretic mobility into zeta potential.

2.4 Phase diagrams

2.4.1 Mixture of polysaccharides

The pure galactomannan solution was centrifuged and insoluble particles were removed before being mixed with starch. The mixture was then transferred to Iwaki 50ml polystyrene plastic centrifuge tubes. All blends were centrifuged at 4200 rpm with a Beckman Coulter Allegra X-22 for 1 hour. The phase separation of the mixtures resulted in clear boundaries between 2 phases.

2.4.2 Determination of phase volumes

Phase separation of S + LBG or GG mixtures were observed after centrifugation, the tubes were held in a vertical position. For the accuracy of volume determinations an error of less than 5% can be expected

The stability of polysaccharide emulsion ± particles was studied using the test tube method by visual observation of the phase separation over a period of time. Freshly made mixtures were prepared, in 75 x 25 mm flat bottom test tubes sealed with plastic cap and Parafilm to prevent sample evaporation, and stored at room temperature (≈22 - 25 °C).

2.5 Rheological measurement

Rheometers are instruments that apply stresses and strains and measure the flow and deformation of the material (Rao, 1999; 2007). Some instruments can be used to analyse all kind of materials whereas some may be able to analyse either liquid or solid material. The type of forces applied and test method used depends upon the physicochemical characteristics of the samples and the kind of information required (McClements, 2005). In order to avoid experimental error and make reliable measurements, it is important to select the most appropriate test method.

Figure 2-4 Image representation of Kinexus rheometer with cone and plate geometries. The images were obtained from Chemeurope.com (2012)

Most rheometers are controlled using a computer and have the ability to analyse multi-parameters in one sequence test. In this thesis, rheological properties were performed with a Kinexus Rheometer – see Figure 2-4 (Malvern Instruments, Worcestershire UK) using the *rSpace* software to control the rheometer, perform measurement and analysis of the result. The environmental controller cartridge holds the lower geometry and controls the temperature of sample as required. The temperature was set at 25 °C in every experiment. Two geometries and cartridges were used: cone with plate cartridge (CP2/60:PL65) for very viscous samples and double gap and bob with cylinder cartridge (DG25:DO25/DI25) for lower viscosity samples.

The rheological properties of each polysaccharide solution have been investigated for different concentrations at 25 ^{o} C. After adding the sample to the geometry, it was then left to achieve steady state for 5 minutes. Viscosities were measured over a range of shear rates using the shear rate mode in rSpace software. The starting shear rate was 0.1 s^{-1} and the final shear rate 100 s^{-1} the whole range taking 16 minutes in total. In frequency sweep tests, the elastic and viscous components G' and

G'' were determined at 1% strain to assure that the conditions were in the linear viscoelastic region (LVR), in the range 0.01 – 1 Hz, taking 26 minutes in total for each run. Silicone oil was layered around the edge of the sample to prevent sample evaporation and drying.

2.5.1 Cone (upper geometry) and Plate (lower geometry) with plate cartridge

Figure 2-5*a* shows a schematic of cone with plate geometry. The plate cartridge is used to hold liquid, pastes and semi-solid samples. The cone has an angle that is designed to ensure that a shear stress acts uniformly across the sample. Each geometry has its own name such as CP*a*/*nn*:PL*xx*, where *a* is the cone angle, *nn* is the cone diameter and *xx* is the bottom plate diameter. The cone and plate geometries are named CP2/60:PL65, meaning a 60 mm diameter with 2^{o} angle cone over a 65 mm plate. The operating gap was 70,000 nm.

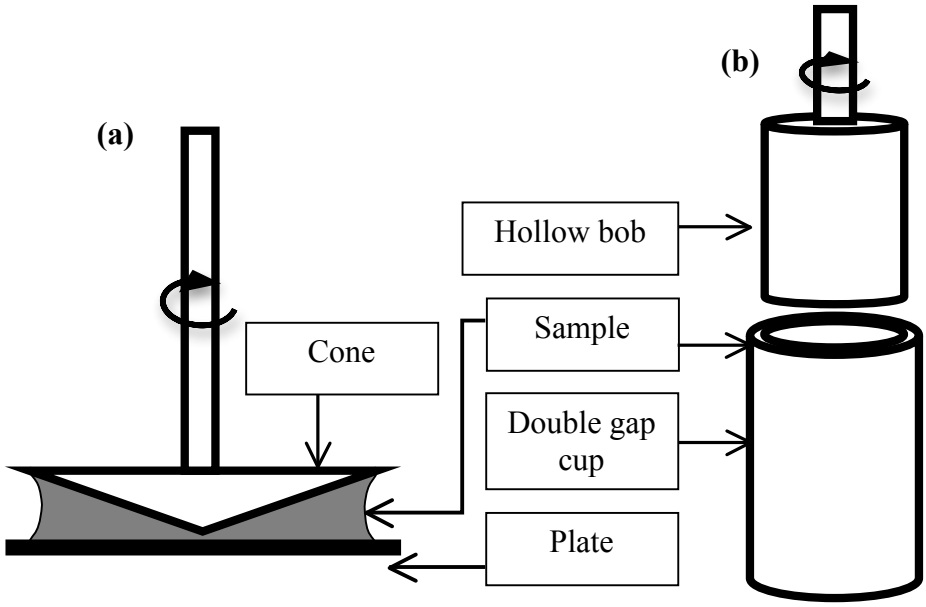

Figure 2-5 Schematic representation of (*a*) cone and plate cartridge geometry; (*b*) Double gap and bob with cylinder cartridge geometry

2.5.2 Bob (upper geometry) and double gap cup (lower geometry) with cylinder cartridge

Figure 2-5*b* shows a schematic of bob and double gap cup. They are usually used to measure low viscosity liquid samples. This type of geometry is named DG*nn*:DO*nn*/DI*nn*, where *nn* is the bob diameter. The bob that was used is named DG25:DO25/DI25, meaning a 25 mm diameter bob with an operating gap at 112,500 nm.

2.6 Confocal laser scanning microscopy (CLSM)

A microscope is a useful instrument to study the morphology of material. Among the several types of microscopes, confocal laser scanning microscopy (CLSM) was selected in this thesis. Before the invention of CLSM, samples had to be cut into sections when observing their microstructure via conventional microscopy; which is not practical for samples that are evolving over time. CLSM provides remarkably valuable information about the microstructure of emulsions (McClements, 2005). The key features of CLSM are (1) a higher clarity of images is possible than normal optical microscopy (2) an ability to visualise the sample without the need for complicated preparation (3) capability to observe the sample in its environment (4) generate three-dimensional (3D) images of structures without the need of physical section specimens (5) distinguish between two or more components using fluorescent dyes (6) capacity to eliminate out-of-focus light, using the pinhole. Figure 2-6 shows a focal plane in CLSM. The resolution in the x-y plane shows a top-view of a two-dimensional image. The resolution in the z plane displays different vertical depths.

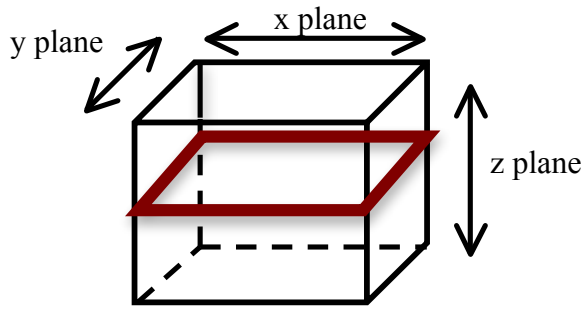

Figure 2-6 Dimension of focal plane in CLSM as x-y-z plane

A simplified diagram of the confocal image principle is shown in Figure 2-7. A photomultiplier tube (PMT) has an ability to detect a laser beam that passes through a pinhole and transforms a light signal to live data on a computer screen. This pinhole is important in the elimination of out-of-focus light hence the areas below or above the in-focus plane are blocked by the pinhole. The laser beam enters through the pinhole aperture; the size of pinhole can be adjusted in order to get the optimum visual image. Moreover, 3D images can be obtained by collection of images at different depth of sample by moving the stage in the z-plane direction (Lorén *et al.,* 2007).

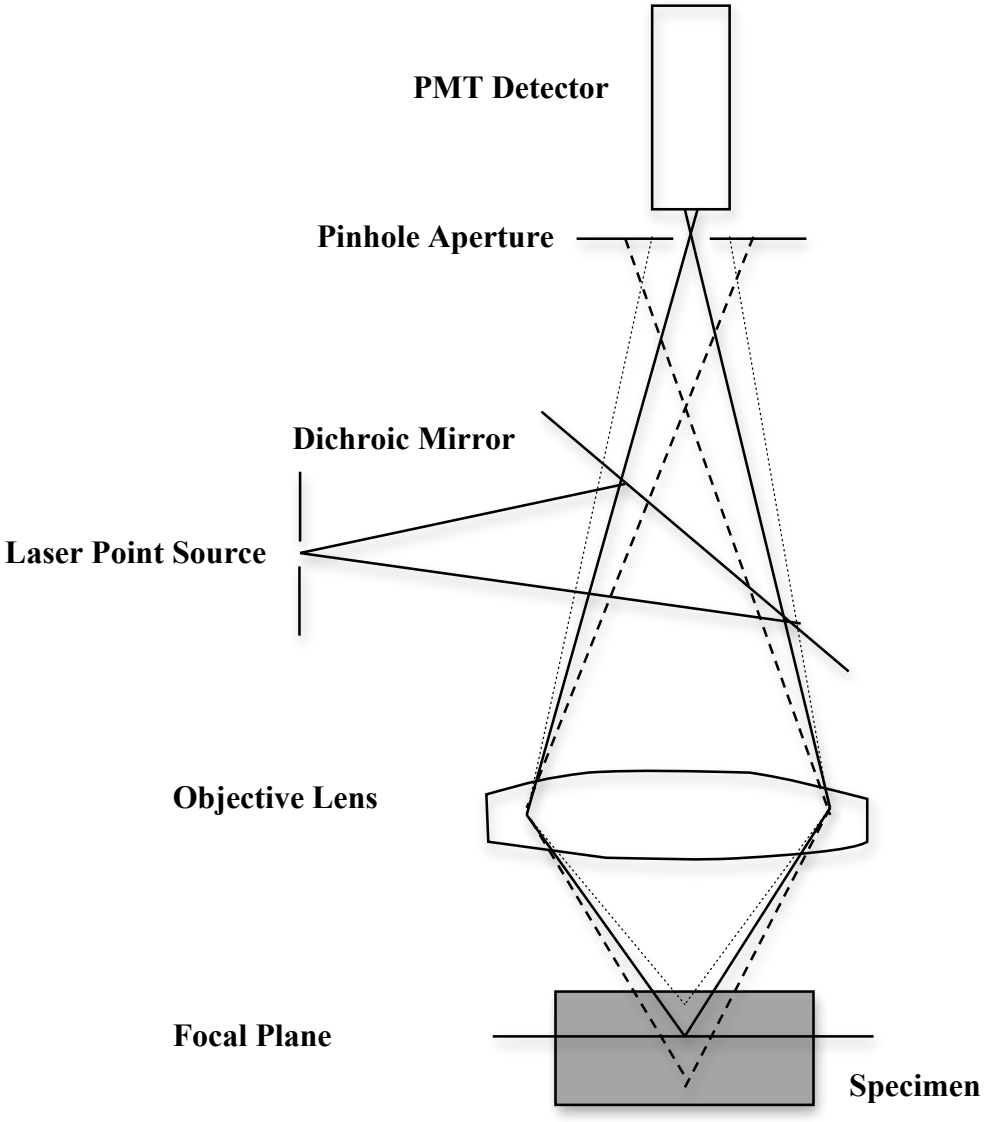

Figure 2-7 The confocal principle in laser scanning microscope. This schematic is adapted from Murphy, 2001, p.210

In CLSM the contrast is obtained by using fluorescent dyes to label the specific regions (Tromp *et al.*, 2001). These dyes can be covalently bonded prior to sample preparation or non-covalently bonded by adding the probe in the dissolved state. The dye molecules will spread over the sample according to its affinity. Although CLSM is a fluorescent microscope it can also work in different modes, e.g. transmission, reflection. Sample images are collected point-by-point and reconstructed with a connected computer.

In the experiments, the CLSM was operated in fluorescent mode. The differences between two polysaccharides and particles were determined by different fluorescent dyes. For mixtures without particles, 100μl of the RB solution were added to 5 ml starch solution before blending with gum. In the presence of particles, 30 μl of the Acridine Orange (AO) or Nile Red (NR) (depending on the type of particles) was added per 5 ml of either the S or gum phase before blending. 30 μl of Rhodamine B (RB) was later added to the mix. After blending the mixtures via the Ultra Turrax samples were immediately poured into a welled slide 30 mm diameter and 3 mm in depth. Rhodamine B showed preferential staining of the starch whilst the NR showed strong affinity for mirodroplets and AO showed an affinity to protein and silica particles. Hence, unlabelled areas were therefore assumed to be gum-rich regions. The recording of images started immediately at room temperature. The position of the confocal plane was held constant throughout the whole sequence of image recoding. To ensure consistency of the results the experiments were duplicated for repeats.

Confocal microscopy was performed using a Leica TCS SP2 confocal laser scanning microscope (Leica Microsystems, Manheim Germany) connected with a Leica Model DM RXE microscope base. The confocal microscope was used with Ar/ArKr (488, 514nm) laser source. Laser excitation of the fluorescent samples was at 514 nm (≈ 29% intensity of laser) for RB and 488 nm (≈ 49% intensity of laser) for NR or AO. A 20x objective with numerical aperture 0.5 was used to obtain all images, at 1024 x 1024 pixel resolution. X-Y-Z focal plane was used in every sample - see Figure 2-6.

2.6.1 Sample holder (slide) for CLSM observations

Plastic welled slides 30 mm diameter and 0.3 mm in depth were used for all samples.

2.6.2 Image analysis

CLSM images were processed using Image J software 1.48v for Mac. Spinodal decomposition structure is normally periodic and usually characterised by only one length scale. Hence, the feature of two-dimensional fast-Fourier transform (2D-FFT) analysis is an appropriate technique to evaluate the evolution of the microstructure of the mixture.

Spinodal decomposition structures often show the fused and elongated solution domains across the position in space which can be defined by a characteristic length (L), the largest dominant dimension in any direction on the image. In this thesis L denotes the waxy corn starch domain size. It was determined from the 2D-FFT of the captured micrographs. This analysis technique has been used in various research, for example in gelatin + starch (Firoozmand *et al.*, 2009a) and solutions of gelatin + maltodextrin (Lorén *et al.*, 2002). 2D-FFT transforms a micrograph from dimensional domain into frequency domain.

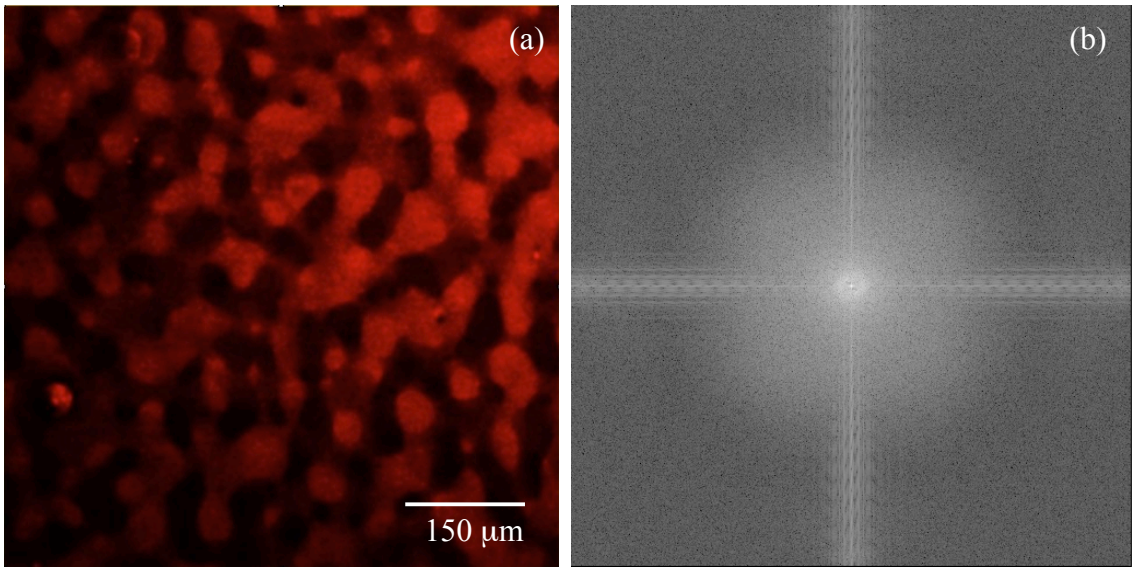

Figure 2-8 (*a*) a typical micrograph of spinodal decomposition in sample containing 2 wt% starch + 0.3 wt% locust bean gum. (*b*) the 2D-FFT of (*a*)

In order to measure the characteristic length (L) of spinodal decomposition using Image J software, the micrographs from CLSM were adjusted to the right contrast and were then converted to 2D-FFT by FFT menu in the program. Figure 2-8*a* shows a typical image of spinodal decomposition obtained via CLSM. Figure 2-8*b* shows the 2D-FFT of image *a*. The FFT images were then used to calculate and plot the normalised intensity of radial profile versus the distance (the radial of the measurement). Figure 2-9 shows the command menu that had been used to construct FFT and calculating the radial profile of the FFT image (circular average).

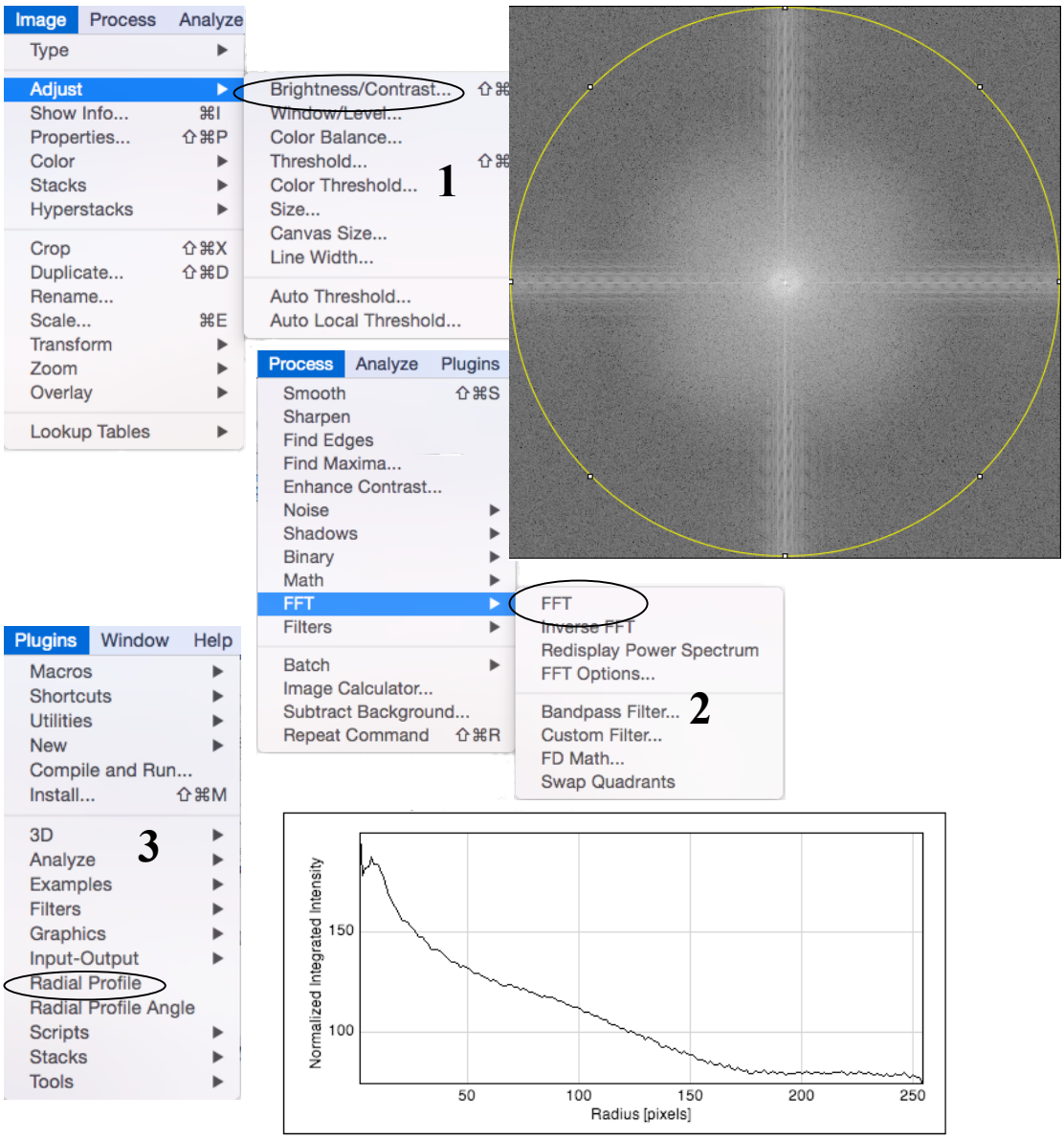

Figure 2-9 Command menus in Image J software to obtain FFT and Radial profile

The peak intensity on Y axis indicates the highest frequency and on the other hand the peck intensity on X axis (δFFT) represents the number of the periods of the periodic feature over the extension of the original micrograph obtained from CLSM. Consequently L is calculated as follows (Equation 2-4) where image width is in pixels, S is the scale factor (µm/pixel) and δFFT is the number of radius distance in pixel.

$$L = image\ width \times S\ /\ \delta FFT \qquad \text{Equation 2-4}$$

Chapter 3

3 Chapter 3. Phase diagrams, phase separation and rheology of waxy corn starch + locust bean gum or guar gum

3.1 Introduction

Waxy corn starch contains exclusively almost 100% amylopectin. Amylopectin is one of the compounds in common starch. It is a highly branched molecule. Galactomannan gums, such as locust bean gum (LBG) and guar gum (GG) have been used in a wide variety of industries in the past decades (Sittikijyothin *et al.*, 2005). In food factories, they are often used as additives to control functional properties of products. They are long chain polymers, which consists of mannan backbones and galactose side chains that produce an entangled solution which has an ability to give a high viscosity at low concentration when dispersed in solvent, i.e. water. One typical property of LBG is that it can yield a gelling system when mixed with other polysaccharides (Ganier *et al.*, 1995; Goff *et al.*, 1999), whilst amylopectin forms very weak gels at relatively high concentrations after heating is induced.

A worldwide trend in the food industry has been developing 'clean food' that does not contain any chemicals or reagents during production. Food hydrocolloids can be an alternative for chemically modified ingredients because they are essentially obtained from natural sources and are safe for humans (Funami, 2009). In the modern food industry starch + non-starch hydrocolloid blends have been used to modify and control texture, help promote moisture retention and control water mobility of the products (Achayuthakan and Suphantharika, 2008). It is well known that the combination of starch and hydrocolloid can lead to a significant viscosity increase and viscoelasticity of starch pastes and gels (Alloncle and Doublier, 1991; Bahnassey and Breene, 1994; Kulicke *et al.*, 1996; Sudhakar *et al.,* 1996; Achayuthakan and Suphantharika, 2008; Nagano *et al.,* 2008; Ptaszek *et al.*, 2009). These kinds of mixtures are commonly found in confectionery products. In the absence of any specific association of biopolymers, this usually leads to phase separation of a mixture into two coexisting phases (Firoozmand *et al.*, 2009a,b). Especially at high polymer concentration, the system typically has a strong tendency for self-association. There are also another key factors influencing phase separation such as chemical structure, ionic strength, pH and temperature.

It is important to have some understanding and be able to control phase separation since excessive phase separation may cause unacceptable changes in the sensory properties or appearance (Semenova and Dickinson 2010; Firoozmand *et al.*, 2012). Whilst at the same time such systems potentially provide a novel way of influencing desired texture and small molecule (flavours, drugs, *etc*.) delivery via dispersions of one type of aqueous phase in another, so called *water-in-water* (W/W) emulsions. Once phase separation occurs, water-water interfaces will be formed in solution, i.e., protein-polysaccharide and polysaccharide-polysaccharide. Moreover, phase separation induced by spinodal decomposition has previously been studied in detail in W/W emulsion for systems containing gelatin + maltodextrin (Lorén *et al.*, 2002), gelatin+maltodextrin (Butler and Heppenstall-Butler, 2003) and gelatin + oxidised starch (Firoozmand *et al.*, 2009a; 2009b). These studies have given some insight into how the microstructure of mixed biopolymers changes during aging.

Food is a complex system which consists of various components. Chaisawang and Suphantharika (2006) stated the interactions of leached amylose in native starch + GG systems are complex. Therefore, in this thesis waxy corn starch, contains virtually all amylopectin, was chosen because it offers the possibility of study of ternary systems without having this complexity. This ternary system contains two different polysaccharides, amylopectin and LBG or GG, and the solvent, i.e. phosphate buffer. Each solution was investigated separately in terms of their rheological properties. Using a rheometer to study solution behaviour, combined with plotted phase diagram data, showed the constituent biopolymers compatibility and incompatibility regions under certain conditions. A simple visual observation was used to study macroscopic phase composition. Subsequently, the microstructure properties of polysaccharide mixtures were investigated using confocal laser scanning microscopy. In this chapter, attention is focused on the phase behaviour of waxy corn starch + galactomannan solutions, which are the model system studied in later chapters. Due to the similarity in chemical structure of LBG and GG, these two gums were often comparatively investigated because it is known that each gum behaves differently in starch solution (Bahnassey and Breene, 1994; Chaisawang and Suphantharika, 2006). The very different conformation of amylopectin and galactomannan means that they have difficulty forming simple mixtures even at relatively low concentrations and this leads to their phase separation. This system was also previously investigated elsewhere (Sudhakar *et al.*, 1996; Closs *et*

al., 1999; Achayuthakan and Suphantharika, 2008; Ptaszek *et al.*, 2009) but there is still lack of information on the rheology of each solution and their mixture microstructures.

3.2 Materials and methods

3.2.1 Materials

Waxy corn starch, GG, LBG, phosphate buffer and Rhodamine B (RB) used in the experiments in this chapter are the same as those stated in chapter 2, section 2.1

Deuterium oxide > 99.92% (D_2O)

The product number is 7789-20-0. It was purchased from Apollo Scientific (Whaley Bridge UK).

Dyes

- 0.1 wt.% Methylene Blue (MB): ($C_{16}H_{18}ClN_3S \bullet xH_2O$) high purity, biological stain (product no. A18174) was obtained from Alfa Aesar, a Johnson Matthey Company. The fluorescence intensity of MB has excitation and emission of 664 and 682 nm, respectively (Lee and Mills, 2003). It was prepared by dissolving 0.02g of Methylene Blue powder in 20 ml Millipore water. The solution was stored in a dark place because of its photosensitivity.
- 1.65 wt.% Iodine Monochloride solution (I_2/KI) product number BDH 7327 was purchased from BDH VWR analytical.

3.2.2 Methods

Preparation of waxy corn starch (S) solutions

Stock solutions of starch (4 wt.%) were prepared by dispersing the starch powder in phosphate buffer pH 7 in a beaker and left for 5 minutes before being placed in a Julabo oil bath. The dispersion was stirred, by hand, at 90 °C for 15 minutes to produce translucent starch paste. The stock solutions were diluted with buffer to the required concentrations.

Preparation of locust bean gum (LBG) or guar gum (GG) solutions

In an early stage of experiment 0.5 wt.% GG and 0.6 wt.% LBG were prepared with the same method as S stock solution then diluted with phosphate buffer to the required concentration. However, when S + galactomannan were mixed together there was difficulty in distinguishing the macroscopic boundary between these two phases as the gum layer was slightly cloudy. It is important for further work that the two phases of the mixtures are clearly distinguishable, hence the clean-up method to obtain clear galactomannan solution was introduced. The method was adapted from Dea and Morrison (1975) and Bourbon and colleagues (2010) and was performed as stated in chapter 2 section 2.2.2. In interfacial measurement, D_2O was used instead of phosphate buffer to prepare gum solutions.

Preparation of mixture of starch + gum

The prepared stock polysaccharide solutions were heated separately before blending these components together. Each step was followed as flow chart in Figure 3-1.

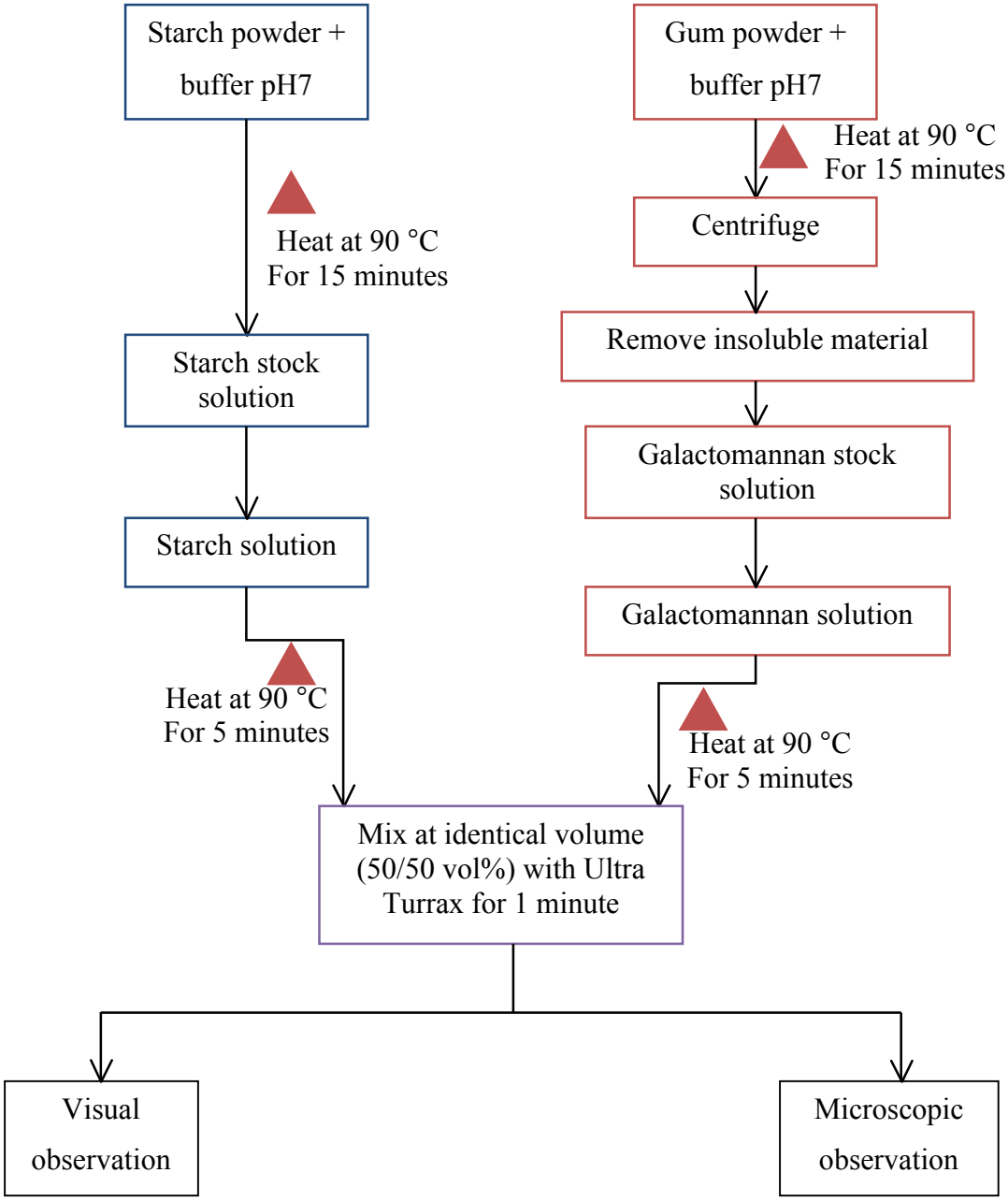

Figure 3-1 Flow chart of preparation method of the mixtures used in chapter 3

Determination of phase separation and phase diagram

The 50/50 vol.% mixtures were transferred to Iwaki 50ml polystyrene plastic centrifuge tubes with accuracy to 0.1 g. All blends were centrifuged at 4200 rpm in a

Beckman Coulter Allegra X-22 for 1 hour. After centrifugation the tubes were held in a vertical position at room temperature. The phase separation of the mixtures resulted in clear boundaries between two phases. The heights of the upper and lower phases were measured and converted to volumes from the known geometry of the tubes.

Effect of changing pH

S, GG and LBG were prepared with the same method as described above using phosphate buffer that has already adjusted pH with NaOH or HCl to pH 5.4 and 8. The stability of emulsion was studied using the tube test method by observation of the sample's phase separation over a period of time. Fresh emulsions were prepared at a different pH in a 75 x 25 mm flat bottom test tube sealed with plastic cap and stored at room temperature (≈22 - 25 °C).

Confocal laser scanning microscopy (CLSM)

For samples intended for confocal microscopy, 100 µl RB was added to starch solution before blending with gum. The mixtures were then placed on a welled slide 30 mm diameter and 3 mm in depth. The first image was captured 5 minutes after blending. The appearance of samples was recorded again at 10, 20, 30 and 1440 minutes.

Interfacial tension measurement

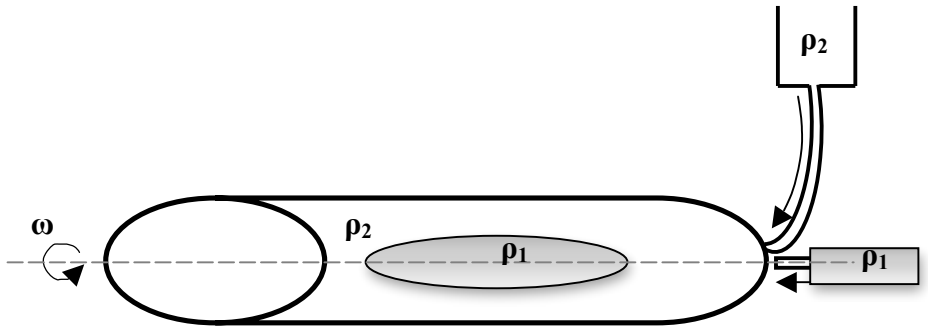

Figure 3-2 Schematic of the spinning drop method.

Spinning drop is a method that was used to measure the interfacial tension of the mixtures. This measurement was completed with help from Professor Bernard Binks and his student, University of Hull. Interfacial tension was performed with a Krüss spinning drop Tensiometer Site 02 (Kruss GmbH, Hamburg Germany) connected with a

Grant LTC 6G thermostat refrigerated circulating bath (Grant instruments, Cambridge UK). The measurements were performed in a rotating horizontal tube where the tube contained denser liquid and a small drop of lighter liquid was injected in later. A drop of starch solution (ρ_1) was injected into a capillary full of galactomannan solution (ρ_2) while the capillary rotated at a known speed (ω). Consequently, the starch liquid drop is elongated along the axis of rotating by the centrifugal force – Figure 3-2. In order to calculate the surface tension, the density of each polysaccharide was measured via Anton Paar DMA 35N density meter (Graz, Austria).

3.2.2.1 Bulk rheology

Rheological measurements were performed as stated in chapter 2, section 2.5.

3.3 Results and discussion

3.3.1 Bulk rheology of different solutions

Steady shear properties

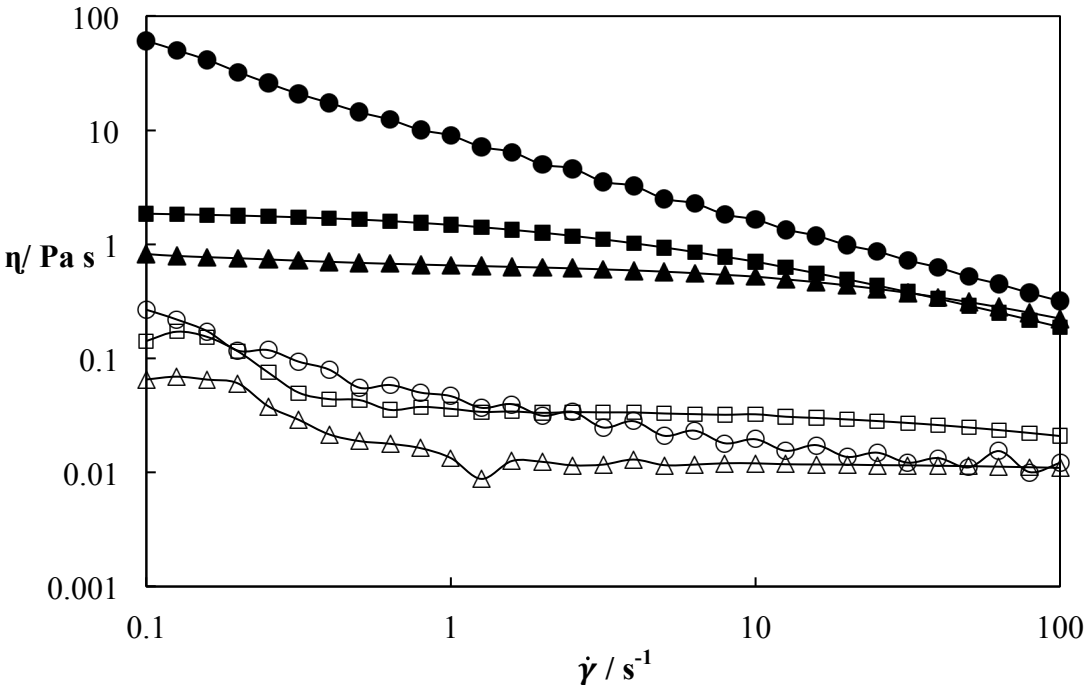

Figure 3-3 Viscosity (η) versus shear rate ($\dot{\gamma}$) for [S] = 4 wt.% (●); [S] = 1 wt.% (○); [GG] = 0.6 wt.% (■); [GG] = 0.2 wt.% (□); [LBG] = 0.6 wt.% (▲); [LBG] = 0.2 wt.% (△).

The effect of the shear rate ($\dot{\gamma}$) in the range 0.1-100 s^{-1} on the viscosity (η) of S, GG and LBG solutions at selected low and high concentration are shown in Figure 3-3. As expected, shear-thinning behaviour was observed in all cases. When fitting the data to a Power law model, Equation 1-7 section 1.7.1, at high polymer concentration S exhibited the strongest shear-thinning followed by GG and LBG, respectively, which is in agreement with Tombs and Harding (1998). Due to the new arrangement of inter-molecular molecules as the shear rate increases, the solution entanglement was disrupted (disentangled), consequently the molecules align with flow and lead to decrease in viscosity. At the same concentration, GG was slightly more viscous than LBG. At selected high [GG] and [LBG], there was a Newtonian plateau in the low shear rate range where the viscosity has constant value ($\eta = \eta_0$). The solution exhibited shear-thinning behaviour at higher shear rates. At selected high [S], the trend line indicates that S is likely to be more shear thinning than LBG and GG, probably because the concentration of S is higher.

Zero-shear rate viscosity, η_0

In terms of structure, GG and LBG are substituted linear polymers that act like 'random coils' in solution (Launay *et al.*, 1997). The relationship between viscosity, their structures and conformations is predictable. When galactomannan is dispersed in water, the galactose side chains interact with water molecules, leading to inter-molecular chain entanglement. Their viscosity may be slightly different from water at low concentrations because there is no interaction between molecules when they are at their most extended, isolated coil. With increase in concentration, individual molecules start to impinge on each other's space leading to the degree of entanglement being enhanced. At this point, the differences in viscosity are dependent upon concentration and their free rotation (Chaplin, 2012).

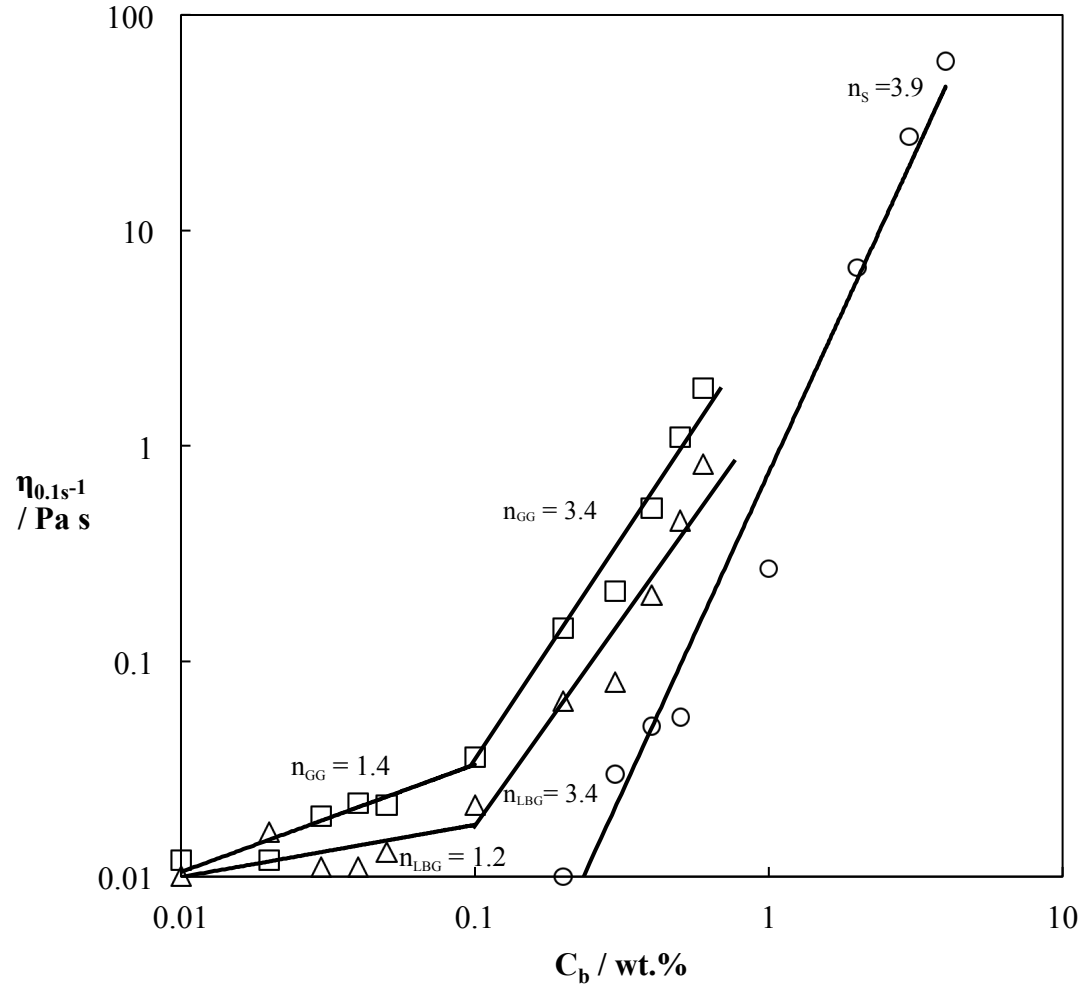

Figure 3-4 Viscosity (η) at $\dot{\gamma}$ = 0.1 s^{-1} versus wt.% concentration (C_b) of different biopolymers: [S] (○); [LBG] (△); [GG] (□); (—) trend line.

The rheology of the galactomannan solutions in Figure 3-4 shows two regions; (1) a region of dilute solution, where the viscosity dependence on concentration follows a 1.2 and 1.4 power law for LBG and GG, respectively and (2) a region of semi-dilute solution where the viscosity dependence on concentration follows a 3.4 power for both gums. In most common polysaccharides, the slope of a double logarithmic plot of η against [C_b] should be close to 1.4 and 3.3 ± 0.3 for dilute and semi-dilute solutions respectively (Morris *et al.*, 1981). However, Smidsrød and Moe (2008) stated that the rheology was frequently found to deviate from above information for galactomannans. The region of semi-dilute solution showed a slope of 5.1 instead of 3.3, which was attributed to specific intermolecular association (hyperentanglements). Launay *et al.* (1986) proposed that, in some cases, there could be two transitions, where the solution changes from dilute to semi-dilute (c = c*) and semi-dilute to a highly concentrated solution (c = c**).

The bulk rheology of each gum and starch solution was measured as a function of their concentrations [C_b]. Viscosity at the lowest shear rate employed (0.1 s^{-1}) is plotted as a function of [S], [GG] and [LBG] - see Figure 3-4. It is seen that at the same concentration, GG gave slightly higher viscosity than LBG, which agrees with numerous other researchers (Glicksman, 1969; Chudzikowski, 1971; Dea and Morrison, 1975; Elfak *et al.*, 1977; Sittikijyothin *et al.*, 2005; Bourbon *et al.*, 2010), whilst the viscosity for starch only reaches similar values at double the concentration, reflecting low overlap molecules. Figure 3-4 also reflects that the GG used in the experiment had slightly larger molecular weight than the LBG used resulting in higher viscosity values at the same concentration. The viscosity at zero shear rate depends strongly on the polymer concentration, reflecting the existence of the critical concentration (c*). At c < c* the solutions usually appear Newtonian. Launay *et al.* (1997) reported that values of c* were close to 0.025 wt.% and c** were equal to 0.25 and 0.28 for LBG and GG, respectively. However in Figure 3-4 the transition where c=c* was unclear and beyond concentration of 0.1 wt.% the viscosity started to increase steeply, hence c* for GG and LBG were estimated to be approximately around 0.1 wt.%. For starch solution, within the concentration observed, it is difficult to determine the critical concentration of starch solution as there was no sign of a clear η transition, with the trend line steadily increasing.

Frequency sweep

In the linear viscoelastic regime (LVR), the complex modulus was measured via low amplitude oscillation. The frequency sweeps for all galactomannan and S solutions are shown in Figure 3-5. Open symbols denoted the storage modulus (G') and filled symbols denote the loss modulus (G"). For an ideal gel, the G' value is expected to be frequency independent (Tzoumaki *et al.,* 2011) and G' should be significantly higher than G". However, all three solutions displayed marked frequency dependence with both G' and G" increasing with frequency, which indicated that all solutions were not an ideal gel. As expected, G' is dominant over the entire frequency range for starch paste, reflecting weak gel behaviour. Starch granules are commonly gelatinised after heat-induction at temperatures above 70 °C and formed opaque thermoreversible gel on cooling. On the other hand, G" is higher than G' for both galactomannan gums. The same result was reported by Sittikijyothin *et al.* (2005) for several galactomannans and random coil polysaccharides where G" > G' at low frequency range the system shows

viscoelastic liquid-like behaviour. However, the range of frequency observed was low, normally ranging between 0.1-10 Hz. G' and G" are expected to show a crossover and exhibit elastic response at higher frequency, i.e., above 1 Hz. Similar experiments performed by Bourbon and colleague (2010) showed a crossover frequency at around 10 Hz for both LBG and GG.

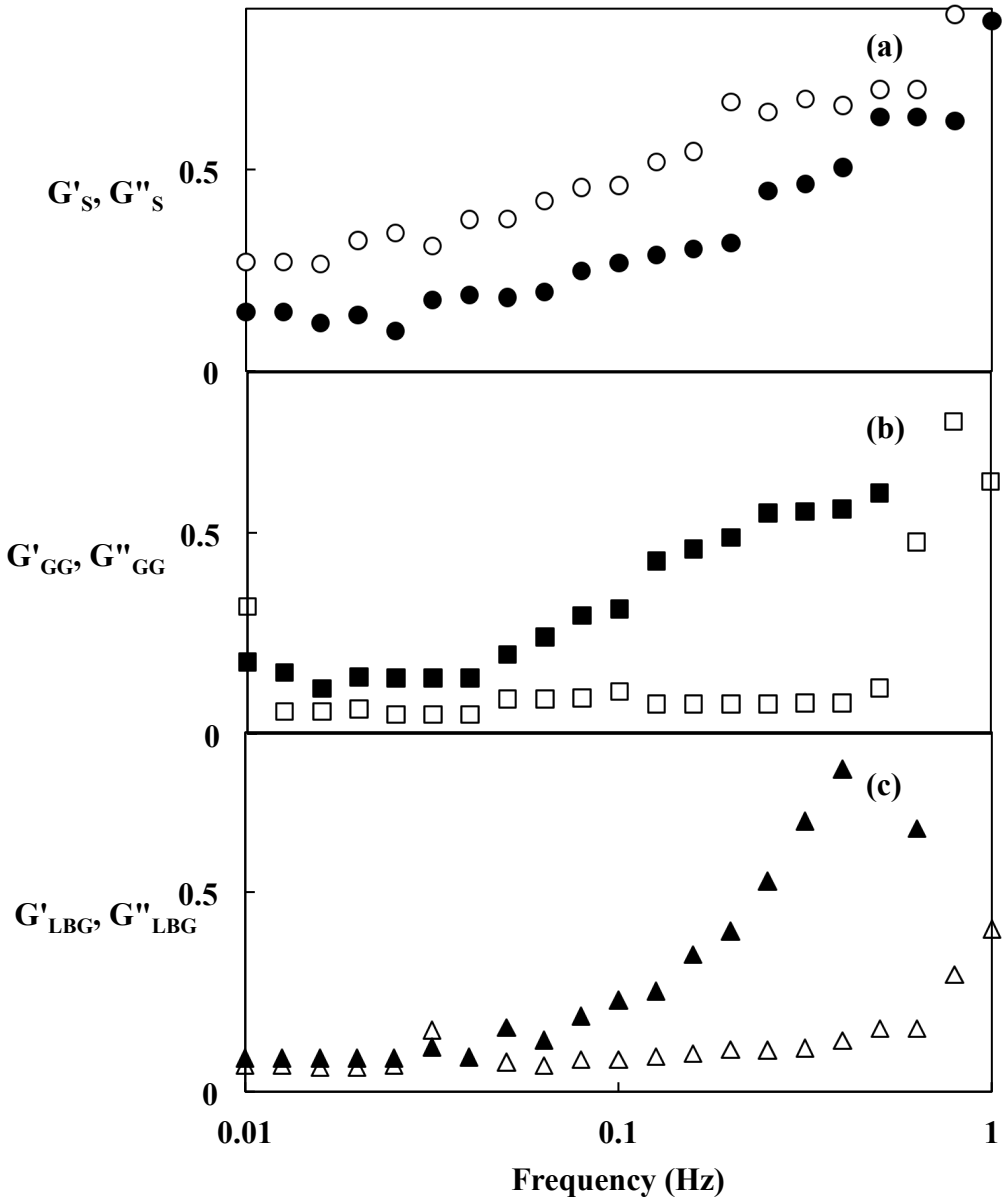

Figure 3-5 Frequency versus storage modulus (open symbol) and loss modulus (filled symbol) for (*a*) [S] = 4 wt.% (○,●); (*b*) [GG] = 0.5 wt.% (□,■); (*c*) [LBG] = 0.6 wt.% (△,▲).

3.3.2 Determination of phase separation and phase diagram

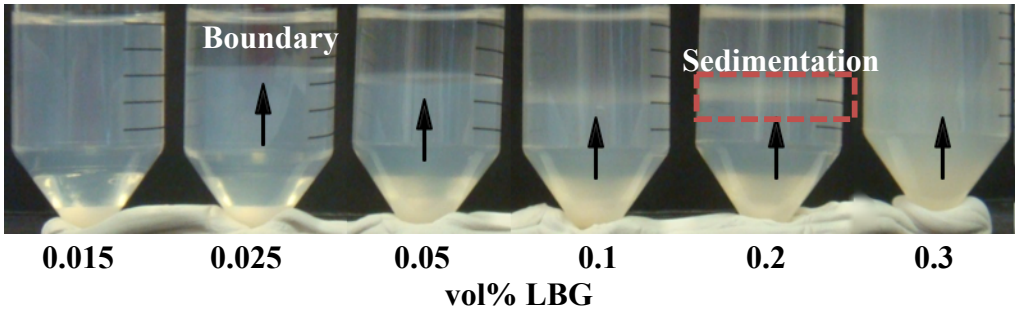

Figure 3-6 Visual observation of 2 wt.% S + different wt.% LBG concentration after centrifugation. Arrow indicates boundary between the two-phases.

The visual observation results showed that the mixtures of S + gum generally underwent initial phase separation within 30 minutes after blending, thus confirming the incompatibility between the two biopolymers previously reported by Closs *et al.* (1999). It took more than 48 hours, under normal gravity, for the samples to fully reach the equilibrium condition. As the S + LBG or GG mixtures formed via segregative phase separation, the full phase equilibrium state may not be observed on the experimental time scale, hence the centrifugation of the mixtures was introduced. Centrifuging the mixtures results in acceleration of the rate of phase separation and the interfacial boundary was slightly clearer. This centrifugation method also provides a measurement of volume ratio of each phase. After an hour centrifugation, the mixtures showed two distinctive layers with a translucent lower phase and an upper clear phase (as can be seen in Figure 3-6). As there was no sharp difference between S + LBG and S + GG mixtures, only S + LBG system is shown. Since the original starch solution was slightly translucent, the lower cloudy phase was assumed to be starch-rich phase. This subsequently was confirmed to be starch after being tested with I_2/KI staining and observed via confocal laser scanning microscopy (CLSM) – see later in section 3.3.6. Therefore the upper phase was assumed to be the gum-rich phase. This bulk phase separation where upper and lower phase were galactomannan-rich and starch-rich phase was also reported by Closs *et al.* (1999). Centrifuging the mixtures further showed no significant change in phase volume. The lower starch phase always presented the larger volume. During centrifugation, at [LBG] > 0.1 wt.%, the samples also developed sedimentation of some insoluble particles at the bottom of the boundary line between

two phases. It was also seen that the turbidity of the top layer increased as the concentration of gum increased, i.e., at 2 wt.% S + 0.3 wt.% LBG the mixture had almost identical turbidity in both top and bottom phase. However, a thin boundary line was still visible between two phases when the sample was put under bright light. Moreover, after 3 weeks storage of 2 wt.% S + 0.3 wt.% LBG mixtures, there was a formation of a weak gel at LBG-rich phase where the upper phase was more opaque and did not flow. It is assumed that this phenomenon is due to its high incompatibility with starch and the high concentration of LBG polymers in definite areas (Garnier *et al.*, 1995). This suggests to self-association via coupled networks via the "smooth" zones of LBG molecules. This self-association depends upon the chemical structure of LBG as the lower the galactose side chain content the higher the association (Goff *et al.*, 1999). However, the formation of gel on top phase was not present with 2 wt.% S + 0.25 wt.% GG mixtures.

In order to obtain rectangular coordination phase diagrams, a series of polysaccharide mixtures were examined. Various concentrations of starch [S] (0.2-4 wt.%) and galactomannans (0.1-0.6 wt.%) were mixed together and centrifuged at 4200 rpm for one hour to identify at which composition the mixture underwent phase separation. Depending on the appearance of the mixtures, either homogeneous or heterogeneous, the position of binodal line in phase diagram was established. Phase diagrams of mixed polysaccharide systems are given in Figure 3-7*a* and Figure 3-7*b* as a function of [S] and [GG] or [LBG]. The line separating homogeneous and heterogeneous mixtures represents an estimation of the binodal line. The binodal lines of both phase diagrams nearly coincide with the concentration axes of both polysaccharides. It is in agreement with the statement from Medin and Janson (1993) that the position of binodal line depends upon molecular weight, the higher the molecular weight the closer to the axis. As the binodal line lay close to the axis this means that in the phase separated solution the individual phases consisted mainly of one of the polymers with only a small fraction of the other. The phase diagram also indicates that the starch (amylopectin) and galactomannan used were highly incompatible under the experimental conditions. The critical point coordinates of S + GG were approximately 0.3 wt.% and 0.04 wt.%, respectively. This result is similar to the research by Closs *et al.* (1999) where critical points of S and GG were 0.27 wt.% and 0.08 wt.%. At around the critical point the difference in density of S and gum

solutions was small which made it difficult to identify the boundary of phase-separated mixture. Therefore the results in this experiment may slightly differ from the published work from Closs *et al.* (1999).

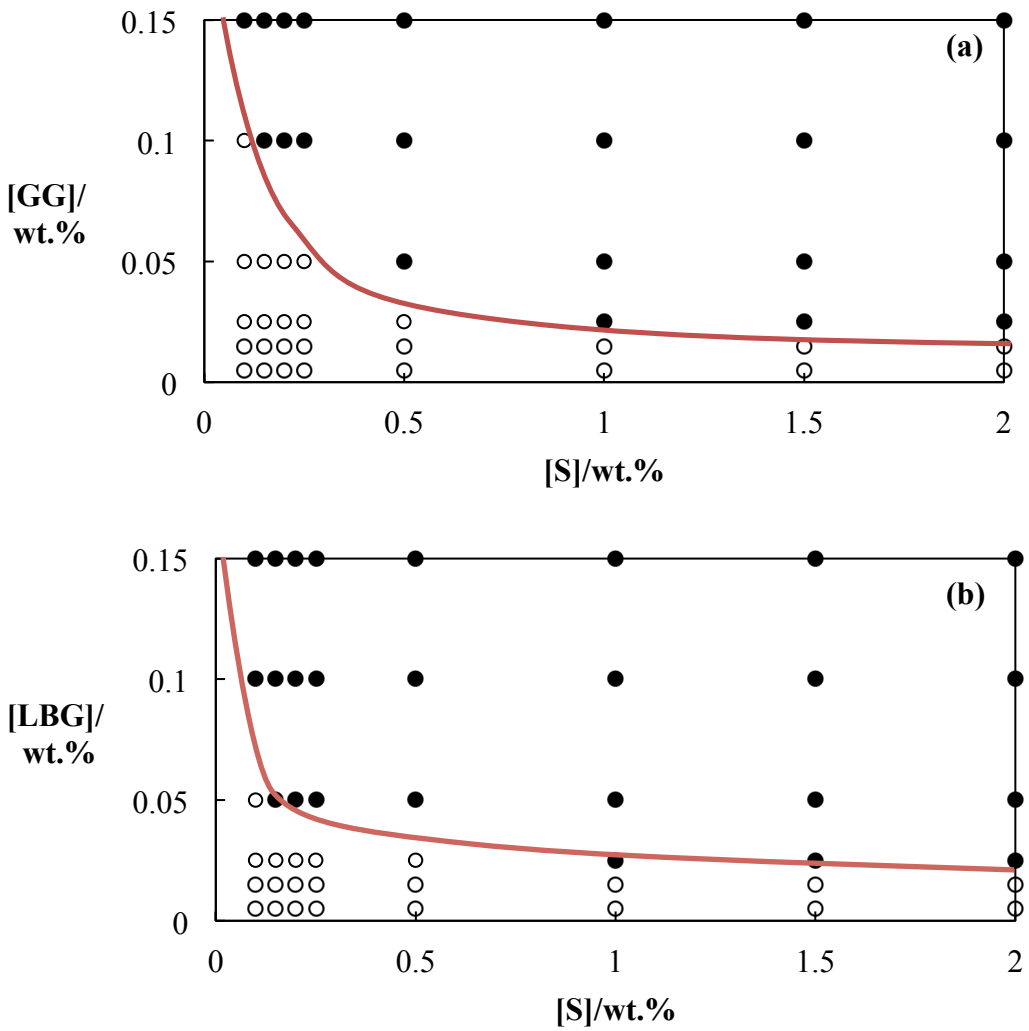

Figure 3-7 Phase diagram showing the estimated binodal (—) between single-phase (○) and biphasic (●) mixtures of (*a*) S + GG; (*b*) S + LBG, as determined by the centrifugation procedure described in the text.

Compositions below critical point where the mixtures had relatively low galactomannan contents (0.005-0.02 wt.%) and various [S] were found to exist as stable homogenous solutions with transparent visual appearance. Figure 3-7*a* indicates that at [GG] > 0.1 wt.% the mixtures exhibited biphasic behaviour at all starch concentrations studied, resulting in the binodal almost joining the gum axis. Although the LBG system (Figure 3-7*b*) appeared to give similar results to GG, LBG seems to have more

incompatibility with starch because the concentration of LBG where phase separation start to occur was lower than that with GG, i.e. [LBG] ≥ 0.05 wt.%. The binodal line of S + gum systems was close to the gum axis, indicating that starch is excluded from the gum-rich phase in this area. Phase separation was observed in a mixture containing 0.15 wt.% LBG and as low as 0.005 wt.% starch, which represented the limit for visual observation.

After the phase diagrams were constructed the same samples were then taken for further investigation. Figure 3-8 shows the volume of upper gum-rich phase after bulk phase separation against the initial gum concentration with different [S]. The volume of upper phase was measured in centimetres and converted to millilitres using basic equations for finding volume of cylinder and conical bottom:

$$V_{cylinder} = \pi r^2 h \qquad \text{Equation 3-1}$$

$$V_{cone} = 1/3\ \pi r^2 h \qquad \text{Equation 3-2}$$

Where π is 3.14, $V_{cylinder}$ is volume of the upper centrifuge tube (ml), V_{cone} is volume of the bottom of the centrifuge tube (ml), h is height measured (cm) and r is the radius of the cone which is 1.15 cm.

From Figure 3-8, as [S] increased, the volume of the upper gum-rich phase was decreased. The rate of phase separation also declined, which may be due to the rise in viscosity of the total mixture that slowed down the speed of phase separation of the total system. For example, at the highest concentration composition in the experiment, 2 wt.% S + 0.25 wt.% GG, the upper phase shows relatively low percentage of gum-rich phase volume. At [S] ≥ 1 wt.%, the volume of upper gum-phase is lower than 50 vol.%. In contrast, at [S] ≤ 0.5 wt.%, the viscosity of each polysaccharide was low which resulted in the volume of upper phase being high and very similar at all gum concentrations. At the same time, the vol.% of gum-rich phase also increased as the concentration of gum increases. This evidence supports the idea that the galactomannan is highly immiscible with starch. Regarding Figure 3-8*b*, the result of S + LBG system was similar to that of GG, however, the overall vol.% of upper phase were slightly higher than GG.

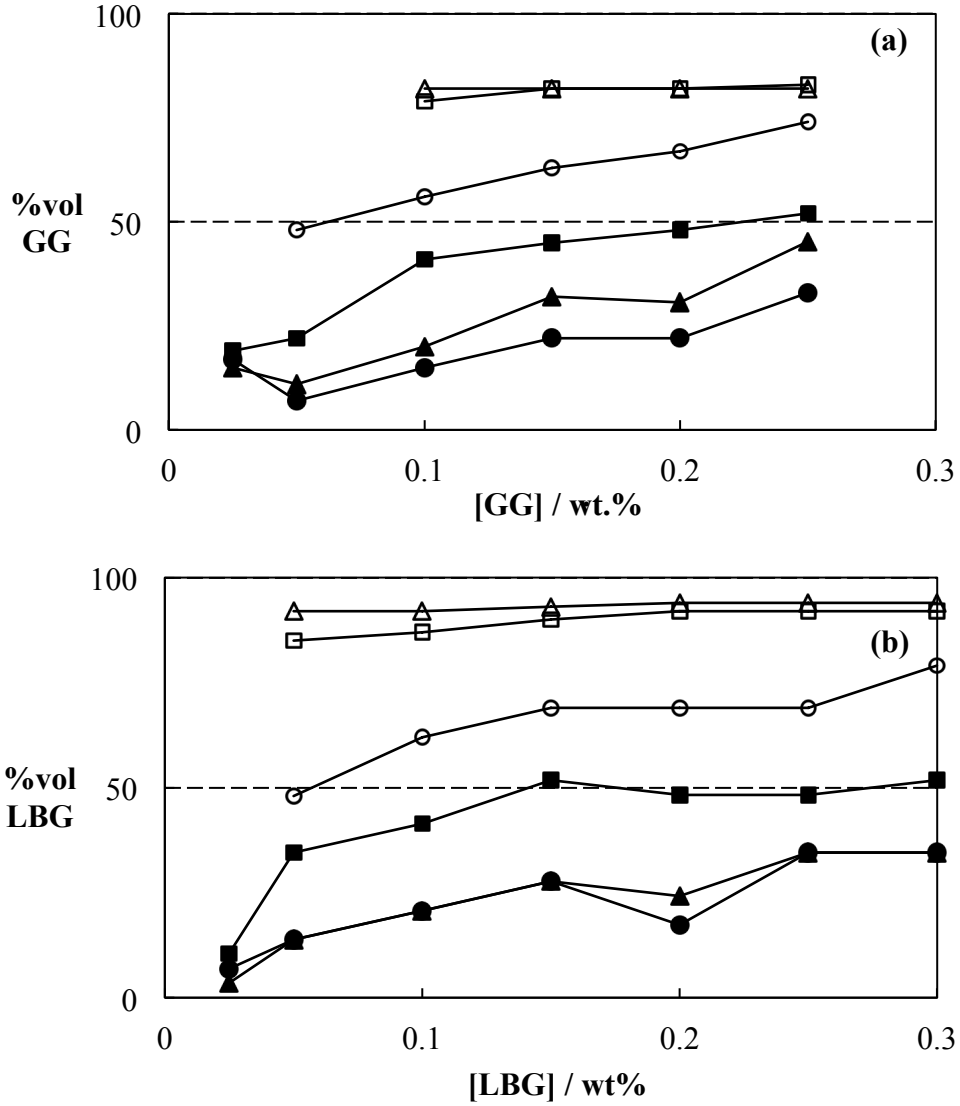

Figure 3-8 Volume of upper (*a*) GG phase and (*b*) LBG phase as a % of the overall volume (%vol gum) versus wt.% of galactomannan in the mixtures at different [S]: 0.15 (□); 0.25 (△); 0.5 (○); 1 (■); 1.5 (▲); 2 (●). The dashed line at 50% indicates initial %volume of gum solution (since equal volumes of solutions were mixed).

An initial assumption was made that upper phase does not entrap any significant amounts of starch, i.e., all of the galactomannan migrates to this region and practically all the starch exists in the lower layer. This hypothesis leads to the calculation of possible maximum concentration [GG'] and [LBG'] of GG and LBG in the top layer. The calculation uses the data from Figure 3-8 with basic dilution equation, see Equation 3-3:

$$C_1V_1 = C_2V_2 \qquad \text{Equation 3-3}$$

Where C_1 is the initial concentration of gum, C_2 is final concentration of gum, V_1 is original volume of gum in the mixture (7.5 ml or 50 vol.%) and V_2 is the final volume of gum after phase separation.

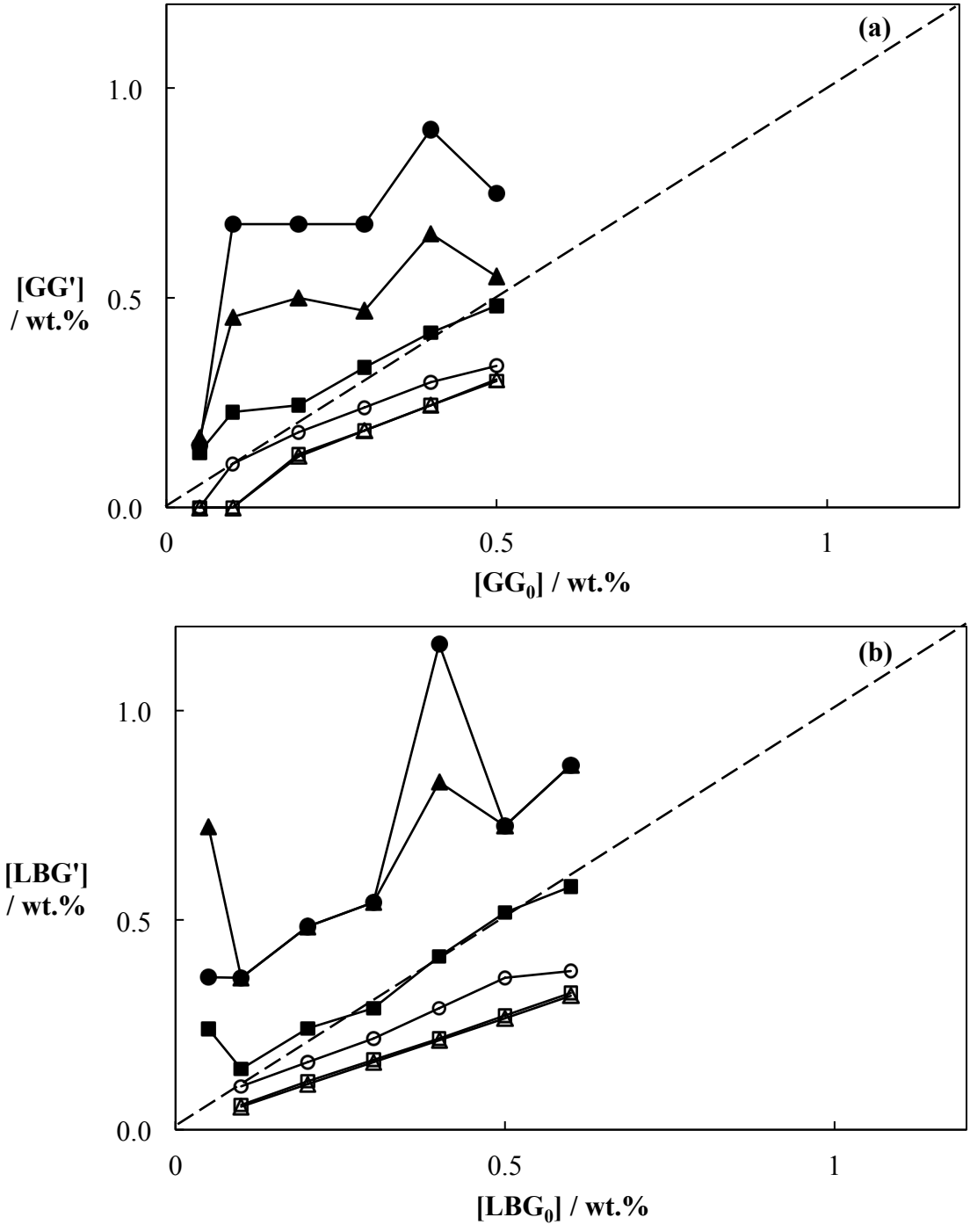

Figure 3-9 Hypothetical maximum concentration (*a*) [GG']; (*b*) [LBG'] of gum in the gum phase separated regions, calculated (see text) on the basis of Figure 3-8, versus initial wt.% of gum in the mixtures at different [S]: 0.15 (□); 0.25 (△); 0.5 (○); 1 (■); 1.5 (▲); 2 (●). Dashed line indicate the volume were [GG'] = [GG_0] or [LBG'] = [LBG_0].

Figure 3-9*a* shows calculated maximum concentration of [GG'] in gum-rich upper phase. It is seen that at [S] > 1 wt.%, the [GG'] >> [GG_0] whilst for [S] < 1 wt.% [GG'] can be < [GG_0]. [GG_0] and [LBG_0] refer to initial concentration of gum before mixing with starch. It is important to understand these concentration effects at higher [GG] or [LBG] where the phase separation is stronger (but the rate of phase separation is slower) because the [GG] (or [LBG]) will strongly affect the viscosity of both polysaccharides and the micro-viscosity of the evolving gum-rich domains.

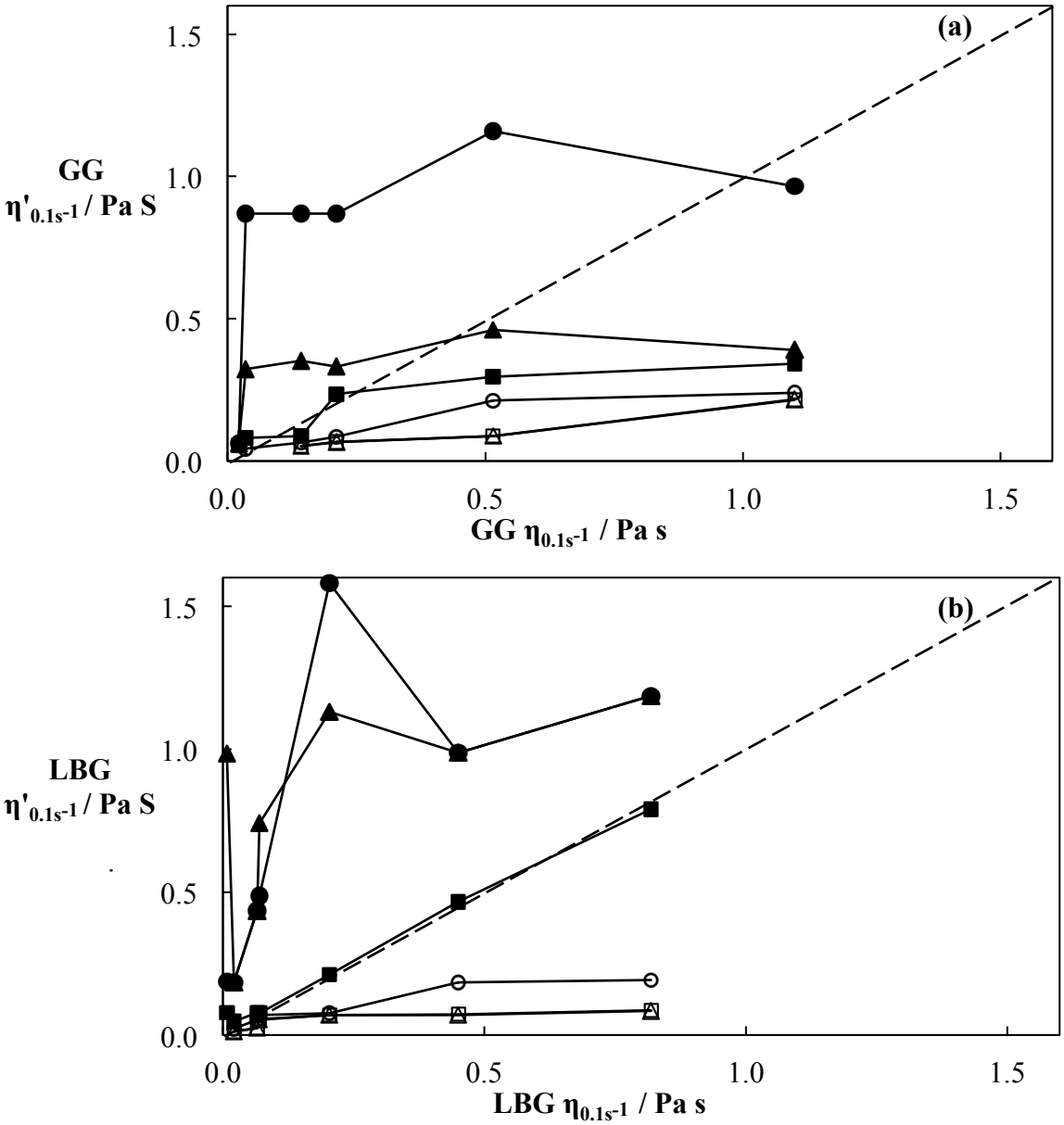

Figure 3-10 Hypothetical maximum viscosity (η') at $\dot{\gamma} = 0.1s^{-1}$ of the (*a*) GG; (*b*) LBG phase separated regions, calculated (see text) on the basis of Figure 3-4 and 3-9, versus viscosity (η) of the original gum phase after mixing with different [S]: 0.15 (□); 0.25 (△); 0.5 (○); 1 (■); 1.5 (▲); 2 (●). The dashed diagonal line indicates the case where η' = η.

Since a shear rate = 0.1 s^{-1} is a relatively low shear rate, the viscosities from Figure 3-4 may be taken as an indication of the 'zero' shear rate. In other words, the viscosity at rest. Therefore, it is instructive to take the hypothetical maximum [GG'] and [LBG'] from Figures 3-9 and combine them with the data obtained from Figure 3-4 to calculate a predicted viscosity of upper gum-rich phase. The results are shown in Figure 3-10*a* and Figure 3-10*b* for GG and LBG respectively with varying [S]. From the graphs, it can be predicted that the increase in the gum concentration leads to a significant increase in the viscosity of upper phase.

At [S] ≥ 1.5 wt.%, it is seen that viscosity of the predicted gum-rich phase ($\eta'_{0.1s^{-1}}$) could be different from the viscosity of the original gum solution ($\eta_{0.1s^{-1}}$), however $\eta'_{0.1s^{-1}}$ still strongly dependent upon initial gum concentration (Figure 3-4), hence above critical concentration of gum, means that $\eta'_{0.1s^{-1}}$ could be very much higher indeed. Increasing microviscosity is expected to slow down the rate of phase separation and in the extreme may inhibit it so greatly that separation is not evident over short time-scales, giving the apparent illusion of mixing. This is one reason why centrifugation to speed up the equilibrium phase separation was needed.

3.3.3 Measured viscosity of each layer in the mixtures

Table 3-1 Measured viscosity η of starch + galactomannan mixtures

Polysaccharide mixtures	Measured viscosity $\eta_{0.1s-1}$ (Pa s)	
	Top layer	Bottom layer
2 wt.% Starch + 0.25 wt.% GG	0.615	0.309
2 wt.% Starch + 0.3 wt.% LBG	1.553	0.238

The real viscosity of the top and bottom layers of starch + galactomannan mixtures has been measured for selected systems. The mixtures were stored for 3 days before measurement. The concentration of S + GG and S + LBG were fixed at 2 wt.%, 0.25 wt.%, 2 wt.% and 0.3 wt.%, respectively, since these concentrations were used in subsequent work as a model system. The starch-rich phase shows similar values of viscosity in both GG and LBG mixtures. However, the GG-rich phase was slightly lower than hypothetical maximum concentration, which could mean that not all GG is in the upper phase. On the other hand, the measured LBG-rich phase viscosity was significantly higher than the maximum viscosity calculated, suggesting that the LBG is in this phase was self-associated or in some way that fractionation of high molecular

weight polymer had occurred. This gel formation of LBG when mixed with another substance also agrees with the theory mentioned in the introduction and also supports the result in section 3.3.2. As discussed in chapter 1 section 1.10.3, LBG consists of mannan backbone and galactose side chains. The structure is composed of a smooth zone and a hairy zone. This smooth region could undergo self-aggregation resulting in gel formation or it is possible that the synergic interaction between starch and LBG occurred which resulted in the formation of mixed junction zones (Grenha and Dionísio, 2012). However, the gelation of LBG is not rapid enough to prevent the phase separation from developing two-coexisting phases.

3.3.4 Interfacial tension measurement

In order to calculate the surface tension, the density of starch and galactomannan gum solutions were measured. 4 wt.% S, 0.5 wt.% GG and 0.6% LBG were tested at two different temperatures (20 °C and 60 °C). The result is shown in Table 3-2.

For W/W emulsion the interfacial tension was predicted to be very low, hence the spinning drop was introduced to measure the interfacial tension of the polysaccharide mixtures. This method has been developed for measuring ultralow interfacial tension. The analysis is based on the shape of a suspended drop of less dense liquid (ρ_1) in more dense liquid (ρ_2) while rotating the capillary at known speed. The elongation of the droplet is stopped when the forces of centrifugal and surface tension balance. The interfacial tension can then be calculated from Vonnegut's fundamental equation:

$$\gamma = \frac{1}{4} r^3 \Delta\rho\omega^2 \qquad \text{Equation 3-4}$$

where γ is interfacial tension, ω is angular velocity, Δρ is the difference between the densities of the droplets and of the surrounding liquid and *r* is radius of droplet.

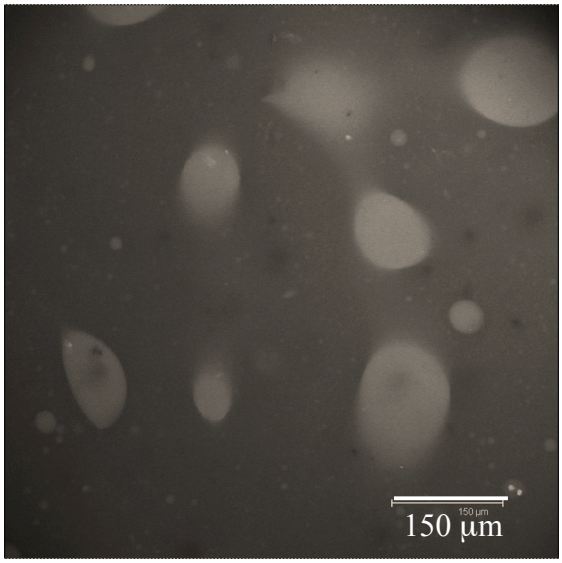

Figure 3-11 Representative confocal micrographs of mixture of 2 wt.% S + 0.3 wt.% LBG. The system was observed at 24 h. Dark regions are gum-rich phase and brighter regions are starch-rich phase.

From the micrograph in Figure 3-11, starch was assumed to be the dispersed phase whereas gum was a continuous phase. Therefore, to make high-density galactomannan, heavy water (D_2O) was used instead of phosphate buffer during preparation stage – see Table 3-2. The GG or LBG solution in D_2O was used to fill the spinning drop capillary. A starch drop was later injected slowly into the capillary while the capillary was rotating. However, as soon as starch was introduced in the capillary, it was rapidly difused in the surrounding gum solution at all rotation speed. This phenomenon indicated ultralow interfacial tension. Thus the radius of the starch droplet could not be measured.

Density

Table 3-2 Measured density of starch, GG and LBG at 20 °C and 60 °C.

Polysaccharide	Temperature	
	20 °C (g/cm^3)	60 °C (g/cm^3)
0.5 wt.% GG in D_2O	1.0990	1.0930
0.6 wt.% LBG in D_2O	1.0985	1.0908
0.5 wt.% GG in H_2O	0.899	0.7990
0.6 wt.% LBG in H_2O	0.885	0.7930
4 wt.% S in H_2O	1.0131	1.0097

3.3.5 Effect of changing pH

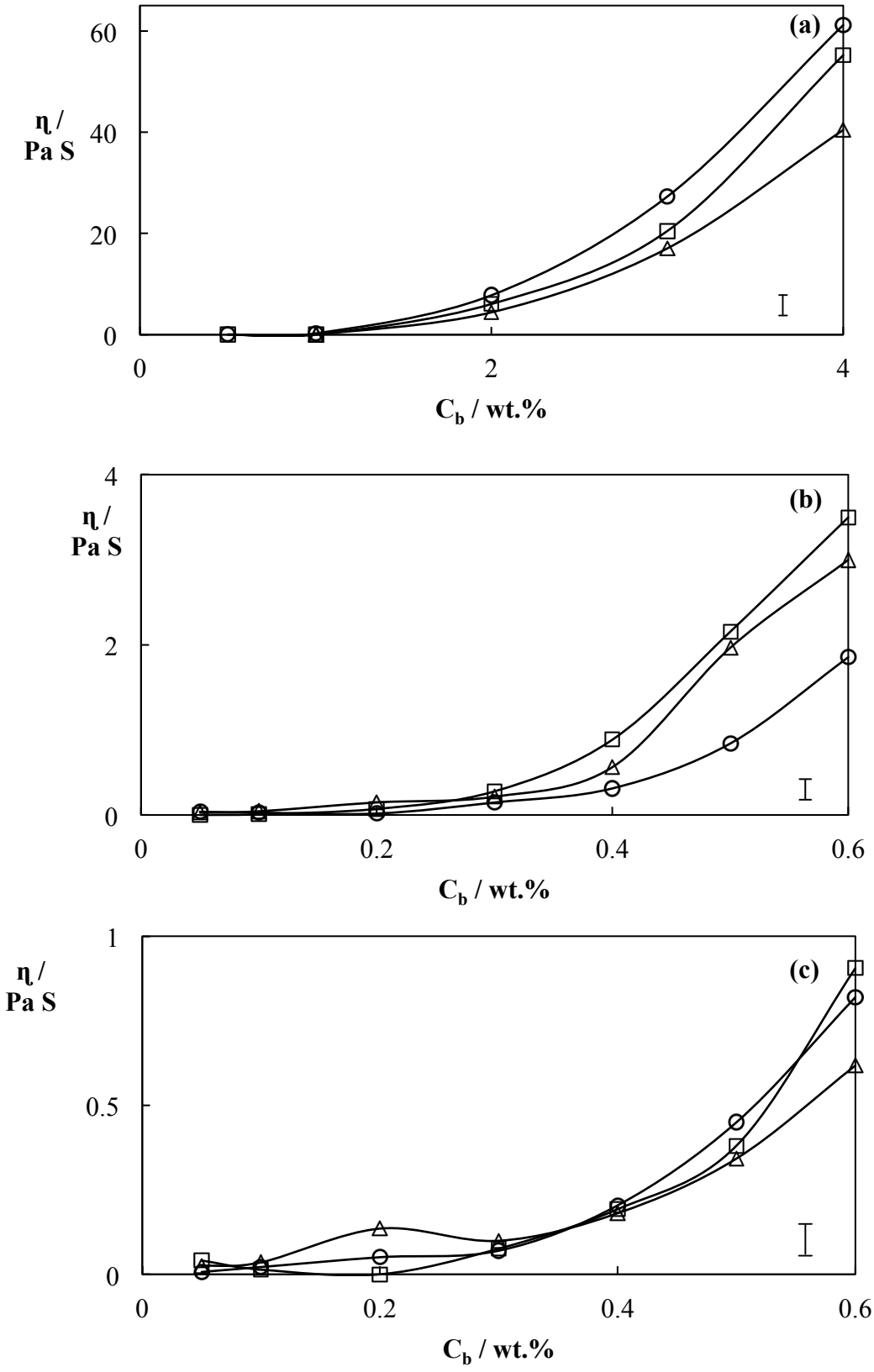

Figure 3-12 Viscosity at $\dot{\gamma}$ = 0.1 s^{-1} versus wt.% concentration [C_b] of different biopolymers: (*a*) waxy corn starch; (*b*) GG; (*c*) LBG at different pH; pH7 (○); pH8 (△); pH5.4 (□). "I" indicates standard error bar.

The purpose of this experiment was to study the effect of the pH conditions on each polysaccharide solution. The pH of starch, GG and LBG were varied between 5.4, 7 and 8. Figure 3-12*a* and Figure 3-12*b* show that changing pH of starch and GG could alter its viscosity. Although all the polysaccharides used in this study are generally accepted as non-ionic polymers, since they are from natural sources, the change in viscosity could be ascribed to the presence of charged contaminants (e.g., protein). In addition, some hydroxyl groups in GG structures could become ionised at extreme pH. The molecules will then expand due to intra chain electrostatic repulsion, hence increase in viscosity of solution is expected (Goycoolea *et al.*, 1995). In contrast, LBG (Figure 3-12*c*) was only slightly affected by changing pH within the range of pH 3-11 (Grenha and Dionísio, 2012). There was no significant change in viscosity. At low concentrations of all polysaccharides, i.e. [S] ≤ 2 wt.%, [GG] and [LBG] ≤ 0.3 wt.% the viscosity remained similar.

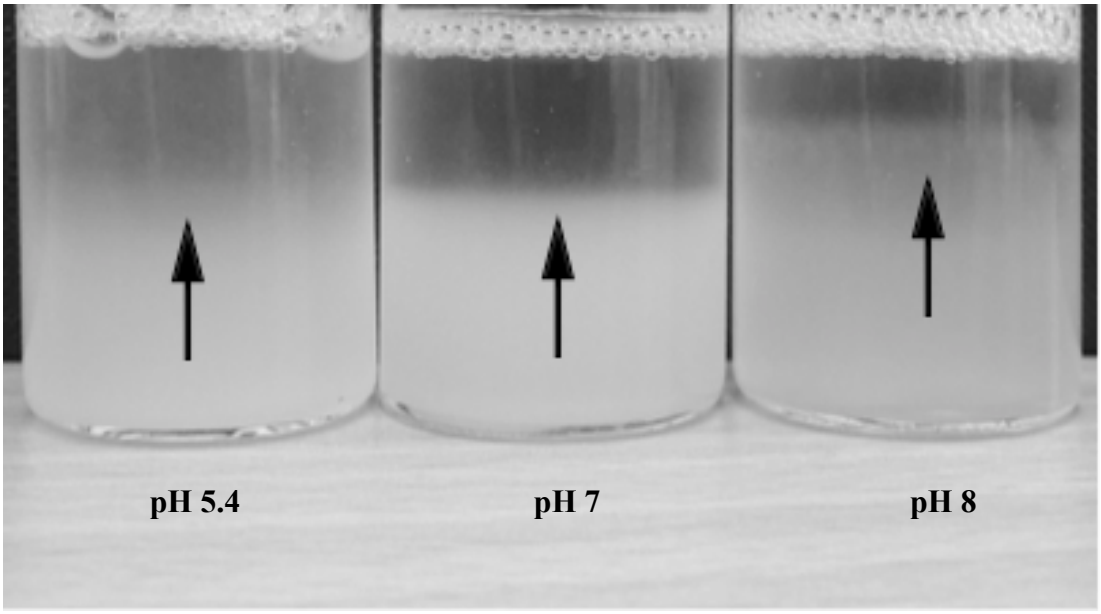

Figure 3-13 Visual observation of 2 wt.% S + 0.25 wt.% GG after strorage at room temperature under normal gravity for 3 days. From left to right: pH 5.4, pH 7 pH 8. Arrow indicates boundary between two-phase.

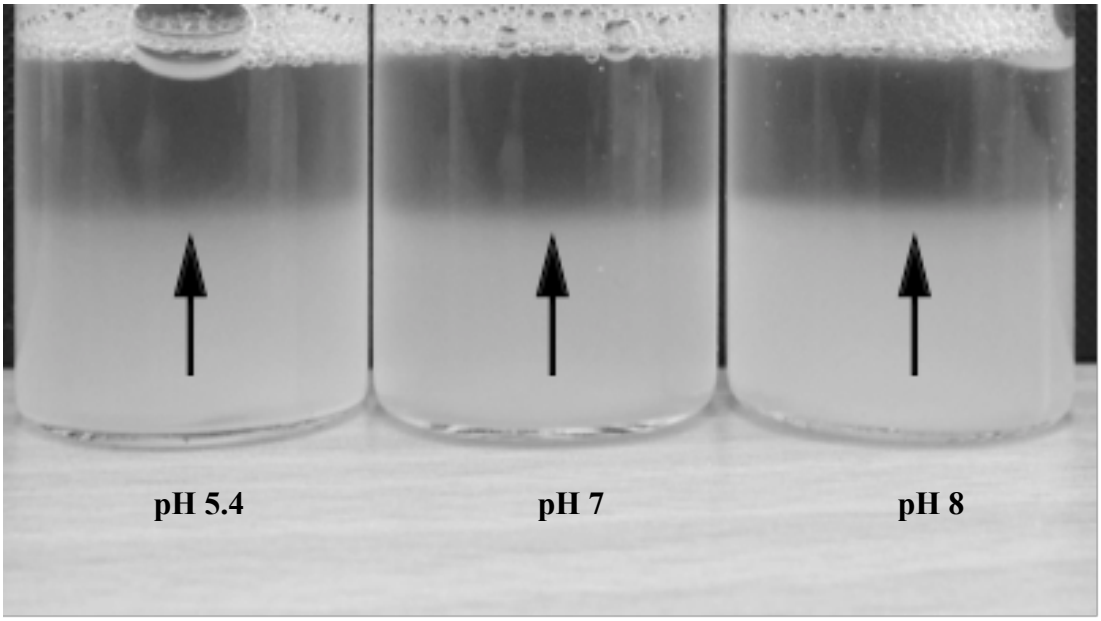

Figure 3-14 Visual observation of 2 wt.% S + 0.3 wt.% LBG after strorage at room temperature under normal gravity for 3 days. From left to right: pH 5.4, pH 7 pH 8. Arrow indicates boundary between two-phase.

After varying the pH, the same volumes (1:1 ratio) of each polysaccharide were mixed and stored at ambient temperature for 3 days before observing the phase

separation. It appeared that phase compositions of 2 wt.% starch + 0.25 wt.% GG were affected by the change in viscosity and pH, (see Figures 3-13). Phase boundaries of the mixtures at pH 5.4 and 8 were not clear and slightly shifted toward GG phase. According to Figure 3-12*b*, there is a possibility that viscosity of GG, that changes with pH, affected the speed of phase separation. On the other hand, Figure 3-14 confirmed that adjusting the pH was not interfering with the speed of phase separation of 2 wt.% starch + 0.3 wt.% LBG mixtures.

3.3.6 Microscopic observations on phase separation

In section 3.3.2, phase separation of polysaccharide mixtures was determined and the composition of the mixtures was mentioned. Figure 3-15 shows the CLSM micrograph under transmission mode of top phase and bottom phase respectively. Transmission mode in CLSM gives the same result as conventional light microscope so there is no fluorescent labelling needed. As expected, the top gum-rich layer displays very little structure apart from a few particles which are assumed to be insoluble materials that remain in the solution after the removal stage. Image from the bottom layer shows signs of swollen starch granules dispersed throughout the area observed, which confirm that it is starch-rich bottom phase.

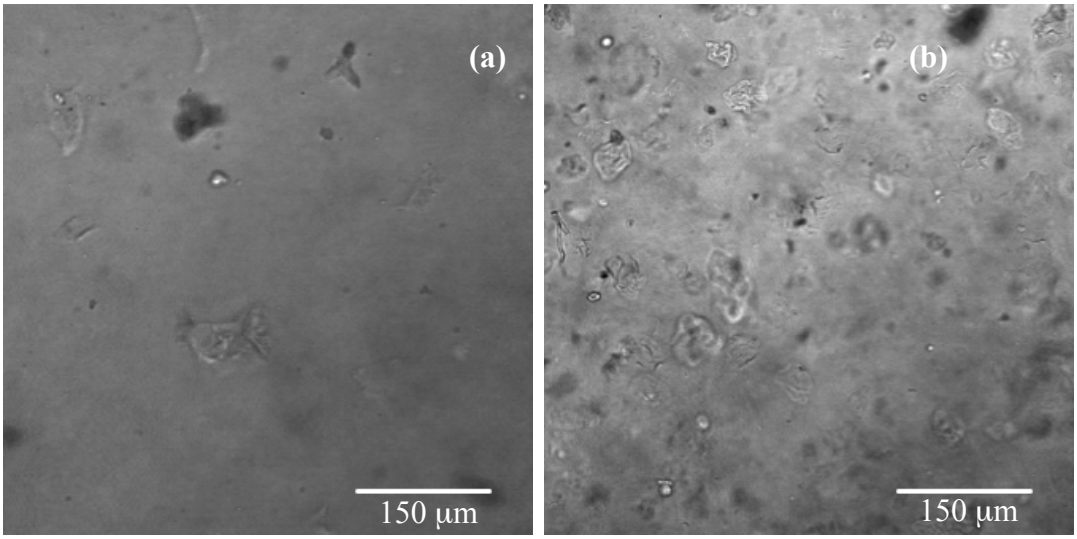

Figure 3-15 CLSM images of (*a*) upper LBG-rich phase; (*b*) lower starch-rich phase in transmission mode.

As the mixtures contain two non-ionic polysaccharides, it is difficult to find fluorescent dyes that stain one and not the other. In an early stage of the experiments, rhodamine B (RB) and methylene blue (MB) were used to stain starch and gum respectively. The images obtained showed similar differences with or without MB. Moreover, as the observation ran for over 24 hours, MB was bleached within 20 hour of observation due to its photosensitivity, hence only RB was used in the later stages of experiments.

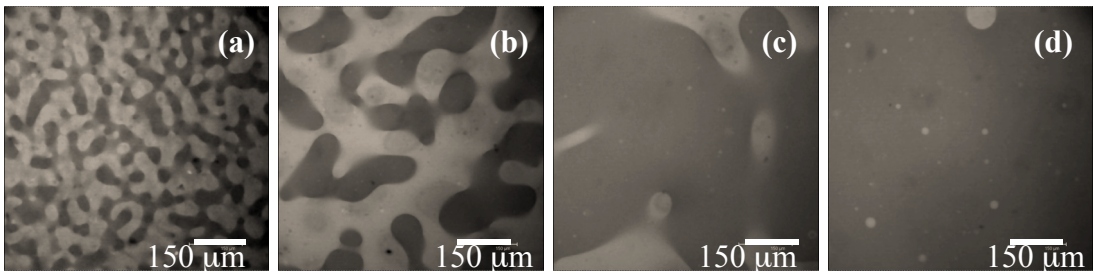

Figure 3-16 Representative confocal micrographs of mixture of 2 wt.% S + 0.25 wt.% GG. The system was observed at different times (*a*) 5min; (*b*) 10 min; (*c*) 20 min; (*d*) 24 h.

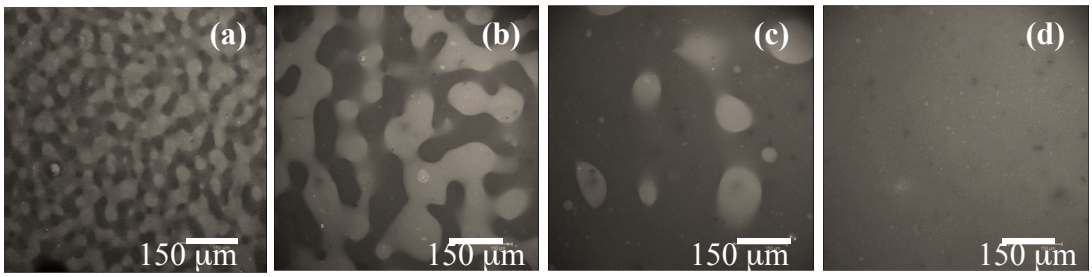

Figure 3-17 Representative confocal micrographs of mixture of 2 wt.% S + 0.3 wt.% LBG. The system was observed at different times (*a*) 5min; (*b*) 10 min; (*c*) 20 min; (*d*) 24 h.

The visually observed phase separation phenomenon between starch + galactomannan was confirmed by CLSM. Figure 3-16 and 3-17 show typical CLSM micrographs of polysaccharide mixture containing 2 wt.% starch + 0.25 wt.% GG and 2 wt.% starch + 0.3 wt.% LBG, respectively. By labeling one of the polysaccharides, it was possible to visualise the polysaccharide-rich zones in the mixtures by CLSM. The starch-rich region was non-covalently labelled with RB. In this mixture composition the ratio of the volumes of gum-rich and starch-rich layers is about 1:3. This was concluded from the thickness of the layers after full separation via centrifugation. The first image was captured within 5 minutes after mixing. The low interfacial tension of these

polysaccharide mixtures resulted in difficulties in forming conventional W/W emulsion (Shum *et al.,* 2012), e.g. nucleation and growth hence phase separation of these mixtures showed a bi-continuous structure. Even after a short ageing time, microscopically the system showed significant phase separation, possessing morphology typical of a spinodal decomposition mechanism. During spinodal decomposition regime, unstable starch domains grow and sink into the bottom of the container until the mixture is well separated by an interface.

In real time the system was quite dynamic, with movement and fusion of the bright (starch-rich) domains and parallel growth of the dark background (gum-rich) domains. The characteristic length (L), i.e., characteristic distance between the starch domains was calculated via the two-dimensional fast Fourier transforms (2D-FFT) as described in chapter 2, section 2.6.2. After 5 minutes L was around 60 ± 2 μm for both gum mixtures. The starch domains within the same systems then grew rapidly, 10 minute after mixing, to ca. > 150 μm - see Figure 3-16*b* and 3-17*b*. When the starch regions grow to a certain size they will start to sink down to the bottom of the slide. Figure 3-16*d* and 3-17*d* shows that 30 minute later no such regions were evident, just an ill-defined background of faint 'blobs' of a wide size range but all below ca. 50 μm. Within this ageing time and the small height (3 mm) of the sample well, almost complete stratification of the galactomannan and starch occurs. The small background blobs may represent the small fraction of starch that still remains within the bulk gum phase.

3.4 Conclusions

The results clarified that both GG and LBG exhibited similar rheological properties, in the range of concentrations and shear rates studied. All polysaccharide solutions exhibited shear-thinning behaviour. There was evidence that LBG formed a gel when mixed with starch. However, the kinetics of this gel formation was not rapid enough to stabilise the system. The phase diagrams for S + LBG and S + GG blends showed the binodal lines that nearly coincide with the axes representing the polysaccharide concentrations which demonstrates the incompatibility of these systems. The rate of phase separation also depends largely on the viscosity of each solution. The

interfacial tension of these mixtures was unable to be determined with the method used which indicated low interfacial tension. The predicted maximum viscosity values of upper gum-rich phase were different from the measured values. For GG mixture the values were slightly lower whereas for LBG mixtures values were somewhat higher than the predicted value. There is no significant effect of changing pH on the viscosity of LBG solution. Whilst, for GG and starch, the viscosities were slightly changed which could be from its natural contamination. Microscopic observation via CLSM revealed phase separation of starch + gum mixtures via spinodal decomposition. The bicontinuous microstructure of the starch domains grew rapidly and within 30 minutes the mixtures were completely phase separated in the welled slides.

Chapter 4

4 Chapter 4. Effect of silica nanoparticles on phase separation of waxy corn starch + locust bean gum or guar gum

4.1 Introduction

As starch + non-starch hydrocolloid mixtures are commonly used as texturing agents, their rheological properties are their most studied aspects. Although the existence of a thermodynamically incompatible mixture of waxy corn starch + non-starch hydrocolloid (i.e. galactomannan) has been studied previously (Closs *et al.*, 1999), much less work has been carried out on the process of stabilising these W/W emulsions. In order to stabilise an emulsion a suitable substance must be added to the system. One method of potentially controlling phase separation is to use particles that strongly adsorb at the interface, whereby solid particles protect the dispersed phase from coalescing. For example, in 1907, Spencer Pickering had shown that oil-water emulsion (paraffin-water) can be stabilised by basic sulphate of copper (solid particulate emulsifiers). Surprisingly, there was little work in this area after the discovery (Chevalier and Bolzinger, 2013), until the last decade where uses of particles as stabiliser has received renewed interest.

In a conventional Pickering emulsion, the presence of closely packed particles around dispersed droplets is required whereas bijels are non-equilibrium stabilised emulsions which form through arrested spinodal decomposition structure. Solid particles are likely to reside in one of the liquids, and this would become the dispersed phase in bijels network (Finkle *et al.*, 1923). Apart from wetting properties, the effectiveness of using particles in stabilising the emulsion also depends upon the particle shape, size, inter-particle interaction and emulsion medium (Hunter *et al.*, 2008).

Most of the works on stabilising emulsions commonly involved model particles, such as silica (Binks and Lumsdon, 2000; Binks and Whitby, 2005; Witt *et al.*, 2013; Murray and Phisarnchananan 2014) or latex particles (Firoozmand *et al.* 2009a; Destribates *et al.*, 2014a; Zhu *et al.*, 2014) as their surface-active properties can be changed by chemical modification. For example, Clegg *et al.* (2005) found

that alcohol-oil emulsions can be stabilised by up to 1 vol.% silica particles. In an oil-water system the interfacial tension can be significantly high and it appears that the energy barrier (ΔE) can easily reach millions of k_BT (k_B is the Boltzmann constant and T is the absolute temperature) per particle (Binks and Horozov, 2006; de Folter, *et al.* 2011; Destribats *et al.* 2014; Murray and Phisarnchananan 2014).

However, with polysaccharide-polysaccharide systems both phases are aqueous and the W/W interfacial tension can be extremely low ($\gamma = 10^{-4} – 10^{-6}$ N m^{-1}: Shum *et al.,* 2012; Hanazawa and Murray, 2013) so that the particle detachment energy is rather weak (Firoozmand *et al.*, 2009a). Therefore, it is assumed that such particles may not be as effective in stabilising the W/W emulsion. Nevertheless, Firoozmand *et al.* (2009a) and Balakrishnan *et al.* (2012) reported that latex particles have an ability to stabilise W/W systems, i.e. for starch + gelatin and dextran + polyethylene oxide phase separating systems, respectively. These systems also showed an accumulation of latex particles at a W/W interface.

The system containing starch + LBG or GG in the absence of particles was demonstrated in detail in chapter 3. Since this system demonstrated a phase-separated network via spinodal decomposition, there is a need for further investigation on adding model colloidal particles to the system in order to observe the change that may occur. This chapter focuses on using a range of fumed silica particles of varying surface hydrophobicities in the specific mixtures to see if they have any effect on the polysaccharide phase separation. Raw fumed silica particles are hydrophilic but they can be chemically modified to give different hydrophobicity. Although the primary size of fumed silica particles is 20 nm in diameter, they can be considered as sub-micron particles with hydrodynamic radius of about 150 nm (Zang *et al.*, 2010) because once they form aggregates they are irreversibly fused together (Chevalier and Bolzinger, 2013). The hypothesis was that silica particles might bind to the interface and prevent droplets of polysaccharide from coalescing, thus causing the system to be uniform for longer period of time. Although only non-modified silica in a certain size range is permitted as a food additive (Berton-Carabin and Schroën, 2015), the objective is to demonstrate the principle of control of polysaccharide-polysaccharide phase separation using solid particles.

4.2 Materials and methods

4.2.1 Materials

Waxy corn starch, GG, LBG, phosphate buffer Aridine Orange (AO) and Rhodamine B (RB) used in the experiments in this chapter are the same as those stated in chapter 2, section 2.1.

Food grade silica particles

They were a gift from Professor Jianshe Chen, University of Leeds. The nominal particles size was 3 μm.

4.2.2 Methods

Preparation of solution

All solutions were prepared according to the standard protocol stated in chapter 2, section 2.2. All the investigated samples contained 2 wt.% starch, 0.25 wt.% guar gum (GG) and 0.3 wt.% locust bean gum (LBG) with or without the presence of varying concentration of silica particles (0.5 - 1 wt.%).

Determination of phase separation

Two methods were used to compare systems. In the first method, the mixtures were left to reach equilibrium under normal gravity for 45 days. The second method, mentioned in chapter 3 section 3.2.2 was where the samples were centrifuged at 4200 rpm in a Beckman Coulter Allegra X-22 for an hour. After centrifugation the samples were taken for analysis under the confocal microscope in order to identify the components in each layer. Each layer was carefully withdrawn with a syringe and labelled with RB or AO.

Confocal laser scanning microscopy (CLSM)

For polysaccharide mixtures intended for confocal microscopy, AO was added to either phase that contained silica particles before blending with the other solution. The mixtures were then placed on a welled slide 30 mm diameter and 3 mm in depth. The first image was captured 5 minutes after blending the mixtures. The appearance of samples was recorded again at 0.5, 3, 6 and 24 hours.

Bulk rheology

The rheological properties of S, LBG or GG solution plus 100SiOH silica particles at [C_p] = 0 - 3 wt.% have been investigated at 25 ^{o} C. Rheological measurements were performed as stated in chapter 2, section 2.5.

4.3 Results and discussion

4.3.1 Determination of phase separation

Various investigations on phase separation of starch + galactomannan mixtures were described earlier in chapter 3. As GG and LBG appeared to behave so similarly only the S + LBG systems were investigated in detail in the presence of fumed silica nanoparticles. The individual particles had a radius of 20 nm, except for food-grade silica particles that had radius of 3 μm. A range of intermediate hydrophilicities with 100-, 80-, 70- and 65-SiOH groups were used for fumed silica and only one type of food-grade silica was used.

Figure 4-1 shows the series of 2 wt.% S + 0.3 wt.% LBG mixtures of equal volume (total volume = 15 ml) in the presence and absence of two different concentrations of silica particles [C_p], i.e. left column [C_p] = 0.5 wt.% and right column [C_p] = 1 wt.%. Pure mixtures of S + LBG in the absence of particles showed macroscopic phase separation of almost equal volumes of top gum-rich phase and bottom starch-rich phase after centrifuged at 4200 rpm for 1 hour. At the same time, the mixtures with the presence of silica particles were separated into three distinctive layers with a translucent lower phase, a transparent middle phase and an upper clear phase. The colours of the top and bottom layers were similar to the pure mixtures without particles. Hence, the lower phase was assumed to be starch-rich phase, an upper phase assumed to be LBG-rich phase and middle phase assumed to be silica sol. This latter assumption was subsequently confirmed via CLSM.

After the centrifugation, one of the samples, 2 wt.% starch + 0.3 wt.% LBG + 0.5 wt.% 100-SiOH, was analysed further under CLSM in order to identify the components of each layer, see Figure 4-3. Both RB and AO were used to stain each layer.

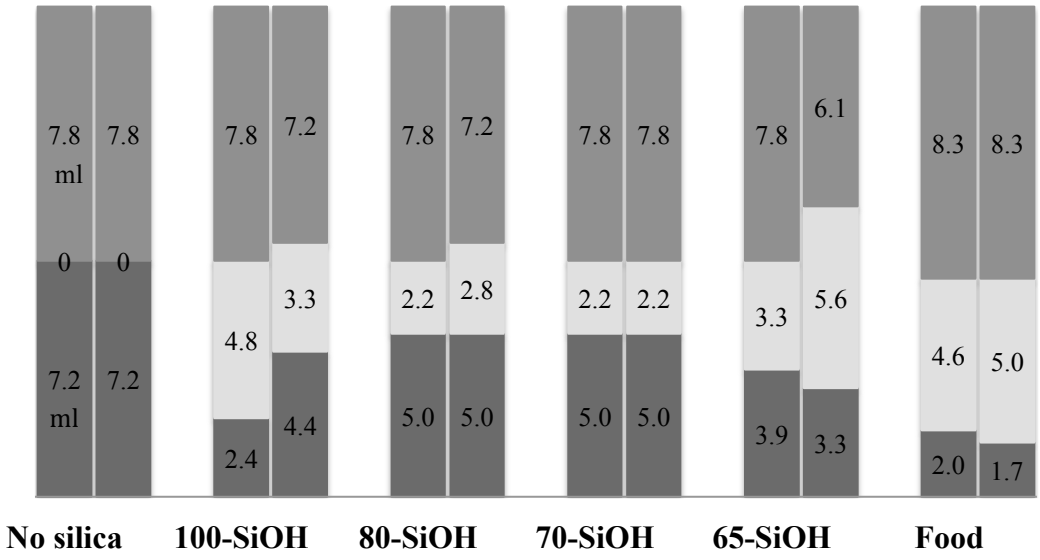

Figure 4-1 Visual observation of centrifuged samples of 2 wt.% S + 0.3 wt.% LBG with the presence of silica particles of varying surface hydrophobicities. From left to right: no partic les; 100-SiOH; 80-SiOH; 70-SiOH; 65-SiOH; food-grade silica particles. Left column = 0.5 wt.%; right column = 1 wt.%. Total volume = 15 ml.

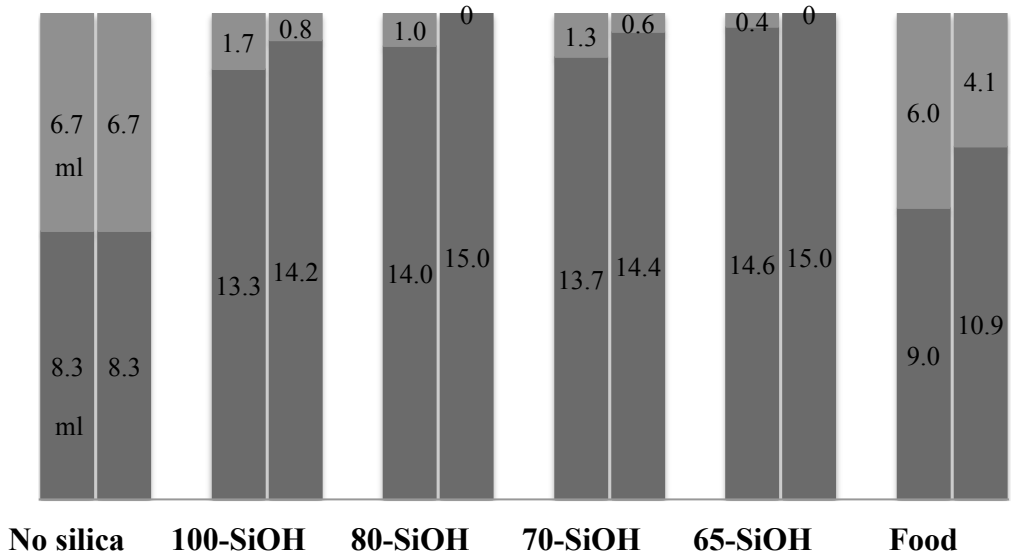

Figure 4-2 Evolution of W/W emulsions formed by S + LBG with the presence of silica particles of varying surface hydrophobicities after leaving under gravity for 45 days. From left to right: no particle; 100-SiOH; 80-SiOH; 70-SiOH; 65-SiOH; food-grade silica particles. Left column = 0.5 wt.%; right column = 1 wt.%. Total volume = 15 ml.

Figure 4-3*a* shows a blank background with no sign of starch granules or silica particles which suggests that this top layer is a gum-rich phase. Figure 4-3*b* displays bright specks that are likely to be silica particles. The bottom layer, on the other hand, shows signs of bright swollen starch granules. The small dark regions may represent the small fraction of LBG or silica sol that still remains within the bulk S phase.

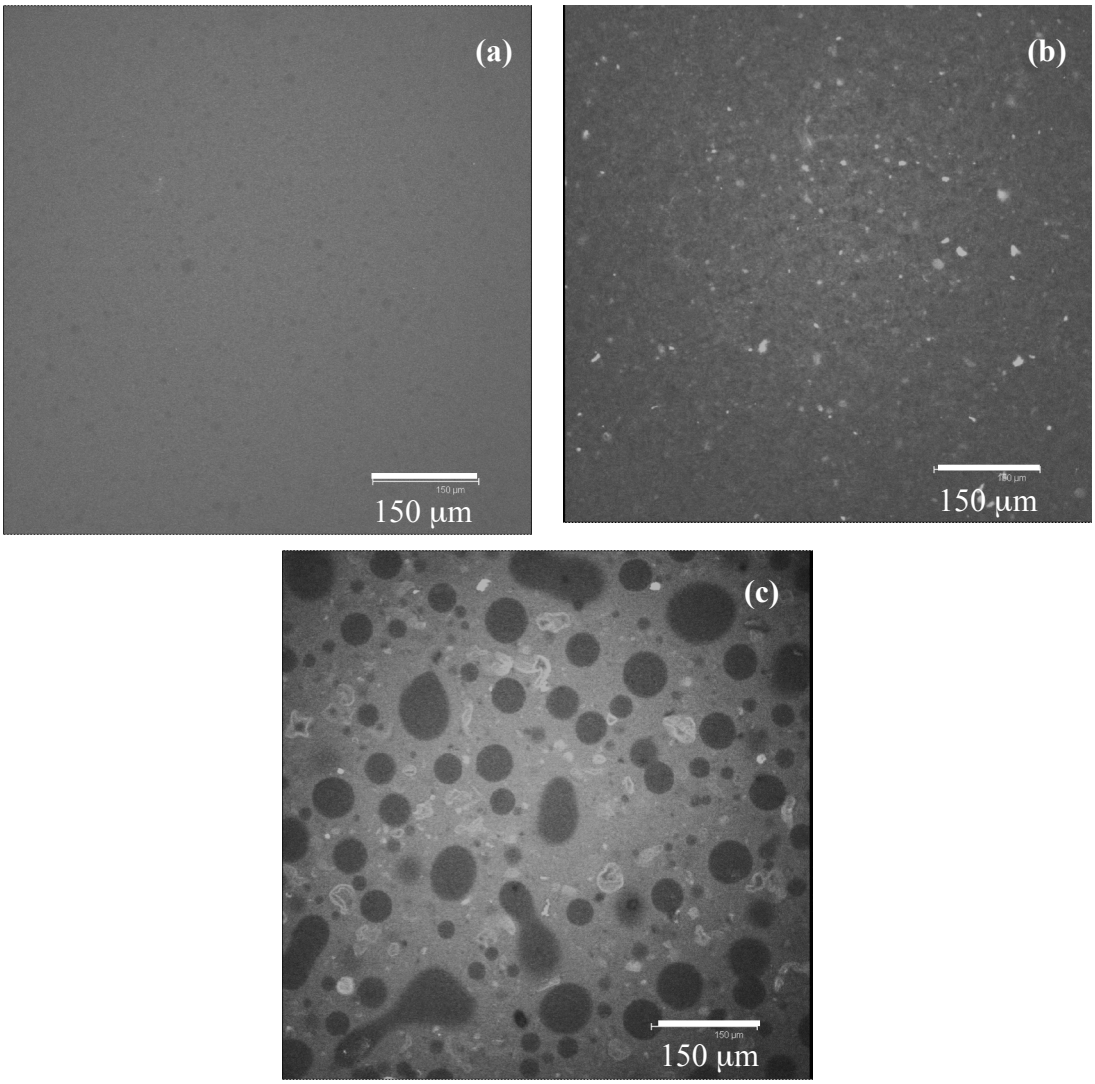

Figure 4-3 Representative confocal micrographs of each layer of centrifuged mixtures of 2 wt.% starch + 0.3 wt.% LBG + 0.5 wt.% 100-SiOH; (*a*) top layer; (*b*) middle layer; (*c*) bottom layer.

Regarding the large distinctive middle phase in the S + LBG mixture in the presence of 100-SiOH, 65-SiOH and food-grade silica particles, see Figure 4-1. As 65-SiOH particles are highly hydrophobic and both polysaccharides are water-based

solutions, there was a high incompatibility between solutions and particles leading to a high volume of silica sol in the middle phase. On the other hand, hydrophilic particles like 100-SiOH and food-grade silica particles might be expected to be compatible with either the gum or starch phase. However, there is currently no obvious explanation why the systems containing these particles also show a significant silica sol phase.

Figure 4-2 shows the same mixture composition as Figure 4-1 after leaving to reach equilibrium under normal gravity for 45 days. In the presence of 0.5 wt.% of 100-, 80-, 70- and 65-SiOH silica particles, the phase separation was significantly altered. Using particles of different silanol content reveals that the volume of gum-rich phase decreased progressively with particle hydrophobicity. For model silica particles, as the concentration of particles increased the more effectively phase separation was inhibited. All mixtures containing model silica particles exhibited almost homogeneous emulsion. Especially at $[C_p]$ = 1 wt.% for the 80- and 65-SiOH, the samples appeared homogeneous for a period of months and/or years. For food-grade silica particles, the mixture showed the weakest affect of particle stabilisation. The explaination will be discussed below in section 4.3.2.

Leaving the samples to separate under normal gravity gave only two distinctive layers, whereas centrifuging the mixtures apparently interferred with the reaction between particles and each polysaccharide. Thus accelerated phase separation via centrifugation seems to affect the process of particle-stabilisation of the W/W emulsions.

4.3.2 Microscopic observations of phase separation

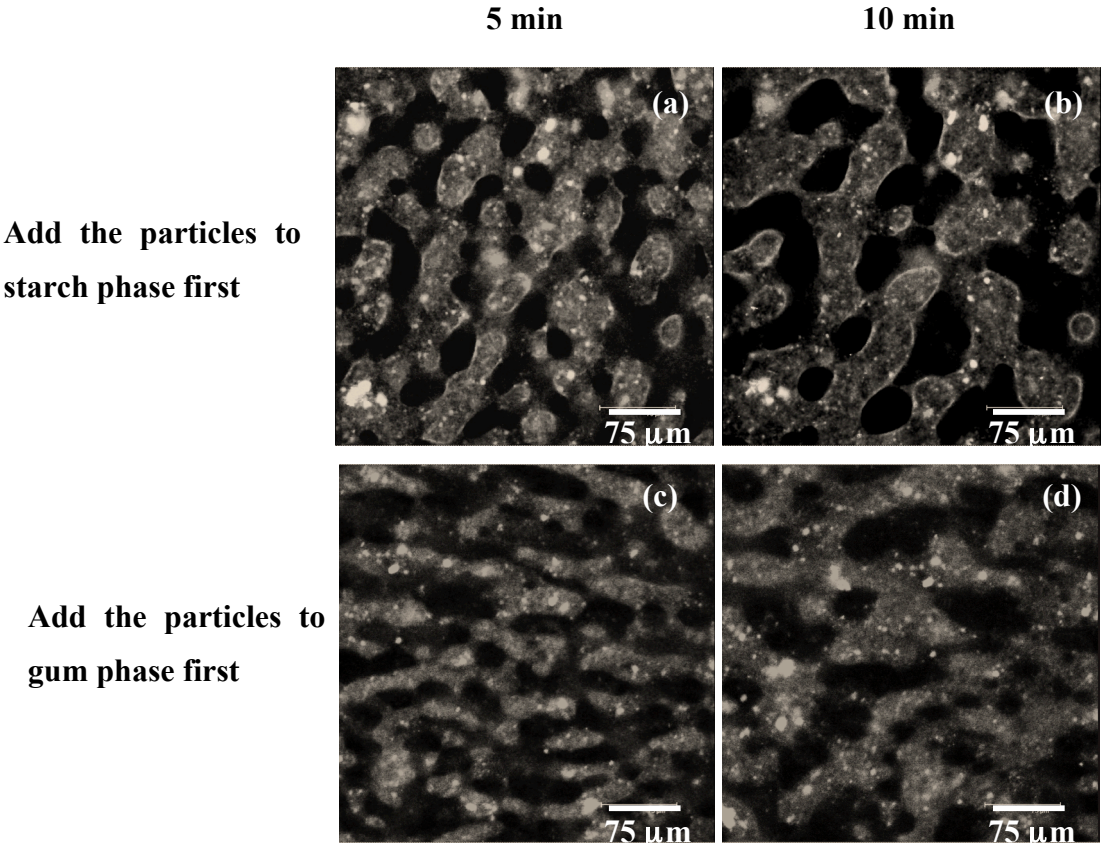

Figure 4-4 Representative confocal micrographs of 2 wt.% S + 0.3 wt.% LBG + 0.5 wt.% 100-SiOH; particles added into the starch phase first, (*a*) age 5 min; (*b*) age 30 min; particles added into the gum phase first, (*c*) age 5 min; (*d*) age 30 min. Dark regions are gum-rich, brighter regions are starch-rich and/or particle-rich, very bright regions are clusters of particles.

Figure 4-4 shows the difference between adding 100-SiOH particles into the S phase before mixing versus adding silica particles into the gum phase before mixing. Being the most hydrophilic, these particles can be easily dispersed in either the S or gum phase. It is of interest to investigate the effect of the initial location of the particles on the emulsion stability. It can clearly be seen that bright specks (particles) are situated inside starch domains, the dark domains indicating regions where there are no colloidal particles. When adding the particles into the starch phase first, the particles were clearly visible around the interface between the two phases – see Figure 4-4*a* and Figure 4-4*b*. In contrast, when adding the particles to the gum phase first, the particles slowly migrated from the gum-rich regions to the

starch-rich regions. Gum-rich domains appeared to be dark and were completely devoid of particles. In Figure 4-4*c* the edge of interface was slightly blurry due to the migration of particles. The edge of interface later sharpened over time (Figure 4-4*d*). Thus, regardless of how the particles were added to the system, the end result was the same. The rate of separation and the domain coalescence rates were similar in all mixtures. This result is in disagreement with the research from Binks and Lumsdon (2000) where they stated that the preference of emulsion type (e.g. O/W or W/O) can depend upon the solution in which particles are first dispersed.

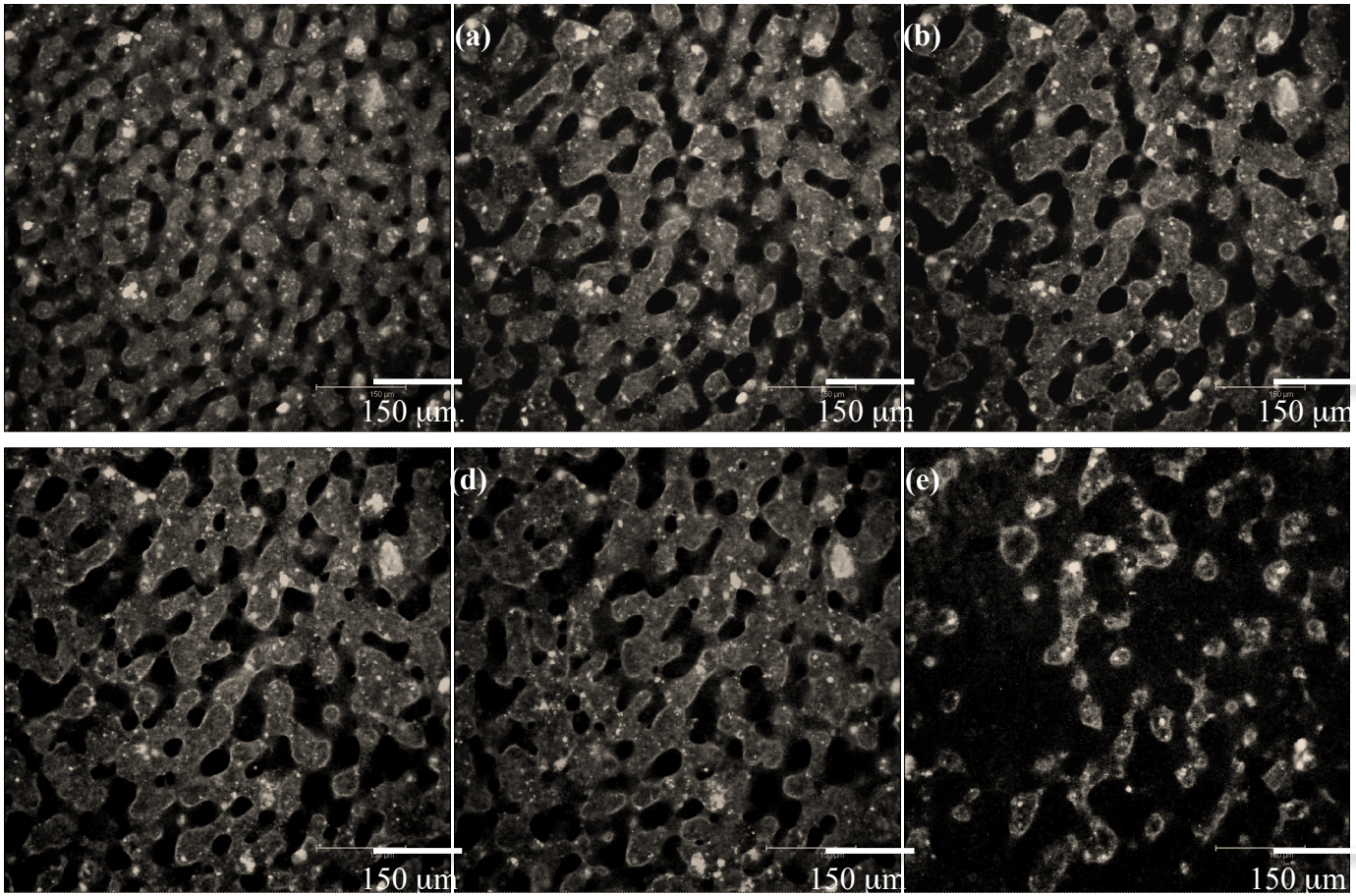

Figure 4-5 Representative confocal micrographs of mixtures of 2 wt.% S + 0.3 wt.% LBG containing 0.5 wt.% 100-SiOH (i.e., unmodified) particles. Observed at (*a*) 5 min; (*b*) 10 min; (*c*) 30 min; (*d*) 3 h; (*e*) 6 h; (*f*) 24 h.

Figure 4-5 displays the evolution of microstructure of 2 wt.% S + 0.3 wt.% LBG with the presence of 0.5 wt.% unmodified silica particles (100-SiOH) over several time intervals. Within the first 5 minutes of observation, there was a clear indication of spinodal decomposition. Observation after 10 minutes demonstrates a slight coarsening of the starch microdomains. As time went on, there were more particles that migrated to the interface of the two phases. The layer of particles at the interface eventually became very dense, resulting in the cessation of starch microdomain growth and they were stable for many hours. Over a period of many hours, the starch regions remained at a similar size as after 10-minutes with only a few areas fusing together. However, after the mixture had been left under normal gravity for 24 hours, the starch blobs started to sink to the bottom of the thin (3 mm) sample well on the microscope slide. Hence, there were only visible small starch blobs ca. 30 μm inside remaining in dark gum regions, as can be seen in Figure 4-5*f*.

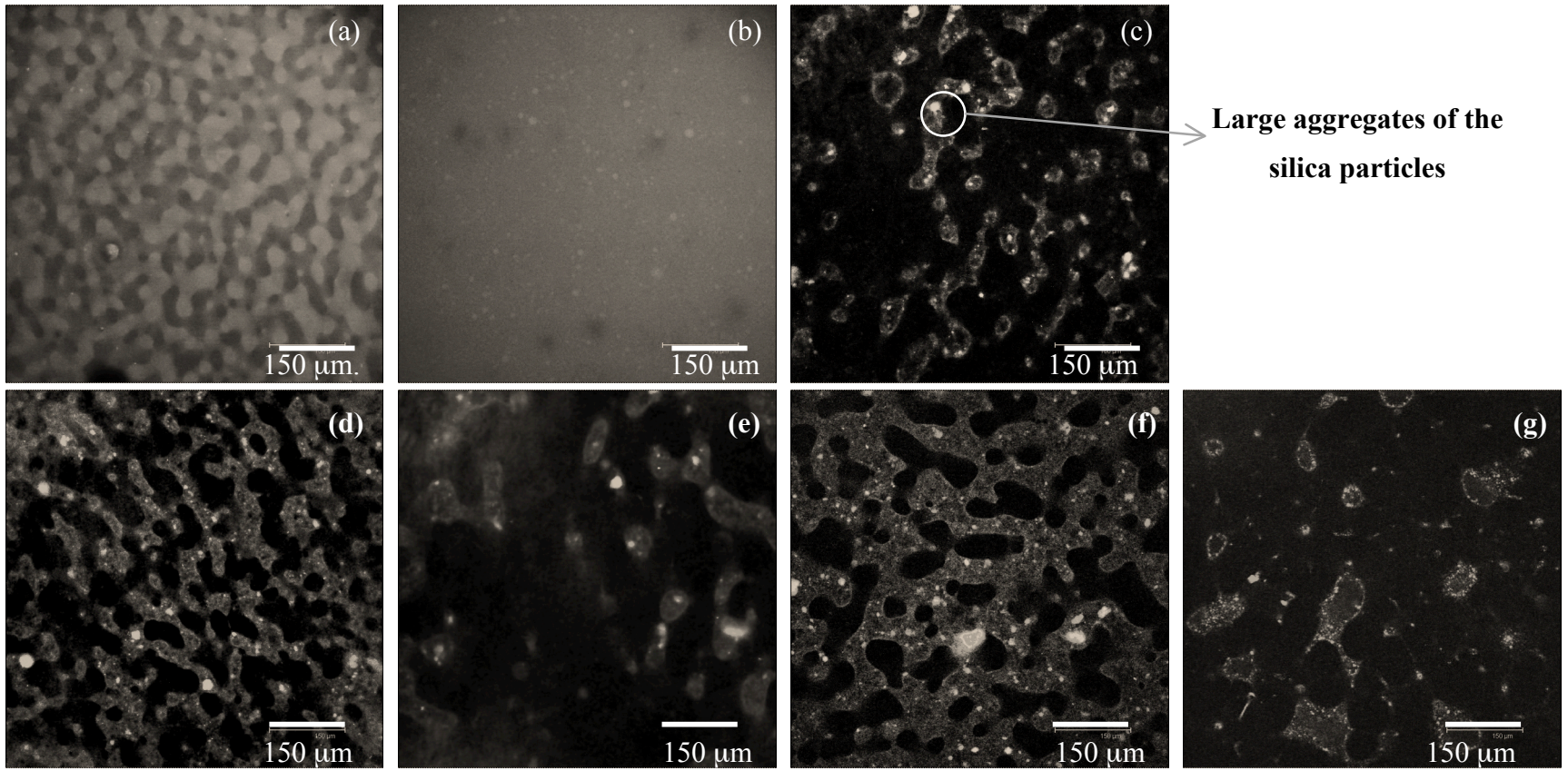

Figure 4-6 Representative confocal micrographs of mixtures of 2 wt.% starch + 0.3 wt.% LBG in the absence and presence of 0.5 wt.% silica particles of varying surface hydrophobicities: (*a*) no particles, age 5 min; (*b*) no particles, age 30 min; (*c*) 100-SiOH (i.e., unmodified) particles; (*d*) 80-SiOH particles; (*e*) 70-SiOH particles; (*f*) 65-SiOH particles; (*g*) Food-grade silica particles. Image *c*-*g* show micrographs at age 24 h.

The mixed polysaccharide systems with or without added silica particles were transformed into a bicontinuous microstructure. Figure 4-6*a* shows a typical image of model system consisting 2 wt.% S + 0.3 wt.% LBG that had been mixed for 5 minutes. It demonstrates common spinodal decomposition structure. In real time this system was quite dynamic, with movement and fusion of the bright (starch-rich) regions and parallel growth of the dark background (LBG-rich) regions. Figure 4-6*b* shows that 30 minutes after preparation within the same system no such regions were evident, just an ill-defined background of faint 'blobs'. The small background blobs may represent the small fraction of starch that still remains within the bulk LBG phase.

Figure 4-6*c* shows the dramatic effect of introducing 0.5 wt.% silica particles to the system. Within 24 hour aging time, there was an evident that the particles affect the phase separation significantly. There was plenty of starch microdomains appeared in continuous LBG phase throughout the sample. In Figure 4-6*c*, the silica particles used were the 100-SiOH particles, i.e., where the silica surface had been unmodified and should possess 100% of the natural surface density of silanol groups. Such particles should be quite hydrophilic and might be expected to be compatible with either the gum or starch phase. The very bright dense regions (ca. 20 μm) that appeared in the image suggested significant aggregation of the silica particles. It should be recalled that the initial particle size of the silica is approximately 20 nm, hence individual particles of this size would not be visible at the resolution used. However, silica particles can form irreversible aggregates and the degree of aggregation depends upon the hydrophobicity of the particles. Moreover, most of the particles and their aggregates appeared to reside largely within the starch-rich domains. The phenomenon where particles appeared both at the interface and within discrete domains also occurred in slightly off neutral wetting silica particles-stabilised oil-water mixture via bijel mechanism (Herzing *et al.*, 2007; 2008). Experiments were repeated many times where the particles were deliberately dispersed within the gum phase before mixing this with the starch phase (Figure 4-4), but this seemed to have no effect on the distribution of particles on aging: after at least 3 hours more than 99% of the particles and their aggregates appeared to reside within the starch-rich phase and/or around the interface. This propensity for particles to prefer one type of phase, for no apparent reason, is a feature that has been noted

previously on completely different systems, for example sodium caseinate + xanthan + emulsion droplet (Hanazawa and Murray, 2014); sodium caseinate + xanthan + latex particles (Moschakis *et al.*, 2006) and also starch + gelatin + latex particles or emulsion droplet particles (Firoozmand, *et al.*, 2009). However, a possible explanation will be discussed in section 4.3.5 below.

To be an effective stabiliser, it is important to have particles and/or their aggregates that have an ability to bind or accumulate at the interface. From Figure 4-6*c* to *g*, it is clearly seen that there are loosely packed silica particles around the interface and the presence of particle aggregates within the starch microdomains. Although in theory ideal Pickering stabilisation required a close packing of particles at the interface, it has frequently been reported that in stable emulsion systems many parts of the interface appear denuded of particles. For example, Yusoff and Murray (2011) have shown a stable oil-water emulsion stabilised by fragments of hydrophobic starch granules with very sparse apparent coverage. Thus a complete coverage may not be necessary if the particles form a strong network at the interface, or again it could be because at the resolution of the confocal microscope a layer of particles just a few tens of nm thick is hard to detect, particularly if there are much larger particle aggregates around which will tend to dominate the fluorescence signal.

Figure 4-6*d* shows a typical micrograph obtained after 24 hours with the presence of the 80-SiOH particles, $[C_p]$ = 0.5 wt.%. Apparently, more hydrophobic particles have a greater tendency to aggregate, which could lead to them forming a strong interfacial network. On the image, there is a greater fraction of the particles and/or particle aggregates situated at the interface. Moreover, this system also showed even greater persistence of the early spinodal decomposition structure than with the 100-SiOH particles. As previously mentioned regarding self-aggregation of hydrophobic particles, there was also a greater density of particle aggregates within the starch-rich domains and indeed there is no obvious reason why more hydrophobic particles would have a greater tendency to aggregate at the interface than in the bulk, unless the particles somehow get trapped at the interface during migration from the gum domains to the starch domains.

Experiments were also conducted with more hydrophobic silica particles, i.e., 70-SiOH and 65-SiOH and representative micrographs for 24 hour old systems are shown in Figure 4-6*e* and Figure 4-6*f*, respectively. For some reason the 70-SiOH

particles were not as effective as the 100-SiOH or 80-SiOH particles in preserving the early spinodal microstructure whereas the 65-SiOH particles gave the most well defined structures with very clear decoration of the interfacial regions with particles. However, individual particles could not be distinguished due to the resolution of confocal microscope. Kim *et al.* (2012) stated that at a certain range of surface hydrophobicity of silica particles, stable water droplets could be created with particles. Being the most hydrophobic, the 65-SiOH particles were the most difficult to disperse. This type of particle will therefore be expected to form large aggregates, which appeared to agree with the confocal images.

Generally, only unmodified silica particles are allowed to be used in food products (Dickinson 2007; Berton-Carabin and Schroën, 2015). Food-grade silica particles, $[C_p]$ = 0.5 wt.%, were also tested on the S + LBG system - see Figure 4-6*g*. These food-grade particles were unmodified; so it acted similarly to the 100-SiOH particles. It can be seen that some starch microdomains still remained in bulk LBG phase with some denuded interfacial area. As expected, food-grade particles did not work as effectively as model silica particles because of their larger particle size (3 μm) and therefore inherently low surface area. It is clearly seen that majority of particles migrate to the interface within 24 hours.

At $[C_p]$ = 0.7 wt.% and 1 wt.%, a reinforcement of the system microstructure is generated. It appeared to slow down or/and inhibit the phase separation. A possible reason for this stabilisation could be the development of a semi-solid character around the particle-rich interface which inhibits structural coalescence. The set of images in Figure 4-7 illustrates the effect of particle concentration on the microstructure of 2 wt.% S + 0.3 wt.% LBG mixtures. Each micrograph was captured 24 hours after mixing. Figure 4-7*a, c, e* and *g* represent the mixtures with added 0.7 wt.% fumed silica whilst Figure 4-7*b, d, f* and *h* represent the mixtures with added 1 wt.% fumed silica for 100-SiOH, 80-SiOH, 70-SiOH and 65-SiOH, respectively. It can be clearly seen that the mixtures illustrated are akin to bijel structures.

Again, within the blobs of the starch-rich phase in Figure 4-7, the silica particles are not uniformly distributed. Numerous large bright specks, particle aggregates, were developed. At 0.7 wt.% 100-SiOH and 80-SiOH (Figure 4-7*a, c*),

there are noticeably more starch blobs remaining in the LBG bulk phase than at concentration 0.5 wt.% particles (Figure 4-6*c, d*) after 24 hour aging. At these specific areas, it can be seen that there is more particle coverage around the interfacial zone. On the other hand, there seems to be an excess of particles in the system containing 0.7 wt.% 70-SiOH and 65-SiOH, see Figure 4-7*e, g*, where the particles were closely packed within the starch microdomains and the thin layer of particle decoration was undetectable, unlike the system at 0.5 wt.%. As the concentration was above certain level, it was difficult to identify the interfacial boundary. There also seemed to be threshold concentration between 0.5 to 0.7 wt.% for 70-SiOH and 65-SiOH. Moreover, a further increase in the concentration of the particles to 1 wt.% (Figure 4-7*b, d*) for 100-SiOH and 80-SiOH indicated that the starch microdomains are smaller compared with Figure 4-7*a, c*. For 70-SiOH and 65-SiOH (Figure 4-7*f, h*). The results did not appear to be significantly affected by increasing [C_p] from 0.7 to 1 wt.%. In fact, the starch microdomains were considerably larger; possibly because the increase in particle concentration resulted in more particle aggregation. Large particle aggregates can clearly be seen in the mixtures containing 1 wt.% 65-SiOH.

Higher particle concentrations than 1 wt.% were not studied because the aim was to keep the effective particle concentration within limits that might have a practical application. Unmodified silica can be added to foods but regulatory limits are around a few wt.% (depending on the particle type), whilst it is also hoped in the long term to mimic these effects of synthetic particles with food-grade materials that have been used elsewhere (Murray, Durga, Yusoff and Stoyanov, 2011).

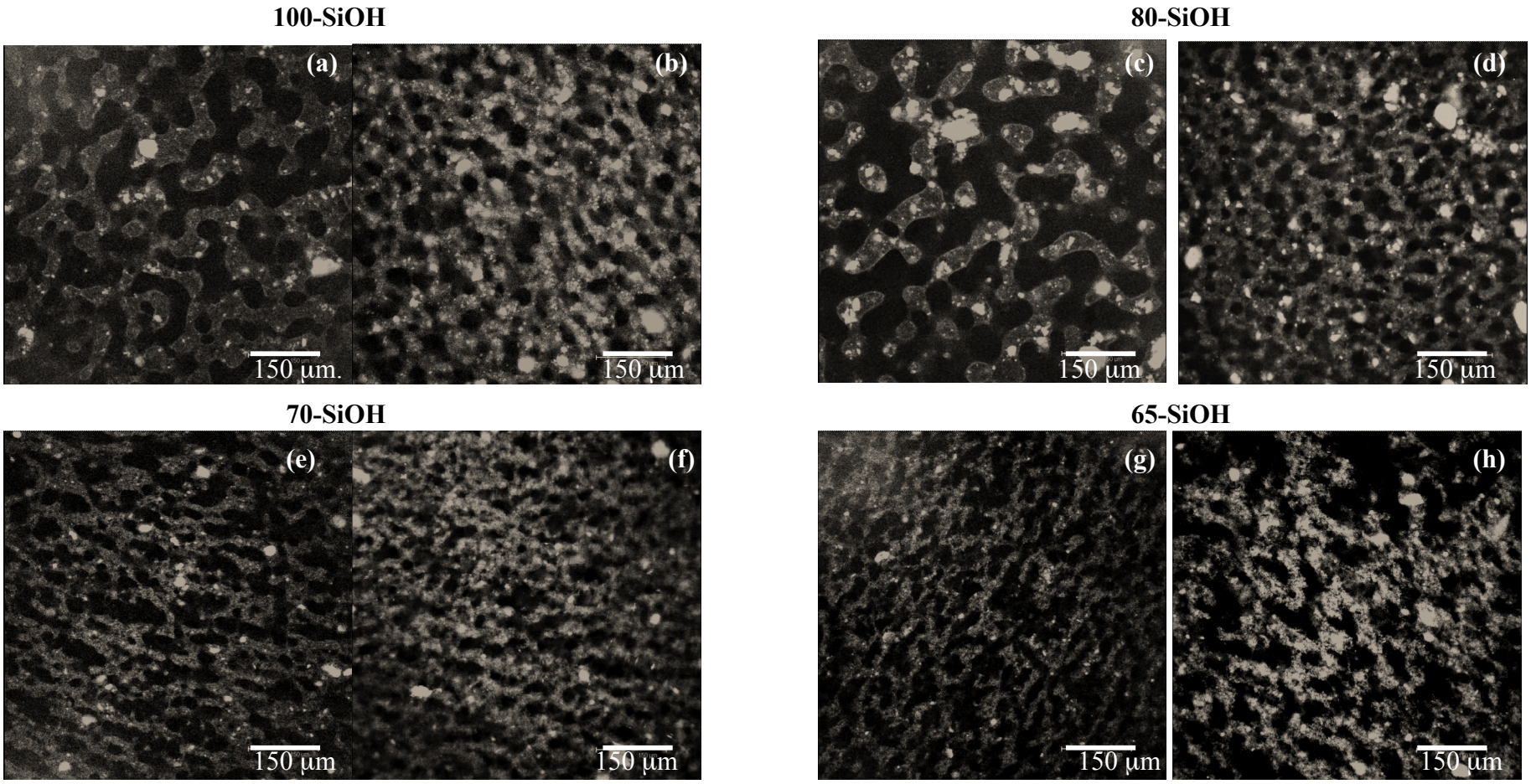

Figure 4-7 Representative confocal micrographs of mixtures of 2 wt.% S + 0.3 wt.% LBG age 24 h in the presence of various surface characteristics silica particle at $[C_p]$ = 0.7 wt.% (left) 1 wt.% (right); (*a,b*) 100-SiOH, (*c,d*) 80-SiOH, (*e,f*) 70-SiOH, (*g,h*) 65-SiOH.

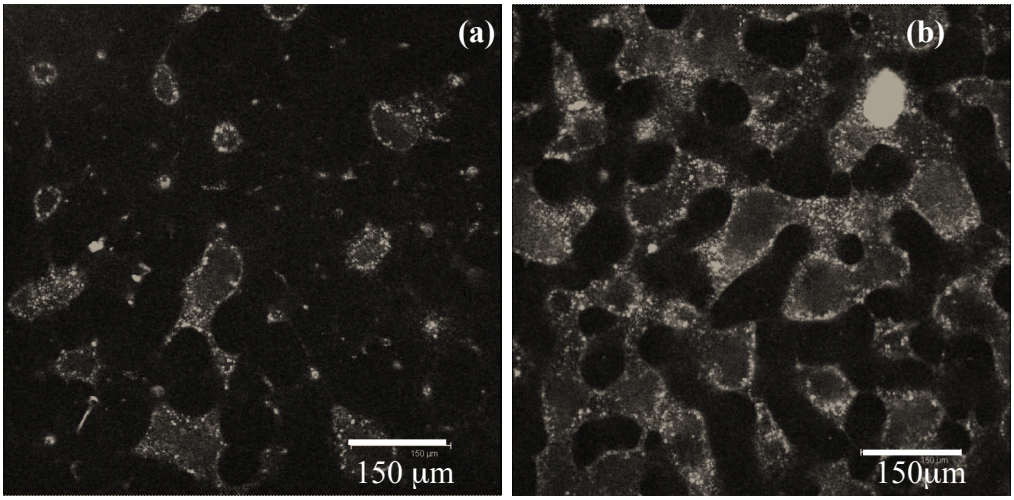

Figure 4-8 Representative confocal micrographs of mixtures of 2 wt.% S + 0.3 wt.% LBG age 24 h in the presence of food-grade silica particles at concentration of (*a*) 0.5 wt.%; (*b*) 1 wt.%.

The progressive increase in stability of 2 wt.% S + 0.3 wt.% LBG on increasing the food-grade particle concentration from 0.5 wt.% to 1 wt.% is shown in Figure 4-8*a*, *b*. Although remarkably more particles appeared around the interface and FDA (Food and Drug Administration) regulations allows up to 2 wt.% food-grade silica particles in food applications; since the particles are quite large it expected that this would give an unappealing food texture, hence higher concentration was not observed.

4.3.3 Image analysis

The size of the resultant starch microdomains is of interest to analyse further. An attempt has been made to quantify the effects of each silica particle type and concentration on the phase separation kinetics of the 2 wt.% S + 0.3 wt.% LBG system by performing image analysis on different sets of images. Figures 4-9*a, b, c* show the extracted characteristic length scale (L) as function of time for the mixture with the presence of 0.5, 0.7 and 1.0 wt.% silica particles, respectively. L was measured in order to evaluate the time dependence of the growth of microdomains. In this analysis only systems containing model silica particles had been analysed. L was calculated using the Equation 2-4 section 2.6.2. In the model system without particles, L was approximately 60 μm at 5 minutes age (the shortest time in which it was possible to obtain images). In less than 30 minutes after preparation, the starch

domain size grew rapidly and domains started sinking down to create separate two distinctive layers in the well of the slide.

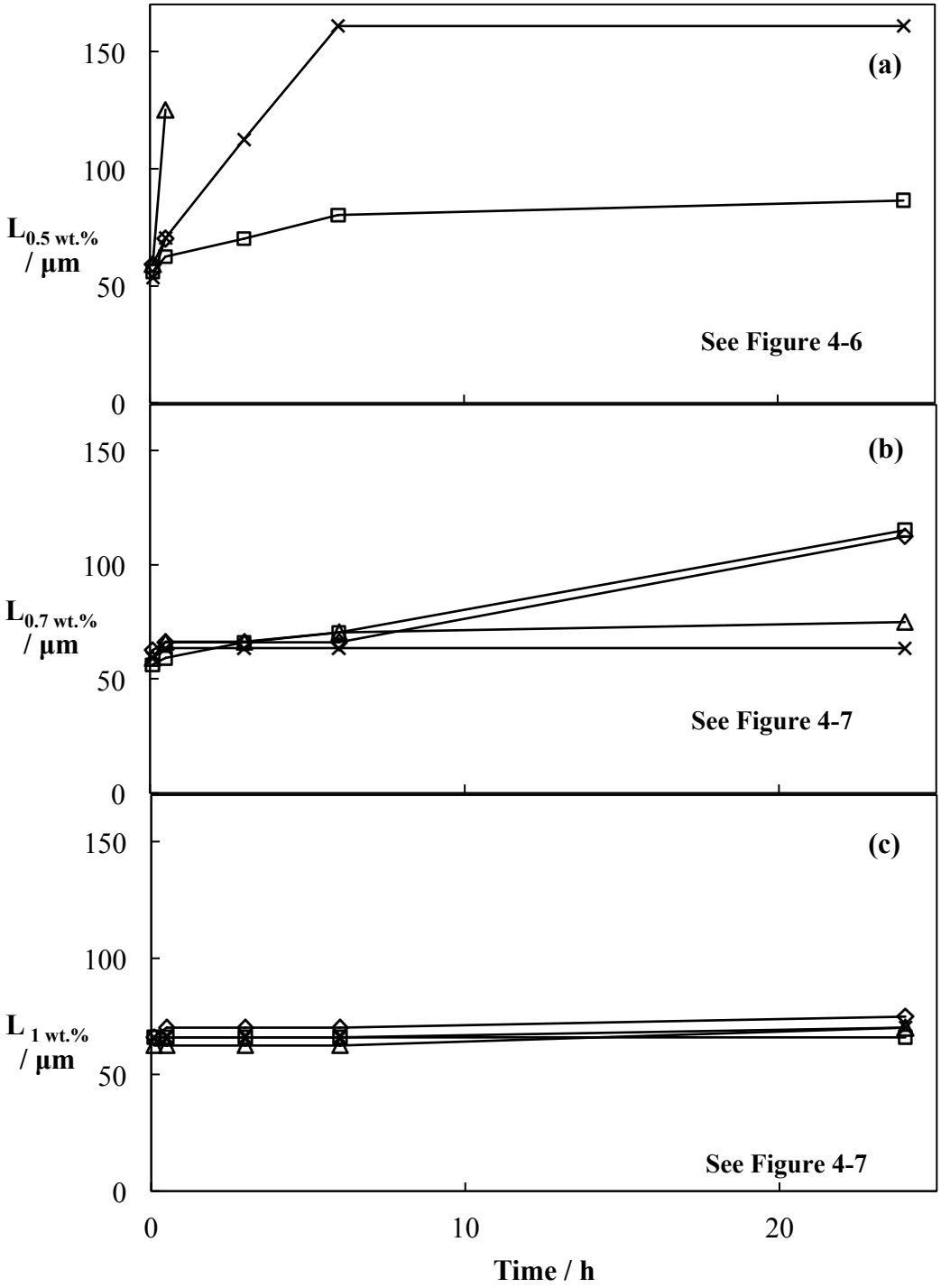

Figure 4-9 Characteristic length scale, *L*, versus time since mixing for mixtures of 2 wt.% starch + 0.3 wt.% LBG plus different [C_p]: (*a*) 0.5 wt.% (*b*) 0.7 wt.%; (*c*) 1 wt.%. Data and representative confocal micrographs are shown for systems with silica particles of different surface characteristics: (◊) 100-SiOH (i.e., unmodified); (□) (80-SiOH); (Δ) 70-SiOH; (X) 65-SiOH.

At [C_p] = 0.5 wt.%, the 80-SiOH particles are effective in keeping *L* below 100 μm after 24 hours, whereas with the 100-SiOH or 70-SiOH particles the domain size is greater than 200 μm after 2 hours of preparation (data points not shown except for 70-SiOH at 0.5 hour). When the domain size grows to a certain size, the blobs will start to sink as the domain forms two separate layers with a starch-rich region at the bottom. It is confirmed with the CLSM result in the previous section that using the most hydrophobic 65-SiOH particles recovers some domain size stability, although *L* is approximately 1.8x larger at 24 hours than with the 80-SiOH particles.

Figure 4-9*b* shows the effect of 0.7 wt.% particles and it is seen that this relatively small increase in particle concentration gave a dramatic increase in stability for all four types of particles. The 70-SiOH and 65-SiOH particles were the most effective, giving approximately the same small increase in *L* from 60 to 70 ± 5 μm in the first 5 hours, within experimental error, *L* was approximately unchanged after 24 hours. The 100-SiOH and 80-SiOH particles gave approximately the same stability in the first 5 hours, but *L* then increased to 115 ± 5 μm after 24 hours. Increasing the particle concentration further to 1.0 wt.% (Figure 4-9*c*) gave a further increase in the stability of *L*, which decreased for all particle types, hardly increasing at all from 60 ± 5 μm between 0.1 and 24 hour for the 80-SiOH, 70-SiOH and 65-SiOH particles, whereas for the 100-SiOH (unmodified) silica *L* was slightly larger ca. = 75 μm. These trends are generally in agreement with the qualitative assessment of the effects at 0.5, 0.7 and 1 wt.% particles in Figure 4-6 and Figure 4-7 discussed above. Overall, *L* decreased with an increased amount of stabilising silica particles.

4.3.4 Estimated minimum domain size that could be covered by the given silica particles

The microscopy demonstrates that the model silica particles of all types observed had a capacity to stabilise W/W emulsions. Nevertheless, it is also instructive to estimate the mean domain size that particles could be expected to stabilise. This theoretical calculation had been done previously (Luo *et al.*, 2011; Yusoff and Murray 2011) for different systems. In order to calculate the minimum domain size of starch, various assumptions about contact angle (θ) and a certain minimum fraction of coverage at the interface ($\emptyset_i$) are required.

In an ideal situation, θ was assumed to be 90° and all particles are present at the interface. An adsorbed particle will then occupy an area of πr^2 at the W/W interface $4\pi R^2$, where $r =$ the particle radius and $R =$ the domain size radius.

With the above assumption one can write:

$$N_p \pi r^2 / \emptyset_i = N_d 4\pi R^2 \qquad \text{Equation 4-1}$$

where N_p is the number of silica particles and N_d is the number of starch domains of radius *R*.

N_p and N_d are given by:

$$N_p = V_p / 4/3\pi r^3 \qquad \text{Equation 4-2}$$

$$N_d = V_d / 4/3\pi R^3 \qquad \text{Equation 4-3}$$

where V_p and V_d are the volume of particles and the volume fraction of the starch domain occupied by the particles, respectively. V_p is from basic equation:

$$V_p = M_p / \rho_p \qquad \text{Equation 4-4}$$

where M_p is the mass per unit volume of particles added and ρ_p is the particle density. Substituting for V_p from Equation 4-4 into Equation 4-2, then N_p and N_d from Equation 4-2 and 4-3 into Equation 4-1 and rearranging the equation as below:

$$V_d = \frac{M_p R}{4 r \rho_p \emptyset_i} \qquad \text{Equation 4-5}$$

The ratio, K, of interfacial area occupied by the particles is:

$$K = \frac{M_p R}{4 V_d r \rho_p \emptyset_i} \qquad \text{Equation 4-6}$$

Since equal volumes of starch and galactomannan phase were mixed, V_d = 0.5. In the absence of the other information, if at least half of the surface of the starch domains should be covered with particles, a value of $\emptyset_i$ = 0.5 should be assumed. The model silica particle had a nominal size of 20 nm and so setting $r =$ 10 nm and the density of silica particles is 2.2 g cm^{-3}, if particle concentration is 1

wt.%, the minimum starch domain size (2R) that the silica cover can be calculated from Equation 4-5 is 2.6 μm. This is close to the maximum resolution of the confocal microscope under the conditions used, hence specific regions of this size would not be clearly visible under the microscope. The minimum ratio of particles to the total interface particle was assumed to be $K = 1$. However, the smallest L that would be seen via the CLSM micrograph was around 60 μm, i.e. to R = 60/2 and made K = 12, so the concentration of particles present could easily stabilise domains of this size. In the absence of more detailed information, it inferred that enough of the model silica particles were available to stabilise the W/W interface of the domains observed.

4.3.5 Bulk rheology of different phases

It is clear that all the particles had an ability to slow down the growth of microscopic domains and macroscopic phase separation. From the CLSM observation, it was clear that there was particle aggregation within the starch microdomains and at the W/W interface. The gelation of silica nanoparticles in the bulk of concentrations, as low as those studied here (i.e. 1 wt.% or less), is a well known phenomenon (Iler, 1979). A question therefore arises whether the change in domain stability is simply due to the formation of silica particle networks within starch microdomains which leads to the gelation or a very significant increase in viscosity of the starch-rich domains. Rheology measurements of each bulk phase with unmodified silica particles is a method that was used to test this hypothesis. Viscosity values were obtained from $\dot{\gamma}$ between 0.1 and 100 s^{-1}. Only low shear conditions close to 'zero' shear were selected as it simulates the conditions typical to spontaneous phase separation. For the oscillatory values, they were obtained from frequency sweeps between 0.01 and 1 Hz.

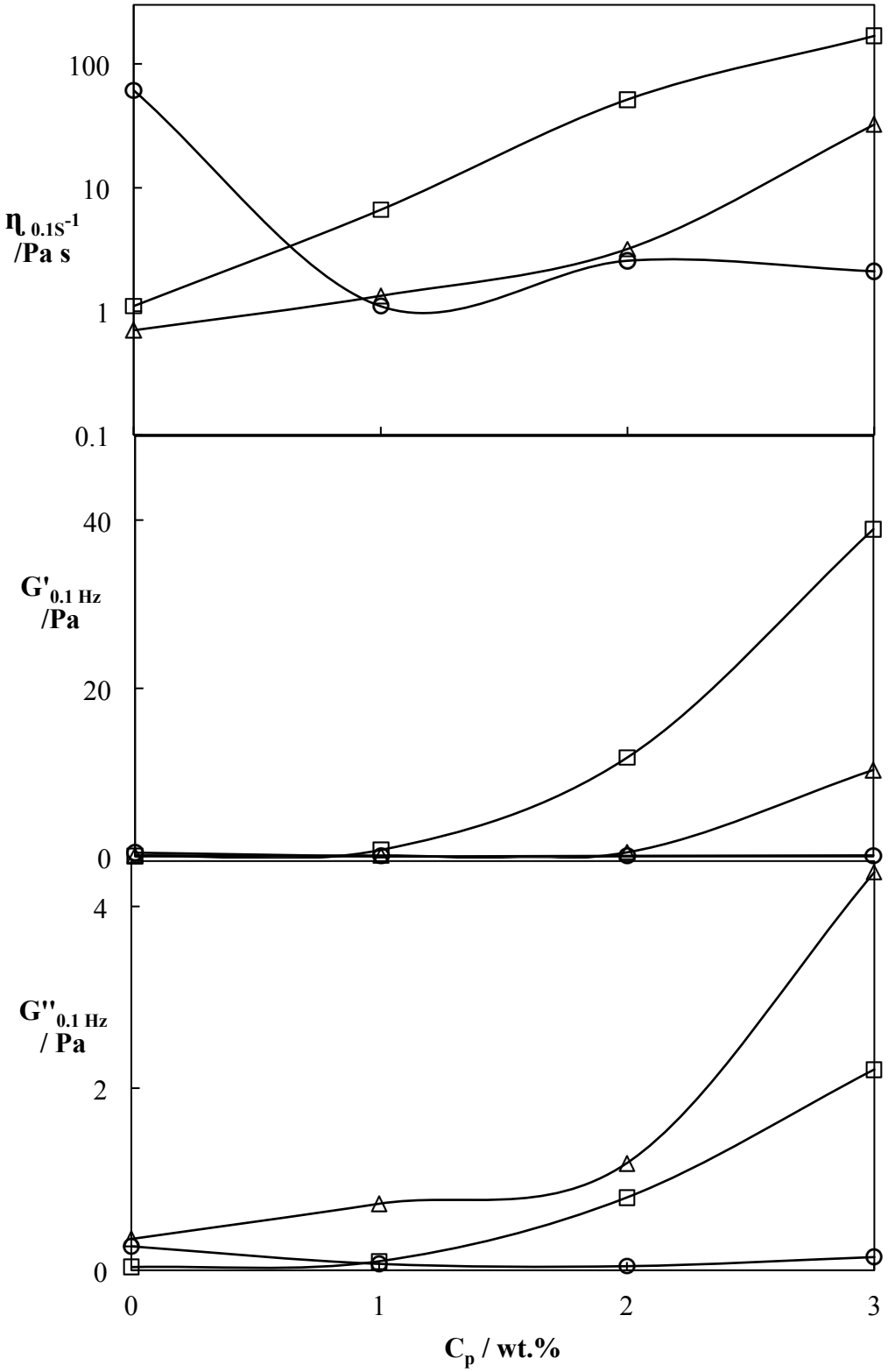

Figure 4-10 (*a*) Viscosity (η) at $\gamma = 0.1\ s^{-1}$; (*b*) loss modulus (G") measured at 0.1 Hz; (*c*) storage modulus (G') at 0.01 Hz for varying concentration of the 100-SiOH particles (C_p) added to individual solutions of 4 wt.% starch (o); 0.6 wt.% LBG (Δ); 0.5 wt.% GG (□).

Figure 4-10 shows the results of three sets of rheology measurements versus particle concentration; the viscosity η at $\dot{\gamma}$ = 0.1 s^{-1} (Figure 4-10*a*) and oscillatory shear rheology at low frequencies and 1% strain: the loss modulus G" at 0.1 Hz (Figure 4-10*b*) and storage modulus G' at 0.1 Hz 1% strain (Figure 4-10*c*). Up to 3 wt.% unmodified silica particles were added to the 4 wt.% S but the bulk S phase showed no significant affect in G' or G". However, the viscosity values were sharply decreased after 1 wt.% of the 100-SiOH was introduced. The values later showed a slight increase at higher particle concentrations (i.e. 2 wt.% and above). In contrast, addition of the 100-SiOH particles in 0.6 wt.% LBG and 0.5 wt.% GG gave a significant increase in both viscosity and elasticity measurements.

From the results in Figure 4-10, it maybe concluded that a combination of starch and silica nanoparticle did not form a strong network within the domains. Interestingly, this silica nanoparticles system showed an effect on viscoelasticity of the gum phases. The well-known phenomenon of "depletion flocculation" of particles was suggested, which leads to a significant increase in all the rheological parameters measured. Consequently, this phenomenon could explain the mechanism of trapping of particles that had aggregated at the W/W interface. This migration of particles into the different regions and the fact that the silica seemed to end up as clusters or aggregates was discussed earlier in section 4.3.2 - see Figure 4-6. Moreover, these large particle lumps could form a high energy barrier at the interface, since the larger the particles the larger the desorption energy (as explained in chapter 1, section 1.9.3), for the particles of the same surface characteristics. In addition, depletion flocculation of particles in the starch phase probably does not occur due to the compact molecule of amylopectin and its smaller hydrodynamic radius. The persistence of depletion-induced particle aggregates within the starch microdomains may be a kinetic effect, since both polymer domains, especially LBG, yield a gelling system when mixed with starch became more viscous, any aggregate re-arrangement or dissociation would be slowed down.

4.4 Conclusion

Phase separation in polysaccharide-polysaccharide systems can be strongly influenced by the addition of a low volume fraction of silica particles. The nanoparticles show a strong preference for the starch domains that form rather than the gum phase, whilst there is an increasing tendency for particle aggregation to occur within the starch domains and at the W/W interface between the two phases as the particle hydrophobicity and particle concentration are increased. Fumed silica nanoparticles effectively inhibit and/or slowdown the phase separation kinetics, whilst the food-grade microparticles showed less of an effect on microstructure. Measurements of the bulk rheology of the gum and starch phases in the presence of particles suggested that the rheology of the interior of the starch domains was hardly affected by the presence of the particles, whereas the gum phase viscoelasticity was significantly increased by the addition of particles. It is suggested that depletion flocculation of the particles in the gum phase may be the driving force behind the formation of particle aggregates at the W/W interface and within the starch domains that somehow slows down phase separation.l

Chapter 5

5 Chapter 5. Effect of bromohexadecane microdroplets on phase separation of waxy corn starch + locust bean gum or guar gum

5.1 Introduction

There are three kinds of nutrients that humans require in large quantities on a day to day basis: polysaccharide, protein and lipid. All of which are the basic components in many food products. Therefore, it is really important to understand the interactions between these components in order to design and control product properties. Polysaccharides are commonly used as thickening and texturing agents, starch and galactomannans are examples. Proteins, such as sodium caseinate, are widely used as emulsion forming and stabilising agents because of their high surface-activity (Neirynck *et al.*, 2007). Oil is another important component in many foods that carries or imparts flavour and aroma. In most aqueous food, oil is commonly presented as oil droplets that are stabilised by proteins.

The previous chapter has shown that the phase separation of model mixtures can be influenced by fumed silica particles. Clearly, if cross-linking between silica particles at the interface could be activated in some way this might give complete inhibition of domain growth. However, most chemicals that exist for this purpose would not be permissible in food-stuffs (Iler, 1979). Protein-stabilised oil droplets strongly impacts the texture of food products (Dickinson, 2012a). The dispersion of these droplets in aqueous media can be made via emulsification processes. Dickinson (1994) and Ye *et al.* (2013) showed evidence that this type of droplet can potentially be adsorbed at the oil-water interface (emulsion-stabilised emulsion). Nonetheless, there has been limited amount of research on using oil-in-water (O/W) emulsion as a stabiliser in W/W emulsion (Firoozmand and Rousseau, 2013; Hanazawa and Murray, 2013; 2014). Hananzawa and Murray (2014) recently extended the principle of stable oil droplets acting as Pickering ‘stabilisers’ in W/W emulsions. The research showed that in the presence of a low volume fraction (up to 2.5 wt.%) of oil droplets covered in protein, phase separation of a xanthan + caseinate system seems to slow down and also provided tentative evidence (Hanazawa and Murray, 2013) that such particles mechanically strengthened the

W/W interface. These multiple emulsions have some advantages over conventional ones, i.e., produce low-fat products that have similar sensorial perception of full-fat food. Hoffmann and Reger (2014) also stated that these kind of protein-stablised oil droplets behave like sticky particles and have gel-like behaviour. Consequently, these particles could be considered as similar to microgels. Ye *et al.* (2013) claimed that soft-solid particles that are used as a Pickering stabiliser behave differently from typical solid particles. Microgels are soft and deformable, hence this deformability at the interface makes it possible to cover a larger interfacial area.

There is a wealth of research about the interaction between proteins and polysaccharides (Syrbe *et al.* 1998; Doublier *et al.*, 2000; de Kruif and Tuinier, 2001; Vazquez-Duhalt and Quintero Ramírez, 2004; Chun *et al.*, 2014). The interaction is mostly the results of thermodynamic incompatibility (Grinberg and Tolstoguzov, 1997). Bourriot *et al.* (1999) reported GG and micellar casein showed phase separation via depletion flocculation at pH 7 even at low concentration of GG (0.1 wt.%). However, the interaction also depends upon the solution conditions, e.g., pH, concentration, temperature, ionic strength etc. For example, Perrechil and Cunha (2012) reported that sodium caseinate + LBG shows no phase separation at pH 7, but exhibits the properties of a heterogeneous mixture at high volume fraction of protein after acidification to pH 5.5. In amylopectin + casein mixtures, only a high concentration (>2wt.%) of amylopection is needed to induce phase separation (de Bont *et al*., 2002; 2004).

This chapter aims to establish a better understanding of multiple emulsions from the mixtures of O/W emulsion stabilised by sodium caseinate (SC) and water-in-water (W/W) emulsions composed of waxy corn starch (S) + locust bean gum (LBG) or guar gum (GG), to see whether these emulsion droplets can act in the same way as the synthetic fumed silica particles in the model starch + galactomannan systems. Although the oil used, 1-bromohexadecane, was a non-food-grade component, it can be seen as an example to illustrate specific mechanisms and potential conceptual opportunities for the food sector. 1-bromohexadecane was chosen as its density is close to that of water (0.99 g cm^{-3}). If the use of O/W droplets is successful in stabilising the model systems, it could mean that this component could be substituted with bioactive compounds, e.g., aroma or flavour compounds in real foods or pharmaceuticals.

5.2 Materials and methods

5.2.1 Materials

The common materials (waxy corn starch, galactomannans, Rhodamine B and Nile Red) used in the experiments in this chapter are the same as those stated in chapter 2, section 2.1

Bromohexadecane microdroplets (BMDs)

Spray-dried sodium caseinate (product code 419491000) and 1-bromohexadecane 97% with density of 0.99 g cm^{-3} (product code 10104510) were purchased from Acros organics (Geel, Belgium).

5.2.2 Methods

Preparation of solution

All solutions were prepared according to the standard protocol stated in chapter 2, section 2.2. All the investigated samples contained 2 wt.% starch, 0.25 wt.% GG and 0.3 wt.% LBG with or without the presence of varied concentration of BMDs (1 -15 vol.%). In order to reduce the pH to pH 4, 29 µl of 0.25 M HCl was added during mixture blending with Ultra Turrax.

Preparation of BMDs

The BMDs were prepared by high-pressure homogenisation using sodium caseinate as the sole emulsifying agent. The BMDs preparation was adapted from Burgaud *et al.* (1990). Sodium caseinate (SC) solutions were prepared as an emulsifier by dispersing the protein (5 wt.%) in phosphate buffer pH 7 and stirred with a magnetic stirrer for 2 hours to ensure a complete solubilisation. O/W emulsions were then produced using a high-pressure jet-homogeniser operating at 300 ± 20 bar at room temperature. The emulsion produced was further passed through the jet-homogeniser three times to ensure production of the smallest possible droplet size. In the final emulsion, the SC concentration was 2.75 wt.% and the concentration of dispersed oil phase was 45 vol.%.

Particle size distribution and ζ-potential measurement

The particle distributions and ζ-potential measurements of the emulsion were determined as stated in chapter 2, section 2.3. Droplet sizes were measured after diluting samples with phosphate buffer. The refractive index of 1-bromohexadecane and dispersion medium were set at 1.460 and 1.33 respectively. The absorbance of the protein was assumed = 0.001. The ζ-potential was determined at pH 7 and 4 at 25 °C.

Bulk rheology

The condition of the measurements were performed as stated in chapter 2, section 2.5. The starting shear rate was 0.1 s^{-1} and the final shear rate 1 s^{-1} the whole range taking 10 minutes in total. The oscillatory values were obtained from frequency sweeps between 0.1 to 1 Hz., taking 15 minutes in total for each run. Viscosities of BMDs, $[C_p]$ = 0 - 15 vol.%, suspended in phosphate buffer were measured at pH 4 and 7.

The rheological properties of each bulk phase, S, LBG and GG solutions, plus BMDs at $[C_p]$ = 0 - 15 vol.% were investigated at pH 4.

Determination of phase separation

The phase separation measurement was mentioned in chapter 2, section 2.4.2.

Confocal laser scanning microscopy (CLSM)

In the absence of BMDs, 20 μl of Rhodamnine B (RB) fluorescent dye was added per 5 ml of the starch solution before blending with gum. For the model, starch + galactomananan gum mixtures in the presence of BMDs, 30 μl of the Nile Red (NR) fluorescent dye was added per 5 ml of gum phase before blending. RB showed preferential staining of the starch and protein whilst the NR showed strong affinity for oil droplets. Unlabelled areas were therefore assumed to be gum-rich regions. Due to bubbles that formed during blending, the first image was captured after 20 minutes of storage. The samples were stirred gently before being poured into a welled slide before observation of microstructure. The appearance of samples was recorded again at 5 minute, 10 minute, 30 minute, 1 hour and 24 hour. Image analysis was performed using Image J software.

5.3 Results and discussion

5.3.1 BMDs characterisation

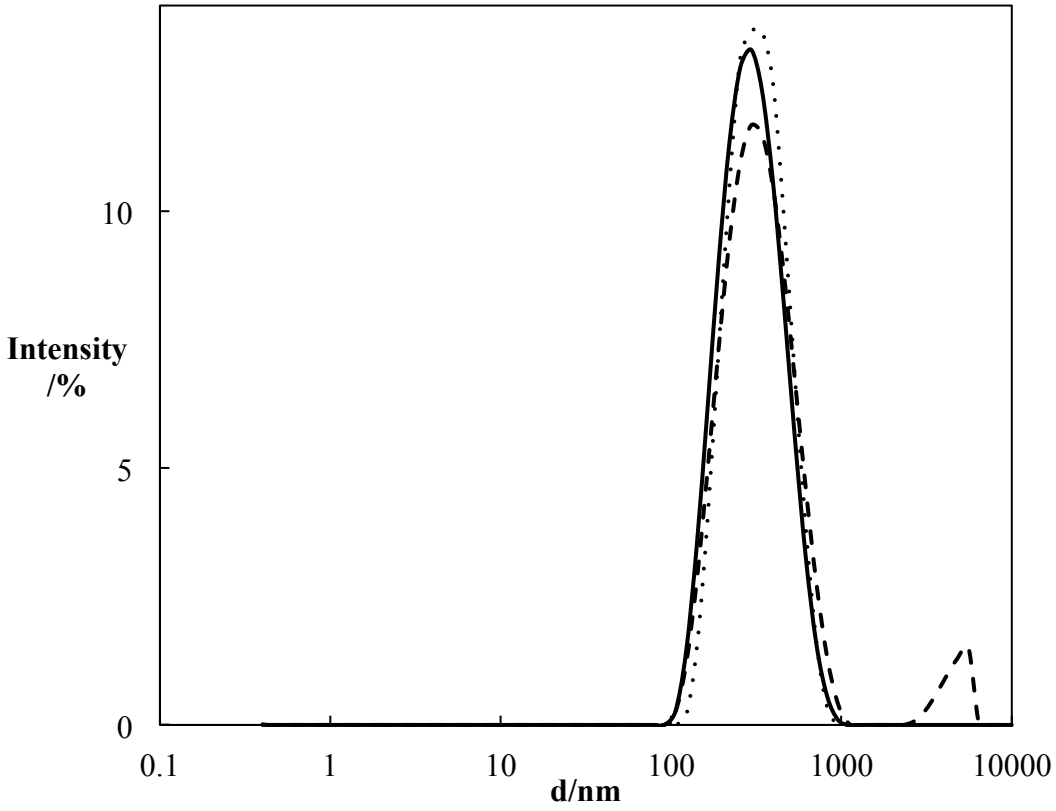

Figure 5-1 Distribution of BMDs dispersion (—) unheated age 1 day; (.....) heated age 1 day; (- - -) unheated age 3 week.

Sodium caseinate is a surface-active molecule that can adopt a variety of configurations in solution. It has amphiphilic character and high surface-activity. Sanchez and Patino (2005) reported that individual caseins, i.e. α_1, α_2 and β have a high tendency to adsorb at air-water and oil-water interfaces. For this reason, sodium caseinate was selected in order to produce stable oil droplets. At an early stage of producing these BMDs, various concentrations of sodium caseinate and oil ratio were used in order to obtain the optimum particle size for further use as particle-stabilised model S + galactomannan systems. The number of passes of BMDs through the homogeniser was also taken into account. There was a notable decrease in droplet diameter with increasing number of passes, which is in agreement with previous studies (Tcholakova *et al.*, 2003; Qian and McClements, 2011). The mean

hydrodynamic particle size decreased from almost 400 nm to 280 nm. Figure 5-1 shows the droplet size distribution of diluted BMDs analysed via light scattering. The solid line in the graph shows the size distribution of the BMD particles at pH 7, aged 1 day. The line illustrates one single peak which means the dispersion was monodisperse, with a Z-average size = 280 nm after passing through the jet-homogeniser 4 times. The dashed line displays the change in a distribution after storage in sealed container for 3 weeks. There were a few small aggregates of particles that appeared during storage. It could be clearly seen that after 3 weeks the smallest dimension of the distribution slightly shifted to ca. 290 nm although the largest was about 5 μm. The large aggregates of BMDs could be from the ruptures of sodium caseinate interfacial film when two or more oil droplets collided. This BMD was also heat stable; the dotted line shows that there was no significant difference between unheated and heated particles (90 C° for 5 minute). The BMD colloidal suspensions appeared milky white in colour with no sign of sedimentation or phase separation throughout the period of storage.

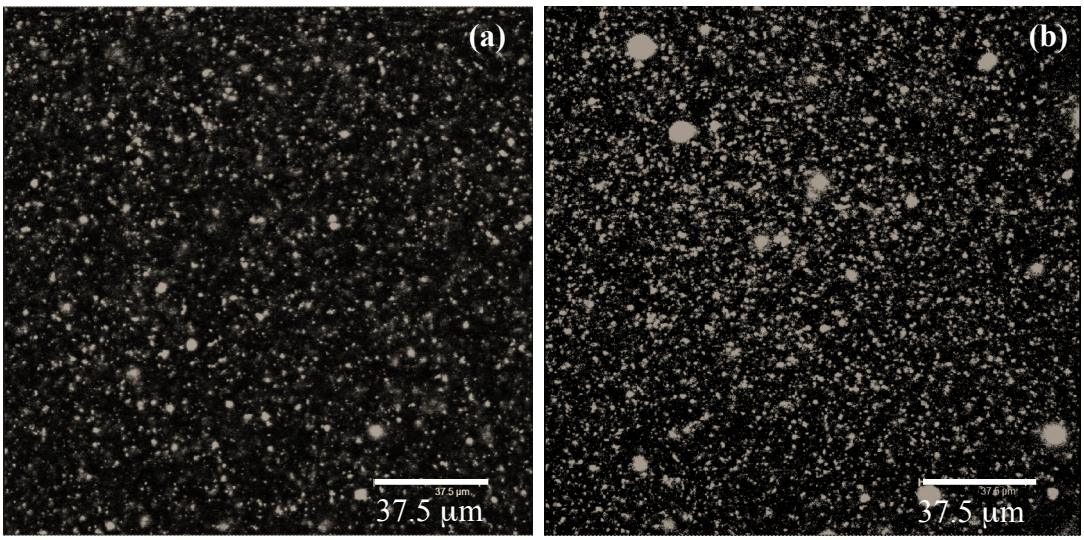

Figure 5-2 CLSM of 1 vol.% of BMDs in phosphate buffer: (*a*) pH7; (*b*) pH4. Bright regions are BMDs, dark regions are phosphate buffer.

Figure 5-2*a* shows a typical micrograph of the morphology of 1 vol.% BMDs diluted with phosphate buffer at pH 7. NR was used to highlight the oil which showed the bright regions. The suspension exhibited fairly uniform droplets with little particle aggregation. Aggregated droplets can form from either having too low

volume of oil (bridging flocculation) or an excess of unabsorbed protein (depletion flocculation) (Dickinson, 2010a). Acidification in the direction of the isoelectric point of sodium caseinate (pI = 4.6) results in decrease of repulsive forces between each molecule (Allen *et al.*, 2006; Dickinson, 2010a). In other words, acidification neutralises the negative charge on the molecules which generally results in particle aggregation (Dickinson, 2012c). The result is in agreement with Hadjsadok *et al.* (2008) and O'Kennedy *et al.* (2006) where they stated that near and below the pI the aggregation number of sodium caseinate is increased. As the suspension passed through pH = pI the uncharged particles are free to collide and aggregate and this aggregation is generally irreversible. Dickinson (2012a) also reported that on lowering the pH of casein toward pI resulted in self-association and gelation. This formation of large BMD aggregates is shown in Figure 5-2*b* and for this reason it was not possible to obtain good quality particle size distributions at pH 4 via the Zetasizer. However, it was possible to measure the electrophoretic mobility and zeta potential of the BMDs suspension. The mobility values obtained were -1.08 and +0.97 at pH 7 and 4. The surface charge of the BMDs displayed initial zeta potential values of -13.8 mV and +12.4 mV at pH 7 and pH 4, respectively.

5.3.2 Bulk rheology of BMDs

As mentioned in the introduction in Chapter 1, one of the influences that impacts on the kinetics of phase separation of S + galactomannan gum is viscosity. For example, if the particles added caused a significant increase in viscosity of either the starch or gum phase, this phenomenon would tend to slow down or inhibit phase separation. Hence, measuring the effect on the bulk viscosity of particles added to the system is crucial. Figure 5-3 shows the microdroplets shear viscosity (η) measured over the shear rate ($\dot{\gamma}$) range 0.1-1 s^{-1} for 1 - 15 vol.% BMDs dispersed in phosphate buffer, at pH 7 and pH 4. It seems that the trend lines on Figure 5-3 follow some kind of power law behaviour, often used to describe data empirically. Further investigation of the viscosities of the BMDs were adequately fitted to a power law model, see Equation 1-7 section 1.7.1. The fitting parameters are shown in Table 5-1 and the trend lines on Figure 5-3 are the fitted power law behaviour. Rheological measurements indicated an almost Newtonian behaviour with flow behaviour index (n) ≅ 0.8 at all concentrations with mean η of 0.005 Pa s at pH 7.

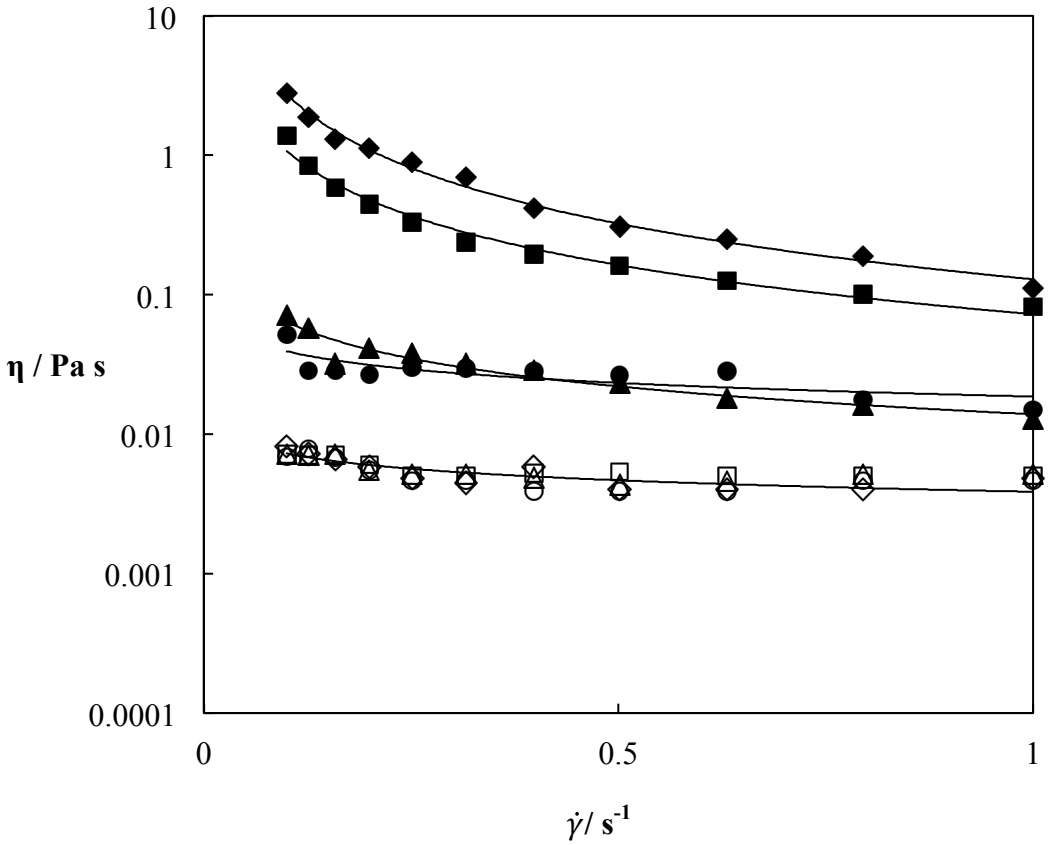

Figure 5-3 Viscosity (η) versus shear rate ($\dot{\gamma}$) for BMDs; at pH 7 (open symbols) and pH 4 (filled symbols): 1 vol.% (○,●); 5 vol.% (△,▲); 10 vol.% (□,■); 15 vol.% (◇,◆).

Nevertheless, after acidification to pH 4, at $[C_p] > 1$ vol.%, BMD dispersions exhibited shear-thinning behaviour ($n < 0.4$) at ambient temperature. In fact, at pH 4 as the $[C_p]$ increased the shear-thinning behaviour was also progressively stronger. The negative n obtained for 10 and 15 vol.% BMDs at pH4 is difficult to explain although negative n had already been reported elsewhere for corn and soy grains mixed solution (Fraiha *et al*., 2011) and potato flour (Mackey *et al.,* 1990). Although the contribution of the factors caused negative n was not clear one might be assumed that sample slip maybe involved.

Table 5-1 Fitting parameters of power law model (Equation 1-7) to viscosity of WPI microgel suspensions of different [C_p] as shown in Figure 5-3. *K* is the flow consistency index, *n* is flow behaviour index and R^2 is goodness-of-fit.

vol.%	*K*	*n*	R^2
pH 7			
1	0.0038	0.74	0.6469
5	0.0045	0.816	0.6391
10	0.0047	0.827	0.7226
15	0.0039	0.73	0.7171
pH 4			
1	0.0186	0.675	0.6310
5	0.0139	0.337	0.9280
10	0.0726	-0.17	0.9833
15	0.1291	-0.326	0.9909

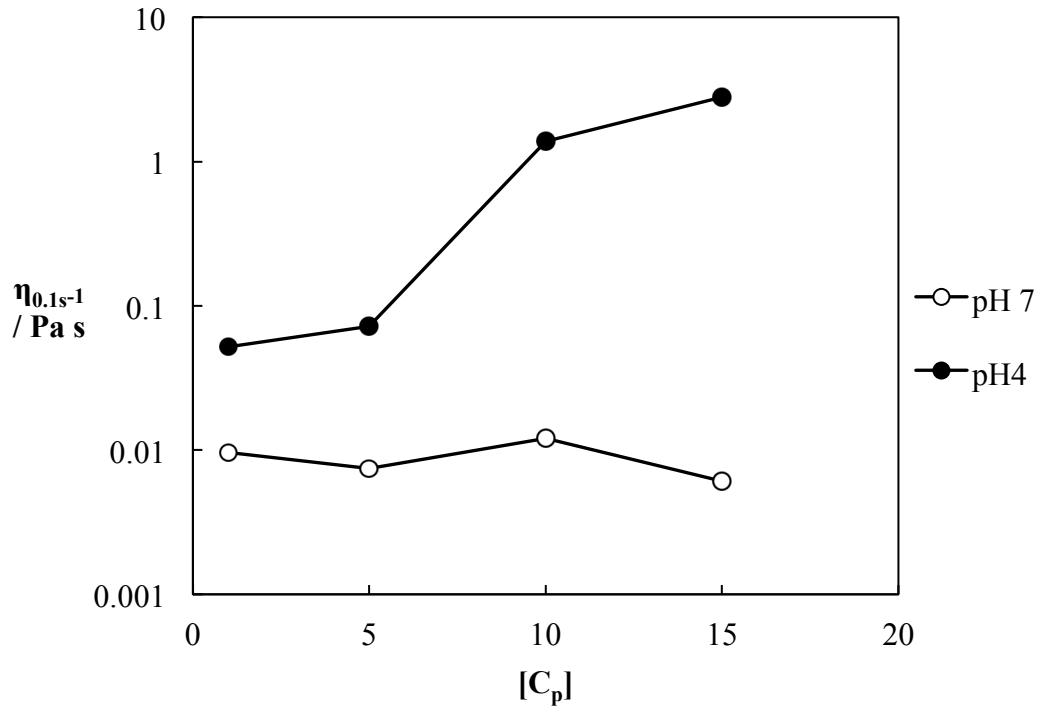

Figure 5-4 Viscosity (η) at $\dot{\gamma}$ = 0.1 s^{-1} of BMDs; at pH 7 (open symbols) and pH 4 (filled symbols).

Figure 5-4 is the graph of η at $\dot{\gamma}$ = 0.1 s^{-1} (lowest shear rate that may be taken as an indication of the 'zero' shear rate) plotted as a function of [C_p] and pH. Based on the results, at pH 7 the η values were likely to be similar in all [C_p] whilst at pH 4 η of BMDs significantly increased as [C_p] is increased. It is seen that at pH 4 where

$[C_p]$ > 5 vol.% the η of dispersion was significantly increased. As expected, the dispersion of 15 vol.% BMDs at pH 4 showed the highest viscosity due to the higher volume fraction of packed particles within the dispersion, and sodium caseinate possibly also formed gel and exhibited high viscosity. Dickinson and Yamamoto (1996) reported that milk protein gels, like casein, are formed with induced acid. As can be seen in Figure 5-2*b* the droplets were aggregated which led to the increased in viscosity of dispersion. From Figure 5-4, it can be concluded that at pH 4 the η of BMDs dispersions depends upon $[C_p]$ whilst at pH 7 the dispersions were not affected when $[C_p]$ of BMDs was increased.

Regardless of the pH, the viscosities of BMD dispersions were still lower than that of 4 wt.% S, 0.5 wt.% GG and 0.6 wt.% LBG, i.e., 60, 1.8 and 0.8 Pa s at $\dot{\gamma}$ = 0.1 s^{-1}. Therefore, in the presence of BMDs in the polysaccharide mixtures, some increase in η of either starch or gum might be expected but not enough to significantly alter the phase separation kinetics. Except at pH4, $[C_p] \geq 10$ vol.%, where the viscosities of BMDs dispersions were close to LBG and GG.

5.3.3 Determination of phase separation

Phase separation in S + LBG or GG (in the absence of particles) has been reported in Chapter 3. The system exhibits macro phase separation and forms a starch-rich bottom phase and gum-rich upper phase. Images of the evolution of macroscopic phase separation with and without particles for the two different systems, S + LBG and S + GG, are shown in Figure 5-5. Pure mixtures of S + LBG or GG show macroscopic phase separation within an hour after mixing and are completely phase separated after 2 weeks. Increasing the volume fraction of BMDs in S + LBG systems seemed to suppress the appearance of phase separation. At concentrations of 10 and 15 vol.% BMDs, the S + LBG mixtures showed no sign of phase separation for a period of months. In contrast, in S + GG systems, addition of emulsion droplets did not seem to have a significant effect on the behaviour of mixtures in the first week of mixing. However, the top phase seemed to be more clear than that of the top phase of S + LBG mixture. Interestingly, the macroscopic phase separation of S + GG mixtures at 10 and 15 vol.% emulsion droplets showed three phase layers after 1 month. The middle phase was assumed to be a mix of all polymers, leaving the top and bottom layers to contain mostly water. An increase in

turbidity of the bottom layers was caused by the presence of excess emulsion droplets. No oiling-off was seen in any samples over 4 weeks of storage indication that there was no coalescence of the BMDs during storage.

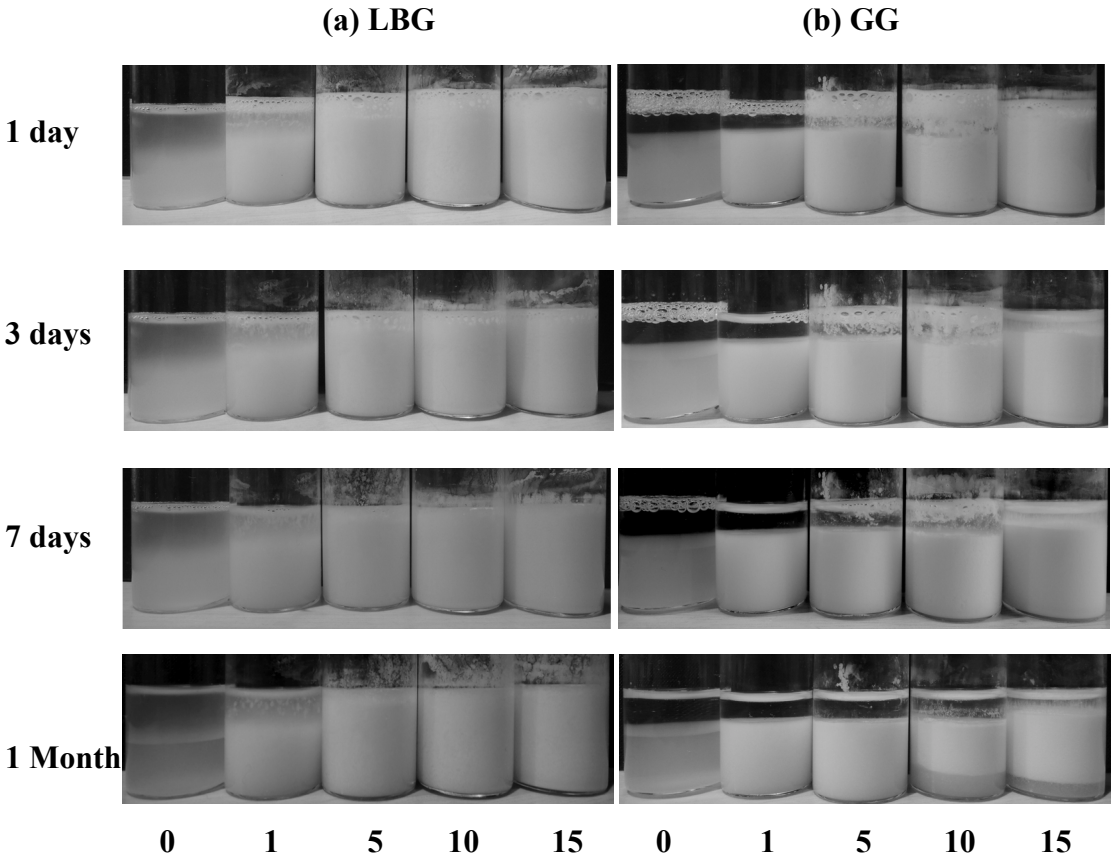

Figure 5-5 W/W emulsions formed by 2 wt.% S + (*a*) 0.3 wt.% LBG; (*b*) 0.25 wt.% GG containing 0 to 15 vol.% BMDs at pH 7. Observed at 1, 3, 7 and 30 days. From left to right: no particle; 1 vol.%; 5 vol.%; 10 vol.%; 15 vol.% BMDs.

The mixtures containing S + galactomannan with the presence of 5 vol.% BMDs were taken for a further analysis via confocal microscopy in order to identify the components of each layer. RB and NR were used to stain each layer. As expected, the bottom layer of both mixtures (Figure 5-6*a* and Figure 5-6*b*) showed bright specks of BMDs when stained with NR and appeared to have starch (bright regions) and gum (dark regions) in the background when stained with RB. Thus, the micrographs confirm that the bottom layer contained all the components, i.e., starch, gum and BMDs. Within the experimental error, the top layer of S + LBG showed

evidence of BMDs, corresponding to the slight turbid top layer in Figure 5-5*a*. When RB was added to the top layer, there was no sign of starch or starch granules which suggests that this layer contained only LBG and BMDs, Regarding Figure 5-6d, there was only small fraction of BMDs with no sign of starch evident.

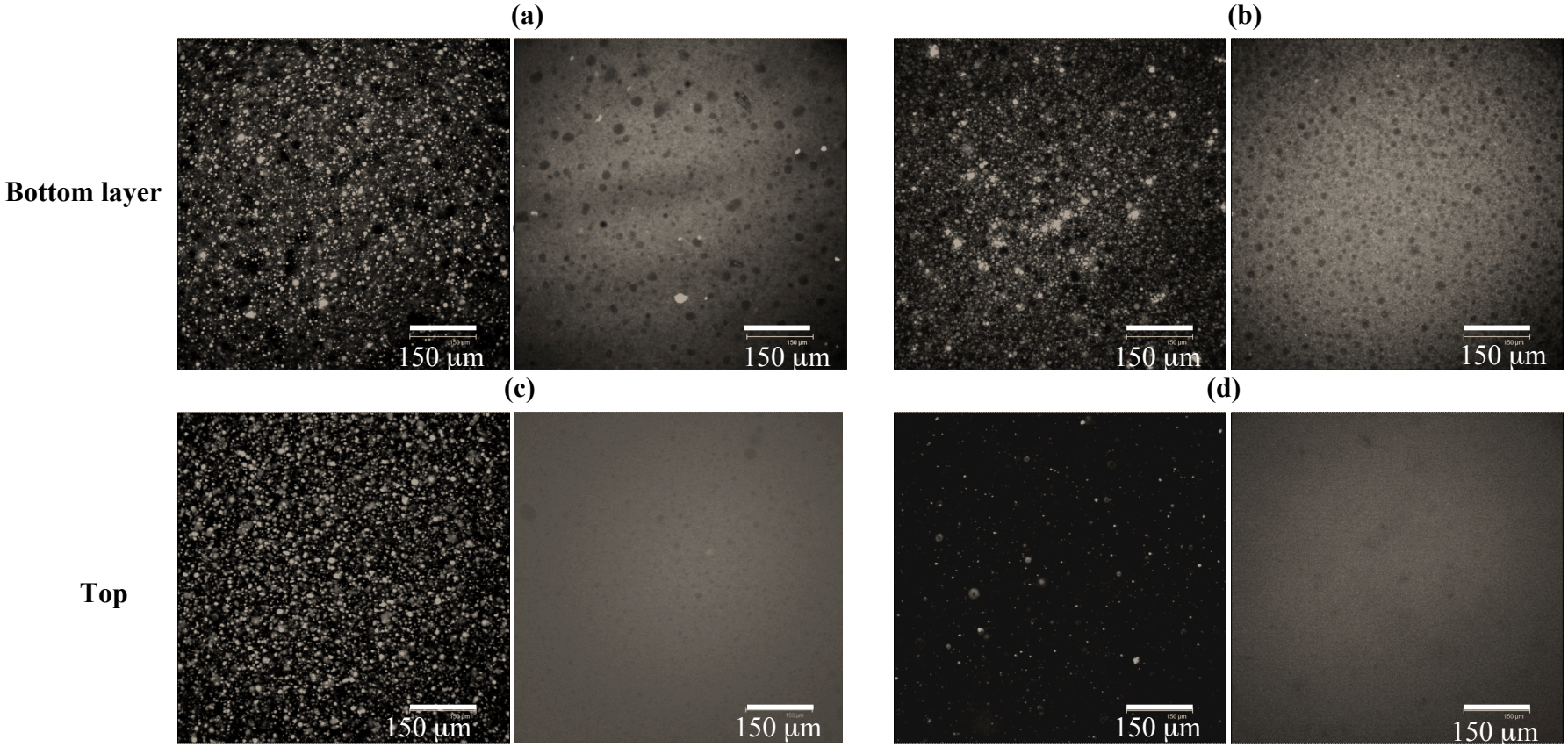

Figure 5-6 Representative confocal micrographs of each layer of 2 wt.% starch + 0.3 wt.% LBG or 0.25 wt.% GG with the presence of 5 vol.% BMDs. (a) S + LBG, bottom layer; (b) S +GG, bottom layer; (c) S+ LBG top layer; (d) S+GG top layer. Left stained with Nile Red; right stained with Rhodamine B.

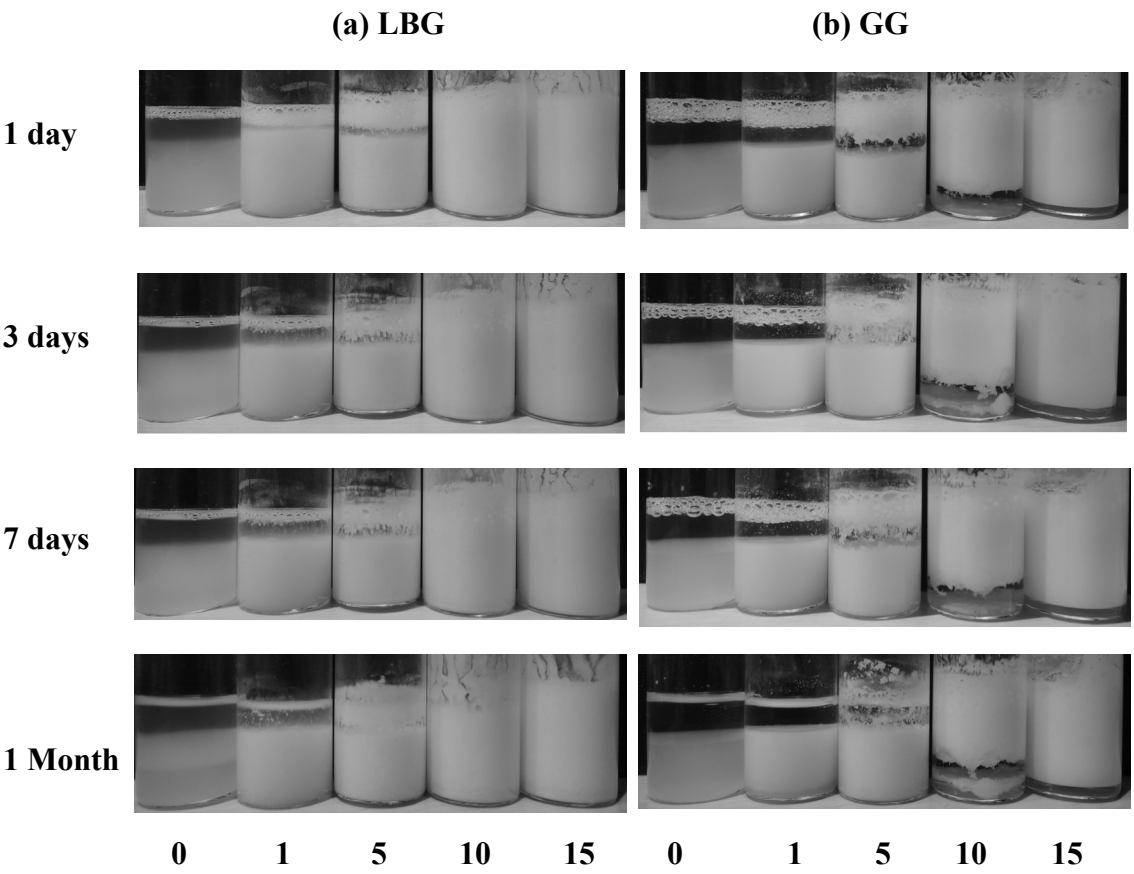

Figure 5-7 W/W emulsions formed by 2 wt.% S + (*a*) 0.3 wt.% LBG; (*b*) 0.25 wt.% GG containing 0 to 15 vol.% BMDs at pH 4. Observed at 1, 3, 7 and 30 days. From left to right: no particle; 1 vol.%; 5 vol.%; 10 vol.%; 15 vol.% BMDs.

Figure 5-7 displays the same system as Figure 5-5 at pH 4. After lowering the pH from 7 to 4 the BMDs tended to self-aggregate and form some kind of network within the S and gum domains. This resulted in an opaque white milky phase at the bottom and clear water-like top layer. The difference in texture of the mixtures was clearly visible compared with the mixtures at pH 7. At $[C_p]$ = 5 vol.% in both S + LBG (Figure 5-7*a*) or GG (Figure 5-7*b*) mixtures showed a thin layer of flocculated droplets on top of the mixtures. No phase separation was observed in the case of S + LBG mixtures stabilised by 10 and 15 vol.% BMDs. However, in the system that contained GG, the separation still persisted. The macro phase separation was changed when increasing the concentration of emulsion droplets to above 5 vol.%. At $[C_p] \geq 10$ vol.% the opaque phase appeared at the top in both model mixtures, i.e. creaming. Phase separation between cream and the aqueous phase at these concentrations can be explained by considering the starch-rich domain density. The hypothesis is that BMDs are closely packed at the domains interface which results in

slightly lower density overall (≤ 0.99 g cm^{-3}) which is close to water density. Although at first sight it seemed that at [C_p] = 15 vol.% the mixture was homogeneous, but actually there was a very thin layer of clear liquid (0.4 ml) at the bottom of the tube after storage for one month. Creaming layer increased with increasing droplet concentration. According to Figure 5-7 all of the mixtures in both polysaccharide systems exhibited good long-term stability to coalescence after one month storage (and up to at least 2 months); the volume of upper and lower phase remained the same even though they had phase separated to different extents. Gelation of sodium caseinate after lowering a pH to below its pI has been studied by numerous researchers (Chen *et al.,* 1999; O'Kennedy *et al*., 2006; Ruis *et al.*, 2007; Hadjsadok *et al.*, 2008). It was reported that after lowering pH toward pI, concentrated liquid-like caseinate is converted to a soft solid-like solution. The S + galactomannan W/W emulsions with 15 vol.% BMDs at pH 4 could be turned upside down without disturbing the sample, indicating the strong gel formation of the mixtures. Gel formation of O/W/W has been reported recently (Firoozmand and Rousseau, 2013) for a starch-gelatin system in the presence of large olive oil droplets, ranging from 2 to 20 μm. These authors also mentioned that the presence of dispersed oil in the system results in a gelatin-stabilised emulsion gel at all oil concentrations (e.g. 1 – 16 wt.%). For the S + galactomannan systems studied here the gel formation only appeared when there was at least 15 vol.% BMDs at pH 4. If one of the components in the mixture forms a gel or exhibits a highly viscous property, the rate of phase separation may be retarded (Ercelebi and Ibanoğlu, 2007).

5.3.4 Microscopic observations on phase separation

As GG and LBG appeared to behave similarly in the CLSM analysis, only micrographs of S + LBG system are presented. Figure 5-8 compares the difference in microstructure of S + LBG mixtures in the absence and presence of BMDs captured at 5 ± 2 minute after mixing. All the systems possessed morphology typical of a spinodal decomposition structure. The bright regions in Figure 5-8*a* correspond to strong RB fluorescence indicative of starch-rich regions whilst in Figure 5-8*b* and Figure 5-8*c* the bright regions are an overlap area of NR and RB, i.e., starch-rich domains plus BMDs or their aggregates. As usual, dark areas in the micrograph represent non-fluorescent regions which assumed to be the gum-rich regions. Figure 5-8*a* represents the microstructure typically observed with no added particles. Figure

5-8*b* shows the same system with added 1 vol.% BMDs at pH 7. BMDs resided largely within starch-rich microdomains. It was not clear in this image whether there was any definite accumulation of particles at the W/W interface. In addition, the phenomenon, where the particles preferred to be situated in the starch phase, for no obvious reason, was also observed as reported for the S + galactomannan gum + silica nanoparticles in Chapter 4. Herzig *et al.*, 2007 explained that when the contact angle of particles/droplets differs from 90° this would be expected to lead to an excess of particles/droplets in one phase. After acidification to pH 4 (Figure 5-8*c*) there was some evidence of BMDs decorating at the interface between two phases, possibly indicating a bijel formation. Regarding the lower tendency of bright specks within the starch-rich domains compared with the Figure 5-8*b,* this might indicate that there was somehow a depletion of BMDs from the starch domain and a flocculation of particles at the interface when lowering the pH to 4. Another assumption is when the starch-rich domain formed, BMDs were at the interface and formed a strong solid network.

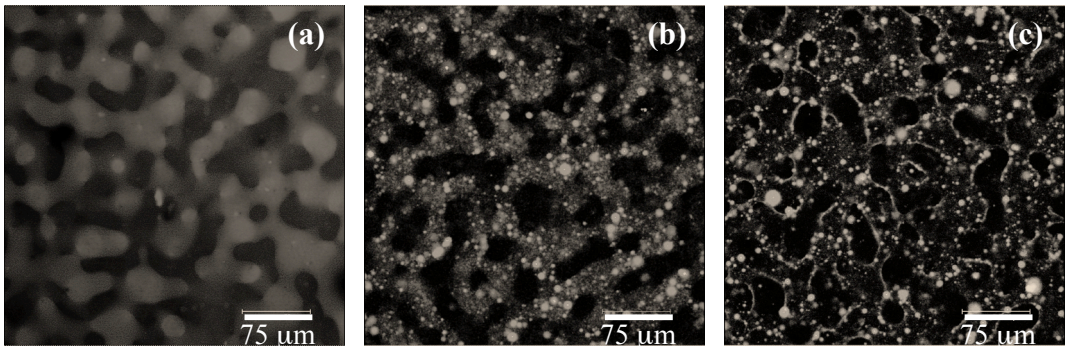

Figure 5-8 Representative confocal micrographs of mixture containing 2wt.% S + 0.3 wt.% LBG in the absence and presence of BMDs captured at 5 ± 2 minute after mixing: (*a*) no particles at pH7, age 5 minute; (*b*) 1 vol.% at pH 7, age 5 minute; (*c*) 1 vol.% at pH 4, age 5 minute.

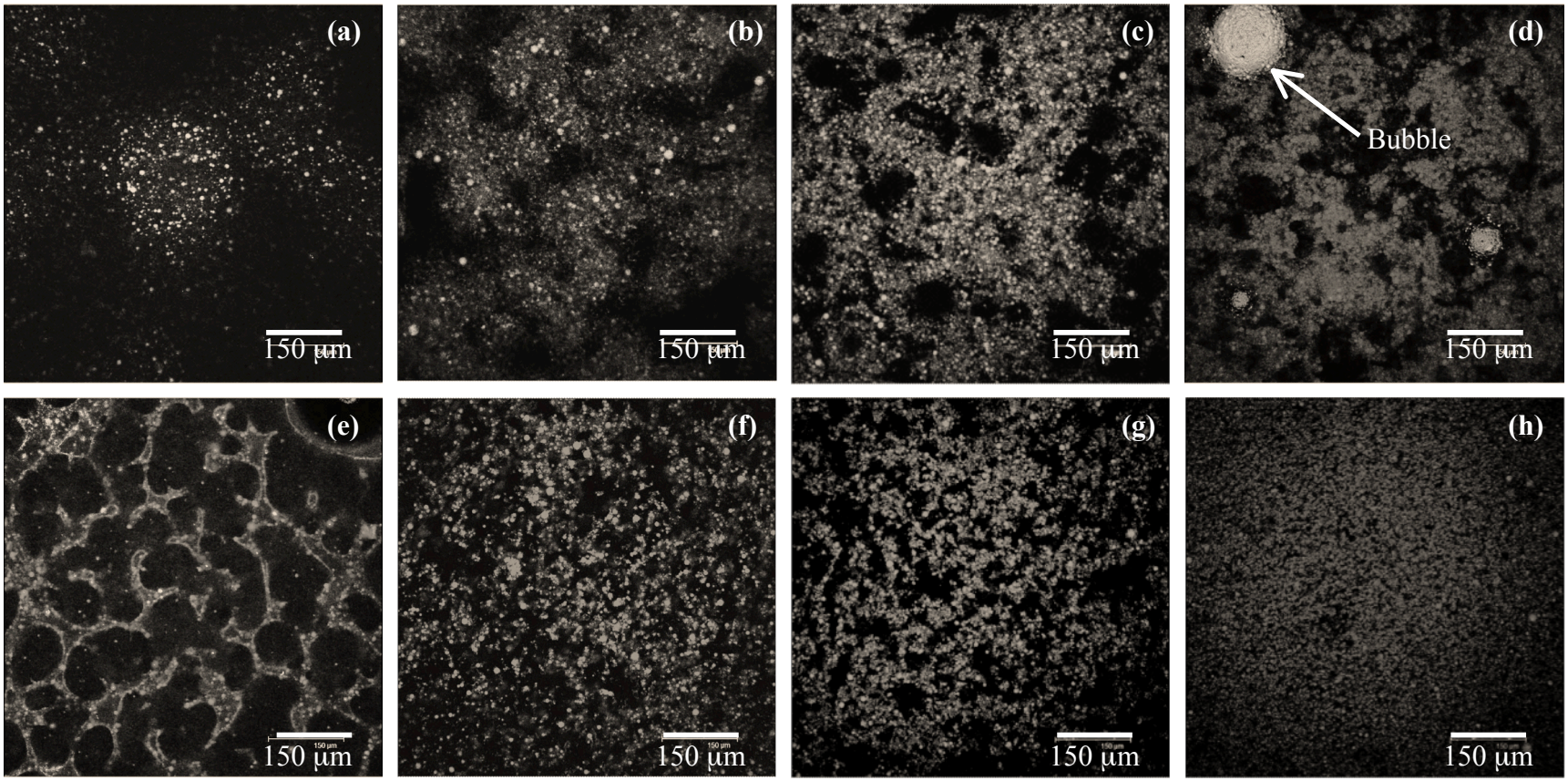

Figure 5-9 Representative confocal micrographs of mixture of 2 wt.% S + 0.3 wt.% LBG in the absence and presence of BMDs captured after 24 h storage: (*a*) 1 vol.%, pH 7; (*b*) 5 vol.%, pH 7; (*c*) 10 vol.%, pH 7; (*d*) 10 vol.%, pH 7; (e) 1 vol.%, pH 4; (*f*) 5 vol.%, pH4; (*g*) 10 vol.%, pH4; (*h*) 15 vol.%, pH4.

Figure 5-9 shows CLSM micrographs of mixtures of 2 wt.% S + 0.3 wt.% LBG after 24 hour storage in the presence of BMDs at different [C_p]. As was mentioned in Chapter 4, the separation kinetics and microstructure were independent of the mixing procedure. Again the bright regions are overlap areas of NR and RB. Dark areas in the micrograph indicate LBG-rich phase. Occasionally, large circular objects were visible in the micrograph, which were air bubbles that were difficult to remove completely in some instances, especially at high BMD concentrations. Figure 5-9 corresponds to the presence of BMDs at concentration between 1 – 15 vol.%. The systems at pH 7 are shown in Figure 5-9*a, b, c, d* whilst the systems at pH 4 are displayed in Figure 5-9 *e, f, g, h.* Figure 5-9*a* shows the effect of 1 vol.% BMD on the system. Due to the strong immiscibility between S and LBG, after 24 hours only a few starch-rich regions were evident at pH 7 and a low concentration of oil droplets had a minor effect on the phase separating microstructure.

The experiment was also conducted with higher [C_p]; 5, 10 and 15 vol.% at this pH. The representative micrographs for 24 hour ageing time are shown in Figure 5-9*b, c, d*, respectively. The growth of starch microdomains was slowed down as the concentration of BMDs increased. There was still a sign of spinodal decomposition even after 24 hours observation - see Figure 5-9*d* and Figure 5-8*a*. Casein is well-known for its foaming and emulsifying properties (Zayas, 1997; Sanchez and Patino, 2005; Abascal and Gracia-Fadrique, 2009). The effect of sodium caseinate-stabilised foam depends upon pH and concentration, the higher the concentration the better the foamability. At pH values near the pI the foamalibilty is decreased (Marinova *et al.*, 2009). As can be seen in Figure 5-9*d,* at pH 7 [C_p] =15 vol.%, there was a sign of bubbles appearing in the mixtures whereas at the same BMD concentration at pH 4 (Figure 5-9*h*) there was no evidence of bubble formation. The bubble layer was clearly visible in macroscopic observations (Figure 5-7), suggesting that the bubbles rose swiftly up to the top. In the presence of 15 vol.% BMDs good CLSM micrographs without the presence of bubbles could not be obtained. Thus, for bubbles which formed during mixing via the Ultra Turrax, whilst some may collapse some still persist in the system, and possibly slightly altered the spinonal decomposition microstructure.

After lowering the pH to pH 4, BMDs showed a much more significant effect on the phase separation. BMDs tended to aggregate during the pH adjustment,

possibly leading them to form a stronger interfacial network, in effect on interfacial emulsion gel (Dickinson, 2012c). Figure 5-9*e* shows a micrograph obtained after 24 hours with 1 vol.% droplets. It is obvious that there are many droplets decorating the interface. However, as [C_p] was increased further, it was very difficult to distinguish an increase in accumulation of BMDs at the interface due to the closely packed droplets in the starch phase. Possibly the BMDs fully covered the interface, resulting in a transition from a more space interfacial droplet layer to a more multilayer. Higher droplet concentrations were not studied because the aim was to find a range of droplet concentrations that might be of practical use in reducing phase separation and because of the problem of increased foaming as the droplet concentration increased.

5.3.5 Image analysis

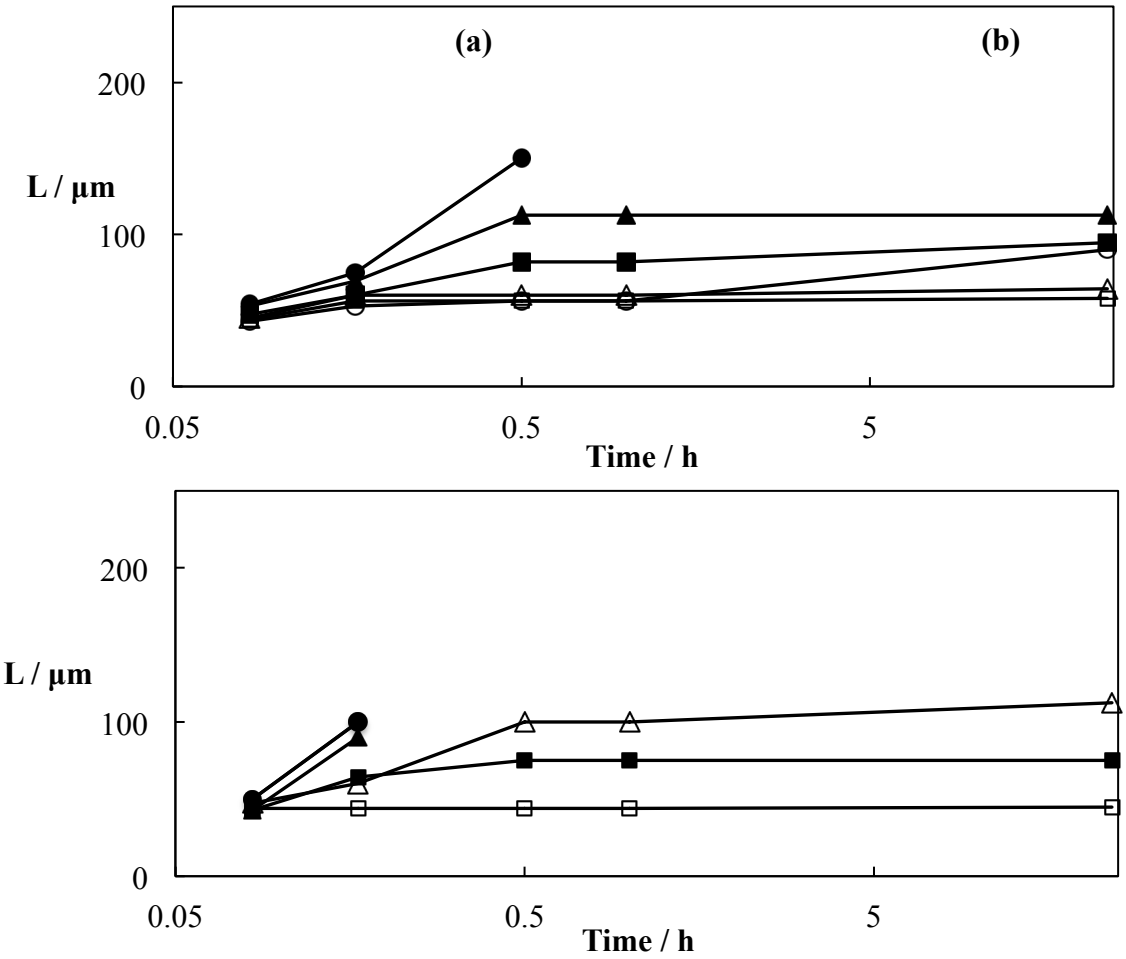

Figure 5-10 Characteristic length scale, *L*, versus time since mixing for mixtures of (*a*) S + LBG; (*b*) S + GG ; at pH 7 (filled symbols) and pH 4 (open symbols) :1 vol.% (●,○); 5 vol.% (▲,△); 10 vol.% (■,□).

Figure 5-10*a, b* shows the quantification of the evaluation of domain size for the different systems mentioned above, Figure 5-10*a* displays S + LBG systems and Figure 5-10*b* displays S + GG systems. The filled and open symbols indicate the condition of the mixture at pH 7 and 4, respectively. Only BMDs concentrations of 1 to 10 vol.% were analysed because at higher concentrations, e.g. 15 vol.% the spinodal decomposition structure was disrupted by the bubbles that formed. In the absence of BMDs in S + galactomannan mixtures, $L \approx 60$ μm after 5 ± 2 minute. However, the starch-rich domain size grew rapidly afterward, consequently the discrete domains were undetectable due to separate layers starting to form in the 3 mm well slide. The data obtained was adequately fitted to Stokes' law:

$$V_s = \frac{g(\Delta\rho)d^2}{18\eta_c} \qquad \text{Equation 5-1}$$

V_s is the velocity, g is gravitational acceleration = 9.8 m/s^2, $\Delta\rho$ the density difference between domain and the continuous phase, d the droplet diameter and η_c the viscosity of the continuous phase. Although this model is used to describe the influence of gravity toward spherical dispersed phase in the binary mixture, but in this case we assume that the size of L is a droplet diameter, hence, the starch microdomain $L = d = 60$ μm. Density of starch, GG and LBG were 1.01, 0.9, 0.89 g cm^{-3}, yielding $\Delta\rho$ = 0.12 and 0.11 g cm^{-3} for S + LBG and S + GG systems, respectively. Viscosity at 0.1 s^{-1} of GG and LBG were 0.15 and 0.07 Pa s and was not significantly different when BMDs were added – see Figure 5-11*a*. The velocity of creaming or sedimentation was quantified by measuring the height of the mixtures as a function of time. The final calculation of velocity of starch domain for S+ GG and S + LBG systems were 0.62 and 1.35 cm h^{-1}. This result predicted that within the height of the welled slide (3 mm), the complete phase separation would be completed within 30 minutes. However, since rate of phase separation was slower in the presence of BMDs it would seem that Stokes model does not apply for the mixture with added BMDs, but this is not a surprise given the complexity of the system, Stokes' law is designed for dilute suspension in a fluid.

At pH 7 for S + LBG mixtures (Figure 5-10*a*) where [C_p] = 1 vol.%, the starch domains grew to $L > 150$ μm within 30 min of observation and the domain size continued growing to over 200 μm after 24 hour (the data point is not shown). At higher concentrations, the starch domains were likely to remain the same size

after 30 minutes. On the other hand, after acidification of the mixtures to pH 4 the results at all particle concentrations show approximately the same *L*. However, there was a slight change in *L* for 1 vol.% where *L* rose to 90 μm after 24 hours. It is also seen that an increase in droplet concentration from 5 to 10 vol.% shows no significant effect on the mixture stability. The BMDs at pH 4 were effective in keeping $L < 90$ μm for 24 hours. These trends are in agreement with the qualitative assessment in Figure 5-9.

Figure 5-10*b* shows the effect of various $[C_p]$ in S + GG systems. At pH 7 where $[C_p] \leq 5$ vol.%, the system was quite dynamic with fast fusion of starch-rich microdomains which led to L > 200 μm within 30 minutes of observation, whereas with 10 vol.% concentration, the BMDs were more effective in keeping $L < 100$ μm for 24 hour. Furthermore, at pH 4 $[C_p]$ =1 vol.% gave approximately the same stability as at pH 7 for the same concentration. Increasing $[C_p]$ further to 10 vol.% gave a further increase in the stability of *L*. Interestingly, only increasing the concentration of BMDs from 5 to 10 vol.% improved the stability of S + GG mixture from $L = 112.5$ to 45 μm.

5.3.6 Bulk rheology of different phases

It is clear that BMDs were capable in slowing down the domain growth and stabilising the system. However, the viscosity of bulk phase also becomes an important consideration when trying to explain the effect of emulsion droplets on the phase separation. So the question arises whether the change in domain stability was due to an increase in viscosity. Consequently, the BMDs were dispersed in the separate bulk phases at $[C_p]$ from 1 – 15 vol.%. Figure 5-11 shows η at $\dot{\gamma} = 0.1\ s^{-1}$ (5-11*a*) plus oscillation shear rheology at low frequencies and 1% strain: in 5-11*b* the storage modulus (G') at 0.1 Hz and in 5-11*c* the loss modulus (G") at 0.1 Hz. These low shear conditions were selected as being close to the solution at rest. Since the major effects of particle addition were at pH 4, the measurements were only conducted at this pH

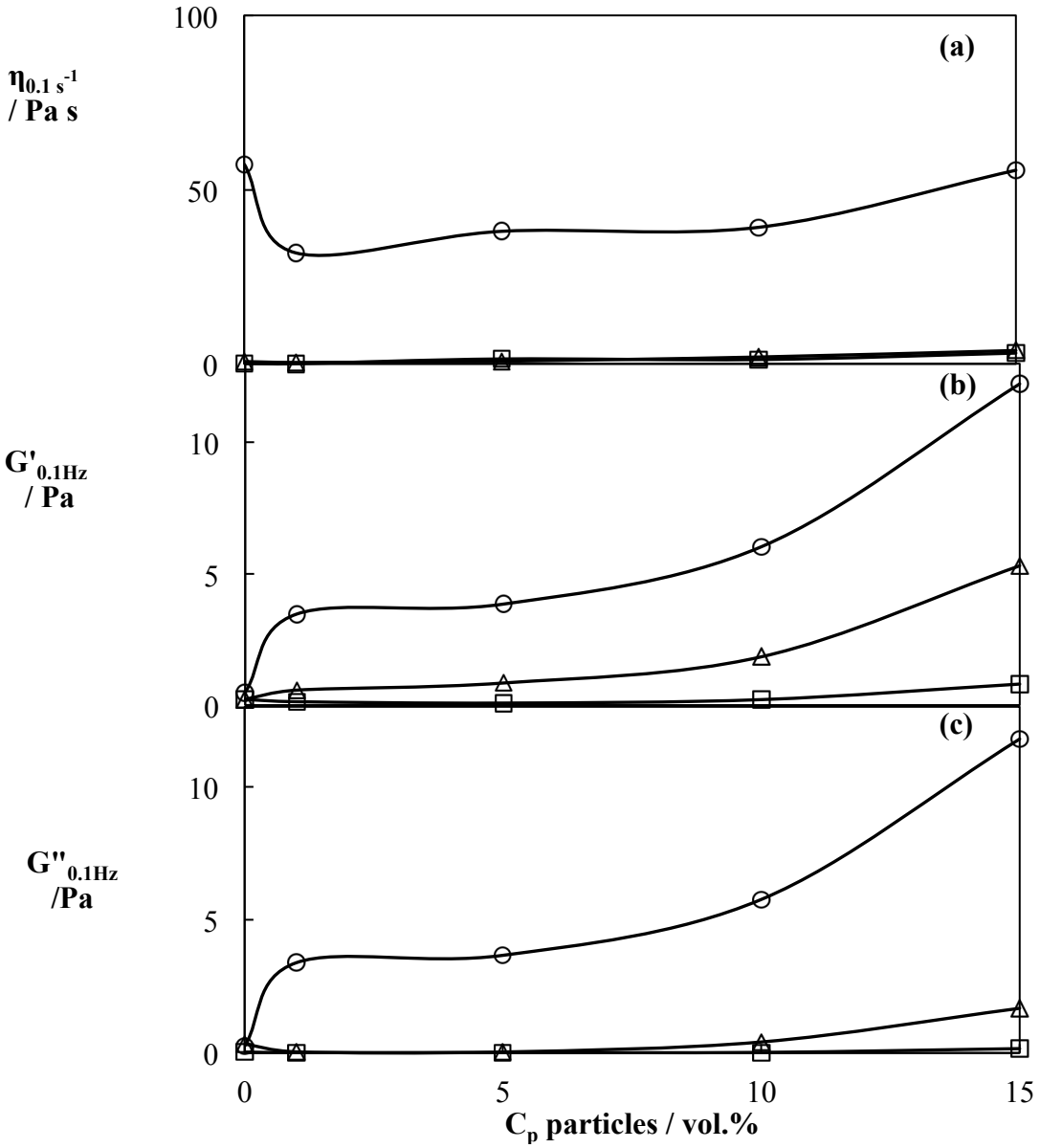

Figure 5-11 At pH4 (*a*) Viscosity (η) at $\dot{\gamma}$ = 0.1 s^{-1}, at pH 4; (*b*) storage modulus (G') measured at 0.1 Hz; (*c*) loss modulus (G") at 0.1 Hz and 0.01 strain versus vol.% (ϕ) of BMDs added to individual solutions of 4 wt.% starch (○); 0.6 wt.% LBG (△); 0.5 wt.% GG (□).

Figure 5-11 clearly shows that for up to 10 vol.% BMDs added to 0.5 wt.% GG, there was no significant increase in η, G' or G" whilst for 0.6 wt.% LBG G' and G" significantly increased at 10 and 15 vol.% BMDs, although η remained similar for the whole concentration observed. At high BMD concentrations, the mixture attained viscoelastic behaviour because the droplets of protein-stabilised droplets were more close packed (Zeeb *et al.*, 2013). An increase in viscoelasticity of the

LBG phase could therefore be reason why S + LBG systems had a better stability than that of GG - see Figure 5-7. Addition of BMDs to 4 wt.% S gave a noticeable increase in G' and G" whereas there was a decrease in η at low percentage of BMD followed by a gradual increase as the concentration of particles increased. The rheological behaviour of S solution in the presence of BMDs particles could be the reason why the decoration of particles at the interface is visible. Probably there is depletion flocculation of particles in the bulk starch phase. Furthermore, the increase in G' suggests an increase in domain rigidity. Figure 5-11*b, c* show that bulk starch and LBG phases form a weak viscoelastic gel (G' > G" over the frequency range observed) after adding BMDs. It is suggested that this gelation could be another reason of slowing down phase separation mechanism.

5.4 Conclusion

The novelty of this research stemmed from the use of 1-bromohexadecane microdroplets (BMDs) as an emulsifier for W/W emulsion system for possible application in food products. The effects on the phase separation of waxy corn starch + locust bean gum or guar gum on adding various concentrations of BMDs has been studied at pH 4 and 7. Above 1 vol.% droplets, at pH 7, phase separation of the W/W systems were significantly inhibited. The stability depended upon concentration of the particles and pH of the system. The particles showed a strong preference for the starch domain rather than the gum phase. Overall, the data obtained indicated that the higher the concentration of BMDs, the better the stability of S + galactomannan mixtures. Moreover, the particles are more effective after acidification. At pH 4, there was some microscope evidence that the droplets actively accumulated at the W/W interface. As the droplets appeared to have positive ζ-potential at pH 4 it is suggested that the charge on the droplets may be the driving force behind the formation of particle aggregates at the W/W interface; which leads to a slowing down of the kinetics of phase separation. Measurements of the bulk rheology of the gums and starch phases in the presence of BMDs suggested that the rheological behaviour of the interior of GG was hardly affected at all, whilst the viscoelasticity of LBG was slightly affected. The starch phase viscoelasticity was significantly

increased which is a sign of gel formation within the starch phase which also possibly contributes to inhibitation the phase separation.

Chapter 6

6 Chapter 6. Effect of whey protein isolate microgel particles on phase separation of waxy corn starch + locust bean gum or guar gum

6.1 Introduction

In the food industry, the use of particles to stabilise emulsions gives advantages in food formulation with novel texture, encapsulation, better stabilisation and good quality overall in the food product. However, most fundamental work on Pickering stabilisation so far has involved non-food grade particles. A challenge is to be able to produce particles that are both effective in stabilising an emulsion and acceptable for use in the food industry (Morris, 2011). Protein particles are an attractive possibility, since their cross-linking, e.g., via hydrogen bonds, salt bridges, changing pH etc., can be controlled by the solution conditions. They can be prepared in various ways such as thermal-induced (Liu and Tang, 2013) and solvent-induced precipitation (de Folter et al., 2012). Microgel particles have featured as part of novel Pickering stabilisers in recent years (Li and Ngai, 2013), since recently they have been used effectively for stabilising O/W emulsion and foams (de Folter *et al.*, 2012; Destribats *et al.*, 2014b,c; Deshmukh *et al.*, 2014). Protein microgel particles (de Folter *et al.*, 2012, Destribats *et al.*, 2014b) are one possible novel food particle that might be able to be used as an emulsifier via Pickering stabilisation. Recently, Nguyen, Nicolai, and Benyahia (2013) reported the W/W stabilisation using protein aggregates as particles in 'semi-polysaccharide' system of dextran + poly (ethylene oxide). In 2011, Schmidt and colleagues proposed a new term for microgel-stabilised emulsions; so called Mickering emulsions due to the basic concepts being similar to that of Pickering emulsions but the underlying mechanisms are different.

There are three main ways to produce a three-dimensional protein gel network: ionotropic gelation, cold-set gelation and heat-set gelation. Especially for globular proteins, e.g., whey protein, they form gels when heated at high enough concentration. Most whey protein components denature and aggregate on heating > 70 °C. In the past few years, gel particles of sub-micron, micro- and nanosize are of growing interest in chemical, food, cosmetics and pharmaceutical industries. One particular use of gel particles is for encapsulation or texture control. Although

protein microgel particles cannot really be considered as classic solid particles but it is not absolutely clear how rigid particles have to be to act as good Pickering stabilisers as long as they maintain a size and contact angle sufficient to maintain their interfacial attachment. In fact, the first person who discovered Pickering stabilisation, Ramsden, also used proteins (i.e., albumin) as particle-stabilised emulsions (Chevalier and Bolzinger, 2013). Li and Ngai (2013) claimed that there are advantages of using microgels over conventionally solid particles. The key advantages are (1) they can cover higher interfacial area due to their soft and porous properties which lead to deformation and flattening at the interface (2) the changes in environmental conditions such as pH, temperature, ionic strength etc. can enhance the stability of emulsions.

As mentioned in chapter 5, mixtures of protein and polysaccharide commonly exhibit phase separation. However, the interaction actually depends upon the conditions of the mixture, i.e. pH, concentration, temperature, ionic strength etc. Chun and colleagues (2014) found that at a concentration of WPI below 1 wt.% mixtures of carrageenan or pectin + non-heated WPI showed no sign of phase separation. Moreover, Simonet and his colleagues (2000) also verified that no protein/polysaccharide phase separation occurred at up to 2 wt.% β-lactoglobulin in guar gum + dextran mixtures. In chapter 5, microemulsion droplets were tested and there was evidence that these particles were able to stablise the model starch + galactomannan systems to some extent. Hence protein microgel particles could also be an alternative possibility. In this chapter, food-grade whey protein isolate (WPI) microgel particles were investigated as Pickering/Mickering stabilisers of W/W emulsions formed by phase separation of waxy corn starch (S) and galactomannan gums. In this chapter protein microgel particles were formed by making a WPI gel via heat processing then breaking it into smaller particles via the jet homogeniser. Visual observations and CLSM were used to characterise the WPI microgel particles and investigate their effect on the phase separation as a function of time and pH. The aim of this research was to formulate an alternative form of stable particle that could possibly be use in food industry for stabilisation of such water-in-water (W/W) emulsions.

6.2 Materials and methods

6.2.1 Materials

The common materials (waxy corn starch, galactomannans, Acriding Orange (AO) and Rhodamine B (RB) used in the experiments in this chapter are the same as those stated in chapter 2, section 2.1.

6.2.1.1 WPI microgel particles

Powdered whey protein isolate (WPI) was obtained from Fonterra Limited (Auckland, New Zealand).

6.2.2 Methods

Preparation of solutions

All solutions were prepared according to the standard protocol stated in chapter 2, section 2.2. All the investigated samples contained 2 wt.% starch, 0.25 wt.% GG and 0.3 wt.% LBG with or without the presence of varying concentrations of WPI microgel particles (1 - 15 vol.%).

Preparation of WPI particle suspensions

For the preparation of the WPI dispersion, the WPI powder was dispersed at 15 wt.% WPI in 200 ml phosphate buffer pH 7 and stirred under mild magnetic stirring overnight for a complete solubilisation. The WPI solution was transferred to a glass bottle with a plastic screwed top and heated in a temperature-controlled water bath at 90°C for 30 minutes. This was followed by cooling under running water for 15 minutes and storage in the refrigerator overnight. The gel was then roughly broken into pieces with a knife and these coarse gel fragments then were added to the 45:55D chamber and homogenised by a jet homogeniser operating at 220 bar. The 45:55D chamber was later filled with finer gel fragments (55% side) and phosphate buffer pH 7 (45% side) and put through jet homogeniser again at 300 ± 20 bar to obtain the microgel dispersion. The WPI microgel dispersion was then passed through the jet-homogeniser twice more to ensure that all gel fragments were broken down. Before conducting any measurements and before adding the microgel particles to in the model systems, the dispersion was sonicated with Vibra-cell (Sonics and Materials, Newtown USA) for 2 min at 40 amplitude with every two-

second pulse. The volume fraction of WPI microgel dispersion was determined by centrifugation of the suspension at 12000 rpm (17400 g) for 45 minutes in a high speed Beckman Coulter (JA-30.50) centrifuge and calculated from the volume fraction of protein sediment. The final suspension was ≈ 40 vol.% microgels. Any bubbles that formed during homogenisation were removed before use.

Particle size distribution and ζ-potential measurement

The particle size distribution and ζ-potential measurements were determined as stated in chapter 2, section 2.3. The refractive index of the microgels and the dispersion medium were set at 1.545 (Purwanti *et al.*, 2012) and 1.33, respectively. The absorbance of the protein was assumed = 0.001. Samples were diluted to approximately 0.01 vol.% before measurement. The ζ-potential was determined at pH 7 and 4 at 25 °C.

Bulk rheology

Rheological measurements were performed as stated in chapter 5 section 5.2.2.

Determination of phase separation

The phase separation measurements were performed as mentioned in chapter 2, section 2.4.2.

Confocal laser scanning microscopy (CLSM)

In the absence of WPI particles, 30 μl of the RB solution were added per 5 ml of the starch solution before blending with gum. For the model, starch + galactomananan gum mixtures in the presence of WPI particles, 30 μl of the AO solution were added per 5 ml of gum phase before blending. RB showed preferential staining of the starch whilst the AO showed strong affinity for the WPI microgel particles. Unlabelled areas were therefore assumed to be gum-rich regions. Due to the bubbles that formed during blending, the first image was captured after 20 minutes of storage. The samples were poured into a welled slide before observing the microstructure. The appearance of samples was recorded again at 5 minute, 30 minute, 1 hour and 24 hour. Image analysis was performed using Image J software as described earlier (section 2.6.2).

6.3 Results and discussion

6.3.1 WPI microgel particles characterisation

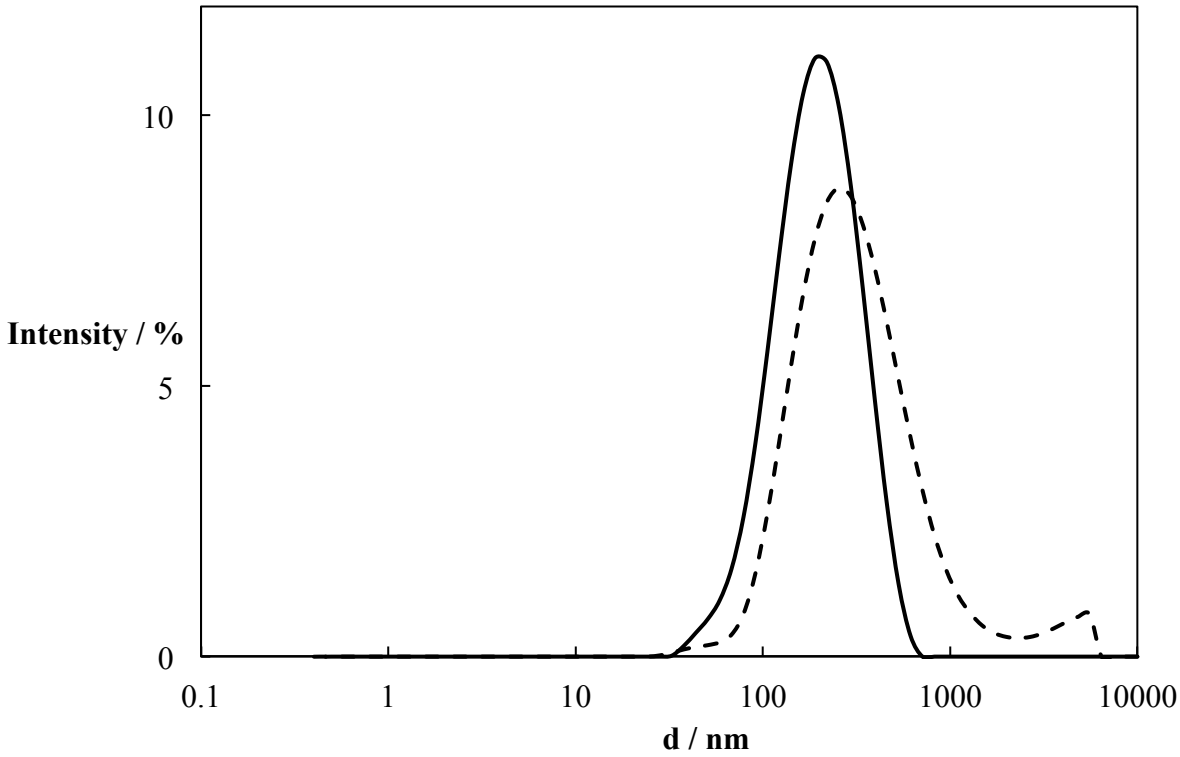

Figure 6-1 Distribution of WPI microgel particles before (- - -) sonication and (—) after sonication.

WPI microgel particles were synthesised from heat-induced protein gel that had been broken down to small fragments by passing through high-pressure jet-homogeniser. The size distribution and morphology of the microgel particles were determined by dynamic light scattering and CLSM techniques. The analytic result of dynamic light scattering is shown in Figure 6-1. The dashed line in Figure 6-1 illustrates the size distribution of the WPI particles at pH 7 after homogenisation. It could be clearly seen that the smallest dimension of the distribution is ca. 220 nm and the largest is about 5 μm. The upper distribution was assumed to be aggregates of particles since Figure 6-1 also shows that after sonication for 2 minutes, the distribution was shifted to lowered particles size (solid line). The distribution showed a significant tail around the 100 nm region. Almost all particles were de-aggregated into a dispersion of individual microgel particles sizes below 1 μm, the

Z-average size = 149 nm. Hence, in all further experiments, only sonicated WPI microgel particles were used.

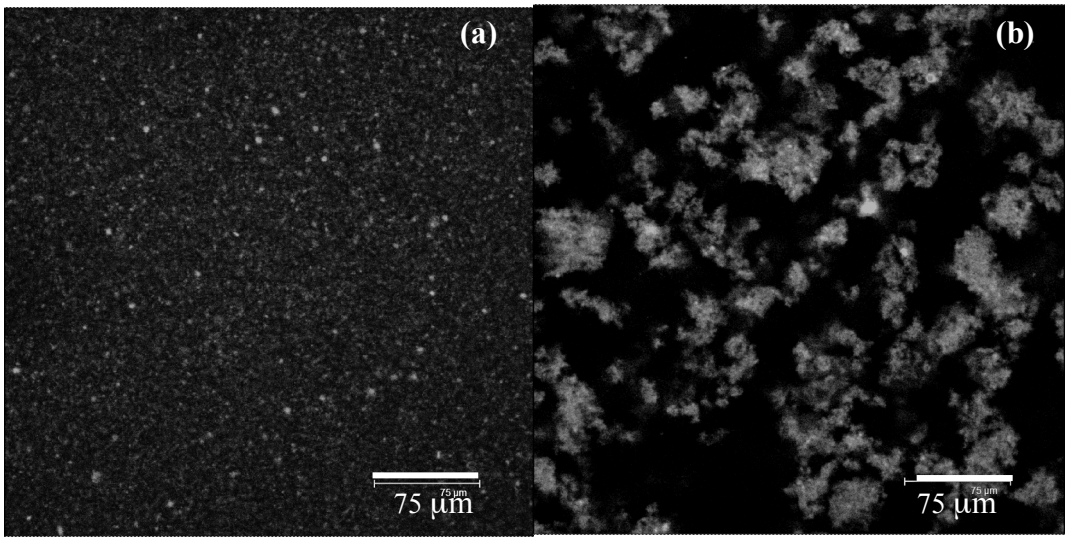

Figure 6-2 CLSM of 5 vol.% of WPI microgels in phosphate buffer: (*a*) pH7; (*b*) pH4. Bright regions are WPI microgel particles, dark regions are phosphate buffer.

The morphology of the WPI microgel particles is shown in Figure 6-2. Figure 6-2*a* shows a CLSM micrograph of the 5 vol.% WPI microgel particles suspension at pH 7 stained with AO to highlight the microgel particles (bright specks). Not surprisingly only a few particles were visible, according to the result of size distribution earlier, which indicated that most of the particles would be below the resolution of the CLSM (ca. 0.55 μm). Moreover, Brownian motion of the particles would result in blurred images. The suspension thus exhibited a fairly uniform microstructure with few particle aggregates. On the other hand, Figure 6-2*b* illustrates the WPI suspension after acidification to pH 4. The impact of acidification showed an evidence of aggregation of the microgel particles. Subsequently, it was not possible to obtain good quality particle size distribution data at pH 4 via the Zetasizer which is limited to size ranges 0.6 nm to 6 μm (Malvern Instruments Ltd., 2005). However, it was possible to measure the electrophoretic mobility of the microgel particles in dilute suspension. The pH change not only triggered the microgel particle morphology but also impacted on their charge. The values of electrophoretic mobility obtained were -1.34 and +0.93 at pH 7 and 4, respectively. Assuming a particle size of 150 nm, these mobility values convert to corresponding

zeta potential values of -17.1 and + 11.8 mV at pH 7 and 4. WPI mainly consists of β-lactoglobulin, α-lactalbumin and the isoelectric point (pI) of these two proteins range between 4.3 to 5.1 (Nicolai *et al.*, 2011;Chun *et al.,* 2014), hence the charge reversal between pH 7 and 4 was expected. Close to the pI the overall electrostatic repulsion between particles will be at a minimum, the proteins contain charges with both positive and negative sign, and this is obviously the cause of aggregation of the microgels where the interaction between opposite charges is involved. Aggregation seemed to occur immediately after pH adjustment. Moreover, the absolute magnitude of the zeta potential at pH 4 is seen to be slightly lower than at pH 7 and these two factors probably account for the greater preponderance of microgel aggregates as the pH is lowered from pH 7 to pH 4.

6.3.2 Bulk rheology of WPI microgel particles

The purpose of using WPI microgel particles in the starch + galactomannan system is to impart the interfacial stability to the immiscible phase separating regions. Therefore, it is important to observe whether the microgels have any impact on the bulk rheology of each biopolymer phase. The dispersion viscosity (η) of 1 - 15 vol.% microgel particles was measured at 25 °C over the shear rate (γ) ranges 0.1 - 1 s^{-1}. The results are shown in Figure 6-3*a, b* for pH 7 and 4, respectively. All WPI microgel dispersions exhibited shear-thinning behaviour to some extent, except for 1 vol.% dispersion at pH 7, which within experimental error was not affected by the change of shear rate. In other words, it was practically Newtonian. Figure 6-4 shows that the viscosities were significantly higher at pH 4 than pH 7 at all other [C_p] due to the high aggregation of WPI microgels, as can be seen in Figure 6-2*b*. At pH 4, 15 vol.% WPI particles, η of the dispersion rose dramatically presumably due to the onset of connection of a weak particle gel.

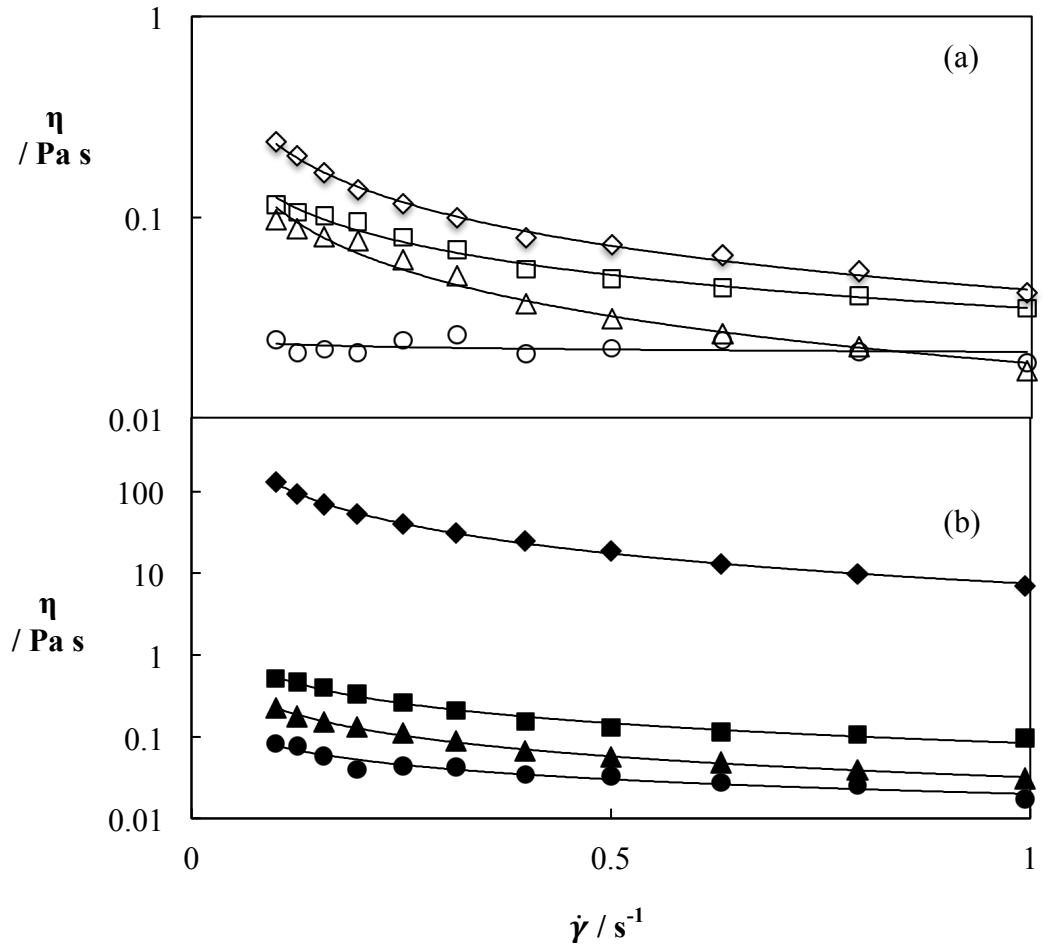

Figure 6-3 Viscosity (η) versus shear rate ($\dot{\gamma}$) for WPI microgel suspensions; (*a*) at pH 7 (open symbols); (*b*) at pH 4 (filled symbols): 1 vol.% (○,●); 5 vol.% (△,▲); 10 vol.% (□,■); 15 vol.% (◇,◆).

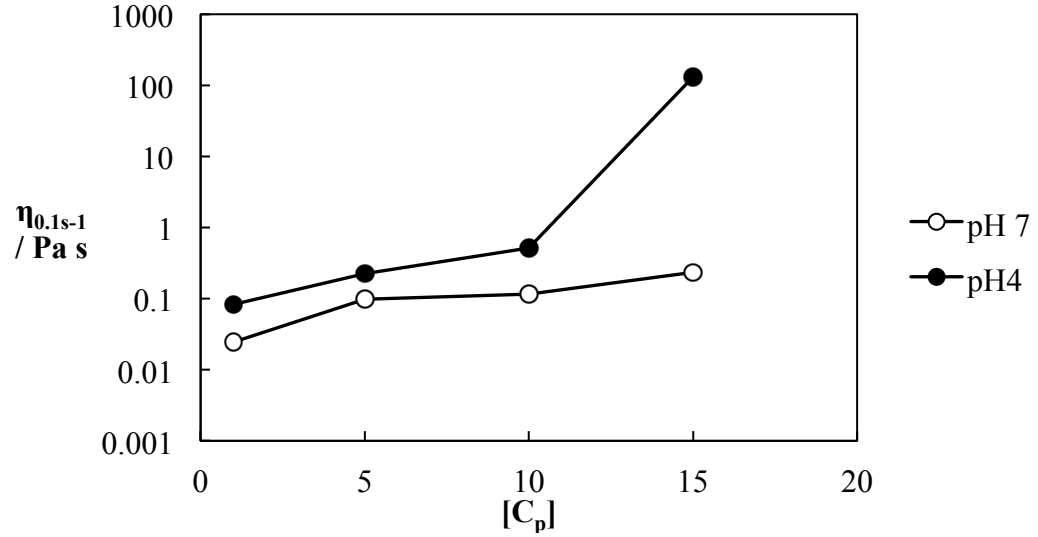

Figure 6-4 Viscosity (η) at $\dot{\gamma}$ = 0.1 s^{-1} of WPI microgel particles; at pH 7 (open symbols) and pH 4 (filled symbols).

Table 6-1 Fitting parameters of power law model (Equation 6-1) to viscosity of WPI microgel suspensions of different concentrations (vol.%), as shown in Figure 6-3. *K* is the flow consistency index, *n* is flow behaviour index and R^2 is goodness-of-fit.

vol.%	*K*	*n*	R^2
pH 7			
1	0.021	0.96	0.1075
5	0.020	0.22	0.9799
10	0.035	0.45	0.9839
15	0.043	0.27	0.9950
pH 4			
1	0.020	0.4	0.9364
5	0.032	0.15	0.9968
10	0.083	0.19	0.9820
15	7.440	-0.23	0.9978

Further investigation of the viscosities of the WPI microgel dispersions were adequately fitted to a power law model, see Equation 1-7 section 1.7.1. The fitting parameters are shown in Table 6-1 and the solid curved lines on Figure 6-3 are the fitted power law behaviour. The fits indicate that all the dispersions were very strongly shear thinning, i.e., $-0.23 < n < 0.45$, except for 1 vol.% WPI dispersion at pH 7 where $n = 0.96$ as noted above was practically Newtonian.

Therefore, when the microgel particles were added to either the starch or LBG phase before the two polymer phases were mixed, one might expect some increase in the viscosity of either phase. However, the viscosities of the 4 wt.% starch and 0.6 wt.% LBG phases before mixing were still considerably greater than the values measured for the WPI microgel dispersions, e.g., 60 and 0.8 Pa s at $\dot{\gamma} = 0.1\ s^{-1}$ for starch and LBG, respectively, except for 15 vol.% microgels where the $\eta_{0.1s\text{-}1} > 100$ Pa s. At this particle concentration any subsequent effect on the phase separation kinetics of including the microgel particles is likely to be due to enhanced viscosity or gel formation of either phase.

6.3.3 Macroscopic observations of the effect of particles on W/W emulsions

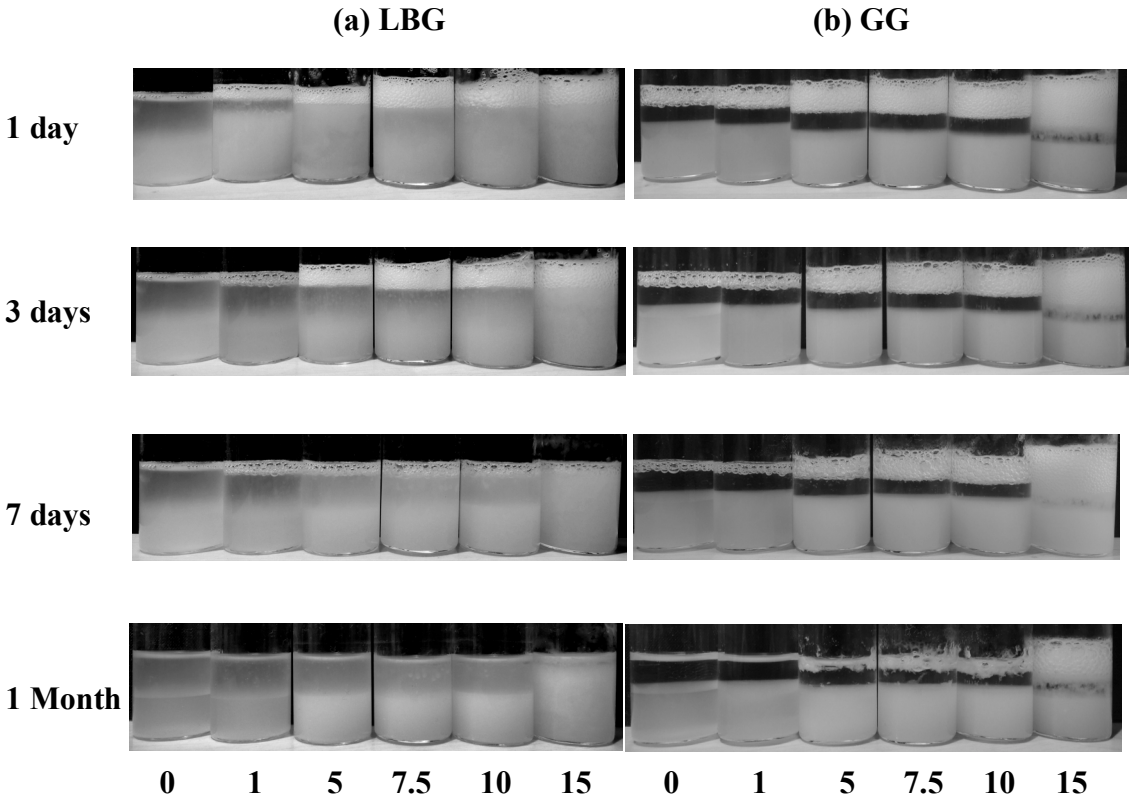

Figure 6-5 W/W emulsions formed by 2 wt.% S + (*a*) 0.3 wt.% LBG; (*b*) 0.25 wt.% GG containing 0 to 15 vol.% WPI microgel particles at pH 7. Observed at 1, 3, 7 and 30 days. From left to right: no particle; 1 vol.% WPI; 5 vol.% WPI; 7.5 vol.% WPI; 10 vol.% WPI; 15 vol.% microgels.

Two series of emulsions were prepared at equal volumes of S + LBG (Figure 6-5*a*) or GG (Figure 6-5*b*) with the presence of different vol.% of WPI microgel particles at pH 7 and observed at different time intervals. Pure mixtures of S + galactomannan shows macroscopic phase separation within an hour after mixing and completely phase separated after 2 weeks. The mixtures formed a gum-rich phase at the top and a starch-rich phase at the bottom. Figure 6-5 shows the appearance of all the mixtures after 1, 3, 7 and 30 days. For S + LBG + microgel particles, within the first week of storage the appearance of phase separation seemed to be reduced as the concentration of particles was increased, since it was progressively more difficult to observe a transparent gum-rich phase. The mixture containing 15 vol.% WPI particles, was at the most stable. After keeping the mixtures for up to one month, the appearance of the mixtures did not significantly change, only the development of a

clearer phase separated boundary and the bursting of bubbles that formed on the top layer. For the S + GG system, increased particle concentration seemed to have no effect on phase separation with the exception of at 15 vol.% particles. It was more difficult to discern phase separation in all the samples containing microgel particles compared to mixtures with silica particles or BMDs due to foam formation. Protein is known as an excellent bubble stabiliser and protein microgel particles can be even better (Schmitt *et al.,* 2014). Subsequently, the samples showed increased foam stability as the vol.% particles was increased, so even after 7 days a layer of bubbles was still visible at the top of the tubes especially for S + GG mixtures. The foam layer appeared to be thicker than that of S + LBG mixtures. GG and LBG are also often used as foaming agents – see Table 1-1, chapter 1. From Figure 6-5 and previous results in chapter 5, section 5.4.1, GG used in this thesis is likely to have better foam formability.

The results in Figure 6-5*a* show that after 1 day at $[C_p]$ = 1 vol.% can slow down the phase separation to some extent. Figure 6-3*a* also shows that the viscosity of 1 vol.% microgels suspension at pH 7 exhibits Newtonian behaviour (ca. 0.02 Pa s) which is much lower than the pure S or gum solution. Thus it is unlikely that the slowing down of the phase separation is due to any significant increase in viscosity of either polysaccharide phase.

Figure 6-6 shows the mixtures S + LBG (Figure 6-6*a*) or GG (Figure 6-6*b*) with the presence of different vol.% of WPI microgel particles at pH 4. Overall the mixtures showed improvement in stability to phase separation at pH 4 compared with the corresponding times and vol.% particles at pH 7. This enhancement in stability could be due to the formation of microgel particles and their aggregates, after reducing pH, that adsorbed around interfacial areas and formed stronger interfacial networks. In the absence of particles, both mixtures containing S + LBG or GG shows a thin clear upper layer within 1 day which is suggestive of syneresis.

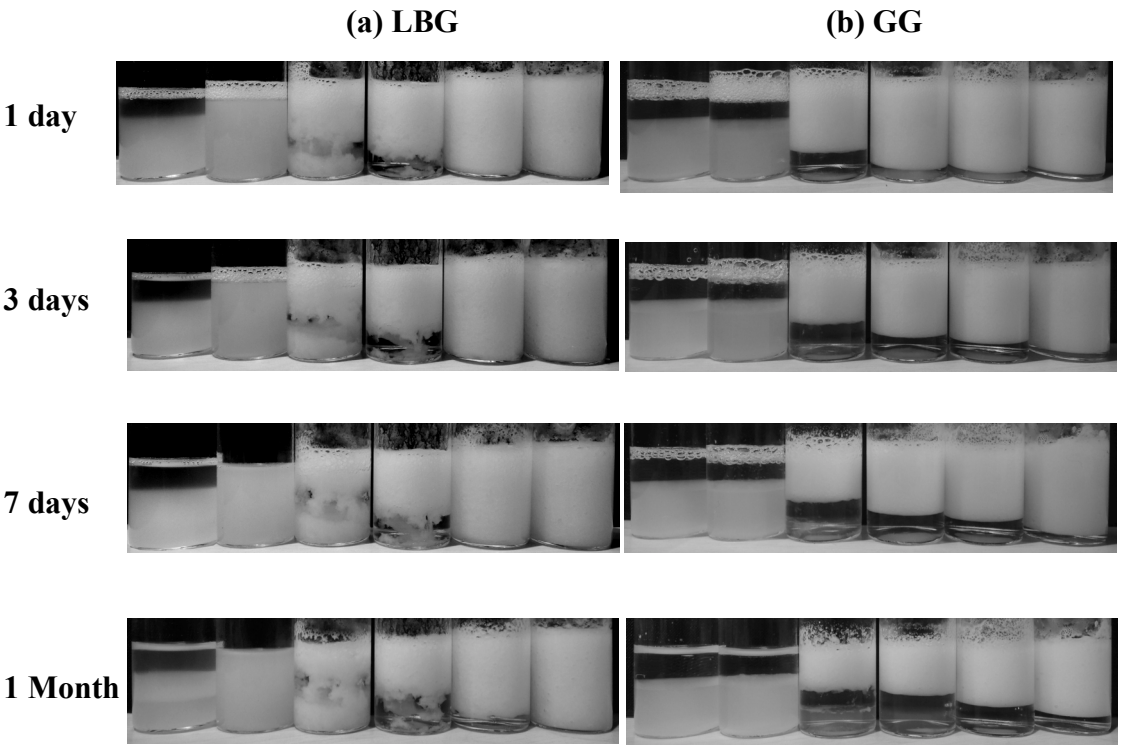

Figure 6-6 W/W emulsions formed by 2 wt.% S + (*a*) 0.3 wt.% LBG; (*b*) 0.25 wt.% GG containing 0 to 15 vol.% WPI microgel particles at pH 4. Observed at 1, 3, 7 and 30 days. From left to right: no particle; 1 vol.% WPI; 5 vol.% WPI; 7.5 vol.% WPI; 10 vol.% WPI; 15 vol.% microgels.

For the S + LBG system (Figure 6-6*a*), even at just 1 vol.% microgel particles, the mixture showed no sign of phase separation over an observation period of 4 weeks and was still stable 12 months later, so possibly indefinitely. Interestingly, at 5 and 7.5 vol.% particles the mixtures appeared to form a single turbid gel-like layer on top of a very clear colourless water-like phase, creaming. At 10 and 15 vol.% particles, the whole mixture was completely turbid and no phase separation was evident within the first week of observation. However, after 1 month storage, at 10 vol.% particles, a turbid layer started to form on top of a thin water-like phase, whilst with 15 vol.% particles the mixture remained homogeneous over an additional period of 8 weeks. Similar results were observed in poly (ethylene oxide) + dextran with the presence of protein particles (Nguyen *et al.,* 2013) where the rate of creaming depends upon [C_p], the higher the [C_p] the slower the rate of creaming. The difference between homogeneous S+ LBG containing 1 vol.% and 15 vol.% is the

flow behaviour; at 1 vol.% the mixture moved after tilting the tube whilst at 15 vol.% the mixture hardly moved at all.

For some reason the microgel particles were more effective in the mixtures containing LBG rather than GG. Figure 6-6*b* shows that the microgel particles had no effect on S + GG system at 1 vol.%. The mixtures formed turbid, gel-like materials at higher concentrations, i.e. 5 to 15 vol.%. The volume of clear, colourless, water-like phase decreased as the concentration of WPI microgels increased and again the sample could be turned upside down without disturbing the sample at $[C_p]$,= 15 vol.%. This phenomenon probably indicates strong aggregation of microgel particles at the W/W interface and/or the bulk phases.

6.3.4 Microscopic observations on phase separation

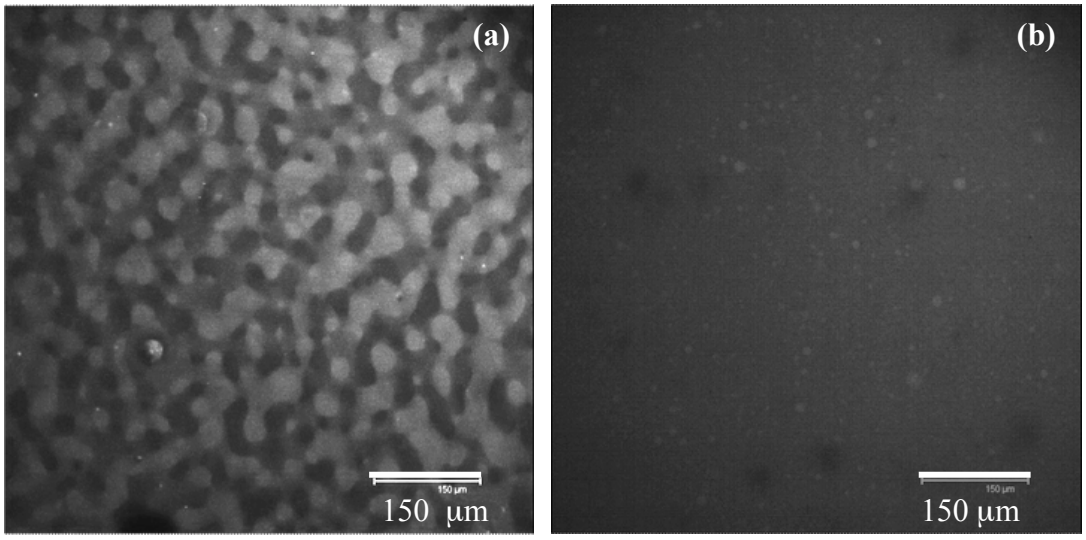

Figure 6-7 Representative confocal micrographs of mixture containing 2wt.% S + 0.3 wt.% LBG in the absence of WPI microgel particles: (*a*) age 5 min; (*b*) age 24 hour.

Figure 6-7*a* shows a typical example of a confocal micrograph from S + galactomannan system, in this case for 2 wt.% starch + 0.3 wt.% LBG in the absence of particles at 5 ± 2 minutes after mixing. It should be recalled from chapter 3 that this specific mixture shows rapid phase separation structure via spinodal decomposition of the W/W emulsion in the absence of particles. In real time the system is dynamic and exhibits movement and fusion of starch domains (bright regions) after short aging times, e.g. 30 minutes and the system showed significant

macroscopic phase separation. Figure 6-7*b* shows that within 24 hours no such regions occur, with only a small fraction of bright faint (starch) blobs remaining within the bulk LBG phase.

Again, as the mixtures of S + GG and S + LBG at pH 7 appeared so similar under the CLSM only S + LBG systems are shown. Figure 6-8*a, b* and *c* represent the model system at pH 7 in the presence of 1 to 10 vol.% particles, respectively, after 24 hour. Compared to the mixtures without added microgel particles, Figure 6-8*c* shows that at 10 vol.% particles there was some effect on microstructure of the system, since large starch-rich domains were still visible, although not as many starch-rich domains throughout the sample as immediately after mixing (Figure 6-7*a*). In the case of low concentration of particles, the microdomains are initially partly covered by the particles and consequently the micodomains coalesce to reduce the interfacial area. This event will eventually stop when the particles adsorption density become high enough.

When the system was acidified to pH 4, Figure 6-8*d*, *e, f*, the systems showed a dramatic effect on the microstructure. Even after 24 hours, something like a fine spinodal decomposition structure still persisted. It possibly means that the starch-rich domains did not merge even though the mixtures creamed or sedimented (Figure 6-6*a*). Figure 6-8*d* at 1 vol.% particles clearly shows that there is an accumulation of particles at the interface between S and LBG domains with some denuded areas. Dickinson (2012c) has stated that a uniform particle monolayer at the interface is rarely achieved due to polydispersity in size of particle aggregation. In fact, it is well-known that full coverage of the interface by particles is unnecessary and gives Pickering stability as long as the adsorbed particles form a rigid network (Binks *et al.*, 2005; Binks and Horozov, 2006; Yusoff and Murray, 2011). In the case of WPI microgel particles, these were already presented at the interface, lowering the pH toward the pI of WPI led to a closely packing onto the interface due to the absence of its charge. It can be seen that apart from the appearance of WPI microgels at the interface, the particles also existed inside the dispersed starch-rich phase. This could mean that the particles and their aggregates formed an interconnected steric barrier both around and within starch microdomains. Nevertheless, the appearance of particles at the W/W interface is good evidence of a bijel formation. Individual particles at the interface cannot be distinguished due to the CLSM resolution.

Increasing the concentrations of particles further to 5 and 10 vol.% (Figure 6-8*e, f*) shows that there are more densely packed region of particles, that are more likely to also form a network, within the starch-rich domains. Excess particles within the starch-rich domains could possibly simultaneously form a gel matrix and kinetically trap the system.

Most of the particles and their aggregates appeared to reside largely within the starch-rich domains even when the particles were deliberately dispersed within LBG phase before mixing with the starch phase. The propensity for particles to prefer one phase over another for no obvious reason was observed also with silica particles and BMDs in Chapters 4 and 5, respectively.

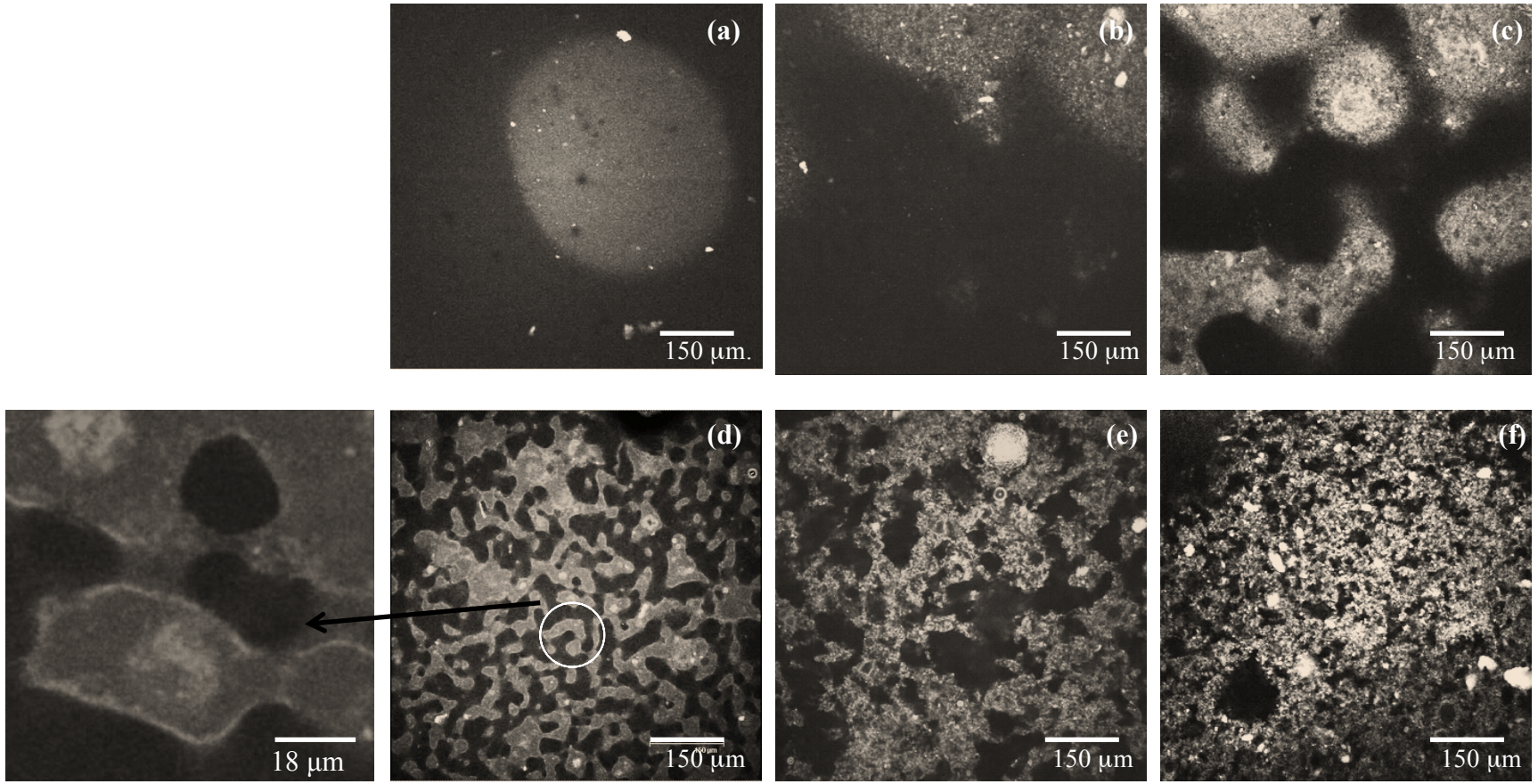

Figure 6-8 Representative confocal micrographs of mixture of 2 wt.% S + 0.3 wt.% LBG in the presence WPI microgel particles, age 24 hour: (*a*) 1 vol.% particles, pH7; (*b*) 5 vol.% particles, pH7 h; (*c*) 10 vol.% particles, pH7; (*d*) 1 vol.% particles, pH4; (*e*) 5 vol.% particles, pH4; (*f*) 10 vol.% particles, pH4.

6.3.5 Estimate of particle detachment energy

The estimation of detachment energy (ΔE) to remove particles from the interface can be calculated by using Equation 1-13 from Chapter 1. In this case we assumed that the contact angle θ = 90° (where attachment is strongest), an initial particle size at pH 7 = 150 nm and an interfacial tension 10^{-6} N m^{-1}, This gives ΔE = 4.3 k_BT. Although the detachment energy is higher than that of thermal energy (4.11×10^{-21} J or 1 k_BT at 25°C) but it might not high enough to stabilise the interfacial area because there could be some particles that can detach itself from the interface. In other words, particles would still be reversibly adsorbed. However, after acidification to pH 4, the particles formed aggregates of indeterminate size. Nevertheless, the minimum particle size that possibly irreversible stabilise the interface could be estimated using the same equation and assume that $\Delta E > 10\ k_BT$. The minimum particle size was predicted to be above 230 nm in diameter. This assumption ignores the additional effects of strong inter-particle attractions reinforcing an interfacial particle network.

6.3.6 Image Analysis of phase separating microdomains

Image analysis was used to quantify the effects of pH and concentration of particles on the phase separation kinetics of the 2 wt.% S + 0.3 wt.% LBG systems. Figure 6-9*a, b* shows the extracted characteristic length scale (L) as a function of time for 1, 5 and 10 vol.% particles at pH 7 and 4, respectively. In the absence of particles, L was approximately 60 μm after 5 minutes and after 30 minutes discrete domains were undetectable because separate layers started to form in the well of the slide. In the presence of 1 to 10 vol.% WPI microgel particles at pH 7 (Figure 6-9*a*), the starch microdomain size shows similar trends at all [C_p], where starch blobs grow rapidly to L > 150 μm after 0.5 hour and continuing to grow to L > 200 μm after 24 hours. At 1 vol.% particles L >> 200 μm within the first 2 hours of preparation (data points not shown except at 0.5 hour). The rise of L obviously reflects the growth of the phase separated starch-rich regions with time, while the decrease in L after 1 hour is a reflection that the larger the domains the faster they tend to sink out of the field of view to form a lower bulk starch-rich phase.

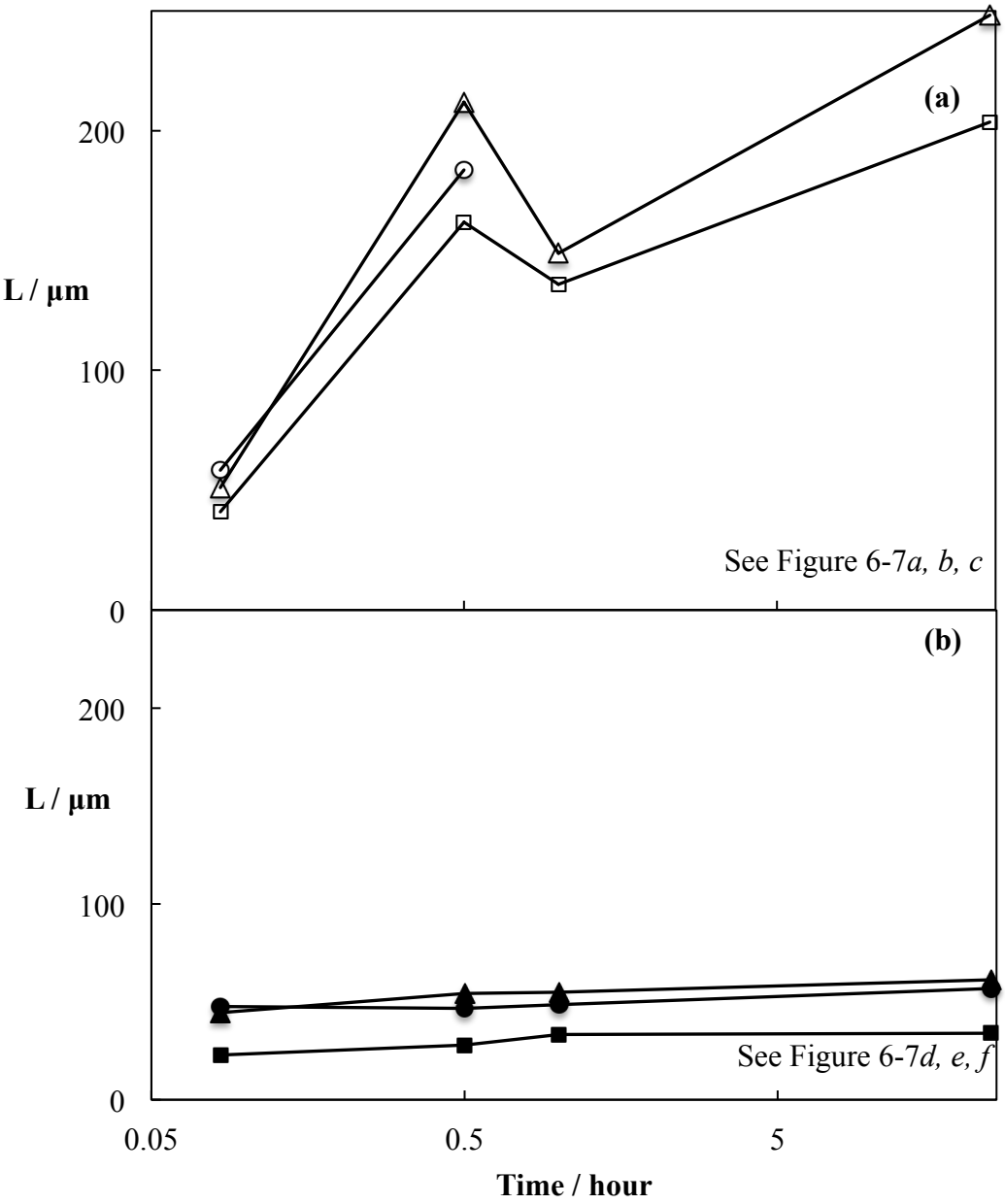

Figure 6-9 Characteristic length scale, *L*, versus time since mixing for mixtures of 2 wt.% S + 0.3 wt.% LBG at (*a*) pH7 (open symbols); (*b*) pH4 (filled symbols). Data and representative micrographs are shown for system with different concentrations of added WPI microgel particles: 1 vol.% (○,●); 5 vol.% (△,▲); 10 vol.% (□,■).

Figure 6-9*b* shows the significant effect of particles after the reduction to pH 4. It is seen that at the lower pH there was a significant W/W emulsions observed, with a relatively small increase in *L* from 45 to 60 µm for 1 and 5 vol.% and 20 to 35 µm for 10 vol.% particles in the first 24 hours. Representative micrographs of some of these compositions can be seen in Figure 6-8.

The analysis of the microstructure is therefore consistent with the macroscopic observations (Figure 6-5*a* and 6-6*a*) and the other microscopic observations (Figure 6-8) that increasing the concentration of particles seems to significantly inhibit phase separation of the S + galactomannan system, especially at pH 4 compared to pH 7.

6.3.7 Bulk rheology of different phases

The results in previous sections indicate that WPI microgel particles have an ability to inhibit and/or slow down domain growth and macroscopic phase separation of W/W emulsions formed from S + galactomannan gum solutions. Some authors (Vincent and Saunders, 2011; Schmitt, *et al.*, 2014) show that WPI and WPI microgel particles can form gel networks in bulk aqueous phase, hence it is important to understand the effect of adding WPI particles in each polysaccharide domain. Therefore, WPI microgel particles were dispersed in separate bulk LBG, GG and S phases at different particle concentrations and the bulk rheology measured. Since the major effects of particle addition were at pH 4, the measurements were only conducted at this pH. Figure 6-11*a* shows the bulk viscosity η at $\dot{\gamma}$ = 0.1 s^{-1} plus the storage modulus (G') and loss modulus (G") at 0.1 Hz and and 1% strain, see Figure 6-11*b* and *c*, respectively. These low shear conditions were selected as close to the solution at rest stage whilst still obtaining reproducible results.

Figure 6-10 clearly shows that up to 10 vol.% WPI microgel particles added to 4 wt.% S, there was a slight decrease in η whilst for 15 vol.% particles η approximately doubled the value compared with the S solution alone, which also agreed with the result from Figure 6-4. For 0.6 wt.% LBG and 0.5 wt.% GG, η remained considerably lower across the whole range of addition of particles. For G' and G'', there was no significant increase in values in any of the gum phases except at particle concentrations between 10 and 15 vol.% where G' and G" values were significantly higher than both gums alone. Whilst, G' and G" for S phase gradually increased as [C_p] increased, G' and G" later dramatically rose up at [C_p] = 15 vol.%. It seems unlikely that an increase in the viscoelasticity of the gum phase on addition of microgel particles can be the explanation of the inhibition of phase separation. However, it does seem that a significant increase in the viscoelasticity of the bulk S phase occurs at all [C_p], probably due to the microgel particle aggregation (as seen in Figure 6-2*b*) via depletion flocculation by the starch molecules. This phenomenon

was also mentioned in Chapter 5 with BMDs and in the presence of silica particles in Chapter 4, although there was no significant increase in bulk phase η occurred on particle addition.

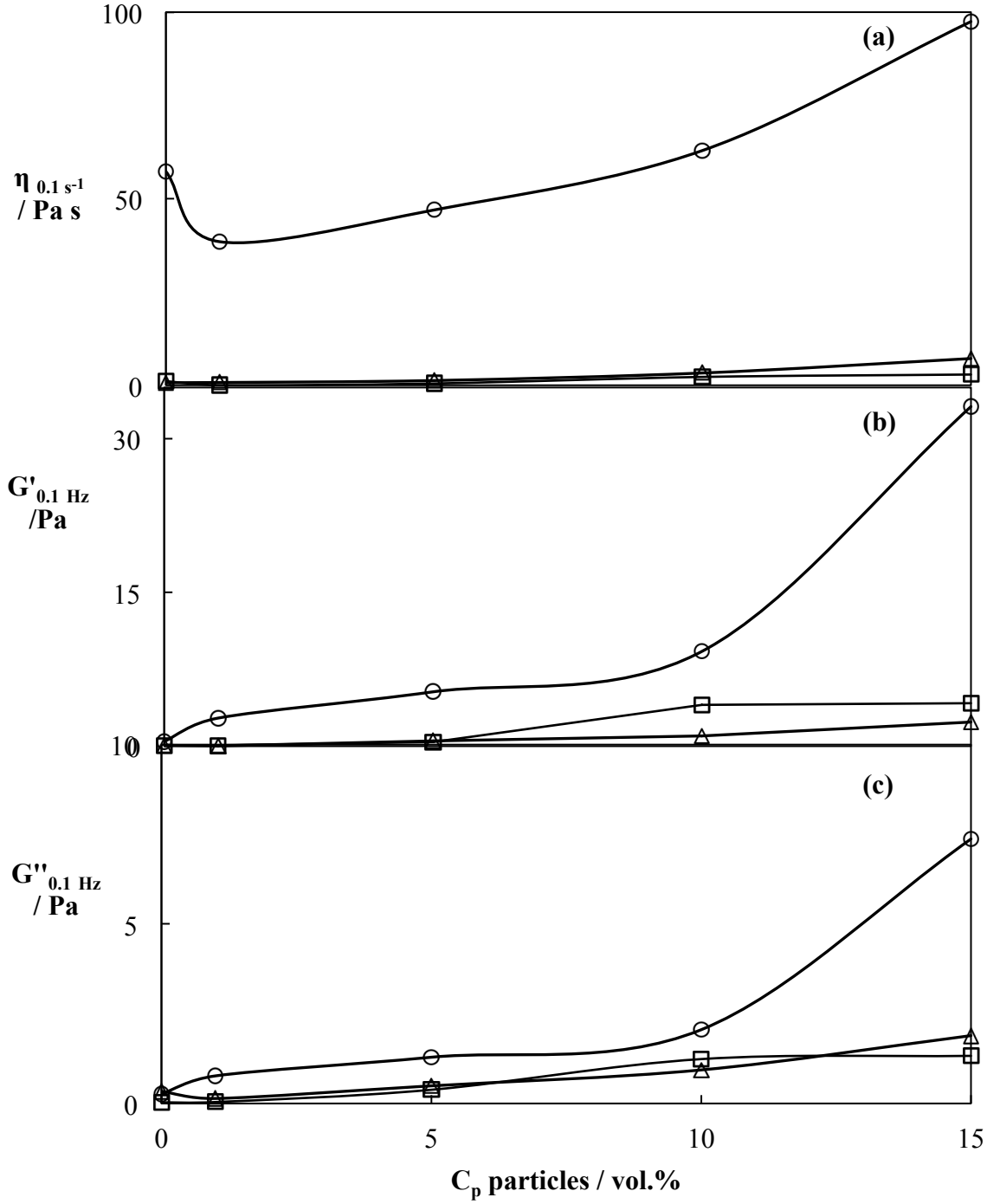

Figure 6-10 At pH4 (*a*) Viscosity (η) at $\dot{\gamma}$ = 0.1 s^{-1}; (*b*) storage modulus (G') measured at 0.1 Hz; (*c*) loss modulus (G") at 0.1 Hz and 0.01 strain versus vol.% (ϕ) of WPI microgel particles added to individual solutions of 4 wt.% starch (○); 0.6 wt.% LBG (△); 0.5 wt.% GG (□).

Another possible explanation is that where G' > G" over the frequency range observed, particles possibly form a gelled network that inhibits the movement of phase separated domains.

6.4 Conclusions

A new class of food-grade "Pickering/Mickering" particles was investigated. Water-in-water (W/W) emulsions formed by mixing waxy corn starch (S) and galactomannan (LBG or GG) solutions could be stabilised by addition of these sub-micron WPI microgel particles. The stability depended upon the concentration of the particles and pH of the system. Clear correlations exist between the macroscopic and microscopic results. At pH 7, stability is increased with increasing concentration of particles in S + LBG system whilst these was no significant change in the S + GG system. Lowering the pH from 7 to 4 showed an improvement in stability in both systems, probably due to aggregation of particles and inter-particle association. At 1 vol.% particles pH 4 the W/W emulsion exhibited long term stability. The particles and their aggregates show a strong preference for the starch domains rather than gum phase under all the condition observed. There was some evidence that the microgel particles tended to preferentially accumulate at the W/W interface, this propensity possibly due to depletion flocculation of particles. Similarly, the enhanced stability of dextran + poly (ethylene oxide) using synthetic cross-linked polymer microgel particles was also proposed by Nguyen *et al.* (2013), where altering the pH or ionic strength can significantly change the stability.

Chapter 7

7 Chapter 7. Overall summaries and conclusions

After investigating the kinetics of phase separation in mixtures containing waxy corn starch + galactomannan ± particles, this chapter provides a summary and conclusions of the thesis overall. All experiments in this thesis have been performed in order to get better knowledge and understanding in these systems with and without the presence of particles, by focusing on the following objectives: (1) determine the phase diagram (2) observe the macroscopic phase separation (3) investigate the microstructure (4) study the rheology of each solution/suspension.

7.1 Phase behaviour of starch + galactomannan

The phase behaviour of various compositions of S + GG or LBG was studied. Based on macroscopic and visual observations of the centrifuged mixtures, the phase diagrams were established. It has been found that phase separation occurred at very low concentrations of polysaccharides for both GG + S and LBG + S systems, i.e., above 0.05 wt.% and 0.1 wt.% for galactomannan and S, respectively. Changing the pH of each polysaccharide to pH 5.4 or 8 showed no significant effect on the rate of phase separation of S + LBG whilst there was a slight effect on S + GG mixtures.

The model system 2 wt.% S + 0.25 wt.% GG or 0.3 wt.% LBG appeared fully phase separated after 2 weeks of preparation where stored at 25 °C under normal gravity. It was shown that after leaving a mixture consisting 2 wt.% S + 0.3 wt.% LBG for 3 weeks, the top LBG-rich phase formed a weak gel, probably due to self-association of the mannan backbone where no galactose side chains exist (‘smooth’ area). Observation of the microstructure via CLSM revealed a spinodal decomposition structure. Microscopically, the mixtures appeared as fully phase separated within 30 minutes of preparation in a 3 mm welled-slide.

7.2 Rheology of each phase

It was found that all polysaccharide solutions used exhibited shear-thinning behaviour. Starch showed the same viscosity as galactomannan gums at double the concentration. In oscillatory viscometry tests, all material showed frequency-dependence. LBG and GG showed viscoelastic behaviour whilst starch solutions exhibited weak gel behaviour.

7.3 Particle size distribution and rheology of particle dispersion

The nominal particle sizes were 20 nm, 3 μm, 280 nm and 149 nm for silica particles, food-grade silica particles, BMDs and WPI microgel particles, respectively. The rheology of particles dispersed in solvent (phosphate buffer) at two different pH values, i.e., pH 7 and 4, were only measured for BMDs and WPI microgel particles. It was shown that the viscosity of BMDs was lower than that of WPI microgel particles at the same volume fraction. At the same particle concentration [C_p], the dispersion with smaller particles should have higher viscosity due to higher number of particles and more particle-particle interaction within the system. The BMDs and WPI microgel particles were stable to aggregation at pH 7 for period of several weeks. It was also shown that upon lowering the pH from 7 to 4 (below the pI of sodium caseinate and WPI), both BMDs and WPI microgel particles aggregated to some extent, which resulted in a significant increase in the viscoelasticity.

7.4 Effect of particles on phase separation

It was found that all the particles used tended to accumulate at the water-water interface. Added particles could slow down and/or inhibit the rate of phase separation in the model mixtures. The degree of inhibition depended upon particle type, particle concentration and environmental conditions (i.e., pH). The microstructure was significantly altered by the presence of particles. Particle-stabilised model mixtures conferred bicontinuous morphologies reminiscent of continuous interfacially jammed emulsion gel (bijels). It seemed like all particles

observed in the phase separation of waxy corn starch + galactomannan had greater attraction toward the starch phase and in some conditions they also accumulated at the water-water interface. This preference for the starch phase more than the other resulted in more particles within the starch microdomains as well as the decoration of particles at the interface. The driving force for an accumulation of particles at the interface is likely to be the result of depletion flocculation by either of the polysaccharide phases.

Moreover, for silica particles, the emulsion stability was shown to be dependent on the particle hydrophobicity and concentration. 80- and 65-SiOH silica particles, [C_p] = 1 wt.%, were the most effective in stabilising W/W emulsions for at least two years, however, they are not permitted for use in food products. Food-grade silica particles, which should have similar surface properties as the 100-SiOH, only slightly affected the phase separation of the mixtures. One of the most important features in stabilising emulsions by particles is the particle size which affects their desorption energy (see Equation 1-13) and the maximum interfacial area they can cover. Thus, the food-grade silica particles were probably too large, which meant that they have low surface area. BMDs showed some an ability to slow down the rate of phase separation but could not fully inhibit the phase-separated network. At [C_p] = 15 vol.% the top layer of the mixtures seemed to form a gel so that the mixtures resisted to flow even after tilting the tubes. The most striking results were with WPI microgel particles where at pH 4 concentrations as low as 1 vol.% particles resulted in S + LBG mixture remaining uniform for at least 12 months. In contrast, in S + GG systems, there was still persistence of macroscopic phase separation in mixtures at the same and higher WPI microgel particles concentrations. There is still no obvious reason why BMDs and WPI microgel particles were more effective in S + LBG system.

7.4.1 Detachment energy, ΔE

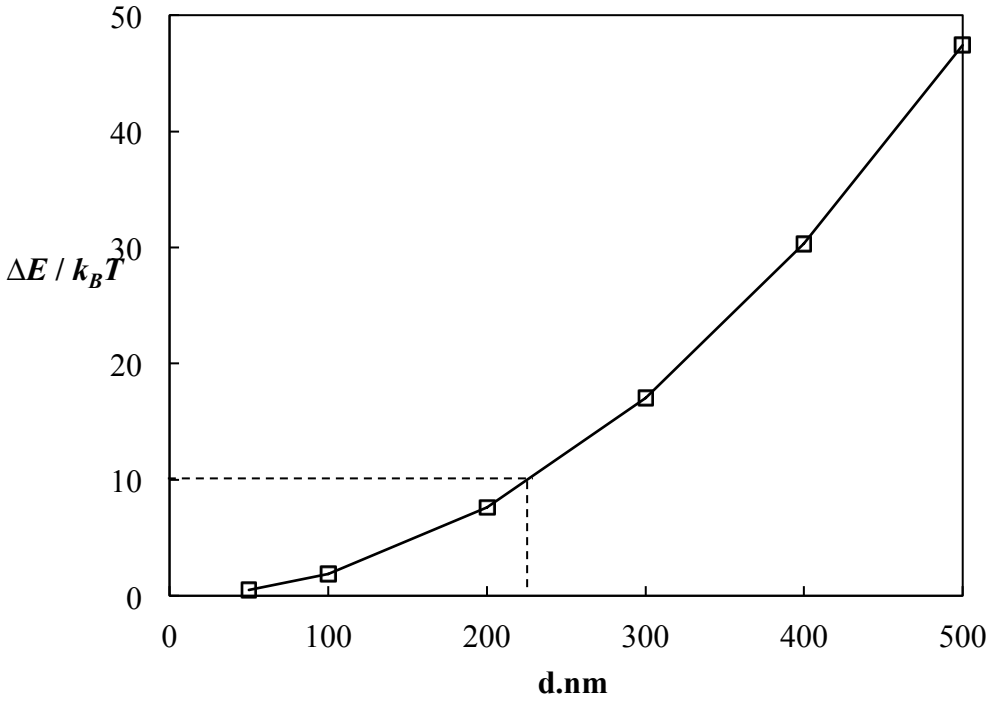

Figure 7-1 Graph shows prediction of particle detachment enery at various particle sizes.

Regarding the particle detachment energy (ΔE), the suitable particle size for W/W emulsion is predicted from Figure 7-1, assuming $\gamma = 10^{-6}\ N\ m^{-1}$ and θ_w = *90°*. According to Dickinson (2012b), ΔE >> 10 k_BT in order to be irreversibly absorbed. The dashed line on the graph shows that particles should therefore be significantly larger than 230 nm. The detachment energy theory is based on the energy needed per single particle. However, the mechanical properties of a particle-stabilised emulsion also depend upon the interaction between particles at the interface. In the case of particles forming a network at the interface (Figure 7-2*a*) the energy needed to remove a collection of aggregated particles simultaneously would be much more than the predicted energy for a single particle. For example, if one particle requires 10 k_BT to be removed from the interface, in Figure 7-2*a*, 50 k_BT is the minimum energy needed in order to remove the layer of particles. Attractive particle-particle interaction provides rigidity to the adsorbed layer (Leal-Calderon and Schmitt, 2008). In the case of particles that form aggregates at the interface, e.g.,

Figure 7-2*b*, this would mean that the effective particle size at the interface and therefore ΔE is likewise increased.

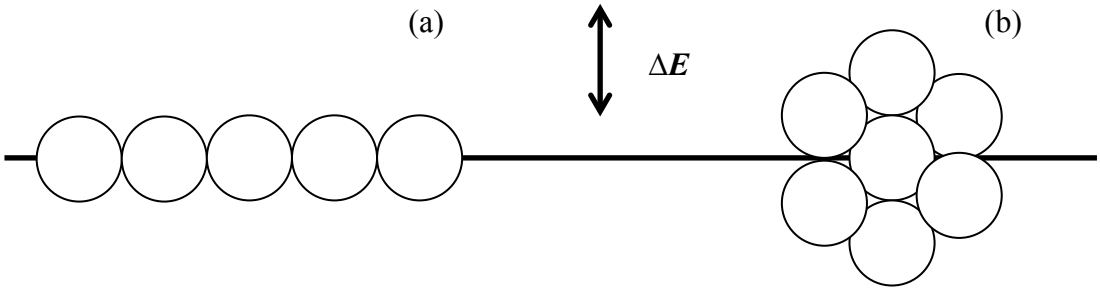

Figure 7-2 Illustration of network of particles at the interface and the energy required to remove them. Particle is strongly linked to its neighbour by some sort of strong bond.

7.5 Future work

This study has demonstrated the possibility of using particles to stabilise polysaccharide mixtures via the Pickering stabilisation mechanism. The WPI microgel particles produced offer a novel type of particle for stabilising W/W food emulsions. Based on the findings from this work, further research could be undertaken in order to fully understand the inhibition process:

- As WPI microgel particles may have a different adsorption mechanism at the interface from that of solid particles, reflecting their deformability, changes in the particle adsorption at different temperatures should be investigated. This could possibly be effective in control and release, i.e., drug or flavor delivery, if the particles shrink and swell at different temperatures.
- There is a need for more detailed investigation of W/W emulsion stability on a bulk scale in order to explore the stabilisation of real foods via WPI microgel particles.
- It might be useful to observe the effect of particle stabilisation as a function of ionic strength because charged particles show different properties at different salt concentrations. Moreover, many food products also contain salt.
- For more insightful information on particle-stabilised emulsions, it would be of great interest to measure the viscosity and viscoelasticity of the whole W/W emulsion containing particles.

There could be potential benefits in using different types of particles in different W/W emulsions which could improve the formulation of a wide range products in foods, cosmetics, textiles, etc. Such concepts need to be further validated. Thus, this research area may generate novel ways of stabilising emulsions, improving shelf-life and possibly enhancing nutrient delivery in food formulations.

References

- Abascal, D.M. and Gracia-Fadrique, J. 2009. Surface tension and foam stability of commercial calcium and sodium caseinates. *Food Hydrocolloids*. 23(7), pp.1848-1852.

- Achayuthakan, P. and Suphantharika, M. 2008. Pasting and rheological properties of waxy corn starch as affected by guar gum and xanthan gum. *Carbohydrate Polymers*. 71(1), pp.9-17.

- Albertsson, P.A. 1962. Partition methods for fractionation of cell particles and macromolecules. *Methods of biochemical analysis*. 10, pp.229-262.

- Allen, K.E., Dickinson, E. and Murray, B.S. 2006. Acidified sodium caseinate emulsion foams containing liquid fat: A comparison with whipped cream. *LWT - Food Science and Technology*. 39(3), pp.225-234.

- Alloncle, M. and Doublier, J.L. 1991. Viscoelastic properties of maize starch/hydrocolloid pastes and gels. *Food Hydrocolloids*. 5(5), pp.455-467.

- Araki, T. and Tanaka, H. 2006. Wetting-induced depletion interaction between particles in a phase-separating liquid mixture. *Physical Review E*. 73(6), pp.061501-061506.

- Aveyard, R., Binks, B.P. and Clint, J.H. 2003. Emulsions stabilised solely by colloidal particles. *Advances in Colloid and Interface Science*. 100-102, pp.503-546.

- Bahnassey, Y.A. and Breene, W.M. 1994. Rapid visco-analyzer (RVA) pasting profiles of wheat, corn, waxy corn, tapioca and amaranth starches (A. hypochondriacus and A. cruentus) in the presence of konjac flour, gellan, guar, xanthan and locust bean gums. *Starch/Stärke*. 46(4), pp.134-141.

- Balakrishnan, G., Nicolai, T., Benyahia, L. and Durand, D. 2012. Particles trapped at the droplet interface in water-in-water emulsions. *Langmuir*. 28(14), pp.5921-5926.

- Batal, H.E., Hasib, A., Ouatmane, A. and Naïmi, M. 2012. Rheology and influence factor of Locust bean gum solution. *Revue de génie industriel*. 8, pp.55-62.

- Berton-Carabin, C.C. and Schroën, K. 2015. Pickering emulsions for food applications: background, trends, and challenges. *Annual Review of Food Science and Technology*. 6(1), pp.263-297.

- Binks, B.P. and Horozov, T.S. 2006. Colloidal particles at liquid interfaces: an introduction *In*: B.P. Binks and T.S. Horozov, ed. *Colloidal particles at liquid interfaces*. Cambridge: Cambridge University Press, pp. 1-74.

- Binks, B.P. and Lumsdon, S.O. 2000. Effects of oil type and aqueous phase composition on oil–water mixtures containing particles of intermediate hydrophobicity. *Physical Chemistry Chemical Physics*. 2(13), pp.2959-2967.

- Binks, B.P. and Lumsdon, S.O. 2001. Pickering emulsions stabilized by monodisperse latex particles: effects of particle size. *Langmuir*. 17(15), pp.4540-4547.

- Binks, B.P. and Whitby, C.P. 2005. Nanoparticle silica-stabilised oil-in-water emulsions: improving emulsion stability. *Colloids and Surfaces A: Physicochemical and Engineering Aspects*. 253(1-3), pp.105-115.

- Binks, B.P., Philip, J. and Rodrigues, J.A. 2005. Inversion of Silica-stabilized emulsions induced by particle concentration. *Langmuir*. 21(8), pp.3296-3302.

- Bourbon, A.I., Pinheiro, A.C., Ribeiro, C., Miranda, C., Maia, J.M., Taixeira, J.A. and Vicente A.A. 2010. Characterization of galactomannans extracted from seeds of Gleditsia triacanthos and Sophora japonica through shear and extensional rheology: Comparison with guar gum and locust bean gum. *Food Hydrocolloids*. 24(2-3), pp.184-192.

- Bourriot, S., Garnier, C. and Doublier, J.L. 1999. Phase separation, rheology and microstructure of micellar casein–guar gum mixtures. *Food Hydrocolloids*. 13(1), pp.43-49.

- Burey, P., Bhandari, B.R., Howes, T. and Gidley, M.J. 2008. Hydrocolloid gel particles: formation, characterization, and application. *Critical Reviews in Food Science and Nutrition*. 48(5), pp.361-377.

- Burgaud, I., Dickinson, E. and Nelson, P.V. 1990. An improved high-pressure homogenizer for making fine emulsions on a small scale. *International Journal of Food Science & Technology*. 25(1), pp.39-46.

- Butler, M.F. and Heppenstall-Butler, M. 2003. Phase separation in gelatin/dextran and gelatin/maltodextrin mixtures. *Food Hydrocolloids*. 17(6), pp.815-830.

- Cates, M.E. and Clegg, P.S. 2008. Bijels: a new class of soft materials. *Soft Matter*. 4(11), pp.2132-2138.

- Chaisawang, M. and Suphantharika, M. 2006. Pasting and rheological properties of native and anionic tapioca starches as modified by guar gum and xanthan gum. *Food Hydrocolloids*. 20(5), pp.641-649.

- Chaplin, M. 2012. Hydrocolloid and gums. *Lsbu.ac.uk* [online]. Available from: http://www.lsbu.ac.uk/water/hyrhe.html [Accessed July 1, 2012].

- Chaplin, M. 2015. Starch. *Lsbu.ac.uk* [online]. Available from: http://www1.lsbu.ac.uk/water/starch.html [Accessed September 11, 2015].

- Chemeurope.com, 2012. Rotational rheometers: Kinexus 'redefines the rheometer'. [online]. Available from: http://www.chemeurope.com/en/products/50351/rotational-rheometer-kinexus.html [Accessed May 11, 2012].

- Chen, J., Dickinson, E. and Edwards, M. 1999. Rheology of acid-treated sodium caseinate stabilized emulsion gels. *Journal of Texture Studies*. 30(4), pp.377-396.

- Chevalier, Y. and Bolzinger, M.A. 2013. Emulsions stabilized with solid nanoparticles: Pickering emulsions. *Colloids and Surfaces A: Physicochemical and Engineering Aspects*. 439, pp.23-34.

- Chudzikowski, R.J. 1971. Guar gum and its applications. *J Soc Cosmet Chem*. 22, pp.43-60.

- Chun, J.Y., Hong G.P., Surassmo, S., Weiss, J., Min, S.G. and Choi, M.J. 2014. Study of the phase separation behaviour of native or preheated WPI with polysaccharides. *Polymer*. 55(16), pp.4379-4384.

- Clegg, P.S., Herzig, E.M., Schofield, A.B., Horozov, T.S., Binks, B.P., Cates, M.E. and Poon, W.C.K. 2005. Colloid-stabilized emulsions: behaviour as the interfacial tension is reduced. *Journal of Physics: Condensed Matter*. 17(45), pp.S3433-S3438.

- Closs, C.B., Conde-Petit, B., Roberts, I.D., Tolstoguzov, V.B. and Escher, F. 1999. Phase separation and rheology of aqueous starch/galactomannan systems. *Carbohydrate Polymers*. 39(1), pp.67-77.

- Conde-Petit, B., Pfirter, A. and Escher, F. 1997. Influence of xanthan on the rheological properties of aqueous starch-emulsifier systems. *Food Hydrocolloids*. 11(4), pp.393-399.

- Dairy Research Institute, 2012. *Whey Protein Heat Stability*. U.S. Dairy Export Council.

- Dakia, P.A, Blecker, C., Robert, C., Wathelet, B. and Paquot, M. 2008. Composition and physicochemical properties of locust bean gum extracted from whole seeds by acid or water dehulling pre-treatment. *Food Hydrocolloids*, 22(5), pp.807-818.

- Dalgleish, D.G. 2004. Food emulsion: their structures and properties *In*: Friberg, S.E., Larsson, K. and Sjöblom, J. ed. *Food Emulsions*. New York: Marcel Dekker.

- de Bont, P.W., Hendricks, C.L.L., van Kempen, G.M.P. and Vreeker, R. 2004. Time evolution of phase separating milk protein and amylopectin mixtures. *Food Hydrocolloids*. 18(6), pp.1023-1031.

- de Bont, P.W., van Kempen, G.M.P. and Vreeker, R. 2002. Phase separation in milk protein and amylopectin mixtures. *Food Hydrocolloids*. 16(2), pp.127-138.

- de Folter, J.W.J., van Ruijven, M.W.M. and Velikov, K.P. 2012. Oil-in-water Pickering emulsions stabilized by colloidal particles from the water-insoluble protein zein. *Soft Matter*. 8(25), pp.6807-6815.

- de Kruif, C.G. and Tuinier, R. 2001. Polysaccharide protein interactions. *Food Hydrocolloids*. 15(4-6), pp.555-563.

- Dea, I.C.M. and Morrison, A. 1975. Chemistry and interactions of seed galactomannans. *Advances in carbohydrate chemistry and biochemistry*. 31, pp.241-312.

- Deshmukh, O.S., Maestro, A., Duits, M.H.G., van den Ende, D., Stuart, M.C. and Mugele, F. 2014. Equation of state and adsorption dynamics of soft microgel particles at an air–water interface. *Soft Matter*. 10(36), pp.7045-7050.

- Destribats, M., Eyharts, M., Lapeyre, V., Sellier, E., Varga, I., Ravaine, V. and Schmitt, V. 2014a. Impact of PNIPAM microgels on its ability to stabilize Pickering emulsions. *Langmuir*. 30(7), pp.1768-1777.

- Destribats, M., Gineste, S., Laurichesse, E., Tanner, H., Leal-Calderon, F., Héroguez, V. and Schmitt, V. 2014b. Pickering emulsions: what are the main parameters determining the emulsion type and interfacial properties?. *Langmuir*. 30(31), pp.9313-9326.

- Destribats, M., Rouvet, M., Gehin-Delval, C., Schmitt, C. and Binks, B.P. 2014. Emulsions stabilised by whey protein microgel particles: towards food-grade Pickering emulsions. *Soft Matter*. 10(36), pp.6941-6954.

- Dickinson, E. 1992. *An introduction to food colloids*. Oxford: Oxford University Press.

- Dickinson, E. 1994. Protein-stabilized emulsions. *Journal of Food Engineering*. 22(1-4), pp.59-74.

- Dickinson, E. 1998. Proteins at interfaces and in emulsions stability, rheology and interactions. *Faraday Trans*. 94(12), pp.1657-1669.

- Dickinson, E. 2001. Milk protein interfacial layers and the relationship to emulsion stability and rheology. *Colloids and Surfaces B: Biointerfaces*. 20(3), pp.197-210.

- Dickinson, E. 2006. Colloid science of mixed ingredients. *Soft Matter*. 2(8), pp.642-652.

- Dickinson, E. 2007. *Food colloids*. London: RSC Publishing.

- Dickinson, E. 2010a. Flocculation of protein-stabilized oil-in-water emulsions. *Colloids and Surfaces B: Biointerfaces*. 81(1), pp.130-140.

- Dickinson, E. 2010b. Food emulsions and foams: Stabilization by particles. *Current Opinion in Colloid & Interface Science*. 15(1), pp.40-49.

- Dickinson, E. 2011. Mixed biopolymers at interfaces: Competitive adsorption and multilayer structures. *Food Hydrocolloids*. 25(8), pp.1966-1983.

- Dickinson, E. 2012a. Emulsion gels: The structuring of soft solids with protein-stabilized oil droplets. *Food Hydrocolloids*. 28(1), pp.224-241.

- Dickinson, E. 2012b. Stabilising emulsion-based colloidal structures with mixed food ingredients. *Journal of the Science of Food and Agriculture*. 93(4), pp.710-721.

- Dickinson, E. 2012c. Use of nanoparticles and microparticles in the formation and stabilization of food emulsions. *Trends in Food Science & Technology*. 24(1), pp.4-12.

- Dickinson, E. and Lorient, D. 1995. *Food macromolecules and colloids*. Cambridge, UK: Royal Society of Chemistry.

- Dickinson, E. and Stainsby, G. 1982. *Colloids in food*. London: Applied Science.

- Dickinson, E. and Vliet, T.V. 2003. *Food colloids, biopolymers and materials*. Cambridge: Royal Society of Chemistry.

- Dickinson, E. and Yamamoto, Y. 1996. Rheology of milk protein gels and protein-stabilized emulsion gels cross-linked with transglutaminase. *J. Agric. Food Chem*. 44(6), pp.1371-1377.

- Dobry, A. and Boyer-Kawenoki, F. 1947. Phase separation in polymer solution. *Journal of Polymer Science*. 2(1), pp.90-100.

- Doublier, J.L. and Launay, B. 1981. Rheology of galactomannan solutions: comparative study of guar gum and locust bean gum. *Journal of Texture Studies*. 12(2), pp.151-172.

- Doublier, J.L., Garnier, C., Renard, D. and Sanchez, C. 2000. Protein-polysaccharide interactions. *Current Opinion in Colloid & Interface Science*. 5, pp.201-214.

- Drelich, J., Fang, C. and White, C.L. 2002. Measurement of interfacial tension in fluid/fluid systems *In*: Hubbard, A.T. ed. *Encyclopedia of Surface and Colloid Science*. New York: Marcel Dekker Inc., pp. 3152-3166.

- Dumitriu, S. 2002. *Polymeric biomaterials* 2nd ed. New York: Marcel Dekker, Inc.

- Dumitriu, S., Vidal, P.F. and Chornet, E. 1996. Hydrogels based on polysaccharides *In*: Dumitriu, S. ed. *Polysaccharides in medicinal applications*. New York: Marcel Dekker.

- Elfak, A.M., Pass, G. and Morley, R.G. 1977. The viscosity of dilute solutions of guar gum and locust bean gum with and without added sugars. *Journal of the Science of Food and Agriculture*. 28(10), pp.895-899.

- Eliasson, A.C. and Gudmundsson, M. 2006. *Carbohydrates in Food* 2nd ed. Boca Raton: CRC Press.

- Ercelebi, E.A. and Ibanoğlu, E. 2007. Influence of hydrocolloids on phase separation and emulsion properties of whey protein isolate. *Journal of Food Engineering*. 80(2), pp.454-459.

- Finkle, P., Draper, H.D. and Hilderbrand, J.H. 1923. The theory of emulsification. *Journal of the American Chemical Society*. 45, pp.2780-2788.

- Firoozmand, H. and Rousseau, D. 2013. Microstructure and elastic modulus of phase-separated gelatin–starch hydrogels containing dispersed oil droplets. *Food Hydrocolloids*. 30(1), pp.333-342.

- Firoozmand, H. and Rousseau, D. 2014. Tailoring the morphology and rheology of phase-separated biopolymer gels using microbial cells as structure modifiers. *Food Hydrocolloids*. 42, pp.204-214.

- Firoozmand, H., Murray, B.S. and Dickinson, E. 2009. Interfacial structuring in a phase-separating mixed biopolymer solution containing colloidal particles. *Langmuir*. 25(3), pp.1300-1305.

- Firoozmand, H., Murray, B.S. and Dickinson, E. 2009. Microstructure and rheology of phase-separated gels of gelatin+oxidized starch. *Food Hydrocolloids*. 23(4), pp.1081-1088.

- Firoozmand, H., Murray, B.S. and Dickinson, E. 2012. Microstructure and elastic modulus of mixed gels of gelatin + oxidized starch: Effect of pH. *Food Hydrocolloids*. 26(1), pp.286-292.

- Fletcher, J. and Hill, A. [no date]. Making the connection - particle size, size distribution and rheology. *Chemeurope.com* [online]. Available from: http://www.chemeurope.com/en/whitepapers/61207/making-the-connection-particle-size-size-distribution-and-rheology.html [Accessed August 17, 2015].

- Flory, P.J. 1953. *Principles of polymer chemistry*. Ithaca: Cornell University Press.

- Fraiha, M., Biagi, J.D. and Ferraz, A.C.D.O. 2011. Rheological behavior of corn and soy mix as feed ingredients. *Ciência e Tecnologia de Alimentos*, 31(1), pp.129-134.

- Frijters, S., Günther, F. and Harting, J. 2012. Effects of nanoparticles and surfactant on droplets in shear flow. *Soft Matter*. 8(24), pp.6542-6556.

- Frijters, S., Günther, F. and Harting, J. 2014. Domain and droplet sizes in emulsions stabilized by colloidal particles. *Physical Review E*. 90(4), p. 042307.

- Frith, W.J. 2010. Mixed biopolymer aqueous solutions – phase behaviour and rheology. *Advances in Colloid and Interface Science*. 161(1-2), pp.48-60.

- Funami, T. 2009. Functions of food polysaccharides to control the gelatinization and retrogradation behaviors of starch in an aqueous system in relation to the macromolecular characteristics of food polysaccharides. *Food science and technology research*. 15(6), pp.557-568.

- García-Ojalvo, J., Lacasta, A, Sancho, J.M. and Toral, R. 1998. Phase separation driven by external fluctuations. *EPL (Europhysics Letters)*. 42(2), p.125.

- Garnier, C., Schorsch, C. and Doublier, J.B. 1995. Phase separation in dextran/locust bean gum mixtures. *Carbohydrate polymers*. 28(4), pp.313-317.

- Girija, V. and Stephen, H.C. 2003. Characterization of lipid in mature enamel using confocal laser scanning microscopy. *Journal of Dentistry*, 31(5), pp.303-311.

- Glicksman, M. 1982. *Food hydrocolloids*. Boca Raton, FL: CRC Press.

- Goff, H.D., Ferdinando, D. and Schorsch, C. 1999. Fluorescence microscopy to study galactomannan structure in frozen sucrose and milk protein solutions. *Food Hydrocolloids*. 13(4), pp.353-362.

- Goycoolea, F.M., Morris, E.R. and Gidley, M.J. 1995. Viscosity of galactomannans at alkaline and neutral pH: evidence of 'hyperentanglement' in solution. *Carbohydrate Polymers*. 27(1), pp.69-71.

- Greb, C. 2012. *Fluorescent Dyes*. [online] Leica Sciencelab. Available at: http://www.leica-microsystems.com/science-lab/fluorescent-dyes/ [Accessed 14 Mar. 2015].

- Greenspan, P. and Fowler, S. D. 1985. Spectrofluorometric studies of the lipid probe, nile red. *Journal of Lipid Research*, 26, pp.781-789.

- Grenha, A. and Dionísio, M. 2012. Locust bean gum: Exploring its potential for biopharmaceutical applications. *Journal of Pharmacy and Bioallied Sciences*, 4(3), pp.175.

- Grinberg, V.Y. and Tolstoguzov, V.B. 1997. Thermodynamic incompatibility of proteins and polysaccharides in solutions. *Food Hydrocolloids*. 11(2), pp.145-158.

- Gupta, R. and Rousseau, D. 2012. Surface-active solid lipid nanoparticles as Pickering stabilizers for oil-in-water emulsions. *Food Funct*. 3(3), pp.302.

- HadjSadok, A., Pitkowski, A., Nicolai, T., Benyahia, L. and Moulai-Mostefa, N. 2008. Characterisation of sodium caseinate as a function of ionic strength, pH and temperature using static and dynamic light scattering. *Food Hydrocolloids*. 22(8), pp.1460-1466.

- Hanazawa, T. and Murray, B.S. 2013. Effect of oil droplets and their solid/liquid composition on the phase separation of protein–polysaccharide mixtures. *Langmuir*. 29(31), pp.9841-9848.

- Hanazawa, T. and Murray, B.S. 2014. The influence of oil droplets on the phase separation of protein–polysaccharide mixtures. *Food Hydrocolloids*. 34, pp.128-137.

- Hans Tromp, R., van de Velde, F. van Riel, J. and Paques, M. 2001. Confocal scanning light microscopy (CSLM) on mixtures of gelatine and polysaccharides. *Food Research International*. 34(10), pp.931-938.

- Harrington, J.C., Foegeding, E.A., Mulvihill, D.M. and Morris, E.R. 2009. Segregative interactions and competitive binding of Ca2+ in gelling mixtures of whey protein isolate with Na+ κ-carrageenan. *Food Hydrocolloids*. 23(2), pp.468-489.

- Heller, M.J. 1994. Fluorescent detection methods for PCR analysis. In: K.B. Mullis, F. Ferre and R.A. Gibbs, ed., *The Polymerase Chain Reaction*, 1st ed. New York: Springer, pp.138.

- Herzig, E.M., White, K.A., Schofield, A.B., Poon, W.C.K. and Clegg, P.S. 2007. Bicontinuous emulsions stabilized solely by colloidal particles. *Nature materials*. 6(12), pp.966-971.

- Herzig, E.M., White, K.A., Schofield, A.B., Poon, W.C.K. Cates, M.E. and Clegg, P.S. 2008. The bijel: a bicontinuous interfacially jammed emulsion gel *In*: Laudon, M. and Romanowicz, B. ed. *NSTI Nanotech 2008, vol. 2, Technical proceedings*. Boca Raton: CRC press, pp. 657-660.

- Hill, S.E. 1998. Emulsions and foams *In*: Hill, S.E., Ledward, D.A. and Mitchell, J.R. ed. *Functional Properties of Food Macromolecules*. London: Elsevier Applied Science Publishers, pp. 302-306.

- Hoffmann, H. and Reger, M. 2014. Emulsions with unique properties from proteins as emulsifiers. *Advances in Colloid and Interface Science*. 205, pp.94-104.

- Hunter, T.N., Pugh, R., Franks, G. and Jameson, G. 2008. The role of particles in stabilising foams and emulsions. *Advances in Colloid and Interface Science*. 137(2), pp.57-81.

- Iler, R.K. 1979. *The Chemistry of Silica*. New York: John Wiley & Sons.

- Izydorczyk, M. 2005. Understanding the chemistry of food polysaccharides *In*: Cui, S.W. ed. *Food Carbohydrates: Chemistry, Physical Properties, and Applications*. Boca Raton: CRC Press.

- Kalichevsky, M.T. and Ring, S.G. 1987. Incompatibility of amylose and amylopectin in aqueous solution. *Carbohydrate Research*. 162(2), pp.323-328.

- Kawamura, Y. 2008. Guar gum *In*: *The Joint FAO/WHO Expert Committee on Food Additives Sixty-ninth meeting*. Rome: World health organization.

- Kim, Y.H., Choi, K.H., Park, C.H. and Oh, S.G. 2012. Preparation of water powders by the adsorption of hydrophobic nanoparticles at the surface of hydrated starch particulates. *Colloids and Surfaces A: Physicochemical and Engineering Aspects*. 403, pp.41-44.

- Knill, C.J. and Kennedy, J.K. 2005. Starch: Commercial Sources and Derived Products *In*: Dumitriu, S. ed. *Polysaccharides*. New York: Marcel Dekker.

- Kristoffersen, A.S., Erga, S.R., Hamre, B. and Frette, Ø. 2014. Testing Fluorescence Lifetime Standards using Two-Photon Excitation and Time-Domain Instrumentation: Rhodamine B, Coumarin 6 and Lucifer Yellow. *J Fluoresc*, 24(4), pp.1015-1024.

- Krog, N.J. and Sparso, F.V. 2004. Food Emulsifiers: Their chemical and physical properties *In*: Friberg, S.E., Larsson, K. and Sjöblom, J. ed. *Food Emulsions*. New York: Marcel Dekker.

- Kulicke, W.M., Eidam, D., Kath, F., Kix, M. and Kull, A.H. 1996. Hydrocolloids and rheology: Regulation of viscoelastic characteristics of waxy rice starch in mixtures with galactomannans. *Starch/Stärke*. 48(3), pp.105-114.

- Launay, B., Cuvelier, G., Martinez-Reyes, S. 1997. Viscosity of locust bean, guar and xanthan gum solutions in the Newtonian domain: a critical examination of the log (ηsp)o-log c[η]o master curves. *Carbohydrate Polymers*. 34(4), pp.385-395.

- Launay, B., Doublier, J.L. and Cuvelier, G. 1986. Flow properties of aqueous solutions and dispersion of polysaccharides *In*: Mitchell, J.R. and Ledward, D.A. ed. *Functional Properties of Food Macromolecules*. London: Elsevier Applied Science, pp. 1-78.

- Leal-Calderon, F. and Schmitt, V. 2008. Solid-stabilized emulsions. *Current Opinion in Colloid & Interface Science*. 13(4), pp.217-227.

- Lee, S.K. and Mills, A. 2003. Novel photochemistry of leuco-Methylene Blue. *Chemical Communications*, (18), pp.2366.

- Lefebvre, J. and Doublier, J.L. 2005. Rheological Behavior of Polysaccharides Aqueous Systems *In*: Dumitriu, S. ed. *Polysaccharides*. New York: Marcel Dekker.

- Levine, S., Bowen, B.D. and Partridge, S.J. 1989a. Stabilization of emulsions by fine particles I. Partitioning of particles between continuous phase and oil/water interface. *Colloids and Surfaces*. 38(2), pp.325-343.

- Levine, S., Bowen, B.D. and Partridge, S.J. 1989b. Stabilization of emulsions by fine particles II: Capillary and van der Waals forces between particles. *Colloids and Surfaces*. 38(2), pp.345-364.

- Li, Z. and Ngai, T. 2013. Microgel particles at the fluid–fluid interfaces. *Nanoscale*. 5(4), pp.1399-1410.

- Liu, F. and Tang, C.H. 2013. Soy protein nanoparticle aggregates as Pickering stabilizers for oil-in-water emulsions. *Journal of Agricultural and Food Chemistry*. 61(37), pp.8888-8898.

- Liu, Q. 2005. Understanding starches and their role in foods *In*: Cui, S.W. ed. *Food Carbohydrates: Chemistry, Physical Properties, and Applications*. Boca Raton: CRC Press.

- Lorén, N. and Hermansson, A.M. 2003. Structure evolution during phase separation and gelation of biopolymer mixtures *In*: Dickinson, E. and Vliet, T.V. ed. *Food colloids, biopolymers and materials*. Cambridge: Royal Society of Chemistry.

- Lorén, N., Langton, M, and Hermansson, A.M. 2002. Determination of temperature dependent structure evolution by fast-Fourier transform at late stage spinodal decomposition in bicontinuous biopolymer mixtures. *J. Chem. Phys*. 116(23), p.10536.

- Lorén, N., Langton, M, and Hermansson, A.M. 2007. Confocal fluorescence microscopy (CLSM) for food structure characterisation *In*: McClements, D.J. ed. *Understanding and controlling the microstructure of complex food*. Cambridge: Woodhead Publishing.

- Luo, Z., Murray, B.S., Yusoff, A., Morgan, M.R.A., Povey, M.J.W. and Day, A.J. 2011. Particle-stabilizing effects of flavonoids at the oil−water interface. *Journal of Agricultural and Food Chemistry*. 59(6), pp.2636-2645.

- Mackey, K.L., Ofoli, R.Y., Morgan, R.G. and Steffe, J.F. 1990. Rheological modeling of potato flour during extrusion cooking. *Journal of Food Process Engineering*, 12(1), pp.1-11.

- Malkin, A.Y. and Isayev, A.I. 2006. *Rheology: concepts, methods and application*. Toronto: ChemTec Pub.

- Malvern Instruments Ltd., 2005. *Zetasizer Nano Series User Manual MAN0317*. Worcestershire, UK: Malvern Instruments Ltd.

- Marinova, K.G., Basheva, E.S., Nenova, B., Temelska, M., Mirarefi, A.Y., Campbell, B. and Ivanov, I.B. 2009. Physico-chemical factors controlling the foamability and foam stability of milk proteins: Sodium caseinate and whey protein concentrates. *Food Hydrocolloids*. 23(7), pp.1864-1876.

- McClements, D.J. 1999. *Food emulsions: Principles, practices, and techniques*. Boca Raton: CRC Press.

- McClements, D.J. 2005. *Food emulsions: Principles, practices, and techniques* 2nd ed. Boca Raton: CRC Press.

- McClements, D.J. 2012. Advances in fabrication of emulsions with enhanced functionality using structural design principles. *Current Opinion in Colloid & Interface Science*. 17(5), pp.235-245.

- McClements, D.J. and Keogh, M.K. 1995. Physical properties of cold-setting gels formed from heat-denatured whey protein isolate. *Journal of the Science of Food and Agriculture*. 69(1), pp.7-14.

- Medin, A.S. and Janson, J.C. 1993. Studies on aqueous polymer two-phase systems containing agarose. *Carbohydrate polymers*. 22(2), pp.127-136.

- Michon, C., Cuvelier, G., Launay, B., Parker, A. and Takerkart, G. 1995. Study of the compatibility/incompatibility of gelatin/iota-carrageenan/water mixtures. *Carbohydrate polymers*. 28(4), pp.333-336.

- Morris, E.R., Cutler, A.N., Ross-Murphy, S.B., Rees, D.A. and Price, J. 1981. Concentration and shear rate dependence of viscosity in random coil polysaccharide solutions. *Carbohydrate Polymers*. 1(1), pp.5-21.

- Morris, V.J. 1998. Gelation of polysaccharides *In*: Hill, S.E., Ledward, D.A. and Mitchell, J.R. ed. *Functional Properties of Food Macromolecules*. London: Elsevier Applied Science Publishers, pp. 182-199.

- Morris, V.J. 2007. Polysaccharide: Their role in food microstructure *In*: McClements, D.J. ed. *Understanding and controlling the microstructure of complex food*. Cambridge: Woodhead Publishing.

- Morris, V.J. 2011. Emerging roles of engineered nanomaterials in the food industry. *Trends in Biotechnology*. 29(10), pp.509-516.

- Moschakis, T., Murray, B.S. and Dickinson, E. 2006. Particle tracking using confocal microscopy to probe the microrheology in a phase-separating emulsion containing nonadsorbing polysaccharide. *Langmuir*. 22(10), pp.4710-4719.

- Murphy, D.B. 2001. *Fundamentals of light microscopy and electronic imaging*. New York: John Wiley & Sons.

- Murray, B.S. 2007. Stabilization of bubbles and foams. *Current Opinion in Colloid & Interface Science*. 12(4), pp.232-241.

- Murray, B.S. and Phisarnchananan, N. 2014. The effect of nanoparticles on the phase separation of waxy corn starch+locust bean gum or guar gum. *Food Hydrocolloids*. 42, pp.92-99.

- Murray, B.S., Durga, K., Yusoff, A. and Stoyanov, S.D. 2011. Stabilization of foams and emulsions by mixtures of surface active food-grade particles and proteins. *Food Hydrocolloids*. 25(4), pp.627-638.

- Murray, B.S. and Phisarnchananan, N. 2016. Whey protein microgel particles as stabilizers of waxy corn starch + locust bean gum water-in-water emulsions. *Food Hydrocolloids*. 56, pp.161-169.

- Nagano, T., Tamaki, E. and Funami, T. 2008. Influence of guar gum on granule morphologies and rheological properties of maize starch. *Carbohydrate Polymers*. 72(1), pp.95-101.

- Neirynck, N., Vanlent, K., Dewettinck, K. and Vandermeeren, P. 2007. Influence of pH and biopolymer ratio on sodium caseinate - guar gum interactions in aqueous solutions and in O/W emulsions. *Food Hydrocolloids*. 21(5-6), pp.862-869.

- Nguyen, B.T., Nicolai, T. and Benyahia, L. 2013. Stabilization of water-in-water emulsions by addition of protein particles. *Langmuir*. 29(34), pp.10658-10664.

- Nicolai, T., Britten, M. and Schmitt, C. 2011. β-Lactoglobulin and WPI aggregates: Formation, structure and applications. *Food Hydrocolloids*. 25(8), pp.1945-1962.

- Nobbmann, U., Connah, M., Fish, B., Varley, P., Gee, C., Mulot, S., Chen, J., Zhou, L., Lu, Y., Sheng, F., Yi, J. and Harding, S.E. 2007. Dynamic light scattering as a relative tool for assessing the molecular integrity and stability of monoclonal antibodies. *Biotechnology and Genetic Engineering Reviews*. 24(1), pp.117-128.

- O'Kennedy, B.T., Mounsey, J.S., Murphy, F., Duggan, E. and Kelly, P.M. 2006. Factors affecting the acid gelation of sodium caseinate. *International Dairy Journal*. 16(10), pp.1132-1141.

- Onov, Y.A.A., Pletenko, M.G. and Tolstoguzov, V.B. 1987. Thermodynamic compatibility of polysaccharides in aqueous media. *Polymer Science USSR*. 29(12), pp.2729-2735.

- Panda, H. 2004. *The complete technology book on natural products (forest based)*. Delhi: Asia Pacific Business Press.

- Pawlik, A.K. and Norton, I.T. 2014. Bridging benchtop research and industrial processed foods: Structuring of model food emulsions. *Food Structure*. 1(1), pp.24-38.

- Perrechil, F.A. and Cunha, R.L. 2012. Development of multiple emulsions based on the repulsive interaction between sodium caseinate and LBG. *Food Hydrocolloids*. 26(1), pp.126-134.

- Pickering, S. 1907. Emulsions. *Journal of the Chemical Society*. 91, pp.2001-2021.

- Picout, D.R., Ross-Murphy, S.B., Errington, N. and Harding, S.E. 2001. Pressure cell assisted solution characterization of polysaccharides. 1. Guar Gum. *Biomacromolecules*, 2(4), pp.1301-1309.

- Picout, D.R., Ross-Murphy, S.B., Jumel, K. and Harding, S.E. 2002. Pressure cell assisted solution characterization of polysaccharides. 2. Locust Bean Gum and Tara Gum. *Biomacromolecules*, 3(4), pp.761-767.

- Ptaszek, A., Berski, W., Ptaszek, P., Witczak, T., Repelewicz, U. and Grzesik, M. 2009. Viscoelastic properties of waxy maize starch and selected non-starch hydrocolloids gels. *Carbohydrate polymers*. 76(4), pp.567-577.

- Purwanti, N., Moerkens, A., van der Goot, A.J. and Boom, R. 2012. Reducing the stiffness of concentrated whey protein isolate (WPI) gels by using WPI microparticles. *Food Hydrocolloids*. 26(1), pp.240-248.

- Qian, C. and McClements, D.J. 2011. Formation of nanoemulsions stabilized by model food-grade emulsifiers using high-pressure homogenization: Factors affecting particle size. *Food Hydrocolloids*. 25(5), pp.1000-1008.

- Ramsden, W. 1903. Separation of solids in the surface-layers of solutions and 'suspensions' (Observations on surface-membranes, bubbles, emulsions, and mechanical coagulation). - Preliminary account. *Proceedings of the Royal Society of London*. 72(477-486), pp.156-164.

- Rao, M.A. 1999. *Rheology of fluid, semisolid, and solid foods*. Maryland: Aspen Publishers, Inc.

- Rao, M.A. 2007. *Rheology of fluid and semisolid foods: principles and applications* 2nd ed. New York: Springer.

- Rao, M.A. 2013. Flow and functional models for rheological properties of fluid foods. *Food Engineering Series*, pp.27-61.

- Rayner, M., Sjöö, M., Timgren, A. and Dejmek, P. 2012. Quinoa starch granules as stabilizing particles for production of Pickering emulsions. *Faraday Discussions*. 158, pp.139-155.

- Ruis, H.G.M., Venema, P. and van der Linden, E. 2007. Relation between pH-induced stickiness and gelation behaviour of sodium caseinate aggregates as determined by light scattering and rheology. *Food Hydrocolloids*. 21(4), pp.545-554.

- Sabin, A. 2011. Problems in particle size: laser diffraction observations. *GXP Journal Articles*. 15(4).

- Sagis, L.M.C. and Scholten, E. 2014. Complex interfaces in food: Structure and mechanical properties. *Trends in Food Science & Technology*. 37(1), pp.59-71.

- Salk Institute for Biological Studies. 2009. Leica Confocal. [online]. Available from: http://cores.salk.edu/ccmi/index.php [Accessed June 22, 2012].

- Sánchez, C.C. and Patino, J.M.R. 2005. Interfacial, foaming and emulsifying characteristics of sodium caseinate as influenced by protein concentration in solution. *Food Hydrocolloids*. 19(3), pp.407-416.

- Schmidt, S., Liu, T., Rütten, S., Phan, K.H., Möller, M. and Richtering, W. 2011. Influence of microgel architecture and oil polarity on stabilization of emulsions by stimuli-sensitive core–shell poly(N-isopropylacrylamide-co-methacrylic acid) microgels: Mickering versus Pickering behavior?. *Langmuir*. 27(16), pp.9801-9806.

- Schmitt, C., Bovay, C. and Rouvet, M. 2014. Bulk self-aggregation drives foam stabilization properties of whey protein microgels. *Food Hydrocolloids*. 42, pp.139-148.

- Schorsch, C., Garnier, C. and Doublier, J.L. 1997. Viscoelastic properties of xanthangalactomannan mixtures: comparison of guar gum with locust bean gum. *Carbohydrate Polymers*. 34(3), pp.165-175.

- Schramm, L.L. 2005. *Emulsions, foams, and suspensions*. Weinheim: John Wiley & Sons.

- Semenova, M.G., Dickinson, E., Burlakova, E.B. and Zaikov, G.E. 2010. *Biopolymers in food colloids: Thermodynamics and Molecular Interactions*. Leiden: Brill.

- Shum, H.C., Varnell, J. and Weitz, D.A. 2012. Microfluidic fabrication of water-in-water (w/w) jets and emulsions. *Biomicrofluidics*. 6(1), pp.012808.

- Simonet, F., Garnier, C. and Doublier, J.L. 2000. Partition of proteins in the aqueous guar/dextran two-phase system. *Food Hydrocolloids*. 14(6), pp.591-600.

- Sittikijyothin, W., Torres, D. and Gonçalves, M.P. 2005. Modelling the rheological behaviour of galactomannan aqueous solutions. *Carbohydrate Polymers*. 59(3), pp.339-350.

- Smidsrød, O. and Moe, S. 2008. *Biopolymer chemistry*. Trondheim: Tapir.

- Stratford, K., Adhikari, R., Pagonabarraga, I., Desplat, J.C. and Cates, M.E. 2005. Colloidal jamming at interfaces: A route to fluid-bicontinuous gels. *Science*. 309(5744), pp.2198-2201.

- Sudhakar, V., Singhal, R.S. and Kulkarni, P.R. 1996. Starch-galactomannan interactions: functionality and rheological aspects. *Food Chemistry*. 55(3), pp.259-264.

- Syrbe, A., Bauer, W.J. and Klostermeyer, H. 1998. Polymer science concepts in dairy systems - an overview of milk protein and food hydrocolloid interaction. *International Dairy Journal*. 8(3), pp.179-193.

- Tadros, T.F. 2007. *Colloid stability: The role of surface forces - Part 1*. Weinheim: John Wiley & Sons.

- Tan, Y., Xu, K., Niu, C., Liu, C., Li, Y., Wang, P. and Binks, B.P. 2014. Triglyceride–water emulsions stabilised by starch-based nanoparticles. *Food Hydrocolloids*. 36, pp.70-75.

- Tcholakova, S., Denkov, N.D., Sidzhakova, D., Ivanov, I.B. and Campbell, B. 2003. Interrelation between drop size and protein adsorption at various emulsification conditions. *Langmuir*. 19(14), pp.5640-5649.

- Timgren, A., Rayner, M., Sjöö, M. and Dejmek, P. 2011. Starch particles for food based Pickering emulsions. *Procedia Food Science*. 1, pp.95-103.

- Tolstoguzov, V.B. 1986. Functional properties of food macromolecules *In*: Mitchell, J.R. and Ledward, D.A. ed. *Functional Properties of Food Macromolecules London*: Elsevier Applied Science, pp. 385.

- Tolstoguzov, V.B. 1986. Functional properties of protein-polysaccharide mixtures *In*: Hill, S.E., Ledward, D.A. and Mitchell, J.R. ed. *Functional Properties of Food Macromolecules*. London: Elsevier Applied Science Publishers, pp. 252-275.

- Tolstoguzov, V.B. 2003. Some thermodynamic considerations in food formulation. *Food Hydrocolloids*. 17(1), pp.1-23.

- Tolstoguzov, V.B. 2006. Phase behaviour in mixed polysaccharide systems *In*: Alistair, M.S., Glyn, O.P. and Peter, A.W. ed. *Food polysaccharides and their application*. Florida: CRC Press, pp. 589-620.

- Tolstoguzov, V.B. 2007. Ingredient interactions in complex foods: aggregation and phase separation *In*: McClements, J. ed. *Understanding and controlling the microstructure of complex food*. Cambridge: Woodhead Publishing.

- Tombs, M.P. and Harding, S.E. 1998. *An introduction to polysaccharide biotechnology*. London: Taylor & Francis.

- Tzoumaki, M.V., Moschakis, T., Kiosseoglou, V. and Biliaderis, C.G. 2011. Oil-in-water emulsions stabilized by chitin nanocrystal particles. *Food Hydrocolloids*. 25(6), pp.1521-1529.

- Vazquez-Duhalt, R. and Quintero-Ramírez, R. 2004. *Petroleum biotechnology*. Amsterdam: Elsevier.

- Vincent, B. and Saunders, B. 2011. Interactions and colloid stability of microgel particles *In*: Fernandez-Nieves, A., Wyss, H.M., Mattsson, J. and Weitz, D.A. ed. *Microgel Suspensions: Fundamentals and Applications*. Weinheim: John Wiley & Sons.

- Walter, R.H. 1998. *Polysaccharide dispersions*. San Diego: Academic Press.

- Wang, F., Sun, Z. and Wang, Y.J. 2001. Study of xanthan gum/waxy corn starch interaction in solution by viscometry. *Food Hydrocolloids*. 15(4-6), pp.575-581.

- Wang, J. and Somasundaran, P. 2007. Study of galactomannose interaction with solids using AFM, IR and allied techniques. *Journal of colloid and interface science*. 309(2), pp.373-383.

- Wang, Q. and Cui, S. 2005. Understanding the physical properties of food polysaccharides *In*: S.W. Cui, ed. *Food carbohydrates: Chemistry, physical properties, and applications*. Boca Raton: CRC Press.

- Wege, H.A., Kim, S., Paunov, V.N., Zhong, Q. and Velev, O.D. 2008. Long-term stabilization of foams and emulsions with in-Situ formed microparticles from hydrophobic cellulose. *Langmuir*. 24(17), pp.9245-9253.

- Whistler, R.L. and BeMiller, J.N 1997. *Carbohydrate chemistry for food scientists*. St. Paul, Minn.: Eagan Press.

- Williams, M.A.K., Fabri, D., Hubbard, C.D., Lundin, L., Foster, T.J., Clark, A.H., Norton, I.T., Loren, N. and Hermansson, A.M. 2001. Kinetics of droplet growth in gelatin/maltodextrin mixtures following thermal quenching. *Langmuir*. 17(11), pp.3412--3418.

- Witt, J.A., Mumm, D.R. and Mohraz, A. 2013. Bijel reinforcement by droplet bridging: a route to bicontinuous materials with large domains. *Soft Matter*. 9(29), pp.6773-6780.

- Wolf, B., Scirocco, R., Frith, W.J. and Norton, I.T. 2000. Shear-induced anisotropic microstructure in phase-separated biopolymer mixtures. *Food Hydrocolloids*. 14(3), pp.217-225.

- Ye, A., Zhu, X. and Singh, H. 2013. Oil-in-water emulsion system stabilized by protein-coated nanoemulsion droplets. *Langmuir*. 29(47), pp.14403-14410.

- Young, T. 1855. Characterisation of oil-water interfaces containing finely divided solids with applications to the coalescence of water-in-oil emulsions: a review *In*: G. Peacock, ed. *Miscellaneous Works*. London: John Murray.

- Yusoff, A. and Murray, B.S. 2011. Modified starch granules as particle-stabilizers of oil-in-water emulsions. *Food Hydrocolloids*. 25(1), pp.42-55.

- Zang, D.Y., Rio, E., Langevin, D., Wei, B. and Binks, B.P. 2010. Viscoelastic properties of silica nanoparticle monolayers at the air-water interface. *The European Physical Journal E*. 31(2), pp.125-134.

- Zayas, J.F. 1997. *Functionality of proteins in food*. New York: Springer.

- Zeeb, B., Beicht, J., Eisele, T., Gibis, M., Fischer, L. and Weiss, J. 2013. Transglutaminase-induced crosslinking of sodium caseinate stabilized oil droplets in oil-in-water emulsions. *Food Research International*. 54(2), pp.1712-1721.

- Zhu, Y., Zhang, S., Hua, Y., Zhang, H. and Chen, J. 2014. Synthesis of latex particles with a complex structure as an emulsifier of Pickering high internal phase emulsions. *Industrial & Engineering Chemistry Research*. 53(12), pp.4642-4649.

Publications and presentations

This thesis has contributed to the following publication:

1. Murray, B.S. and Phisarnchananan, N. 2014. The effect of nanoparticles on the phase separation of waxy corn starch+locust bean gum or guar gum. *Food Hydrocolloids*. 42, pp.92-99.
2. Murray, B.S. and Phisarnchananan, N. 2016. Whey protein microgel particles as stabilizers of waxy corn starch + locust bean gum water-in-water emulsions. *Food Hydrocolloids*. 56, pp.161-169.

This work has also been presented by the author at the following events:

1. Oral presentation: "Phase separation of amylopectin + guar gum mixtures", Food colloids seminar, 18th July 2012, University of Leeds, UK.
2. Oral presentation: "Effect of silica particles on phase separation of waxy corn starch + locust bean gum mixture", Food colloids seminar, 8th May 2013, University of Leeds, UK.
3. Poster presentation: "Effect of silica particles on phase separation of polysaccharide mixtures", 14th European Student Conference on Colloid and Interface Science (ESC), 10th – 13th June 2013, Potsdam-Golm, Germany.
4. Poster presentation: "Effect of silica particles on phase separation of polysaccharide mixtures", the Biosciences KTN early career researchers food sector event, 23rd May 2013, Painter's Hall, London, UK.
5. Oral presentation: "Effect of nanoparticles on phase separation of waxy corn starch + locust bean gum mixtures", Food colloids seminar, 14th May 2014, University of Leeds, UK.
6. Poster presentation: "The effect of nanoparticles on the phase separation of waxy corn starch + locust bean gum", 15th Food Colloids Conference, 13th - 16th June 2014, Karlsruhe, Germany.
7. Oral Presentation: "The effect of nanoparticles on the phase separation of waxy corn starch + locust bean gum", the SoftComp Annual meeting, 26th - 29th May 2014, Heraklion, Greece.

8. Oral presentation: “The effect of nanoparticles on the phase separation of waxy corn starch + locust bean gum”, PhD conference, 24th September 2014, University of Leeds, UK.

Nomenclature

Annotations

ΔG_{mix}	Gibbs free energy of mixing (J/mol)
ΔH_{mix}	Change of enthalpy of mixing (J/mol)
ΔS_{mix}	Change of entropy of mixing (J/Kmol)
ΔE	Particle detachment energy (J)
C_b	Biopolymer concentration
C_p	Particle concentration
c*	Critic biopolymer overlap concentration
c**	Second critic biopolymer concentration
R^2	Goodness of fit
T	Absolute temperature (°K)
k_B	Boltzmann's constant (1.38 x 10^{-23} m^2 kg s^{-2} K^{-1})
V_s	Velocity of spherical droplet (m s^{-1})
V_p	Volume of particles
V_d	Volume fraction of starch domain occupied by the particles
N_p	Number of particles
N_d	Number of starch domains
$\emptyset_i$	Fraction of coverage at the interface
g	Gravitational acceleration (9.8 m/s^2)
M	Mass per unit volume
R	Domain radius (m)

r, a	Particle radius (m)
d	Particle/droplet hydrodynamic diameter (m)
D	Translational diffusion coefficient
S	Scale factor (μm/pixel)
δFFT	Number of radius distance (pixel)
G’	Storage modulus (Pa)
G”	Loss modulus (Pa)
G*	Complex modulus (Pa)
K	Flow consistency index (Pa s^n)
K	Ratio of interfacial area occupied by the particles
n	Power law flow behaviour index
C	Cross constant
m	Dimensionless exponents
E	Electrical field
V	Particle velocity (m s^{-1})
U	Electrophoretic mobility

Greek letters

$\Delta\rho$	Density difference (kg L^{-1})
η_c	Viscosity of the continuous phase (Pa s)
η_0	Zero shear rate viscosity (Pa s)
η_∞	Limiting value of the viscosity at high shear rate (Pa s)

η	Viscosity (Pa s)
σ	Shear stress (Pa)
$\dot{\gamma}$	Shear rate (s^{-1})
γ	Interfacial tension ($N\ m^{-1}$)
θ	Contact angle
ω	Angular velocity or frequency (rad)
ζ-potential	Zeta potential (mV)
ε	Dielectric constant
f(κa)	Henry's function
κ	Debye length

Abbreviations and subscripts

LVR	The linear viscoelastic region
LBG	Locust bean gum
GG	Guar gum
S	Waxy corn starch
SC	Sodium caseinate
BMDs	1-Bromohexadecane microdroplets
WPI	Whey protein isolate
RB	Rhodamine B dye
AO	Acridine Orange dye
NR	Nile Red dye
SiOH	Silanol group
FFT	Fast-Fourier transform

F	Force (N)
A	Area
D	Displacement; Diffusion coefficient
H	Height
L	Characteristic length
CLSM	Confocal laser scanning microscopy